DISCLAIMER NOTICE

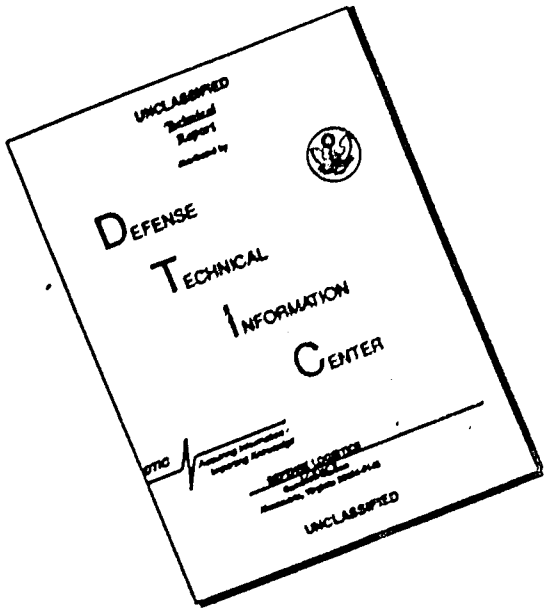

THIS DOCUMENT IS BEST QUALITY AVAILABLE. THE COPY FURNISHED TO DTIC CONTAINED A SIGNIFICANT NUMBER OF PAGES WHICH DO NOT REPRODUCE LEGIBLY.

WEB SUBTASK 13.009
THE RESPONSE OF SOILS
TO DYNAMIC LOADINGS, REPORT 17

STRESS-STRAIN-TIME BEHAVIOR OF SOIL IN ONE DIMENSIONAL COMPRESSION

Robert V. Whitman

May 1963

MIT

DEPARTMENT
OF
CIVIL
ENGINEERING

SCHOOL OF ENGINEERING
MASSACHUSETTS INSTITUTE OF TECHNOLOGY
Cambridge 39, Massachusetts

Department of Civil Engineering Research Report R63-25

THE RESPONSE OF SOILS TO DYNAMIC LOADINGS
Report No. 17: Stress-Strain-Time Behavior of Soil in One Dimensional Compression

Robert V. Whitman

May 1963

Contract No. DA-22-079-eng-224
with
U. S. Army Engineers Waterways Experiment Station
Department of the Army, Rand D Subproject 8-S12-95-002
under Weapons Effect Board Subtask No. 13.009

ABSTRACT

Ground motion prediction formulas based upon elastic wave propagation in one-dimension (no strain transverse to the propagation direction) have been used widely in protective construction work. Actual soil materials of course exhibit many deviations from elastic behavior. This report assesses the probable influence of these non-elastic effects upon the accuracy of the above-mentioned prediction formulas, and upon the question of stress attenuation with depth.

Toward this end, three different models of soil behavior are assumed: a standard 3-element visco-elastic model (spring in series with spring-dashpot combination); a compacting model (straight line loading and unloading curves); and an "elastic" model in which any arbitrary shape may be assigned to the loading stress-strain curve. This report deals primarily with the first of these three models; the possible significance and probable importance of the third model are discussed briefly.

The theory necessary for estimating the effects of visco-elasticity and inelasticity has been presented in various papers and reports by other workers. In order to assign numbers to the pertinent parameters, a large number of one-dimensional compression tests have been carried out upon granular specimens and specimens of both re-molded and undisturbed cohesive soils. A step loading with a rise-time of about 15-20 milliseconds has been used in these tests. Several cycles of stress were applied to each specimen.

By combining the theoretical and experimental results, it is shown that the elastic ground motion prediction formulas are generally valid (for cases where it is appropriate to think of one-dimensional motion); i.e. the possible effects of viscosity and inelasticity are no greater than uncertainties as to the order of magnitude of the compressibility of an in situ soil mass.

PREFACE

This report serves two purposes. First, the appendices present certain test programs and results not previously reported. These testing efforts were carried out during the period commencing in the early months of 1961 and ending in May 1962. Second, the main body of the report is essentially a final report for the one-dimensional compression testing phase of the total research effort. The main body presents the rationale for the testing program, summarizes the test data, and discusses the implications of the data with regard to propagation of high intensity stress waves through earth. The origianl effort of compiling and interpreting the data was carried out during the spring of 1962; the validity of the data and of the interpretations were rechecked during the winter of 1962.

It is worth noting that the total period of time used for the one-dimensional testing program (the first results were given in Report No. 3 dated October 1959) overlapped the time during which hardened facilities for intercontinental ballistic missiles were designed and constructed in this country. The research already underway on this contract, and especially the testing procedures already under development, proved to be of great value during this mammoth engineering undertaking; for example, see the article "Sites for Hardened ICBM Facilities" by V. E. Zadnik in the April 1962 issue of CIVIL ENGINEERING. At the same time the engineering effort for the hardened bases aided the research effort, for the engineering effort provided an opportunity to test undisturbed samples of a variety of earth materials. The data from these tests appears in a series of reports which the author prepared for The Ralph M. Parsons Company and for the firm of Shannon and Wilson. These reports are referenced in the main body.

This is the seventeenth in a series of reports issued by M.I.T. under its present contract with the U. S. Army Engineers Waterways Experiment Station. A list of the earlier reports follows this preface. The work has been carried out in the Soil Laboratories of the Civil Engineering Department. The author is Robert V. Whitman, Associate Professor of Civil Engineering. The author has been aided in this research by numerous research assistants, as noted in the prefaces to the several appendices.

PREVIOUS REPORTS

1. "Scope of Test Program and Equipment Specifications," November 1957
2. "Test Equipment for High Speed Triaxial Tests," January 1959
3. "First Interim Report on Dynamic Soil Tests," October 1959
4. "One-Dimensional Compression and Wave Velocity Tests," August 1960
5. "Pore Pressure Measurements During Transient Loadings," November 1960
6. "Effects of Rate-of-Strain on Stress-Strain Behavior of Saturated Soils," April 1961
7. "Adaptation and Use of the Boynton Device for Rapid One-Dimensional Compression Tests," June 1961
8. "Laboratory Measurement of Dilatational Wave Propagation Velocity," July 1961
9. "Shearing Resistance of Sands During Rapid Loadings," May 1962
10. "Strength of Saturated Fat Clay," June 1962
11. "Triaxial Tests upon Saturated Fine Silty Sand," September 1962
12. "Static Tests upon Thin Domes Buried in Sand," December 1962
13. "The Dependence of Dilation in Sand on Rate of Shear Strain," February 1963
14. "Propagation Velocity of Ultrasonic Waves through Sand," March 1963
15. "Undrained Strength of Saturated Clayey Silt, March 1963
16. "Effective Stress Versus Strength: Saturated Fat Clay," April 1963

TABLE OF CONTENTS

		Page No.
1.	Introduction	1
	1.1 Objectives and scope of research	1
	1.2 Definition of one-dimensional compression	1
	1.3 Importance of one-dimensional wave propagation	3
	1.4 Elastic wave propagation theory	5
	1.5 Possible shortcomings in modified "elastic" formulas	7
	1.6 Present status of knowledge	8
	1.7 Method of attack	9
2.	Test equipment	15
	2.1 History of one-dimensional compression test devices	15
	2.2 Oedometer I	16
	2.3 Tests with explosive loading system	16
	2.4 Oedometer II	16
	2.5 Wave propagation during compression test	19
	2.6 Laboratory measurement of seismic wave velocity	20
3.	Test results	31
	3.1 Test program	31
	3.2 Magnitude of modulus	35
	3.3 Data regarding time dependency	38
	3.4 Data regarding irreversibility	41
	3.5 Data regarding non-linearity	44
4.	Implications regarding wave propagation	61
	4.1 Wave propagation effects within visco-elastic material	61
	4.1.1 Importance of stress attenuation from visco-elasticity	63
	4.1.2 Influence of visco-elasticity upon maximum displacement and particle velocity	65
	4.1.3 Effect of visco-elasticity upon maximum acceleration	65

Page No.

4.2 Wave propagation effects within irreversible material 66
4.2.1 Importance of stress attenuation by irreversibility 67
4.2.2 Effect of irreversibility upon maximum ground displacement and particle velocity 68
4.3 Wave propagation effects within non-linear material 70
5. Summary and final remarks 85
5.1 Predicting free field effects from explosions of megaton size 86
5.1.1 Stress attenuation 86
5.1.2 Ground motion predictions 86
5.1.3 Selection of "Design Velocity" 87
5.2 Analysis of free field effects measured during explosion of kiloton size 88
5.3 Problems for further study 88
5.4 Conclusions 89

Appendix A First Series of Cyclic Loading Tests
Appendix B Second Series of Cyclic Loading Tests
Appendix C Improvement of One-Dimensional Compression Test Apparatus
Appendix D First Series of Rapid Loading Tests upon Granular Materials
Appendix E Second Series of Rapid Loading Tests upon Granular Materials
Appendix F Triaxial Tests Using Cyclic Loading

LIST OF FIGURES FOR MAIN BODY

		Page No.
1.1	One-Dimensional State of Strain	12
1.2	Air Blast Loading	12
1.3	Superseismic Case	13
1.4	Elastic One-Dimensional Wave Propagation	13
1.5	Models for Soil Behavior	14
2.1	Early Arrangement for Rapid Compression Tests	22
2.2	Oedometer I	23
2.3	General Arrangement of Explosive Loading System	24
2.4	Specimen Container and Strain Measurement System - Explosive Loading System	25
2.5	Oedometer II for Rapid Compression Tests	26
2.6	Pattern of Applied Stress	27
2.7	Actual and Apparent Stress-Strain Curves from Hypothetical Compression Test	28
2.8	Schematic of Ultrasonic Wave Propagation Apparatus	29
2.9	Specimen Container for Ultrasonic Wave Propagation Apparatus	30
3.1	Typical Oscilloscope Photographs from Compression Tests	47
3.2	Summary of Data for Modulus of Ottawa Sand	48
3.3	Creep at Early Time - Cemented Silty Clay	49
3.4	Creep at Late Times - Cemented Silty Clay	50
3.5	Creep at Early Time - Ottawa Sand	51
3.6	Creep at Early Times - Several Soils	52
3.7	Response of Visco-Elastic Model to Step Load	53
3.8	Symbols Associated with Irreversible Model	54
3.9	Hysteresis Loops for Ottawa Sand	55
3.10	Stress-Strain Curves for Ottawa Sand	56
3.11	Modulus of Ottawa Sand vs. Stress Increment - First Cycle of Loading	57
3.12	Modulus of Ottawa Sand vs. Stress Increment - After Many Cycles of Loading	58
3.13	Typical Stress-Strain Curve for Soil During Rapid Loading	59

		Page No.
4.1	Patterns of Applied Stress for Visco-Elastic Model	72
4.2	Distribution of Stress Along Visco-Elastic Column at Several Times - Step of Stress	73
4.3	Stress vs. Time at Several Points Along Visco-Elastic Column - Step of Stress	74
4.4	Strain vs. Time at Several Points Along Visco-Elastic Column - Step of Stress	75
4.5	Stress Attenuation in Visco-Elastic Column - Stress Pulse of Finite Duration	76
4.6	Stress vs. Time at Several Points Along Column - Blast Stress	77
4.7	Stress Attenuation in Visco-Elastic Column - Blast Stress	78
4.8	Stress Attenuation in Visco-Elastic Column - Blast Stress from Large Explosions	79
4.9	Particle Velocity vs. Time at Several Points Along Visco-Elastic Column - Blast Stress	80
4.10	Characteristics Diagram for Study of Wave Propagation Through Irreversible Material	81
4.11	Triangular Approximation to Blast Wave	82
4.12	Example to Study Effect of Irreversibility Upon Surface Displacements	83
4.13	Example to Illustrate Effect of Irreversibility Upon Displacements at Depth	84

Figures are found at the end of each chapter. Figures for the appendices are listed at the beginning of each appendix.

LIST OF TABLES FOR MAIN BODY

		Page No.
3.1	Summary of Test Program	32
3.2	Reference for Detailed Test Data	33
3.3	General Order of Magnitude of Modulus	36
3.4	Total Accumulation of Creep - Various Soils	40
3.5	Parameters for Visco-Elastic Model	42
3.6	Data Regarding Recovery Ratio	43

Tables for the appendices are listed at the beginning of each appendix.

LIST OF SYMBOLS

M - constrained modulus = ρc^2

ρ - mass density

c - wave propagation velocity

$\Delta\sigma$ - stress increment

$\Delta\varepsilon$ - change in strain corresponding to stress change $\Delta\sigma$

M_o - loading modulus in irreversible model = ρc_o^2

M_1 - unloading modulus in irreversible model = ρc_1^2

r - recovery ratio = $M_o/M_1 = 1/m^2$

t - time from start of loading

μ - viscosity coefficient in visco-elastic model

T - dimensionless time = t/t_o, where $t_o = 1/\mu M_o$

X - dimensionless distance = $x/c_o t_o$

T_s - dimensionless time of arrival of wave front at dimensionless distance X

$\hat{\sigma}$ - dimensionless stress = $\Delta\sigma/\Delta\sigma_s$

$\Delta\sigma_s$ - stress step

$\hat{\varepsilon}$ - dimensionless strain = $(M_o/\Delta\sigma_s)\,\Delta\varepsilon$

v - particle velocity

u - ground displacement

Chapter 1

INTRODUCTION

1.1 Objectives and Scope of Research

This report represents the end product of several year's research into the stress-strain-time behavior of soil during one-dimensional compression. This research has been aimed specifically toward a better understanding of the relation between soil behavior and the one-dimensional propagation through soil of high-intensity stress waves (say, greater than 10 lbs/in^2, and ranging up into the thousands of lbs/in^2) such as those resulting from a nuclear explosion.

The objective of the laboratory testing program has been to block-out in a general way the pertinent behavior characteristics of soil such as the ratio of dynamic to static modulus, the apparent range of relaxation times, the degree of strain recovery upon unloading, the nature of the non-linearities in the stress-strain relation, etc. The laboratory tests have been relatively crude and "heavy-handed," and the emphasis has been upon measurements which suffice for engineering estimates as to the importance of the various effects. This emphasis has of course meant that scientific exactness, thoroughness and sophistication have been sacrificed.

This introductory chapter will review the reasons for interest in the one-dimensional wave propagation case, will discuss the simple formulas that have been developed for making ground motion predictions and the shortcomings of these formulas, will analyze the present state of our knowledge regarding wave propagation phenomena, and finally will outline the method of attack to be followed in the report.

1.2 Definition of one-dimensional compression

The prime characteristic of one-dimensional compression is that all motion takes place in one direction only: along the axis of

the material element. The sketch in Figure 1.1 indicates these conditions. If lateral strains occur, as in the typical compression test upon a billet of metal, the situation is not truly one-dimensional. Propagation of stress waves along a long slender rod suspended freely in air is likewise not a truly one-dimensional problem, although this problem can be treated by one-dimensional theory provided that the wave fronts are not too sharp. The essence of the one-dimensional case is that resistance to volume change, rather than resistance to shear, is the governing aspect of the material behavior. Shear stresses and strains are present in the one-dimensional case, but are limited in magnitude and importance by the boundary conditions. The distinction between the rod case and the one-dimensional case is of obvious importance when large stresses are applied to a soil.

During one-dimensional wave propagation, each element of soil is in the same state of strain as a chunk of soil during an ordinary consolidation test. When conducting such a test, we are usually interested in studying the compression or expansion of the soil as water flows out of or into the soil. During wave propagation, there generally will be no movement of the soil moisture through the soil. Hence, to be precise, we shall subsequently be talking about undrained one-dimensional compression. The modulus for this state of strain will generally be called the "constrained" modulus.

If a soil were completely saturated, its behavior in undrained one-dimensional compression would be primarily controlled by the compressibility of water. Such a soil would be more-or-less elastic in its behavior. While there are some interesting questions concerning wave propagation phenomena in a saturated soil (for example, see BIOT, 1956), this report is almost entirely concerned with soils that can compress significantly; i.e. partially-saturated or dry soils.

1.3 Importance of one-dimensional wave propagation

One valid reason for studying one-dimensional wave propagation is that this case is far easier to treat than cases involving strains and movements in more than one direction. The mathematical theory for one-dimensional propagation is now well advanced and reasonably simple, whereas theoretical work involving several dimensions is complex and is just getting off the ground. Corresponding statements can be made concerning the experimental determination of the necessary stress-strain-time relations. In addition, however, the one-dimensional case is a reasonable representation for an important group of protective construction problems; those where the air-blast induced ground shock is of primary importance.*

The loading of the ground surface by a blast wave (see Figure 1.2) has some obvious similarities to the loading of the ground surface by a building or an embankment. Moreover, the maximum displacement of the ground surface is of important concern in protective construction studies, just as the settlement is of concern in connection with foundation engineering problems. The foundation engineer is accustomed to assuming a one-dimensional case for his settlement studies, and it is most natural to make the same assumptions for the air blast loading case.

In the simplest form of settlement analysis, the engineer considers a soil column extending down to the depth of the "pressure bulb," and estimates settlement as the product of (1) the column length, (2) the applied stress, and (3) a compressibility factor obtained from ordinary (one-dimensional) consolidation tests. If the soil column is short compared to the width of the loaded area, as when harder soil or rock

---

*The ground shock which originates as the air blast wave from the explosion sweeps outward over the ground surface, as contrasted to the ground shock coming directly through the ground from the point of a surface or underground explosion.

underlies the compressible soil at shallow depth, this procedure involves a close approximation to the actual stress and strain condition. In the more general case, the procedure, which ignores decrease of stress increment with depth, change of compressibility with depth, strains below the pressure bulb, etc., is still a useful engineering tool however crude the approximation. Even the more sophisticated settlement calculation techniques, such as those by TAYLOR (1948) and SKEMPTON and BJERRUM (1957), are quasi-one-dimensional; i.e. the stresses come from a two-dimension theory, but the compressibility factors from a one-dimensional test.

Thus there is ample precedent for analyzing the air blast induced ground shock case by considering the strains developed within a column of soil, extending downward from the ground surface and assumed to be in a one-dimensional state of strain: see Figure 1.2. The loading upon the end of this column is now time dependent, as determined by the space distribution of the blast pressure at various times. For explosions of megation size, the wave lengths of the blast waves through the air are quite long; as long as one-half mile. To the extent that the ground motions result primarily from compressive strains within, say, the top 500 feet of the earth's crust, the assumption of the one-dimensional case should provide a very good approximation to the actual conditions. In the more general case, the assumption should still provide a useful engineering tool.

The use of one-dimensional theory can be justified further by reference to the theory for a superseismic blast wave sweeping over the ground surface: see COLE and HUTH (1958). As indicated in Figure 1.3, a superseismic blast wave is one whose shock front propagation velocity exceeds the velocity of stress wave propagation in the earth.* The theory predicts a plane wave front advancing through the ground; and thus one-dimensional conditions at the front and for some distance behind the front.

---

*When the shock front air overpressure is 100 lbs/in^2, for example, the shock front propagation velocity is 2000 ft/sec.

While the conditions assumed in construction of this theory differ somewhat from the actual conditions, the theory does give special credance for the assumption of the one-dimensional state whenever superseismic conditions prevail.

1.4 Elastic wave propagation theory

The theory for elastic wave propagation for the one-dimensional case (TIMOSHENKO, 1934) yields several simple and particularly useful results. First of all, the theory indicates that a wave will propagate along homogeneous column with unchanged wave shape, as indicated in Figure 1.4. Each station will experience the same maximum stress. Next, by considering the momentum conditions at a wave front, it can be shown that the particle velocity** increase as a wave front passes it:

$$\Delta v = \Delta\sigma (c/M) = \Delta\sigma/\rho c \qquad (1.1)$$

where

Δ signifies a change
$v = \partial u/\partial t$, particle velocity
u = particle displacement
σ = stress
c = wave front propagation velocity
M = modulus, $\sigma \div \partial u/\partial x$
x = distance from end of column
ρ = mass density

Finally, by adding up all the strains behind the wave front, it is found that the displacement of the end of the column is:

**It is important to distinguish between particle velocity, or the rate at which an element of matter moves, and the wave front velocity.

$$u_o = cI/M = I/\rho c \qquad (1.2)$$

where u_o = displacement at $x = 0$ at time t

$I = \int_0^t \sigma_o \, dt$, the impulse in the applied pressure-time relation up until time t

σ_o = applied pressure at $x = 0$

Starting with these equations, it is possible to derive formulas for the maximum ground displacement and maximum particle velocity for explosions of varying size and for various air blast pressure levels. The formulas in Chapter XI of ASCE Manual No. 42 (MURPHY, et al, 1961) were obtained in this way. The chief problem in the application of these formulas lies in selection of the wave propagation velocity, since it is this parameter that reflects the stiffness of the earth material. Where the overpressure level $(\sigma_o)_{max.}$ is small, the earth will likely behave linearly, and c may be taken equal to the seismic velocity. Higher overpressures will undoubtedly stress the earth into its non-linear range. In order to use Eq. (1.1) and (1.2) under these circumstances, an "effective" wave velocity c must be chosen with an eye toward the increased compressibility of the soil, an approach which SAUER (1959) has termed quasi-elasticity. Based upon an analysis of available data from explosion tests, Sauer has recommended that c be taken as 3/4 of the seismic wave velocity.

Whereas the maximum displacement and particle velocity can thus be estimated without a detailed knowledge of the wave shape, such information is necessary for predictions of particle acceleration. If the advancing wave front does have a sharp distinct rise, then the peak acceleration can be estimated from the quotient of the velocity jump and the rise-time. However, if the very short rise-times in the air blast shock front are used, one gets in this way accelerations much larger than those actually measured in the ground. Thus it is necessary to resort to empirical data. The ASCE Manual suggests that a 0.001 second rise-time should be used near the ground surface. Moreover, it has been observed that the peak acceleration attenuates

with distance into the ground, even in situations where the peak stress and particle velocity remain unchanged with distance. Again, the ASCE Manual suggests a simple correction to the formulas based upon elastic theory.

1.5 Possible shortcomings in modified "elastic" formulas

The foregoing discussion has indicated that the results from elastic, one-dimensional wave propagation theory, with simple corrections to account for non-linearity and degradation of rise-time, can be used as a basis for ground motion predictions. Two questions inevitably arise: just how to select the "effective" wave propagation velocity for a given earth material, and in what way is the degradation of rise-time related to the properties of the particular earth material in question?

A more serious question is frequently directed at the use of the elastic formulas, to wit: the actual peak stress must certainly decrease with depth into the ground, and since the elastic theory fails to predict such a decrease, may not formulas based upon this theory fail seriously to preduct the maximum ground displacement!

Of course, one reason why the peak stress decreases with depth has to do with the geometry of the problem; the wave fronts are not really plane and the problem is really not one-dimensional. The possible departure from a one-dimensional state is not the concern of this report. The ASCE Manual provides a formula for estimating the rate of attenuation of peak stress with depth, and for megaton-sized explosions this attenuation rate is surprisingly small. WILSON and SIBLEY (1962) have proposed a method for incorporating the stress attenuation effect into the elastic wave propagation approach; this method bears many similarities in philosophy to that outlined by Taylor for static settlement problems. However, even if the one-dimensional approach is accepted, there are still possible reasons why the peak stress might decrease with depth; e.g. energy attenuation due to viscous or hysteresis effects. Perhaps, it can be

argued, the same phenomena that degrade with depth the rise-time of the soil stress wave will lead to significant attenuation of stress and invalidate the prediction formulas based upon elastic theory.

Thus we have generated three questions which need to be answered by research into one-dimensional wave propagation through earth materials:

(a) How do actual soil properties effect the peak stress as a function of depth?

(b) In what way is the transmission of high frequency motions (those which give a short rise-time) controlled by soil properties?

(c) Despite the obvious shortcomings to the elastic theory as applied to soils, can reasonable estimates of ground motion be made on the basis of Eq. (1.1) and (1.2)?

1.6 Present status of knowledge

A completely organized body of knowledge concerning one-dimensional stress waves in soil would have these components: (1) systematic data regarding stress-strain-time behavior; (2) a set of theoretical tools to predict wave patterns, given any stress-strain-time relation and any set of initial and boundary conditions; and (3) confirming observations from laboratory and field tests.

Direct observations from tests are scant indeed. There have, of course, been measurements of acceleration vs. time, strain vs. time, and stress vs. time at various depths below surface during nuclear field tests in Nevada. These data have been put to very good use in the protective construction effort to date, but there are many, many questions that simply cannot be asnwered on the basis of these data. For example, consider the question of attenuation of peak stress and peak strain with depth. Such decreases were indeed observed to occur.

On one hand, however, WILSON and SIBLEY (1962) attributed the stress decrease to three-dimensional effects, and used the observed strain attenuation to validate their theory for change in soil compressibility with depth, while on the other hand Paul Weidlinger and his associates used the same results to back up their theory concerning stress attenuation as a result of irreversible straining.(Report to Air Force Special Weapons Center).

To date (1962) there have been almost no satisfactory laboratory tests*, although efforts are underway at numerous laboratories; e.g. see KRIEBEL (1961), THOMPSON (1960), WALSH (1960), and BLOEDOW (1962). The problem of preventing lateral strains without inhibiting axial movements is almost overwhelming, but must somehow be overcome. Failure to consider the side friction effect casts doubt upon some of the results which appear in the listed references. If any dynamic test result is to be convincing, the data must include some direct observation of the magnitude of the axial stress "lost" to the container walls.

Lacking the essential direct observations, we can at best speculate intelligently concerning wave propagation patterns, making use of available stress-strain-time data and available theories. Such an approach can never provide final answers, but considerable guidance can be obtained as to the relative importance of the various phenomena.

1.7 Method of attack

The first step will be to study the one-elastic aspects of soil behavior, so as to give answers to questions (a) through (c) of Section 1.5. For this purpose, the three models of soil behavior shown in Figure 1.5 will be used. No one model by itself represents all aspects of soil

---

*The early tests at M.I.T., described by PARKIN (1961), were not truly one-dimensional. The tests of HEIERLI (1962) were satisfactory only when very loose soils were involved.

behavior; however, the sum total of the three models, if they were to be combined into a single model, does encompass most of the important aspects. In Chapter 3, the available stress-strain-time data will be organized in terms of these models. Then, in Chapter 4, the implications of each model will be examined from the standpoint of wave propagation, and then theory and data will be combined so as to evaluate the possible importance of the effect represented by each model.

REFERENCE

BIOT, M. A., 1956: "Elastic Waves in Porous Solids, I and II," J. Acoustical Soc. Amer., Vol. 28, pp 168-191

BLOWDOE, F. H., 1962: "Radiographic Instrumentation Study," Report by American Machine and Foundry Co. to Air Force Special Weapons Center, SWC-TDR-62-44

COLE, J. D. and HUTH, J. H., 1958: "Elastic Stresses Products in a Half-Plane by Steadily Moving Loads," J. Appl. Mech., Vol. 25

HEIERLI, W., 1962: "Inelastic Wave Propagation in Soil Columns", Proc. ASCE, Vol. 88, No. SM6

KRIEBEL, H. W., 1961: "Feasibility Study of an Experimental Apparatus for Unidimensional Stress Propagation in Soil," Stanford Research Institute Report to Defense Atomic Support Agency, DASA-1266-2

MURPHY, H. L., and others, 1961: "Design of Structures to Resist Nuclear Weapons Effects," ASCE Manual of Engineering Practice No. 42

PARKIN, B. R., 1961, "Impact Waves in Sand: Theory Compared with Experiments on Sand Columns," Proc. ASCE, Vol. 87, No. SM3

SKEMPTON, A. W., and BJERRUM, L., 1957, "A Contribution to the Settlement Analysis of Foundations on Clay," Geotechnique Vol. VII

TAYLOR, D. W., 1948: "The Fundamentals of Soil Mechanics," John Wiley and Sons, Chapter 12

THOMPSON, A. A., 1960: "A Comparison of the Dynamic and the Static Stress-Strain Curve in Sand Under Confined and Unconfined Conditions," Ballistic Research Laboratories, Memo Report No. 1262

TIMOSHENKO, S., 1934: "Theory of Elasticity," United Engineering Trustees, Inc.

WALSH, H. R. J., 1960: "An Experiment on Soils Loaded Dynamically by a Shock Tube," Air Force Special Weapons Center, Technical Note AFSWC-TN-60-39

WILSON, S. D., and SIBLEY, E. A., 1962: "Ground Displacements from Air Blast Loading," Proc. ASCE, Vol. 88, No. SM6

No shear stresses on x, y or z faces

Motions in y and z direction, and hence εy and εz will be zero

Stresses σ_y and σ_z generally will be > 0

Motion in x direction can occur

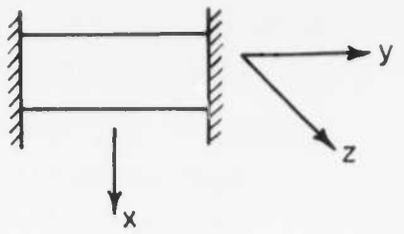

FIGURE 1.1 ONE-DIMENSIONAL STATE OF STRAIN

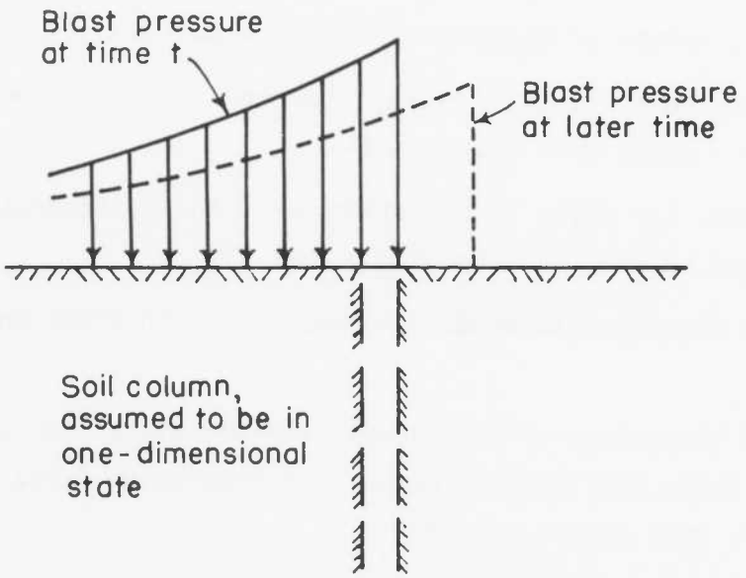

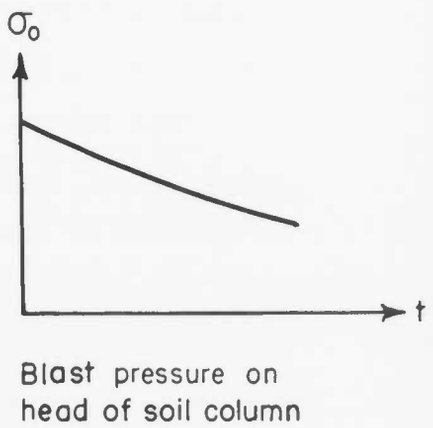

FIGURE 1.2 AIR BLAST LOADING

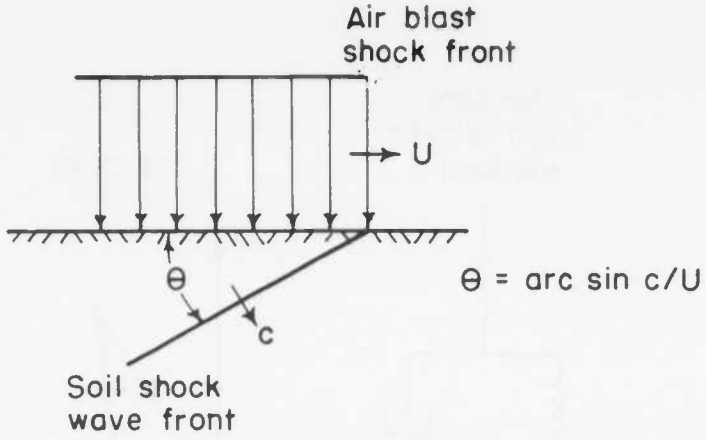

FIGURE 1.3 SUPERSEISMIC CASE

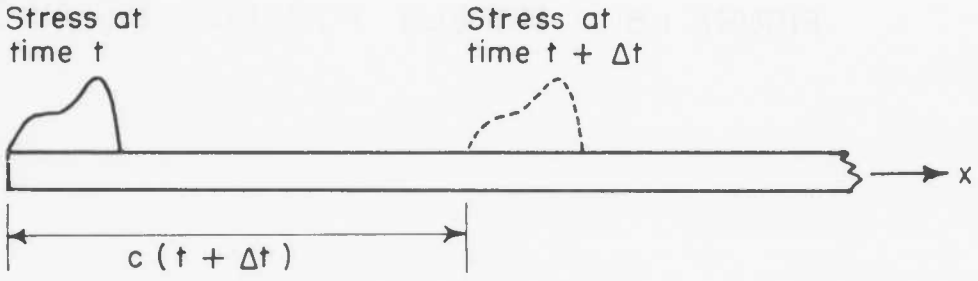

FIGURE 1.4 ELASTIC ONE-DIMENSIONAL WAVE PROPAGATION

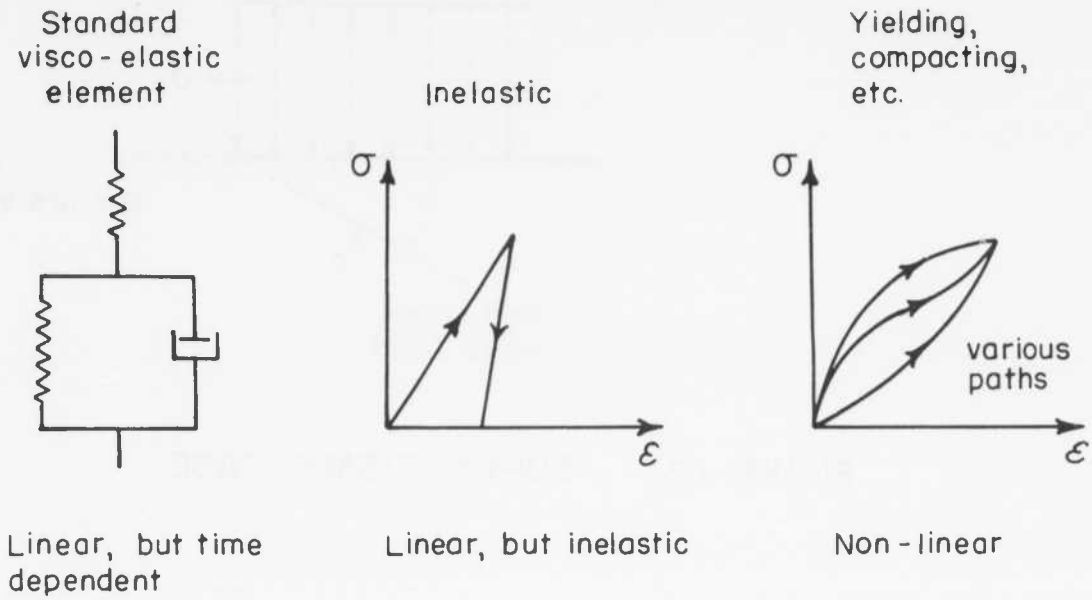

FIGURE 1.5 MODELS FOR SOIL BEHAVIOR

Chapter 2

TEST EQUIPMENT

2.1 History of one-dimensional compression test devices

Devices for one-dimensional compression tests upon soils are commonplace in soil mechanics laboratories. In Europe and in Commonwealth countries, such devices are commonly called oedometers. In the United States, these devices are usually referred to as consolidometers, since their principal use is for evaluating the consolidation characteristics of saturated soils. In this study, we are specifically interested in undrained compression (or at least compression which involves no loss of water) and hence the phenomenon of consolidation is not involved. Hence the term oedometer will be applied to the devices used in this study.

Consolidometers can of course be adapted to permit undrained compression tests. However, careful attention must be given to the deformability of the various parts of the device: the porous stones, loading cap, and sphere used to transmit force to the loading cap. Such deformations are usually of little consequence in ordinary engineering practice, for most consolidation tests involve soils with modulus values less than 1000 lb/in^2. In the present study, we are interested in soils with modulus values of 10,000 lb/in^2 to 100,000 lb/in^2 and even greater. In very early studies (Whitman et al, 1954), ordinary devices proved to be far too deformable for use with such soils. Hence, it became necessary to develop special oedometers.

The first of these special oedometers was described in Report No. 3 of this series, and is shown in Figure 2.1. The significant features are: (1) the stiff, self-contained cell; (2) the membrane covering the soil; (3) loading by means of fluid pressure directly against this membrane; and (4) the strain-measurement system involving a disk in contact with that part of the soil which was unaffected by side friction. This device was the direct forerunner of Oedometer II which has been used for the majority of the work reported in this volume.

2.2 Oedometer I

The device shown in Figure 2.2 was first described in Report No. 4 of this series. The strain-sensing device was placed below the specimen container for two reasons: (1) In order to obtain accurate control of the pressure applied to the soil, it was necessary that the chamber above the soil be free from leaks. Hence the rod to the transducer could not pass out through the top of the cell. (2) An explosive loading arrangement (see section 2.3) was being developed, and in such a system it would not be possible to have the transducer exposed to the blast. The transducer arrangement shown in Figure 2.2 was developed in anticipation of the explosure loading arrangement.

Oedometer I has been employed for cyclic loading tests upon sand, as described in Appendices A and B. More details concerning this apparatus and its use appear in these appendices. Compression test data for a compacted clay have also been obtained using this apparatus, using rise times of about 30 milliseconds: see Report No. 4. For testing remolded specimens, the rod and sleeve through the specimen did not present any major difficulties. However, it proved to be very difficult to achieve satisfactory tests upon specimens of undisturbed soils.

2.3 Tests with explosive loading system

This system has been described in Report No. 7; the essential features appear in Figures 2.3 and 2.4. A rise time of 1 millisecond and load dwell of about 100 milliseconds could be achieved with this arrangement. While satisfactory tests were accomplished upon compacted clay specimens, undisturbed soils could not be tested satisfactorily.

2.4 Oedometer II

Figure 2.5 shows the essential features of this apparatus; Appendix C describes the apparatus in detail. This apparatus was used to obtain the data reported in Appendices D and E and to obtain all data for undisturbed soils. The output of the pressure and displacement trans-

ducers were displayed by a dual-beam oscilloscope. Specimens of sand and of remolded clay, 1.57 inches thick by 4.38 inches in diameter, were formed by compacting the soil directly into the well in the lower part of the apparatus. A rubber membrane was stretched across the top of the specimen, and the specimen was loaded by fluid pressure. When undisturbed soils were tested, the soil was left within the sampling tube, this unit was placed within the well, and the remaining portion of the well was packed with sand. A membrane was stretched over the soil and packing.

Changes in the thickness of the specimen were determined by measuring the movement of an aluminum disk resting on top of the specimen. This disk covered only that portion of the specimen which was assumed to be unaffected by friction between the side of the specimen and its container. Because of this arrangement, it is a reasonable presumption that the vertical stress in the soil under the disk equalled the applied pressure, and that the strain in this region was uniform.

The LVDT (linear variable differential transformer) which sensed motion of the disk was mounted on the upper plate of the apparatus, and any distortion within the apparatus thus caused the measured movement to be greater than the actual change in thickness. With no soil within the oedometer, the relative movement between the LVDT and the center of the bottom of the well was measured to be about 0.00035 inches per 100 lbs/in^2 of pressure change. The following tabulation indicates the error introduced by this "apparatus compressibility" for a soil specimen which is 1 inch thick.

Observed ratio of change in stress to change in unit strain	Ratio corrected for apparatus compressibility
10,000 lbs/in^2	10,400 lbs/in^2
50,000 lbs/in^2	60,500 lbs/in^2
100,000 lbs/in^2	154,000 lbs/in^2
200,000 lbs/in^2	667,000 lbs/in^2

Clearly the error from this source was important if the stress-strain ratio of the soil exceeded 50,000 lbs/in^2.

The pattern of stress application used in this study had the features shown in Figure 2.6. The initial stress simulated the effects of an in situ overburden pressure and served to seat the specimen into the apparatus and the aluminum disk against the specimen. In order to isolate and evaluate any time-dependent phenomena, a flat topped stress-time function was used instead of a stress which decayed immediately after the initial peak. The maximum pressure within the apparatus was limited to 300 lbs/in^2.

Stress was applied to the soil by compressed gas. The chamber immediately above the specimen was filled with water. Thus, only a small volume of air had to flow through the control valves. The throttle valve controlled the rise-time and minimized the overshoot. The overshoot is the amount by which the peak pressure oscillation exceeds the mean pressure in which the effects of the oscillation have been averaged out (see Figure 2.6). Rise-times as short as 2 milliseconds could be achieved, but only at the expense of having considerable overshoot. By using rise-times as long as 30 milliseconds, the overshoot could be eliminated completely. Rise-times of 10 to 20 milliseconds were used for most tests, and the overshoot was generally less than 10%.

Because there was only a limited volume of compressed gas in the nitrogen accumulator, the applied pressure actually reached only 75 per cent to 90 per cent of its final level during the initial rapid rise. As additional compressed air flowed through the reducing valve, the applied pressure crept up to its final level within from 1 to 15 seconds.

During the course of a test, water would leak out through the bushing for the rod to the LVDT. To unload the specimen, the inlet through the accumulator was closed, and leakage then reduced the pressure within the test chamber. Unloading was complete within about 15 seconds. In many of the tests a water accumulator was used such that water could be added to the test chamber when the chamber was pressurized.

From the foregoing remarks, it is clear that a number of compromises

were made so as to "get on" with the test program. The rise-times were longer than would have been desirable. The applied stress actually was not constant following the initial rapid rise of pressure. Short decay times were not achieved during the test program. All of these compromises affected the usefulness of the test data.

Steps to improve the apparatus have been and still are underway. Some of these steps are described in Appendix C.

2.5 Wave propagation during compression test

When stress is applied suddenly to the upper surface of a test specimen, a stress wave starts through the specimen. Successive reflections of the wave will occur at both the top and bottom surfaces of the specimen. Depending upon the rate of stress application and the propagation velocity for the stress wave, stress and strain may well not be uniform over the thickness of the specimen.

The implications of the presence of wave propagation effects are illustrated in Figure 2.7; the curve of measured strain (change in overall thickness divided by thickness) vs. applied stress may be non-linear, even though the true stress-strain curve for the material is linear. In particular, the measured strain appears to lag the measured stress right at the start of the test. The test system thus can make it appear that non-linearities are present even though the material under test is perfectly linear. Such a situation arises because the test system measures stress at the top of the specimen but strain averaged over the thickness of the specimen.

Appendix C contains a numerical analysis of these effects. This analysis leads to the following criterion: If the maximum error in measured strain is to be less than 2% of the maximum measured strain (see Figure 2.7), then:

$$t_L > 25\ L/C$$

where t_L: rise-time of the applied stress

L: thickness of specimen

C: wave propagation velocity through specimen

The results of applying this criterion are shown by the following tabulation, assuming a specimen thickness of one inch.

Modulus lb/in^2	Wave velocity ft/sec	Minimum rise time milliseconds
10,000	650	3.2
30,000	1200	1.7
100,000	2000	1.0

As will be seen subsequently, the criterion was satisfied by the great majority of the tests. At the same time, it is clear that difficulties must be anticipated when one attempts to use rise times of one-millisecond or less.

2.6 Laboratory measurement of seismic wave velocity

The test system described in Reports No. 8 and 14 has been used to measure the ultrasonic wave propagation velocity through the soils included in the one-dimensional compression test program. The essential elements of this system are shown in Figures 2.8 and 2.9. A signal is sent through the specimen 50 times per second, but each signal damps-out completely before the next signal appears. The propagation velocity was computed from the observed time delay between the sent and received signals. It is believed that the propagation velocity so measured corresponds to the seismic velocity for dilatational waves.

REFERENCE

LAWRENCE, F. V., "The Response of Soils to Dynamic Loads: Report 8, Laboratory Measurement of Dilatational Wave Propagation Velocity," Report to U. S. Army Engineer Waterways Experiment Station by M. I. T. Department of Civil Engineering, July 1961.

LAWRENCE, F. V., "The Response of Soils to Dynamic Loads: Report 14, Propagation Velocity of Ultrasonic Waves Through Sand," Report to U. S. Army Engineer Waterways Experiment Station by M. I. T. Department of Civil Engineering, No. R63-8, 1963.

MOORE, P. J., "The Response of Soils to Dynamic Loads: Report 7, Adaptation and Use of the Boynton Device for Rapid One-Dimensional Compression Tests," Report to U. S. Army Engineer Waterways Experiment Station by M. I. T. Department of Civil Engineering, June 1961.

WHITMAN, R. V., et al, 1954: The Behavior of Soils Under Dynamic Loadings, 3: Final Report on Laboratory Studies (AFSWP-118).

"The Response of Soils to Dynamic Loads: Report 3, First Interim Report on Dynamic Soil Tests," Report to U. S. Army Engineer Waterways Experiment Station by M. I. T. Department of Civil Engineering, Oct. 1959.

"The Response of Soils to Dynamic Loads: Report 4, One-Dimensional Compression and Wave Velocity Tests," Report to U. S. Army Engineer Waterways Experiment Station by M. I. T. Department of Civil Engineering, Aug. 1960.

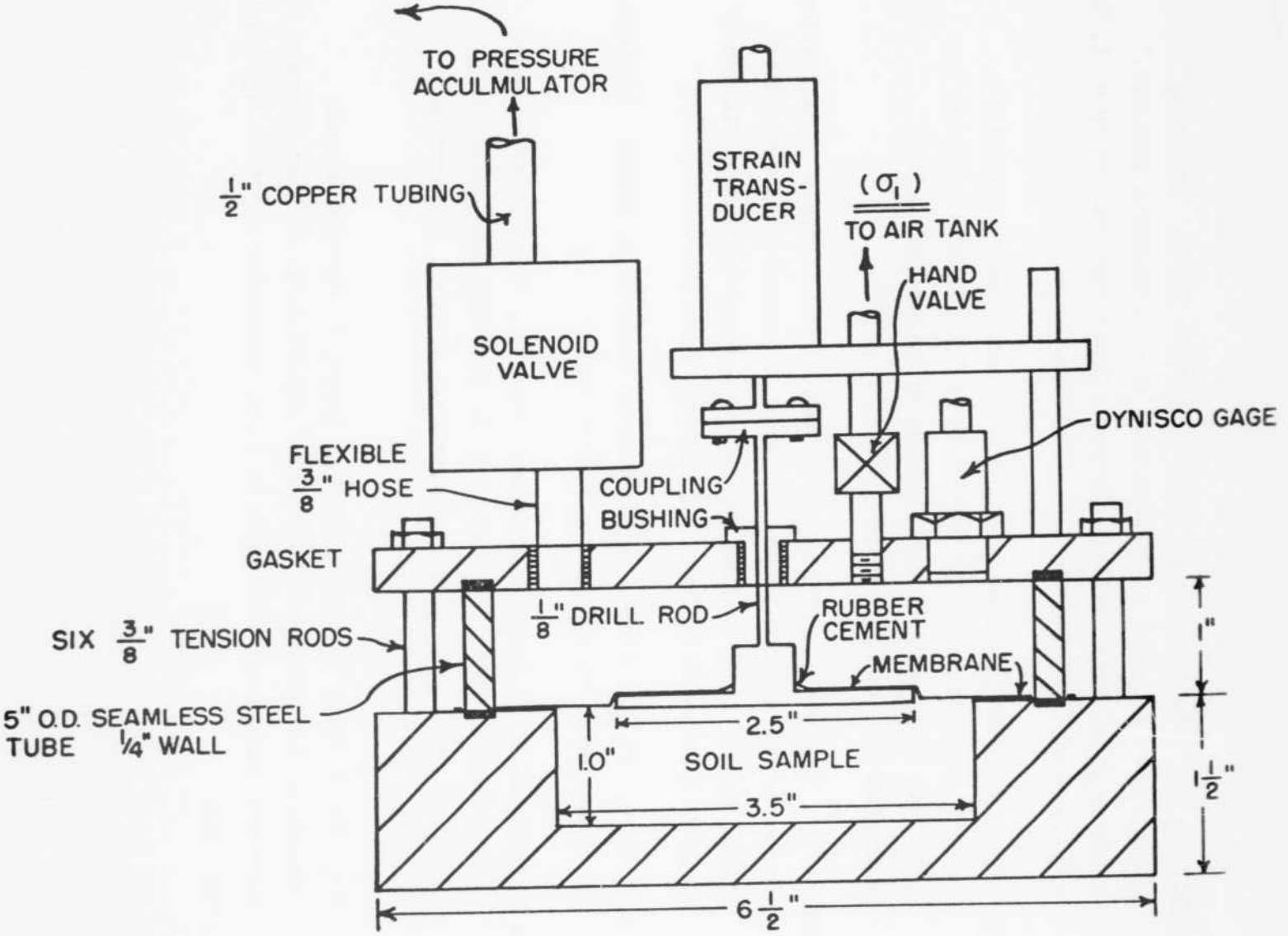

FIGURE 2.1 EARLY ARRANGEMENT FOR RAPID COMPRESSION TESTS

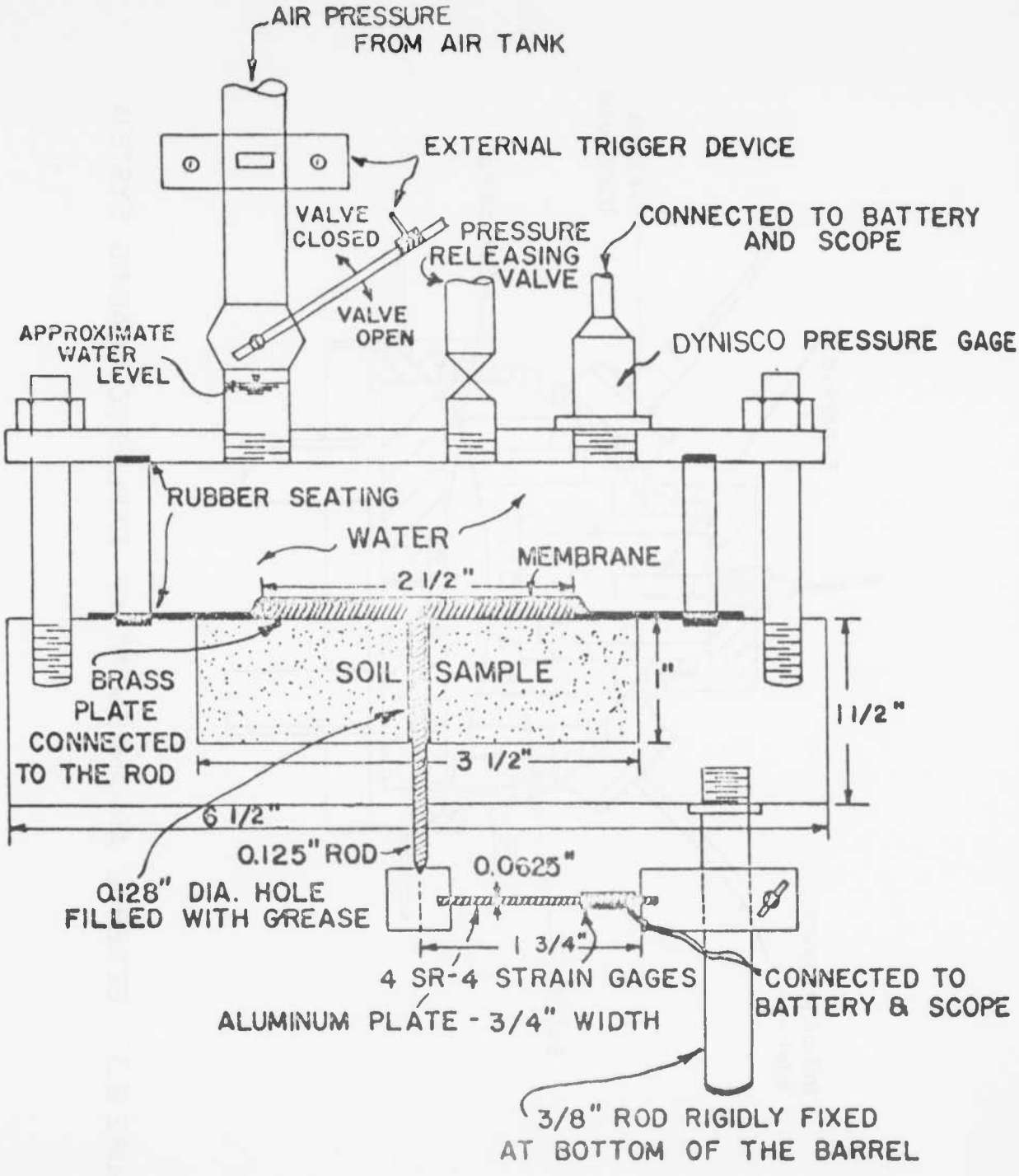

FIGURE 2.2 OEDOMETER I

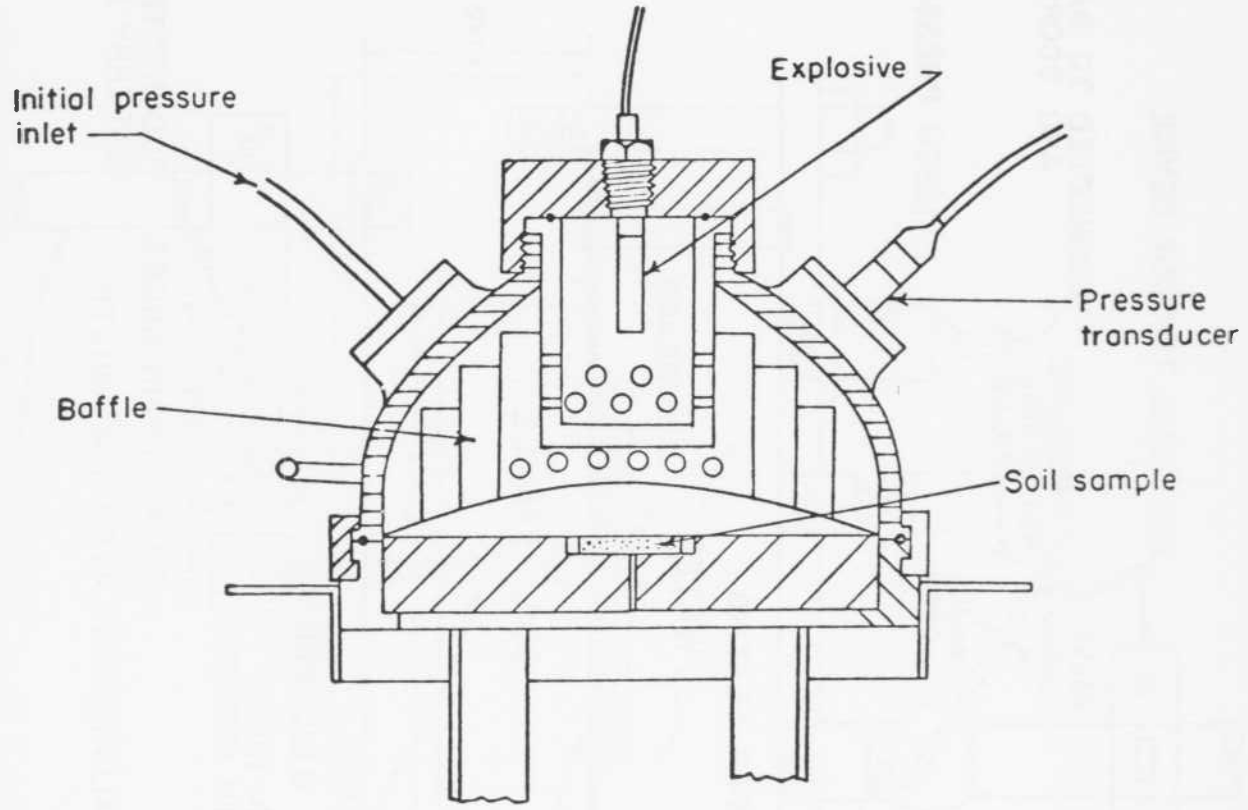

FIGURE 2.3 GENERAL ARRANGEMENT OF EXPLOSIVE LOADING SYSTEM

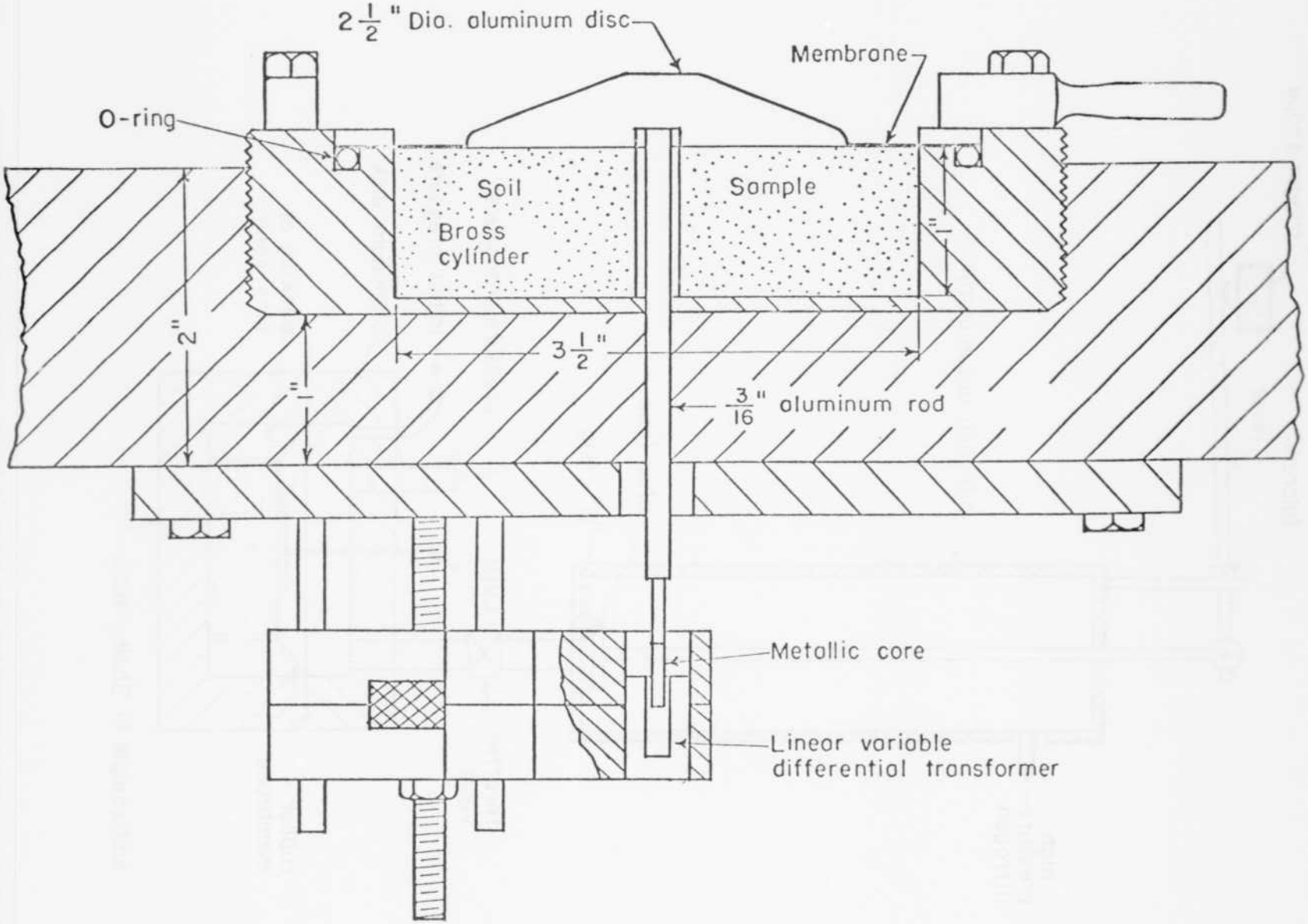

FIGURE 2.4 SPECIMEN CONTAINER AND STRAIN MEASUREMENT SYSTEM - EXPLOSIVE LOADING SYSTEM

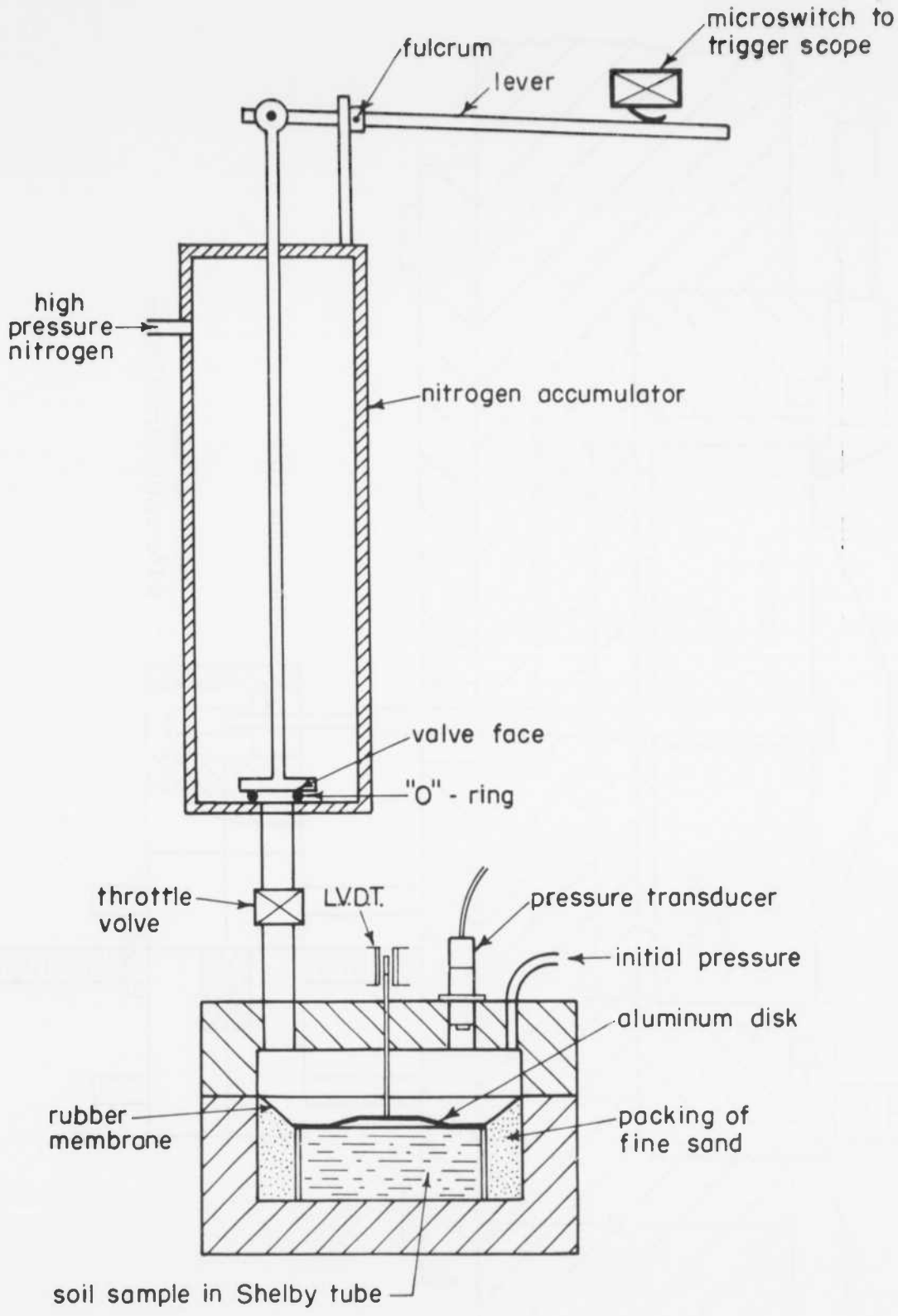

FIGURE 2.5 OEDOMETER II FOR RAPID COMPRESSION TESTS

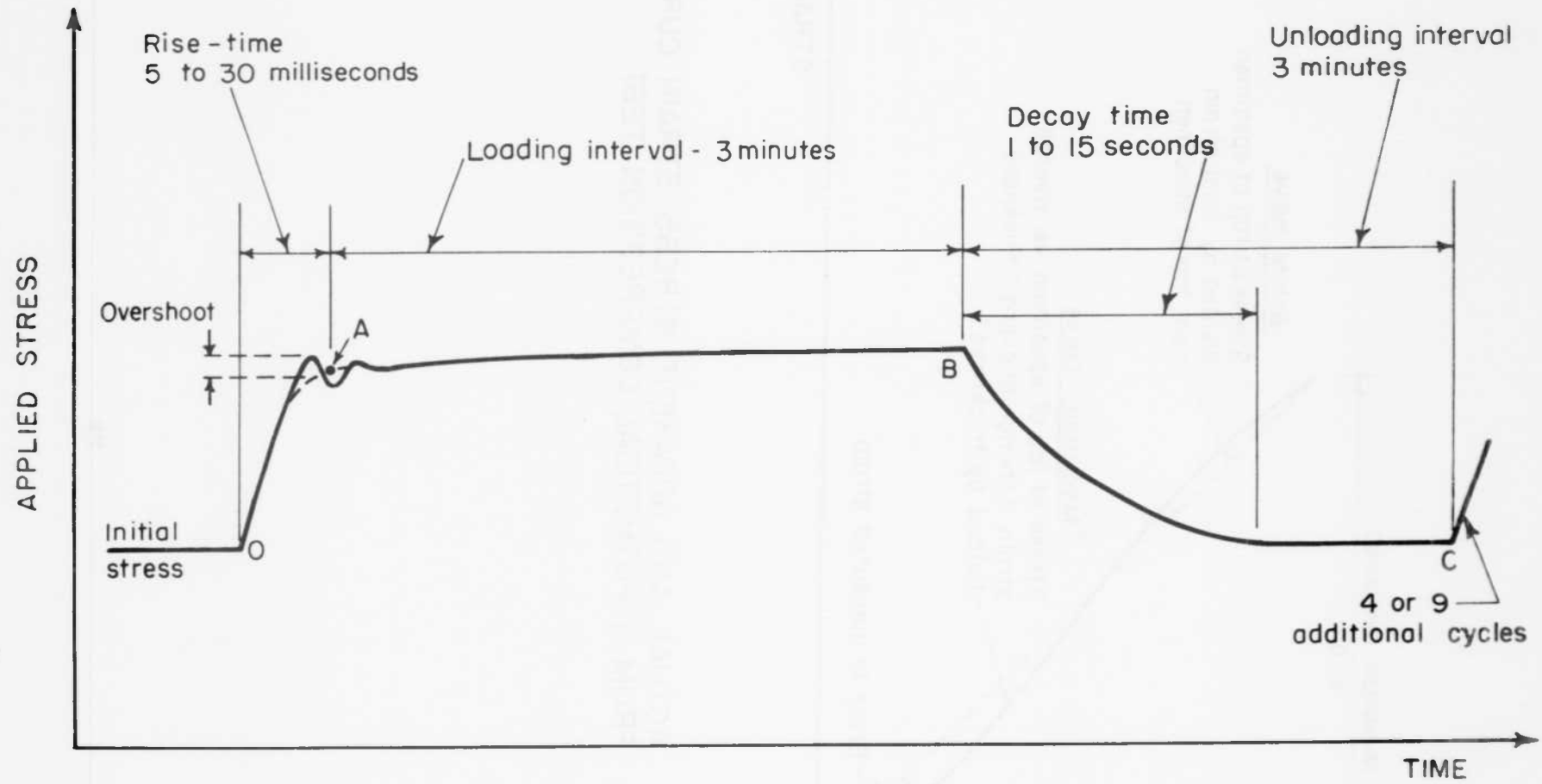

FIGURE 2.6 PATTERN OF APPLIED STRESS

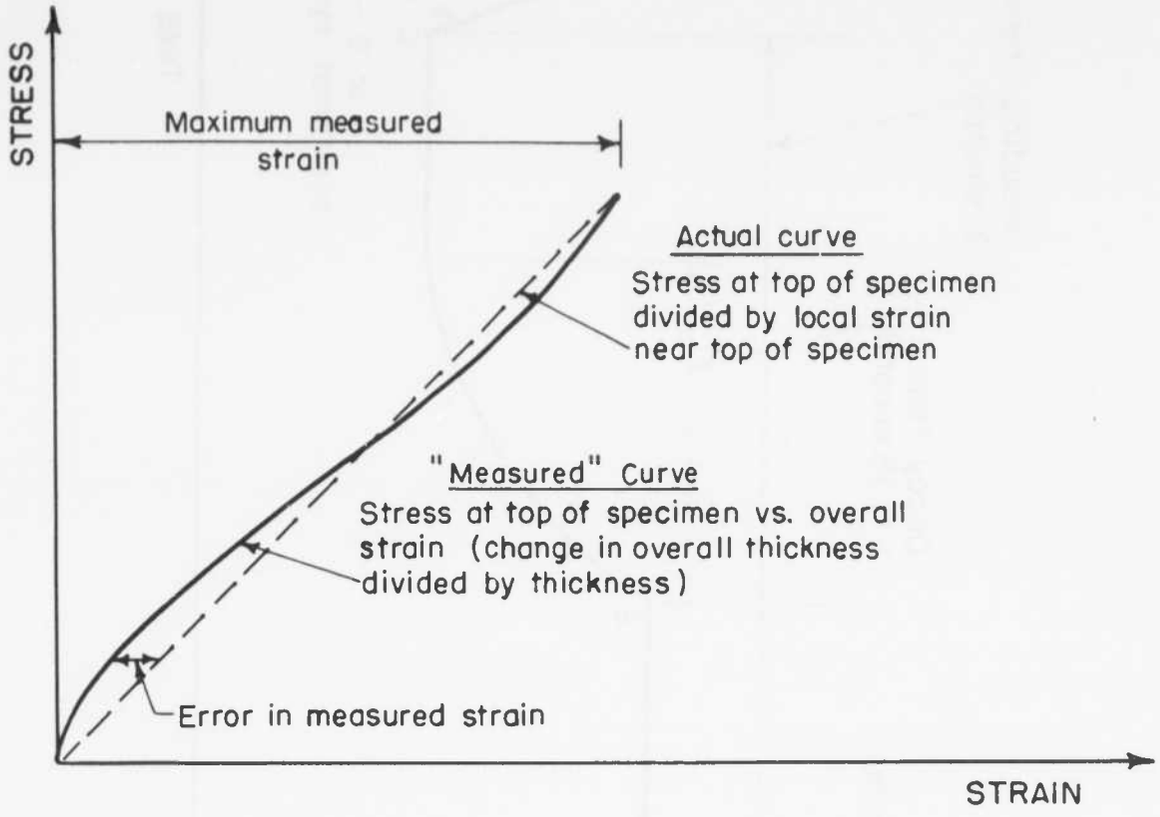

FIGURE 2.7 ACTUAL AND APPARENT STRESS-STRAIN CURVES FROM HYPOTHETICAL COMPRESSION TEST

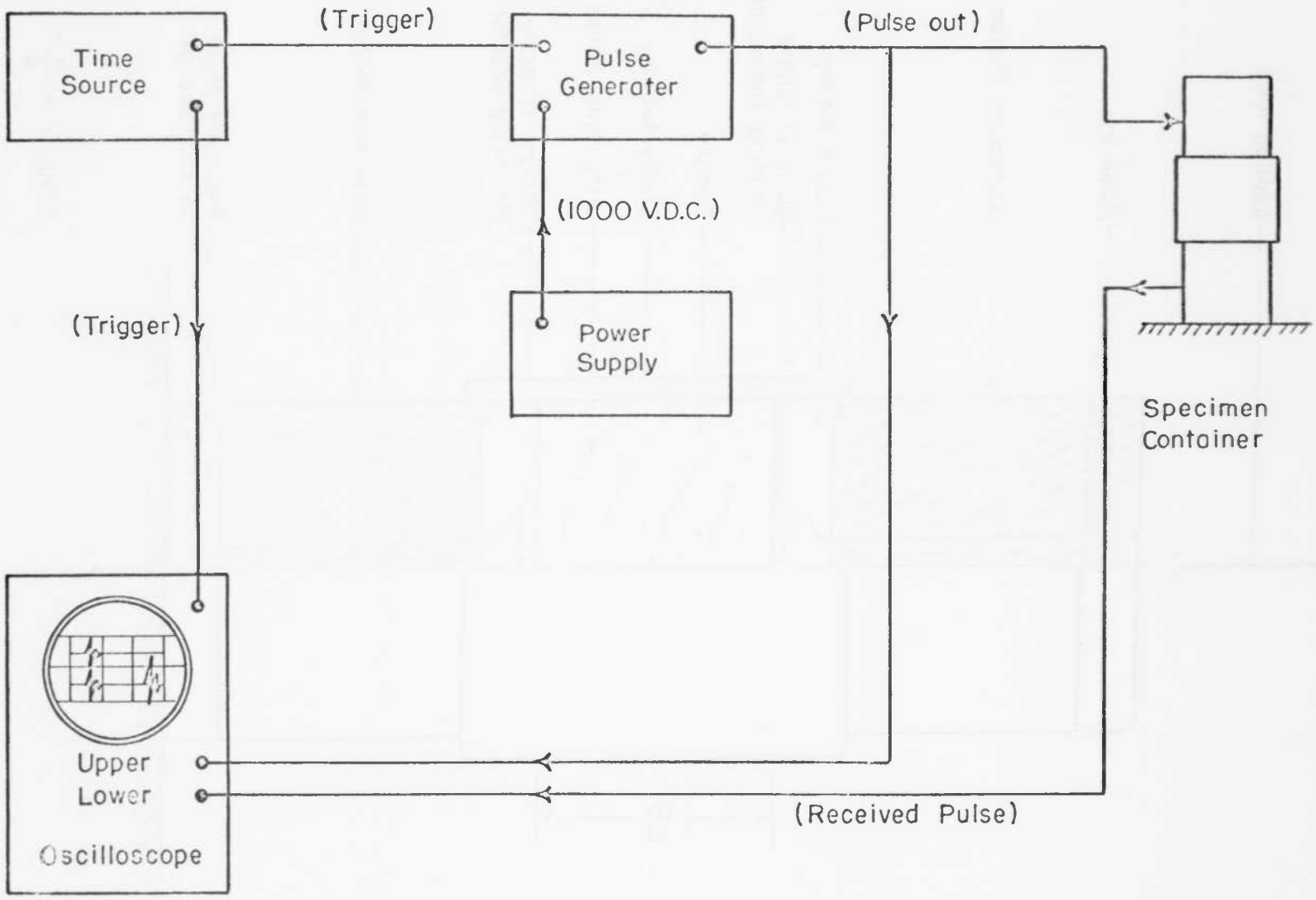

FIGURE 2.8 SCHEMATIC OF ULTRASONIC WAVE PROPAGATION APPARATUS

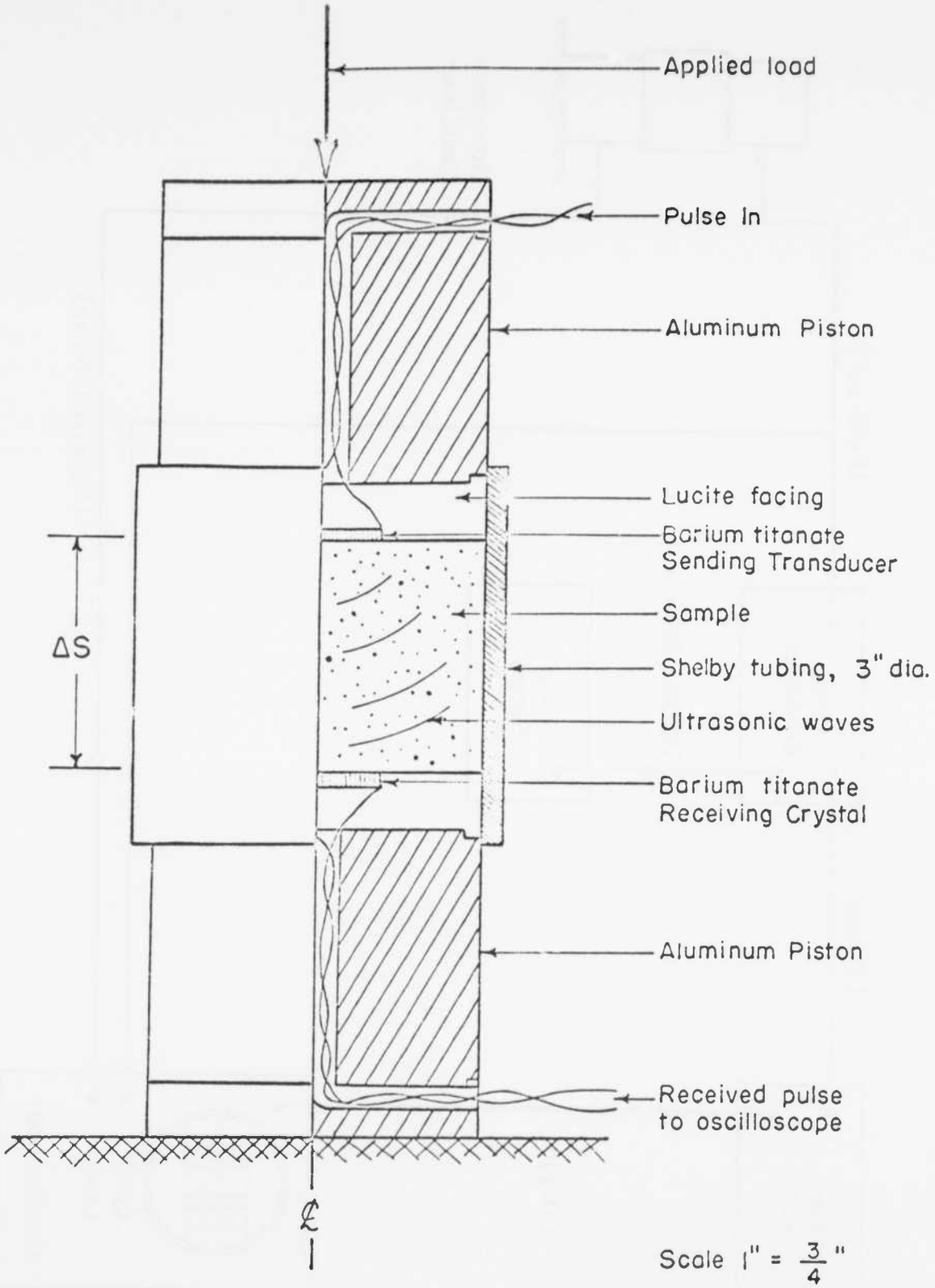

FIGURE 2.9 SPECIMEN CONTAINER FOR ULTRASONIC WAVE PROPAGATION APPARATUS

Chapter 3

TEST RESULTS

3.1 Test program

Table 3.1 lists the soils for which data have been obtained, and indicates the scope of the compression test program for each of these soils. The basic reference for the data regarding each of these soils is shown in Table 3.2.

The two granular materials (E and F) were compacted to essentially 100 per cent relative density. Generally each soil was tested using several different stress increments, and the rise times achieved scattered somewhat from test to test. The soils have been listed in the chronological order of testing. The test procedures were relatively crude for soils A, B and C, and the data for these soils are sparse and of limited reliability. The data are more extensive and more reliable for the soils listed near the bottom of Table 3.1.

A typical set of data for a single cycle of load upon a single specimen consisted of: (1) a photograph of the oscilloscope screen showing applied stress and measured strain as a function of time (see examples in Figure 3.1); (2) a table showing stress and strain at selected times (1/4, 1, 2, 3 minutes) following application of stress, as determined by visual observation of the oscilloscope screen; and (3) a similar table showing stress and strain at selected times following release of stress.

From each photograph it was possible:

(a) To determine the "fast modulus": ratio of stress increment to strain increment at end of initial rapid rise of stress; i.e. at point A, Figure 2.6.

(b) To study the shape of the curve of stress vs. strain during the initial rapid rise of stress. This stress-strain curve could be evaluated with accuracy only when the oscilloscope was set for a fast sweep, so that the interval of rapid pressure rise was stretched out over one-quarter to one-half

Table 3.1

SUMMARY OF TEST PROGRAM

Code	Description of Soil	Dry Unit Weight lb/ft^3	Degree of Saturation %	Initial Stress lb/in^2	Stress Increment lb/in^2	Typical Rise-Time M sec.
A	Fat clay, compacted	90-95	85-90	25 & 10	100 & 50	1 & 30
B	Silt from desert playa, undisturbed	89	60	55	100, 200	10-20
C1	Boulder clay, unweathered, undisturbed	113	82	75	125	2
C2	Boulder clay, weathered, undisturbed	110	94	10	100, 200	2
D1	Weakly cemented sand, unweathered, undisturbed	122	72	135	50, 165	20
D2	Weakly cemented sand, slightly weathered, undisturbed	106	71	40	100, 260	15-20
D3	Weakly cemented sand, weathered, undisturbed	107	83	10	100, 290	20-25
E	Ottawa sand, 20-30 mesh, compacted	110	0	15, 100	10, 100	5-20
F	Glass beads, 40-60 mesh, compacted	97	0	15, 100	10, 100	5-20
G	Weakly cemented clayey silt, undisturbed	80	94	30	30,100,270	25-30

NOTE: All tests were conducted with Oedometer II with the following exceptions:

(i) Oedometer I and the explosive loading system were used for Code A.
(ii) Oedometers II and III and the Oedometer in Figure 1 of Appendix A were used for Code E.

Table 3.2

REFERENCE FOR DETAILED TEST DATA

Code	Description of Soil	Basic Reference
A	Fat clay, compacted	Reports No. 4 and 7, this series
B	Silt from desert playa	"Compressibility of Silt from Frenchmans Flat, Nevada," report by Robert V. Whitman to Shannon and Wilson, August 1961
C	Boulder clay	"Compressibility of Glacial Till from above Water Table: Minot, North Dakota," report by Robert V. Whitman to Shannon and Wilson, September 1961
D	Weakly cemented sand	"Special Compression Studies: Lubbock, Texas," report by Robert V. Whitman to Shannon and Wilson, February, 1962
E	Ottawa sand	Appendices A, B, D, E and F, this report
F	Glass beads	Appendices D, E and F, this report
G	Weakly cemented clayey silt	"Special Compression Studies: Cheyenne, Wyoming," report by Robert V. Whitman to Shannon and Wilson, July 1962

of the screen. Satisfactory stress-strain data were not obtained from all tests.

(c) To evaluate the creep in strain following the initial rapid rise of stress. If the oscilloscope was set for a fast sweep (as was the case in most tests), only the initial rate of creep was observed. In a few tests, use of a slower sweep rate made it possible to observe creep over an interval lasting almost 1/2 second.

From the visual readings of the oscilloscope screen following loading, the following information was determined:

(d) The "slow modulus": ratio of stress increment to strain increment at the end of 3 minutes at the increased stress level.

(e) The development of strain creep over the 3-minute interval following loading.

From the visual readings of the oscilloscope following unloading, this information was calculated.

(f) The "unloading modulus": ratio of stress increment to strain increment at the end of three minutes at the reduced stress level.*

These various types of information are recorded in detail in the basic references. The information bearing upon the various aspects of soil behavior is summarized in the following subsections.

---

*Usually there was little or no change in strain between 1/4 minute and 3 minutes following unloading. Except as noted in Appendix E and in the report for soil G, creep effects immediately following a rapid unloading were not studied in this test program.

Certain information from tests involving slow loadings has also proved to be of use in this study. Appendices A and B to this report present data regarding the modulus and energy loss during a slow repetitive loading (6 cycles per minute). The data have been useful in the evaluation of irreversible and non-linear effects. Appendix F presents data from tri-axial compression tests involving several cycles of slowly applied stressings. These latter data shed light upon the magnitude of the modulus to be expected during one-dimensional compression.

3.2 Magnitude of modulus

Table 3.3 indicates the general order of magnitude of the stress-strain ratio immediately following the initial rapid rise of applied stress; i.e. the fast modulus. The values given in this table have been corrected for the error introduced by apparatus compressibility. As will be discussed in a subsequent section, the magnitude of the stress increment generally did have some effect upon the observed stress-strain ratio; i.e. the stress-strain curves were generally non-linear. Where there was such an effect, the ratios given in Table 3.3 are for the smaller stress increments.

The last column of Table 3.3 gives the modulus M backfigured from the ultrasonic wave propagation velocity measured in the laboratory, using the formula:

$$M = \rho c^2$$

where M: modulus

ρ: mass density

c: wave propagation velocity

For soils B, D2, D3 and G, the velocity measured in the laboratory agreed well with the seismic velocity reported from field investigations. For all other undisturbed specimens, the laboratory value was larger than the field value, by a factor of 1.5 to 2. In these later cases, the soil samples came from points just above a velocity discontinuity. The velocity as measured in the laboratory agreed with the velocity below this discontinuity.

Table 3.3

GENERAL ORDER OF MAGNITUDE OF MODULUS

Code	Description of Soil	Initial Stress lb/in^2	From Compression Tests 1st Loading lb/in^2	From Compression Tests 5th Loading lb/in^2	From Lab. Seismic Wave Velocity lb/in^2
A	Fat clay, compacted		8,000	-	150,000
B	Silt from desert playa		15,000	40,000	180,000
C1	Boulder clay, unweathered		25,000	30,000	1,200,000
C2	Boulder clay, weathered		10,000	20,000	450,000
D1	Sandstone, unweathered		120,000	135,000	650,000
D2	Sandstone, slightly weathered		45,000	55,000	220,000
D3	Sandstone, weathered		20,000	25,000	150,000
E	Ottawa sand	15	35,000	45,000	70,000
		100	120,000	150,000	155,000
F	Glass beads	15	45,000	65,000	80,000
		100	125,000	150,000	175,000
G	Siltstone		15,000	30,000	220,000

As is generally the case, the data in the table reveal a great discrepancy between the modulus as measured in a compression test and as backfigured from ultrasonic or seismic wave propagation velocity. The modulus from the first cycle of loading during a compression test ranged, for the soils studied here, from 1/4 to 1/50 of the modulus backfigured from ultrasonic velocity. In order to minimize the effects of sampling disturbance and testing errors, it is often suggested that the choice of a modulus from a compression test should be based upon the second or subsequent loading. However, even adopting this procedure, the ratio of the types of modulus still ranges from 1/4 to 1/25. The discrepancy between the two types of modulus is of the greatest importance in many practical problems, and will be discussed again later in the report.

It would seem that this discrepancy should disappear if the compression is measured using a very small increment of stress following many previous cycles of stress. Figure 3.2 summarizes the available data for the "slow modulus" of Ottawa sand (see Appendices B, D and E), and compares these results with the modulus backfigured from ultrasonic wave propagation velocity (see Report No. 14). The curves in this figure indicate average values for rather widely scattered data, corrected for effects of apparatus compressibility. Although this figure gives only a tentative picture of general trends, it would appear that, after many cycles of load had been applied, the slow modulus during compression did indeed agree (within the uncertainty of the data) with the modulus backfigured from the ultrasonic wave propagation velocity. From the available data for "fast modulus", there is a preliminary indication that agreement is reached after a relatively small number of cycles of loading.

The measured and backfigured modulus should also agree for a saturated soil.

In rapid compression tests upon a saturated soil (not included in Tables I and II), the observed stress-strain ratios were reasonably consistent with those expected for water, once a correction was made for apparatus compressibility and several cycles of load used to remove

seating errors.*

Thus, the two methods for determining modulus did agree in those cases where agreement would be most expected. These observations indicate the creditability of the data obtained from the compression tests.

3.3 Data regarding time dependency

Data regarding time-dependent effects are most complete in the case of the weakly cemented clayey silt (Soil G). The range of these data are represented by the bands in Figures 3.3 and 3.4. The ordinate of these figures expresses the following ratio:

$$\frac{\Delta\varepsilon \text{ at any time divided by } \Delta\sigma \text{ at that time}}{\Delta\varepsilon \text{ at Point A of Fig. 2.6 divided by } \Delta\sigma \text{ at Pt. A.}}$$

where $\Delta\sigma$ and $\Delta\varepsilon$ are measured with regard to the stress and strain at the beginning of the loading cycle. Use of this normalization scheme was necessary since the stress did not remain constant following the initial rapid rise of stress. Figure 3.3 shows that some creep occurred quite rapidly, but Figure 3.4 emphasizes that creep continued to occur at a slow rate for a long time. There was considerable scattering of the results, primarily because of the difficulties involved in abstracting the data from the photographs (the same statement applied to the data for the other soils, also).

Figure 3.5 shows the creep at early times for tests upon Ottawa sand. The curves represent the average results from a number of tests. In substantially all tests, creep was complete by 15 seconds, and the normalized strain/stress ratio was only slightly more at 15 seconds than it was at 180 milliseconds. Tests upon the glass beads showed no creep over the first 40 milliseconds, and only a slight amount of creep over longer time intervals.

---

*These data are in "Evaluation of Constrained Modulus of Glacial Till from Vicinity of Minot, North Dakota," report by Robert V. Whitman to the Ralph M. Parsons Co., June 1961.

The data regarding creep are much less complete for the remaining soils. Typically it was possible to determine the initial rate of creep during the first 25, 50 or 100 milliseconds after the start of loading and the total accumulation of creep over a period of several minutes. However, the in-between history of strain was unknown. Figure 3.6 shows the initial creep rates; the total accumulation of creep is indicated in Table 3.4. There was only one valid test for Soil B; this test would suggest that the early creep for this soil was much like that for Soil G. No early creep could be detected in the case of the unweathered sandstone (Soil D1).

Figure 3.7 shows the response of the three-parameter visco-elastic model to an ideal step-stress of magnitude $\Delta\sigma_s$. The strain is given by the equation:

$$\Delta\varepsilon = \frac{\Delta\sigma_s}{Mo}\left[1 + \frac{Mo}{M_1}\left(1 - e^{-\nu u\ M_1 t}\right)\right]$$

Comparing Figures 3.3 and 3.4 with Figure 3.7, it is evident that the simple three-parameter model does not provide a complete analogy to the creep behavior of the soil. That is to say, a more complete model is needed in order to represent both the early and long-time creep effects. However, if attention is focused upon the behavior within the first second of loading, then the model does provide a reasonable analogy. Since the stresses caused by an explosion do substantially disappear within one second, it seems proper to ignore the long term creep effects. (Some of the long term creep of undisturbed soils may have been the result of consolidation, since there was no positive prevention against the loss of water from the specimen to the void spaces of the sand packing.)

As will be seen in section 4.1, values of the parameters m^2 and $1/\nu uMo$ are needed for application of the wave propagation theory. The parameter $1/\nu uMo$, the so-called visco-elastic time constant, is related to the initial slope of the strain-time diagram. For example, $1/\nu uMo$ for the weathered sandstone is given by 25 milliseconds / 0.1 = 250 milliseconds (compare Figure 3.7 with last diagram of Figure 3.6). For our purposes, the modulus

Table 3.4

TOTAL ACCUMULATION OF CREEP - VARIOUS SOILS

Code	Description of Soil	Ratio $\frac{\text{(Strain} \div \text{Stress) at 3 min.}}{\text{(Strain} \div \text{Stress) at Point A}}$ 1st Loading	5th Loading
A	Compacted fat clay	~2.0	-
B	Silt from desert playa	1.3	1.3
C1	Boulder clay, unweathered	1.7	1.6
C2	Boulder clay, weathered	1.3	1.4
D1	Sandstone, unweathered	2.0	1.4
D2	Sandstone, slightly weathered	2.1	1.7
D3	Sandstone, weathered	1.7	1.7
E	Ottawa sand	1.4	1.2
F	Glass beads	1.3	1.2
G	Siltstone	1.4	1.2

ratio, m^2, is related to the total strain accumulated over the first second. In the case of the compacted fat clay, for example, $1/m^2 = 0.6$ and hence $m^2 \approx 1.5$ (compare Figure 3.7 with first diagram of Figure 3.6). Since the strain at the end of one second was not recorded for all of the soils tested, the data in Table 3.4 have been used to evaluate m^2 for certain soils. Values of m^2 based upon Table 3.4 presumably are too small.

Table 3.5 lists values of these two parameters for the various soils, based upon the "average" curves in Figures 3.3, 3.5 and 3.6. The slope of the curves at Point A was used to determine $1/\mu M_o$. Despite the wide scattering in the data, and the fact that the rise-times used in the tests were sometimes as long as 30 milliseconds, it is felt that the data in Table 3.5 indicate the approximate range of values for the parameters.

3.4 Data regarding irreversibility

If the stress-strain law is as in Figure 3.8, the parameter $r = M_o/M_1$ controls the wave propagation patterns. The parameter r, which is a means for expressing irreversibility, is also equal to the ratio of recovered strain to maximum strain, and to the ratio of energy recovered to energy input for one complete cycle of loading and unloading.

Table 3.6 lists values for the recovery ratio r, based upon the strain accumulated during the entire interval of loading (Point O to Point B, Figure 2.6) and the strain recovered during the slow unloading (Point B to Point C). Presumably the recovery ratio would be even larger as the result of a rapid loading and unloading.

For several reasons, the in situ recovery ratio of a natural soil is probably greater than the ratio measured during the first cycle of loading upon an undisturbed sample of this soil: expansion of the soil during sampling, poor seating within the test apparatus, etc.

It is possible for energy to be lost during a cycle of loading and unloading even though there is complete recovery of strain during the cycle. Figure 3.9 shows hysteresis loops obtained for dense Ottawa sand after many cycles of loading at about 6 cycles per minute (see Appendix A).

Table 3.5

PARAMETERS FOR VISCOELASTIC MODEL

Code	Description of Soil	$1/\mu_{Mo}$ milliseconds	m^2 From $\Delta\varepsilon$ at 1 sec.	m^2 From $\Delta\varepsilon$ at 3 min.
A	Fat clay, compacted	80-400	1.5	-
B	Silt from desert playa	500	-	3
C1	Boulder clay, unweathered	250	-	1.4
C2	Boulder clay, weathered	350	-	3
D1	Sandstone, unweathered	Very large	-	-
D2	Sandstone, slightly weathered	600	-	0.9
D3	Sandstone, weathered	250	-	1.4
E	Ottawa sand	50-175	5-16	
F	Glass beads	Very large	-	-
G	Siltstone	500	7	-

Table 3.6

DATA REGARDING RECOVERY RATIO

Code	Description of Soil	Average Recovery Ratio		
		1st Loading	2nd Loading	5th Loading
B	Silt from desert playa	-		0.70
C1	Boulder clay, unweathered	0.30		1.00
C2	Bounder clay, weathered	0.45		0.70
D1	Sandstone, unweathered	0.55		0.90
D2	Sandstone, slightly weathered	0.55		0.80
D3	Sandstone, weathered	0.75		0.90
E	Ottawa sand	0.57	0.87	0.98
F	Glass beads	0.63	0.92	0.94
G	Siltstone	0.46		0.95

Appendices A and B contain data regarding the energy loss associated with such hysteresis loops. The data contain some inconsistencies and are affected somewhat by experimental errors. However, as long as the initial stress level exceeded some small value such as 5 lbs/in^2, it can be said that the ratio of energy recovered to energy input was about 0.90 or greater. The energy loss associated with a stable hysteresis loop must be added to the energy loss associated with incomplete recovery of strain, and the value of r selected for analysis purposes should reflect both of these phenomena.

Loose sands and cohesive soils of low density exhibit small recovery ratios if their degree of saturation is low. Values as low as 0.05 have been observed for such soils. However, for the soil deposits usually involved in the type of protective construction problem considered in this paper, the writer believes that 0.50 is a lower limit for the recovery ratio, and that typical values are 0.80 or greater.

3.5 Data regarding non-linearity

The shape of the loading branch of the stress-strain curve was observed from the tests upon Soils E, F and G. Some results are also available from tests upon Soils D1, D2 and D3, but these results are relatively crude.

The results for Ottawa sand (see Appendix E) are shown in Figure 3.10. Each of the curves in this figure were obtained by averaging the results of from 5 to 10 tests. The curves in the upper part of the figure came from tests using a stress increment of 100 or 200 lbs/in^2. Stress increments of 5, 10 and 20 lbs/in^2 were used to obtain the curves in the lower part of the figure. The curves in the upper part represent results during the second and subsequent loadings; results from first loadings scattered considerably, but lay somewhat to the right of the curves shown. For small stress increments (the lower part of the figure) the results were the same for first and subsequent loadings.

For very small stress changes, the stress-strain curves for Ottawa sand are concave toward the strain axis. The initial downward concavity becomes more marked as the initial stress increases. As the stress increment

is increased further, the curves become straight or concave toward the stress axis. Figures 3.11 and 3.12 further illustrate the effect of the magnitude of the stress increment.

This same pattern of behavior was also observed during tests upon the glass beads and upon weakly cemented silty clay. When small stress increments were used, the stress-strain curves tended to be concave toward the strain axis. The direction of the concavity reversed as the stress increment was increased. The same general patterns appeared in the relatively crude results for the weakly cemented sandstone and for the glass beads. Wilson and Sibley (1962) suggest that silt from a desery playa behaves in this same way, and Heierli (1962) shows similar results for loose granular soils.

From these various observations, the stress-strain curve for soils is as shown in Figure 3.13, at least when the soils are loaded rapidly. For small stress increments, the strains presumably result from deformations of the mineral particles at the points of contact. As the stress is increased further, the shear resistance presumably is exceeded at contact points and the particles slide relative to one another. This behavior would explain the discrepancy between the modulus as measured in compression tests (which typically employ large stress increments) and as backfigured from seismic velocity measurements (which inherently involve small stress increments).

These preliminary findings concerning the shape of the stress-strain curve are one of the most important results of the research to date. It is, of course, very difficult to get accurate data using small stress increments. More and very careful tests are underway to confirm this pattern of behavior, to establish accurate numerical values for the initial tangent modulus, and to ascertain the effect of rise-time upon the shape of the stress-strain curve.

REFERENCES

HEIERLI, W., "Inelastic Wave Propagation in Soil Columns," Proc. ASCE, Vol. 88, No. SM6, Dec. 1962.

LAWRENCE, F. V., "The Response of Soils to Dynamic Loads: Report 14, Propagation Velocity of Ultrasonic Waves Through Sand," Report to U. S. Army Engineer Waterways Experiment Station by M. I. T. Department of Civil Engineering, No. R63-8, 1963.

WILSON, S. D. and SIBLEY, E. A., "Ground Displacements from Air Blast Loading," Proc. ASCE, Vol. 88, No. SM6, Dec. 1962.

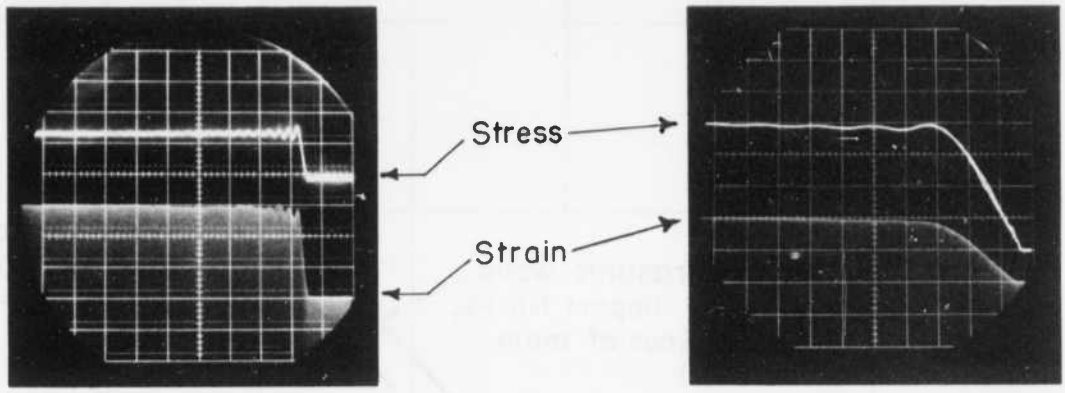

Soil E
20 msec / grid space
sweep rate

Soil G
5 msec / grid space
sweep rate

FIGURE 3.1 TYPICAL OSCILLOSCOPE PHOTOGRAPHS FROM COMPRESSION TESTS

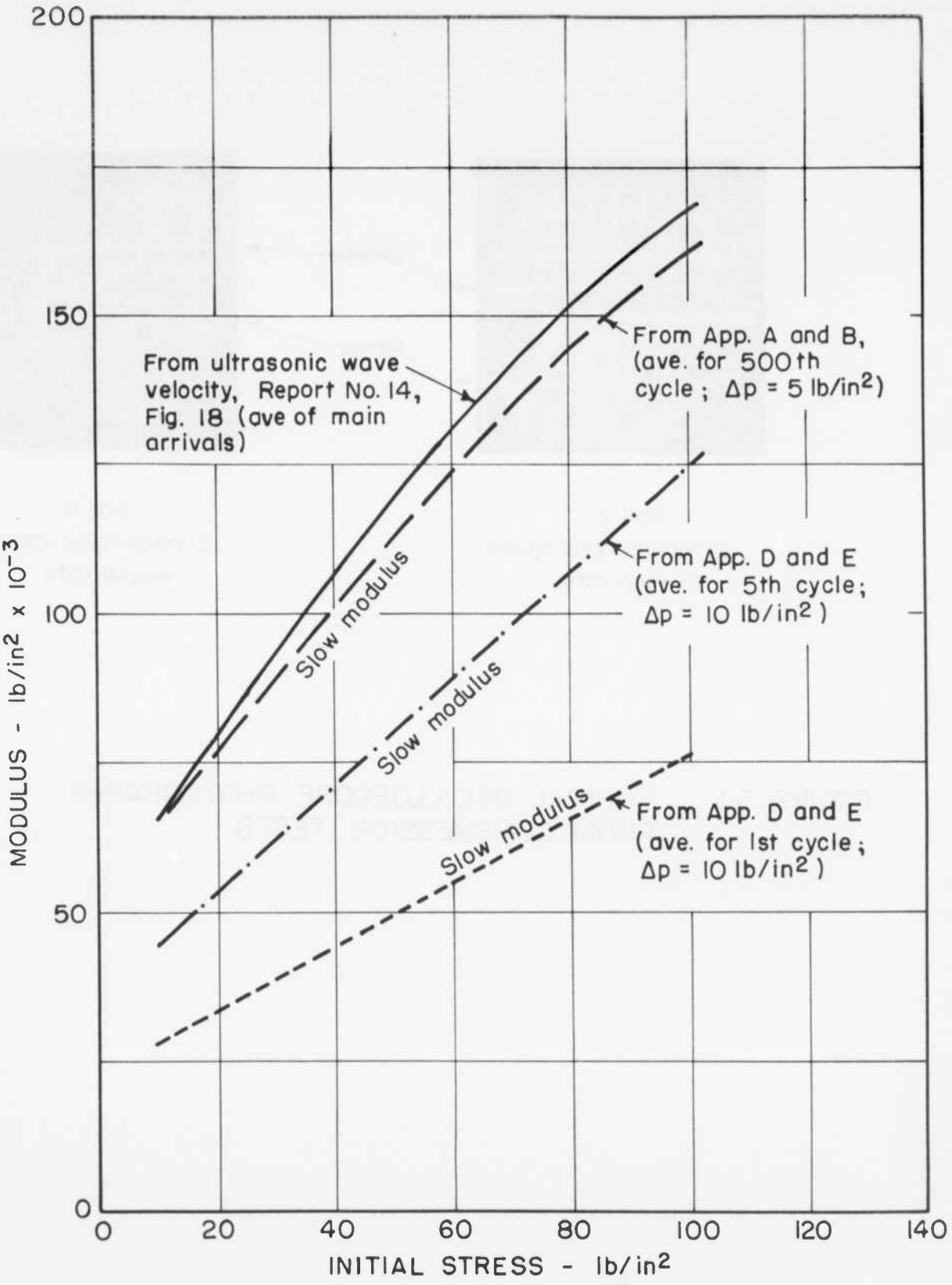

FIGURE 3.2 SUMMARY OF DATA FOR MODULUS OF OTTAWA SAND

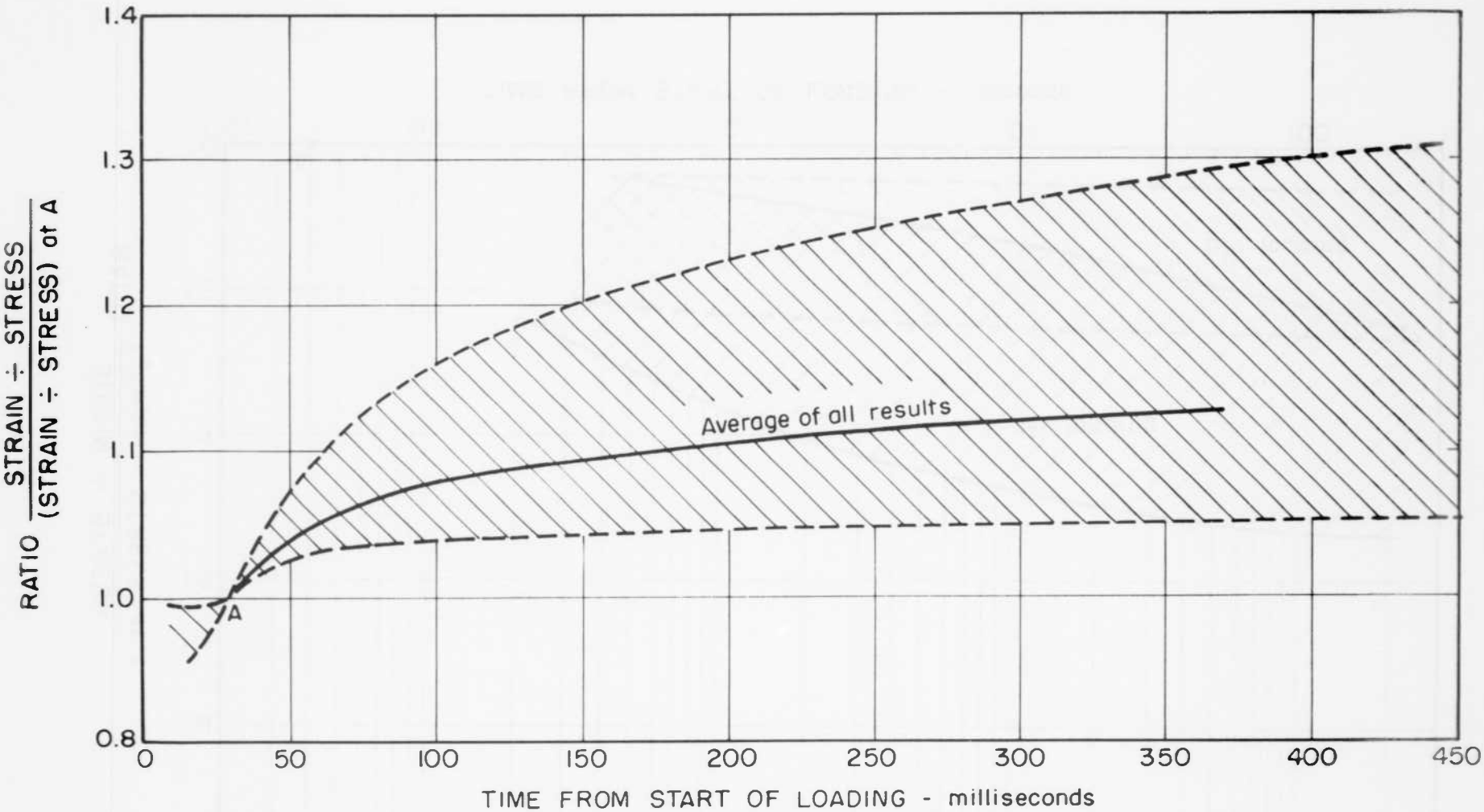

FIGURE 3.3 CREEP AT EARLY TIME - CEMENTED SILTY CLAY

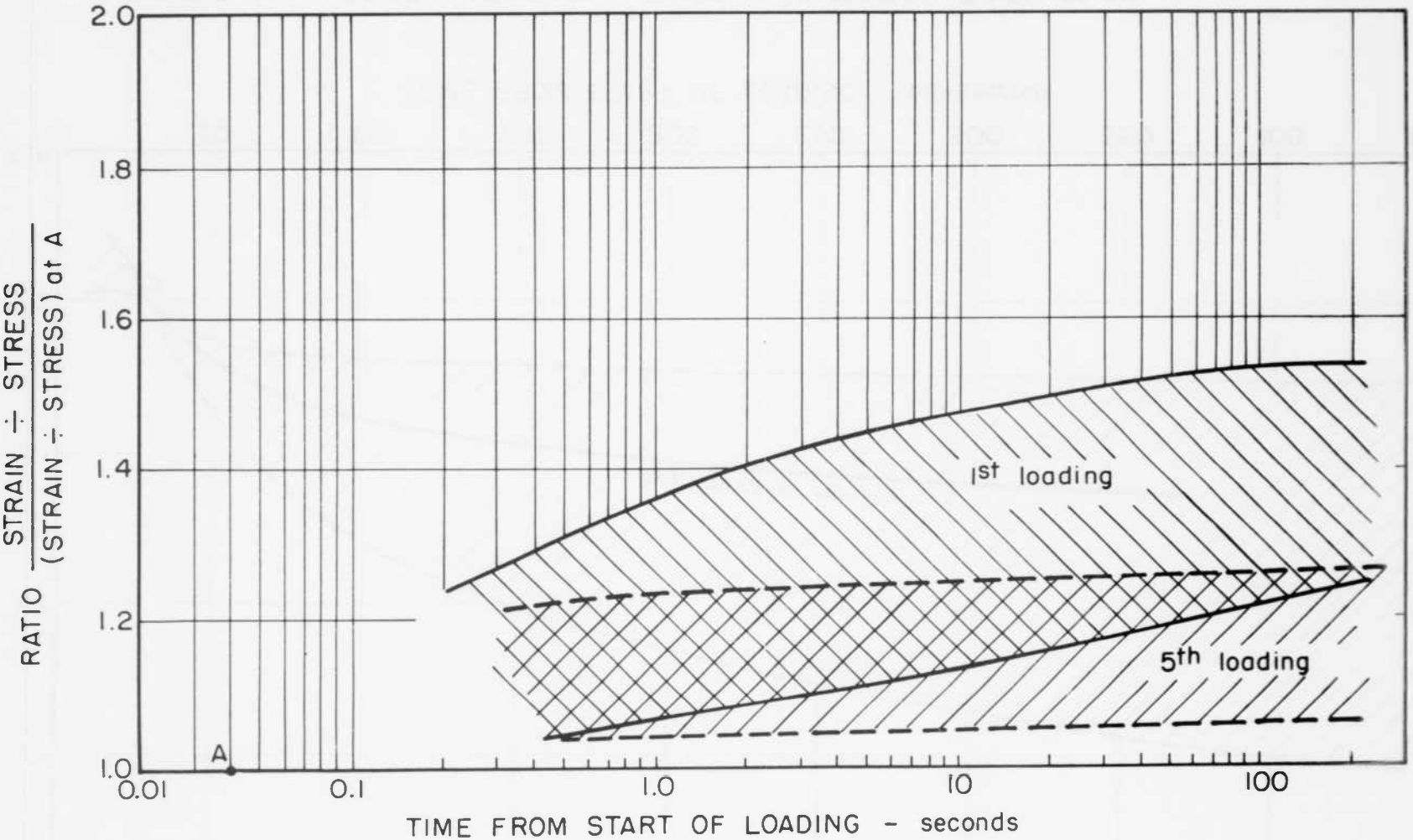

FIGURE 3.4 CREEP AT LATE TIMES - CEMENTED SILTY CLAY

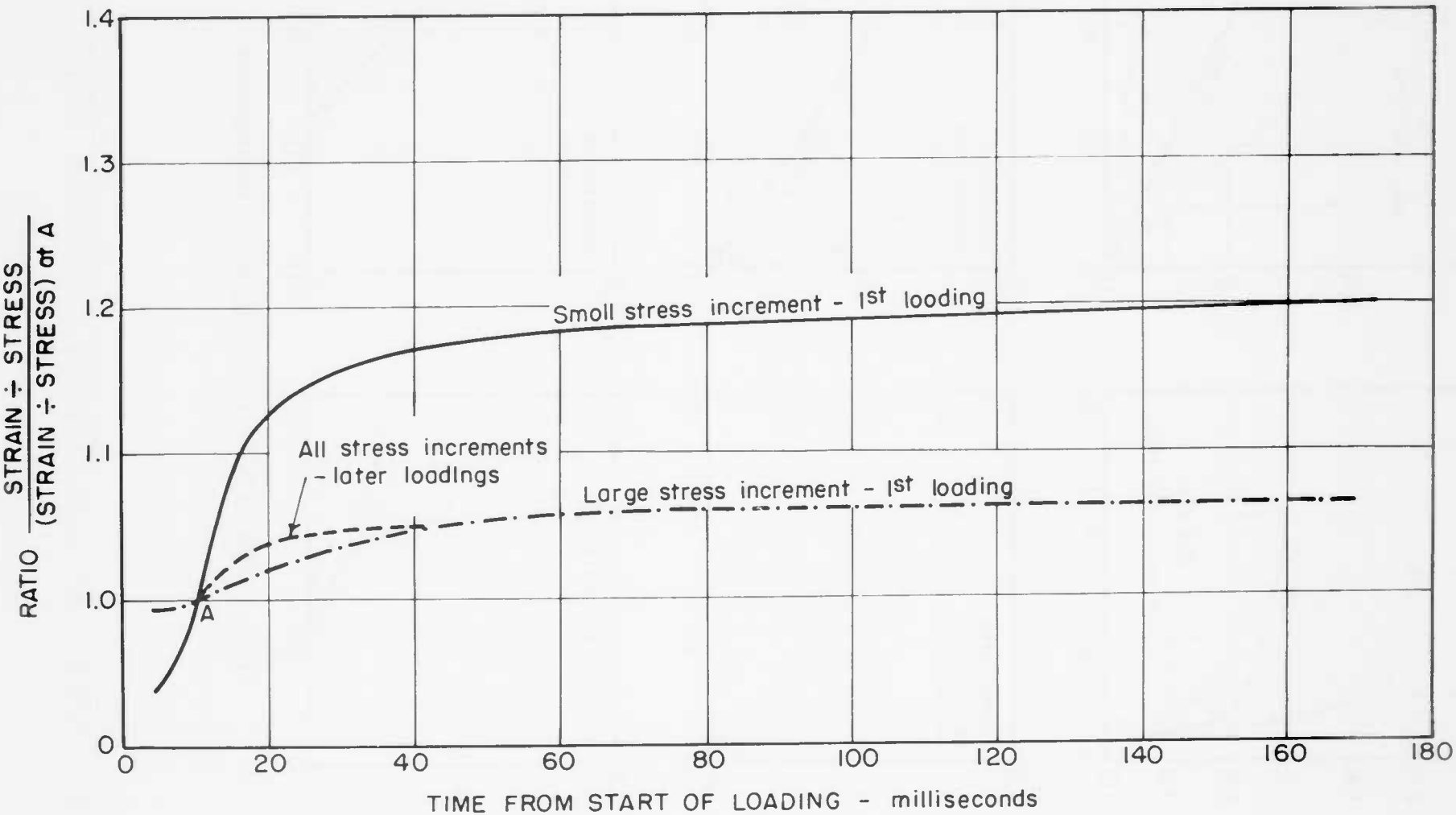

FIGURE 3.5 CREEP AT EARLY TIME - OTTAWA SAND

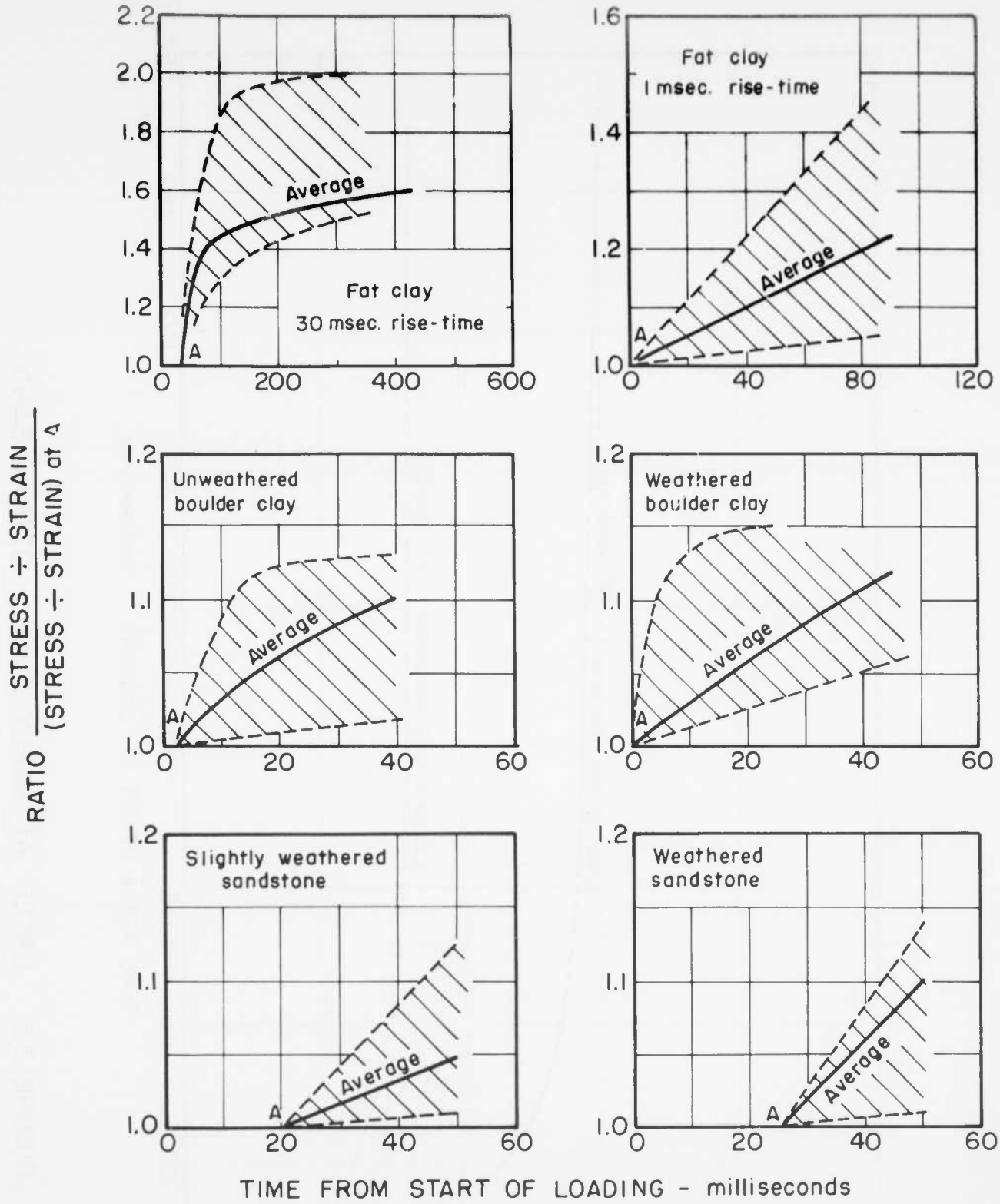

FIGURE 3.6 CREEP AT EARLY TIMES - SEVERAL SOILS

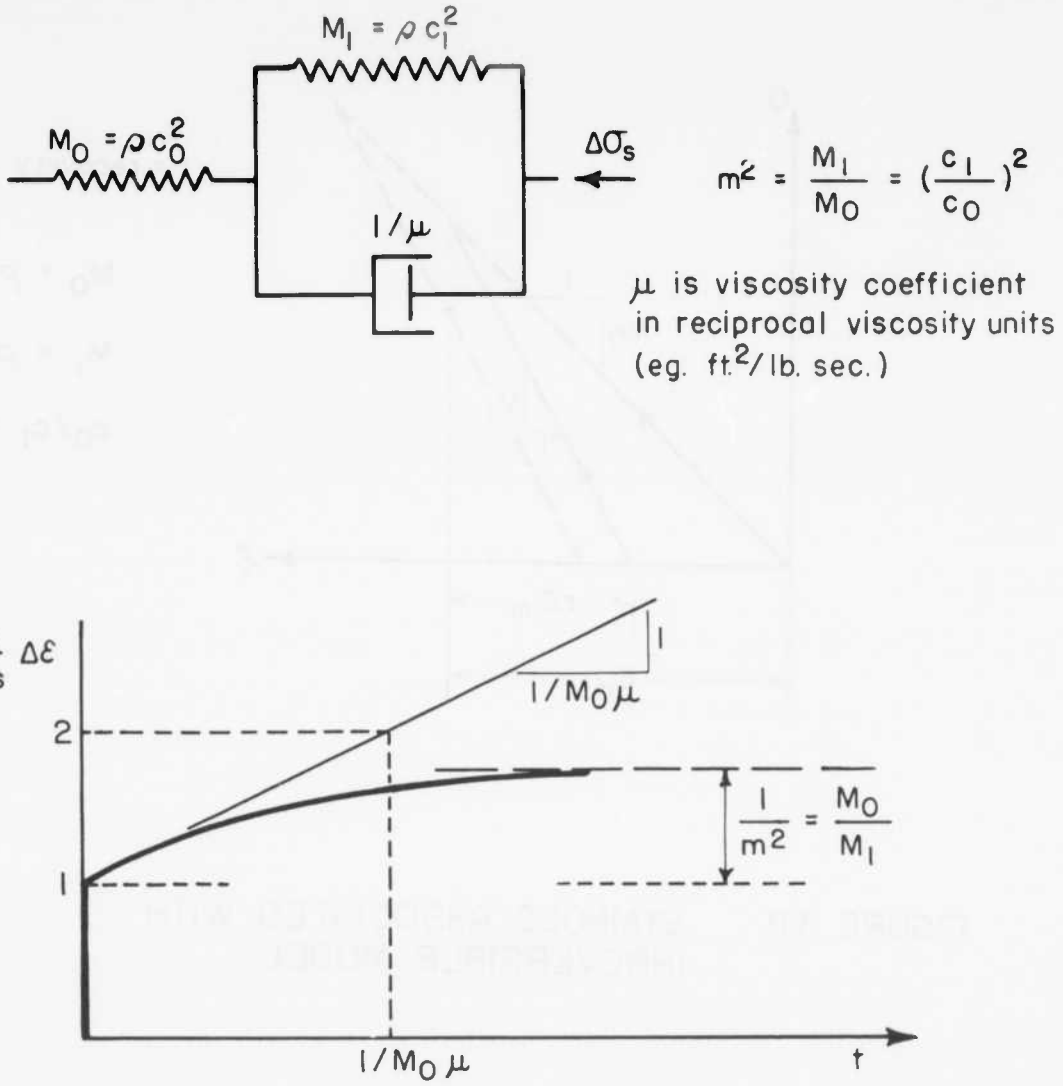

FIGURE 3.7 RESPONSE OF VISCOELASTIC MODEL TO STEP LOAD

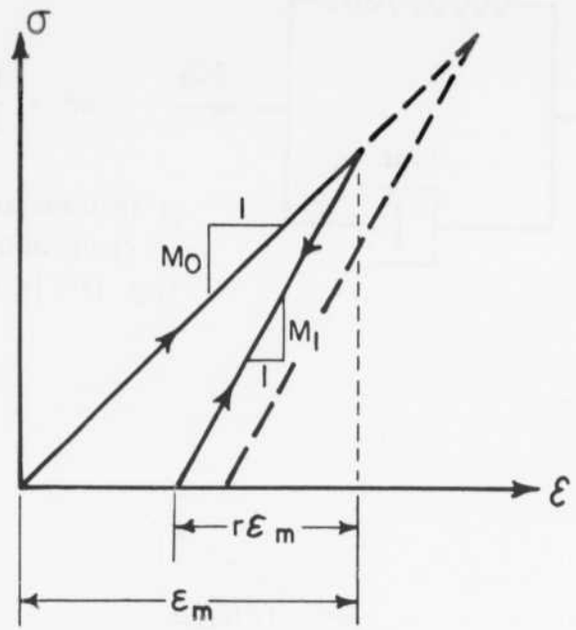

$$r = \text{recovery ratio} = \frac{M_0}{M_1}$$

$$M_0 = \rho c_0^2$$

$$M_1 = \rho c_1^2$$

$$c_0 / c_1 = \sqrt{r}$$

FIGURE 3.8 SYMBOLS ASSOCIATED WITH IRREVERSIBLE MODEL

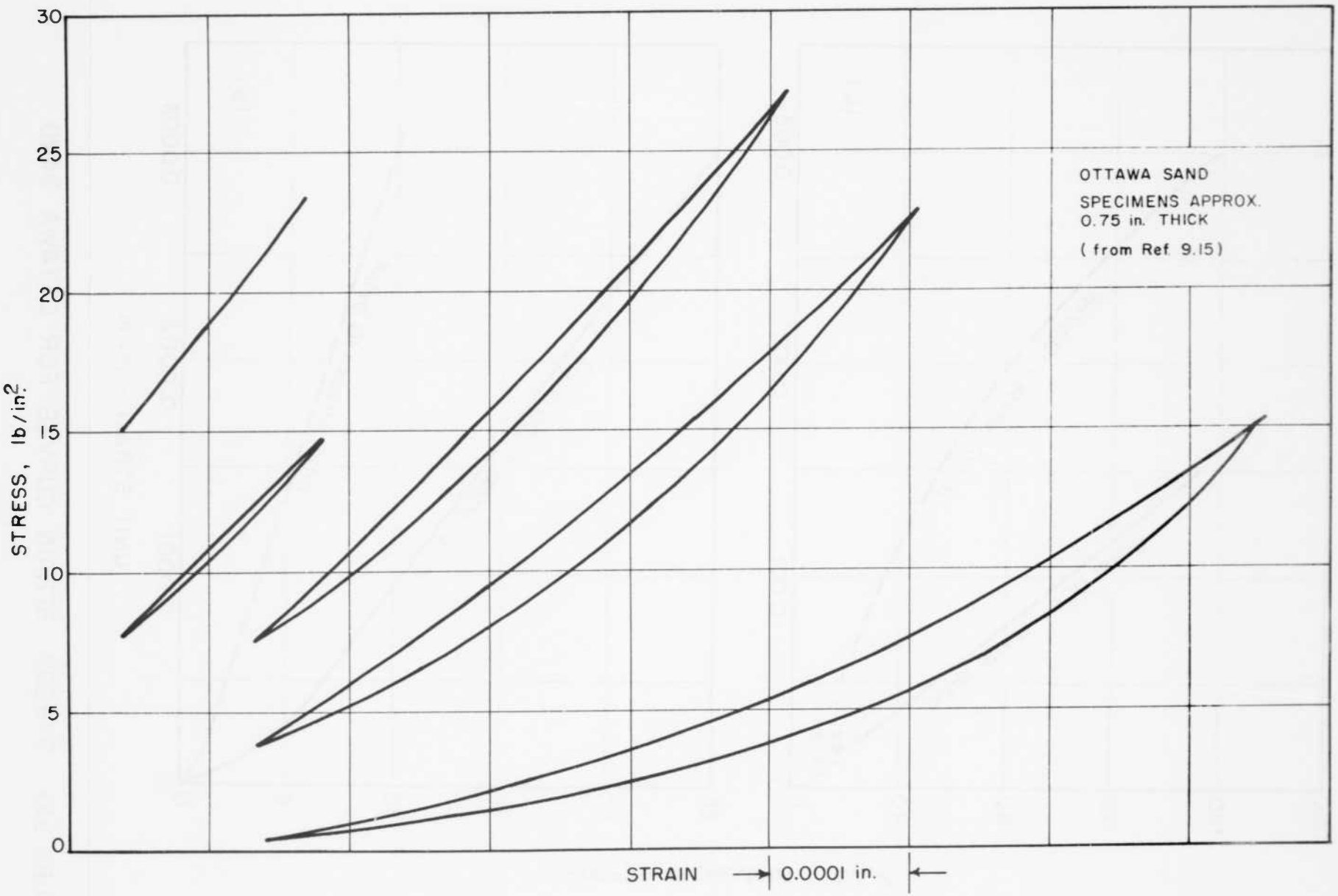

FIGURE 3.9 HYSTERESIS LOOPS FOR OTTAWA SAND

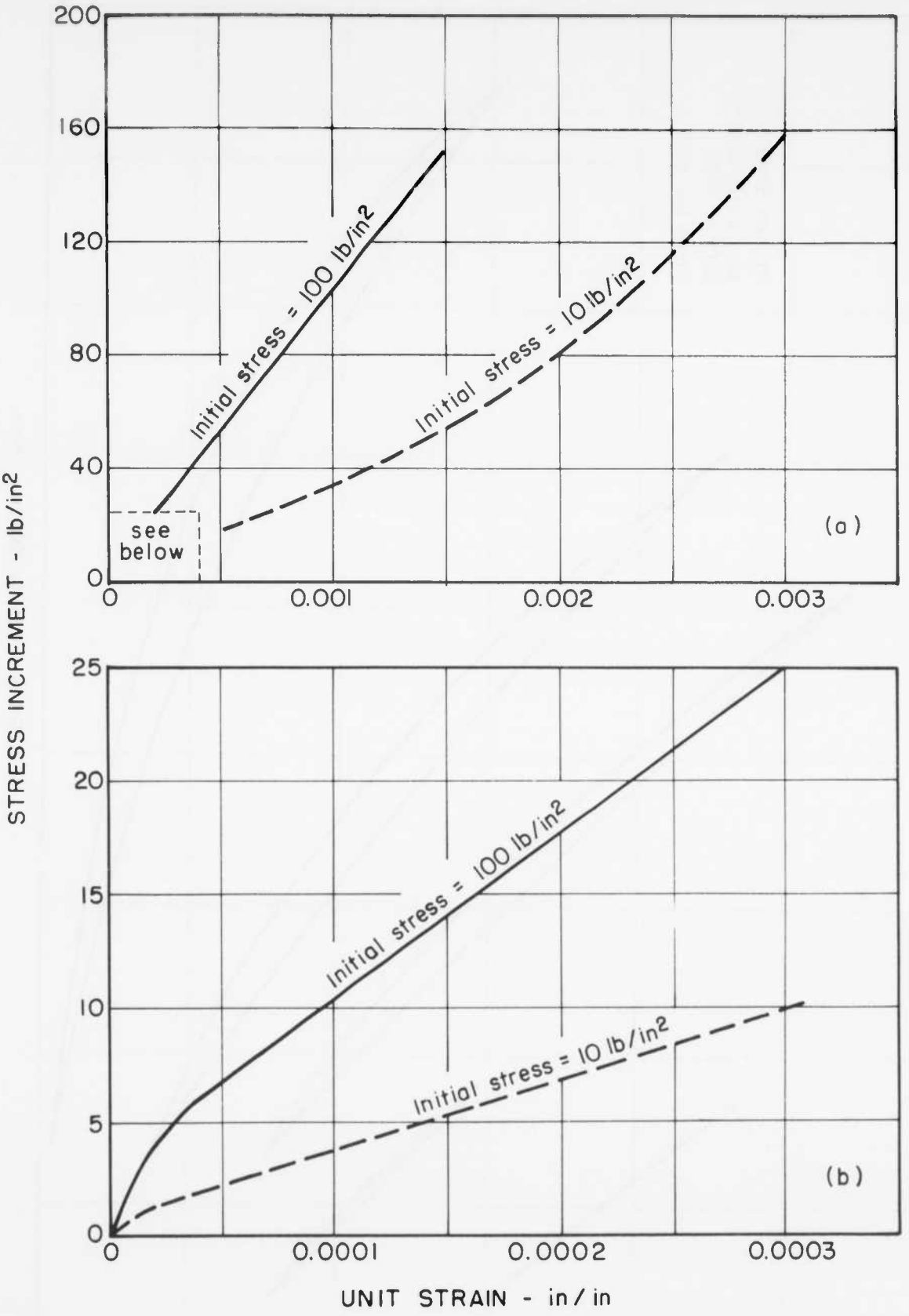

FIGURE 3.10 STRESS - STRAIN CURVES FOR OTTAWA SAND

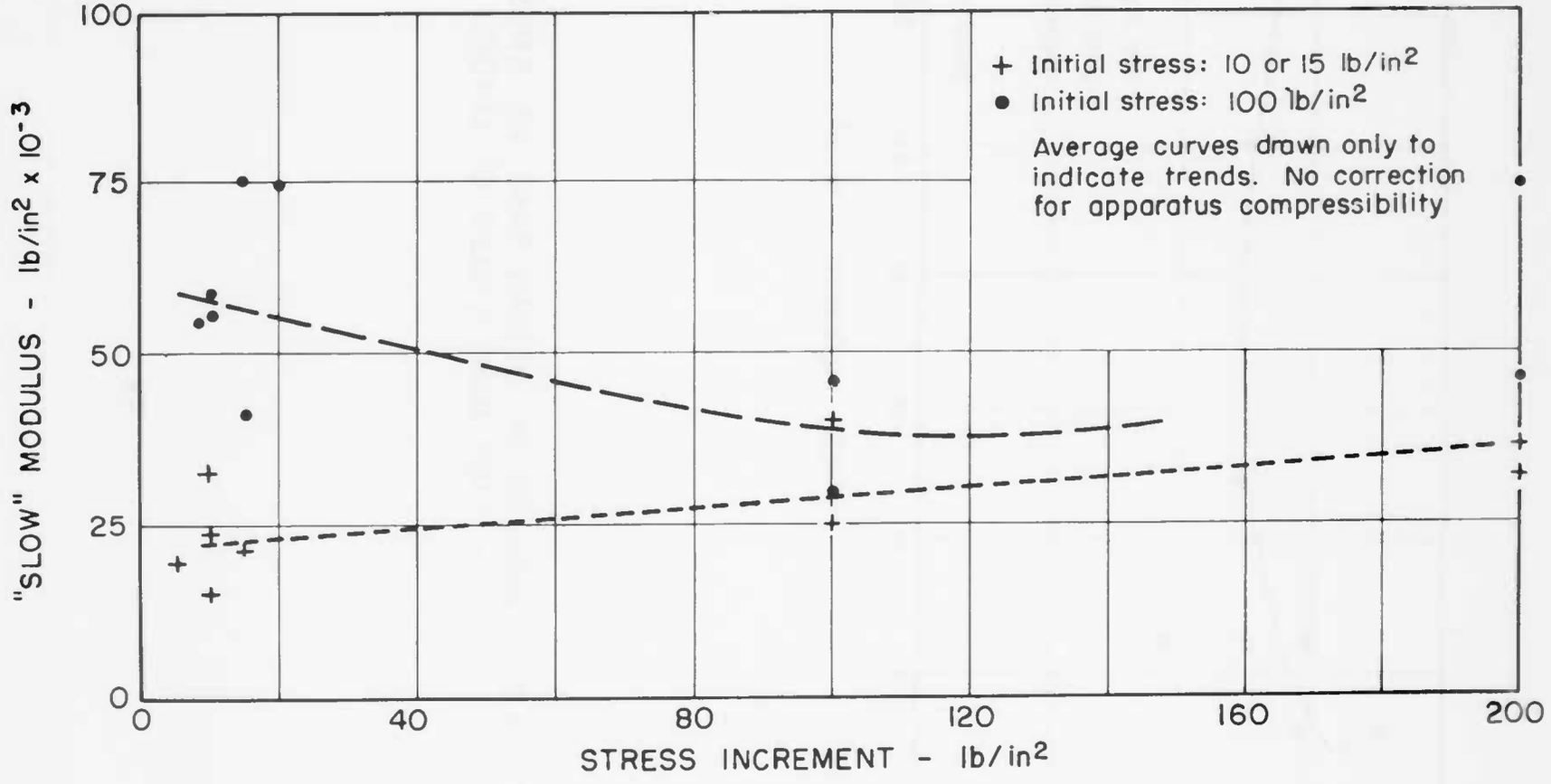

FIGURE 3.11 MODULUS OF OTTAWA SAND vs STRESS INCREMENT - FIRST CYCLE OF LOADING

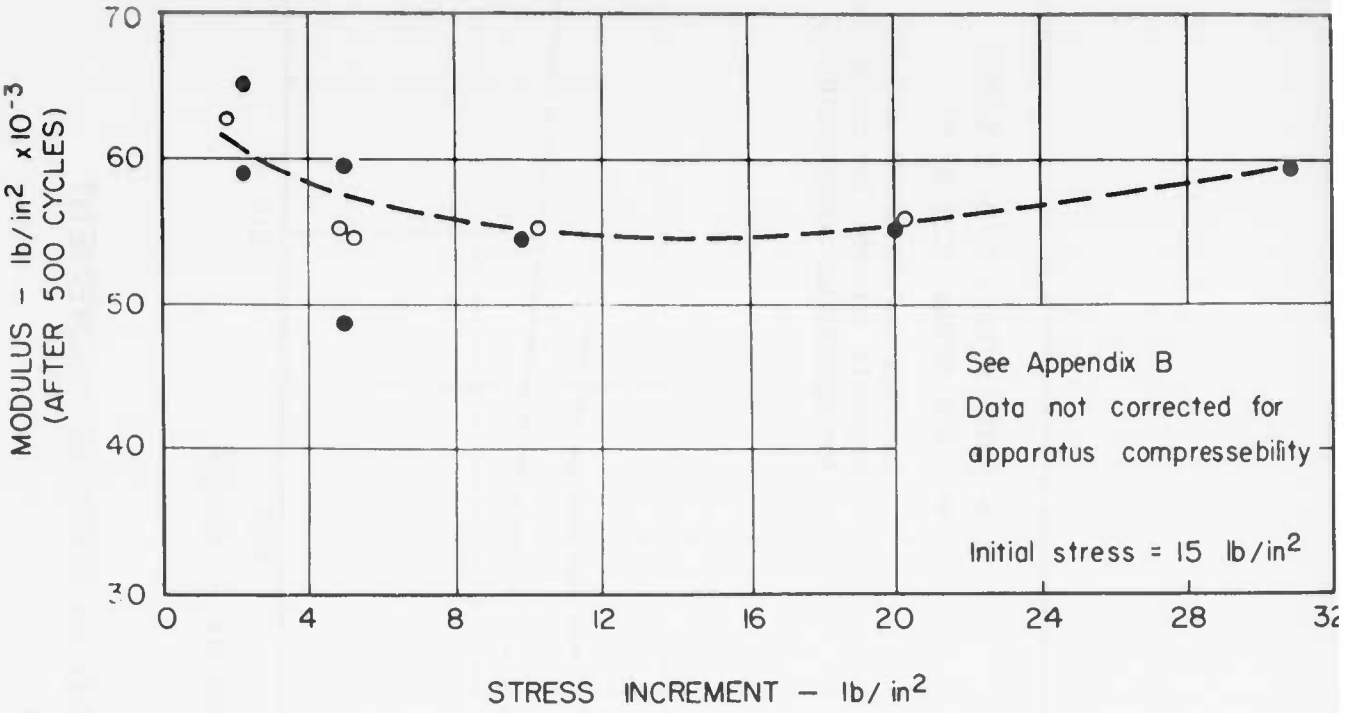

FIGURE 3.12 MODULUS OF OTTAWA SAND VS. STRESS INCREMENT —AFTER MANY CYCLES OF LOADING

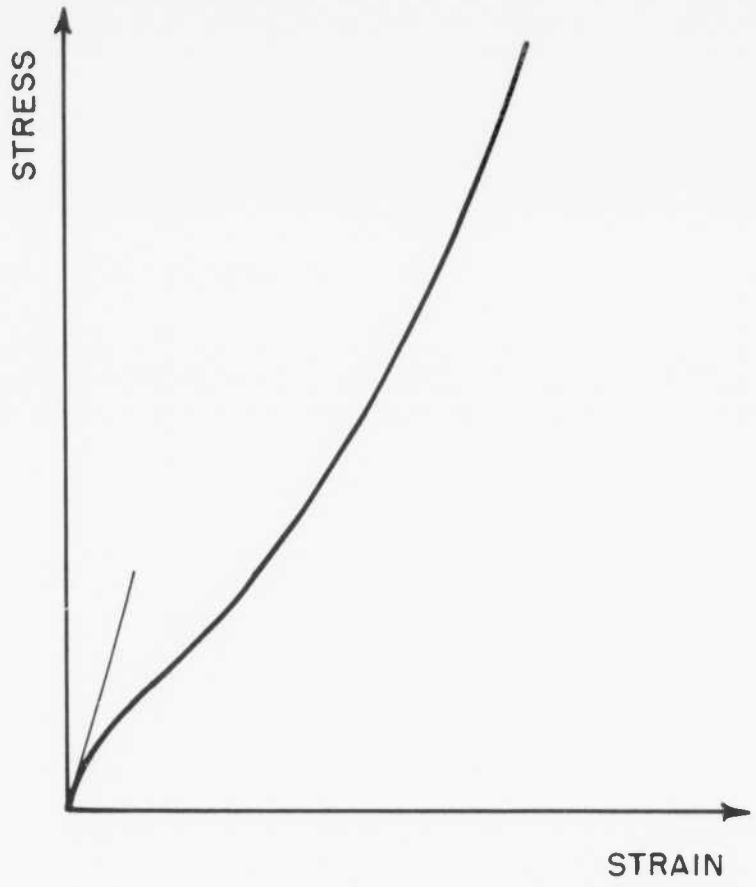

FIGURE 3.13 TYPICAL STRESS-STRAIN CURVE FOR SOIL DURING RAPID LOADING

Chapter 4

IMPLICATIONS REGARDING WAVE PROPAGATION

4.1 Wave propagation effects within visco-elastic material

To illustrate the nature of the wave propagation patterns within a visco-elastic material, let us consider the response of such a material to the step loading shown in Figure 4.1(a). Let: t = time from start of loading; x = distance along rod; $t_o = 1/\mu M_o = 1/\rho\mu c_o^2$ = visco-elastic time constant; $\Delta\sigma$ = the stress increment at any point, and $\Delta\varepsilon$ = the strain increment at any point. Other symbols are as defined in Figure 3.7. The following dimensionless parameters are useful:

dimensionless time	$T = t/t_o$
dimensionless distance	$X = x/c_o t_o$
dimensionless time of arrival of wave front at dimensionless distance X	$T_s = X$
dimensionless stress	$\hat{\sigma} = \Delta\sigma/\Delta\sigma_s$
dimensionless strain	$\hat{\varepsilon} = (M_o/\Delta\sigma_s)\,\Delta\varepsilon$

With this formulation, $c_o t_o$ plays the role of a characteristic wave length.

Figures 4.2, 4.3 and 4.4 show various aspects of the wave propagation patterns resulting from a step of loading. When the wave first arrives at any point along the column, the stress increment is less than the applied stress increment. Therafter, the stress and strain at this point increase continuously with time until the stress equals the input stress and the corresponding static strain level is reached. The stress change across the leading wave front is given by the very simple expression (Lee and Kantner, 1953):

$$\hat{\sigma} = e^{-X/2} \tag{4.1}$$

Morrison (1956) obtained an analytical solution for the time history of

stress and strain behind the wave front. This solution involves Bessel functions, and available tables permit evaluation only for small X and T. Using the method of characteristics, with a power series expansion near the origin, Lai and Sauer (1961) have prepared a very complete set of charts for m^2 of 1/4, 1/2, 3/4, 1, 2 and 4.

Since the viscoelastic model is linear, superposition can be used to find the wave patterns resulting from a stress pulse of finite duration (Figure 4.1(b)). Figure 4.5(a) illustrates the use of superposition to establish the time history of stress at a particular station. Note that the maximum stress reached at this station is less than the peak input stress; i.e. there is attenuation of peak stress with distance along the rod. The degree of attenuation is shown in Figure 4.5(b) as a function of the dimensionless duration of the stress: $T = {}^{t_1}/_{t_o}$.

Lai and Sauer (1961) have presented chart solutions for the blast wave type of stress input (Figure 4.1(c). The symbol $\Delta\sigma_s$ now denotes the peak stress applied at the surface. The duration of the blast wave is expressed by the dimensionless parameter.

$$\hat{T} = {}^{at}/_{\mathcal{A}} \qquad (4.2)$$

where a = speed of sound in air (1085 ft/sec for standard atmospheric conditions

$\mathcal{A}$ = nuclear distance scaling factor, proportional to the cube root of the explosive yield ($\mathcal{A}$ = 1134 for 1 kiloton at standard atmospheric conditions)

Figure 4.6 shows a specific example of the time-history of stress at various points along the length of the column. For small X, the stress decreases once the leading wave front has passed. So long as this condition is met, the attenuation of peak stress with distance is given by equation (4.1). At large X, however, the stress increases for a time after passage of the leading wave front. Extensive numerical calculations are then necessary to determine peak stress as a function of distance. Figure 4.7 illustrates the attenuation of

peak stress with dimensionless distance. Large values of the parameter $\mu Mo(d/a)$ means that the duration of the blast wave input is very long compared to the visco-elastic time constant. Strain and particle velocity exhibit similar variations with distance and time.

Lai and Sauer have also shown that the maximum ground displacement is:

$$u_{max} = (u_e)_{max} \sqrt{1 + \frac{1}{m^2}} \qquad (4.3)$$

where $(u_e)_{max}$ is the maximum displacement for an elastic material with wave propagation velocity c_o. Equation (4.3) applies for all depths, and is independent of the time history of the applied surface pressure.

4.1.1 Importance of stress attenuation from visco-elasticity

The charts in Lai and Sauer have been used to establish curves of peak stress with depth for some typical design situations as shown in Figure 4.8. The values of m^2 and $1/\mu Mo$ used for curves 1, 2 and 3 are typical for the undisturbed soils. If anything, the experimental values of these parameters were greater than the typical value chosen; using a larger value for these two parameters would lead to less stress attenuation. Curves 5 and 6 are based upon the extreme results for the compacted fat clay, while Curve 6 corresponds to the parametric values observed for Ottawa sand.

To illustrate the significance of these results, assume that a structure is buried 100 feet deep in a soil with a modulus M_o = 28,000 lbs/in^2. The corresponding wave propagation velocity c_o for this soil would be 1000 ft/sec. Based upon the typical properties for undisturbed soils (Curves 1, 2 or 3), the peak stress reaching the structure would be 82 per cent of the peak surface pressure. From the practical standpoint, this structure would undoubtedly be designed to resist the full surface overpressure. For most practical design problems, the modulus Mo will be greater than the value chosen here, and hence the attenuation within the top 100 feet of the soil will be even less. Attenuation will be significant

in the case of high overpressure levels and/or greater depths of burial for the structure. However, it is doubtful whether the one-dimensional analysis will apply for such conditions. Attenuation begins to become significant if the visco-elastic time constant is 1/10 sec. rather than 1/4 sec., although such a result has been observed only in the case of reconstituted soils. Note that decreasing the size of the explosion will not change the position of Curves 1, 2, 3 and 6 in Figure 4.8 (for the range of x/c_o covered in this figure.) Thus, on the basis of measured time-dependent effects, visco-elastic type of phenomena should not have caused significant stress attenuation in the Nevada field tests.

The data presented in this report are based upon tests in which the applied stress rise-times were generally 5 milliseconds or longer. Hence these results do not preclude the possibility that very short relaxation times are present. (The presence of such short relaxation times is suggested by the results of Leonards, 1962.) Consider, for example, the discrepancy between the two types of modulus listed in Table 3.3. This discrepancy might be explained by the existence of a relaxation time of 1 millisecond or less.

Assume for the moment that this explanation is correct. On the basis of the data in Table 3.3, m^2 might range from 1/5 to as low as 1/40. Lai and Sauer (1961) have provided charts for $m^2 = 1/4$. Using these charts, one obtains the following values for $\Delta\sigma / \Delta\sigma_s$ at $x/c_o = 0.1$, for a 30 megaton explosion.

$1/\nu M_o$	$\Delta\sigma_s = 60$ lbs/in^2	$\Delta\sigma_s = 450$ lbs/in^2
0.1 msec.	0.88	0.70
0.5 msec.	0.85	0.63

Hence the existence of very short relaxation times would imply significant attenuation of the overpressure produced by a very large explosion, at least for the case of high surface overpressures. For a 1 kiloton explosion, the numbers in this table would be much smaller:

$1/\nu M_o$	$\Delta\sigma_s$ = 60 lb/in^2	$\Delta\sigma_s$ = 450 lb/in^2
0.1 msec.	0.47	0.17
0.5 msec.	0.37	0.12

Thus it is conceivable (if the presence of very short relaxation times is assumed) that visco-elastic effects might have caused significant attenuation in Nevada field tests.

4.1.2 Influence of visco-elasticity upon maximum displacement and particle velocity

From the results in Table 3.5, it would appear that m^2 is no smaller than unity. On the basis of equation (4.3), the error which results from ignoring visco-elasticity is no greater than 41 per cent. Actually, in the author's engineering judgment, m^2 for typical undisturbed soils is probably more like 5, and the error is more like 10 per cent.

If one used in equation (1.2) the propagation velocity deduced from a test with a 5 millisecond rise-time, and if very short relaxation times were actually present, one would overestimate the maximum ground displacement. Comparison of the two types of modulus values in Table 3.3 provides a basis for estimating this error. It would appear that the error would be no more than 25 per cent.

Lai and Sauer also provide charts for the maximum particle velocity. For the range of variables considered in Figure 4.8, the ratio $v_{max}/(v_e)_{max}$, varies from 1.09 to 1.00 at x = 0 and from 0.90 to 0.55 at x/c_o = 0.1. The quantity $(v_e)_{max}$ is the maximum particle velocity for an elastic material with wave propagation velocity c_o.

4.1.3 Effect of viscoelasticity upon maximum acceleration

Theoretically there is always an infinite particle acceleration whenever a sharp fronted wave passes through a visco-elastic column; i.e. the particle velocity increases immediately as the front passes, and in direct proportion to the change in stress. However, as the magnitude of

the stress at the wave front attenuates, it can be said that the maximum particle velocity becomes "less infinite".

Figure 4.9 shows curves of particle velocity vs. time at various distances, for a set of parameters which might apply if there were relaxation times of less than a millisecond. Although the peak particle velocity does not change much with distance, the time to achieve the peak particle velocity lengthens. Thus, in theory the average acceleration does decrease with distance. If the "less infinite" acceleration at $(T - T_s) = 0$ is ignored, then perhaps visco-elasticity can explain the attenuation of peak acceleration which has been observed in field tests.

However, for situations in which there is little stress attenuation with distance, it is hard to ignore the "large" infinite acceleration which theory ascribes to the wave front. For such conditions, viscoelasticity does not explain the observed attenuation of maximum acceleration.

4.2 Wave propagation effects within irreversible material

Techniques for evaluating these effects with distance have been presented by Salvadori, Skalak and Weidlinger (1960) and by Heierli (1962). The general procedure is illustrated by the characteristics diagram in Figure 4.10. On this diagram, the lines represent wave fronts, and the amplitudes of stress and particle velocity between the wave fronts are represented by the boxed quantities. For the problem studied in Figure 4.10 a stress pulse of magnitude $\Delta\sigma_s$ is applied for a time t_o. Dimensionless time and distance are defined as in section 4.1. Dimensionless particle velocity is defined by:

$$V = \frac{M_o}{\Delta\sigma_s} \quad \frac{v}{c_o}$$

where v is the actual particle velocity.

Because the modulus upon unloading is greater than that upon loading, the unloading wave front catches up with the loading wave front at point X_1. As a result, the stress intensity across the continuing front is decreased; i.e. stress has been attenuated with distance. A

reflected wave is generated at point X_1, and this wave is in turn reflected from the surface. Successive reflections then occur.

This basic graphical procedure can be used for any input stress history. Analytical solutions are available for certain special cases.

4.2.1 Importance of stress attenuation by irreversibility

For the case of a triangular relation between applied pressure and time (see Figure 4.11), the maximum stress $\Delta\sigma$ at any depth x is given by:

$$\frac{\Delta\sigma}{\Delta\sigma_s} = 1 - \frac{x}{c_o t_o}\left(\frac{1-r}{2}\right) \qquad (4.4)$$

where $c_o = \sqrt{Mo/\rho}$. This formula is accurate only for $x < c_o t_o/(1-\sqrt{r})$. At greater depths, the formula underestimates the peak stress.

Equation (4.4), together with the data presented in section 3.3, may be used to estimate the stress attenuation arising from irreversibility. The time t_o has been determined from the initial rate of decay for the applied stress for the overpressure level in question.* The results of the calculation are given in the following table, assuming a 30 megaton explosion.

$\frac{x}{c_o}$	$\Delta\sigma/\Delta\sigma_s$			
	$\Delta\sigma_s = 60$ lbs/in^2		$\Delta\sigma_s = 450$ lbs/in^2	
Sec.	r = 0.5	r = 0.8	r = 0.5	r = 0.8
0.05	0.98	0.99	0.84	0.92
0.10	0.95	0.98	0.72	0.89
0.20	0.90	0.96	0.45	0.78

Since the applied surface stress decays more slowly than is assumed (see Figure 4.11), the peak stress ratios given in this table are too small.

To illustrate the significance of these results, consider again the case of a structure buried 100 feet deep in a soil with a modulus $M_o = 28{,}000$ lbs/in^2, $c_o = 1000$ ft/sec.). For $\Delta\sigma_s = 450$ lbs/in^2 and r = 0.8,

*Figure 25 of Lai and Sauer (1961) is useful in this connection.

the peak stress reaching the structure would be 89 per cent of the peak surface pressure. From the practical standpoint, this result is the same as no attenuation.

The attenuation of stress will become significant if one considers explosions of kiloton size and/or great depths of burial for the structure. Once again, however, it is doubtful whether the one-dimensional analysis will apply for such conditions.

4.2.2 Effect of irreversibility upon maximum ground displacement and particle velocity

Assuming a semi-infinite column and an applied loading as shown by the triangle in Figure 4.11, theory indicates that the maximum surface displacement is infinite (for example, see Heierli, 1962). To avoid this obviously incorrect result, it is necessary to consider that natural soil deposits are not homogeneous with depth. While the surface portion of a natural soil deposit generally will exhibit $r<1$, the deeper layers probably are elastic.

In order to investigate the effects of layering, the example shown in Figure 4.12 has been evaluated. In Part (a) of this example, the inelasticity of the surface layer is considered, whereas this inelasticity is ignored in Part (b). The depth of the upper layer has been selected so that the wave reflected from this layer in Part (a) just reaches the ground surface at the very end of the loading.

Simple formulas in Salvadori, Skalak and Weidlinger (1960) may be used to determine the surface particle velocity in Part (a) for $t<t_o$. For $t>t_o$, the surface particle velocity proves to be zero. Thus the maximum surface displacement in Part (a) may be found by integrating the particle velocity from $t = 0$ to $t = t_o$.

For Part (b), the reflected wave reaches the surface after the end of the applied loading. The maximum surface displacement thus occurs at $t = t_o$, and may be computed from equation (1.2). The maximum surface displacement calculated for Part (a) is $(3-r)/2$ times greater than that for Part (b).

Thus, by ignoring the effects of inelasticity, the maximum ground displacements are underestimated for points near ground surface. For the example in Figure 4.12, the error which arises from neglecting irreversibility is only 10 per cent if r = 0.8. In most practical problems, the transition from inelastic to elastic soil will probably occur at a depth less than that assumed in the example. While it will be necessary to work out many more examples to establish the typical magnitude of this error, the writer estimates that the error will usually be less than 20 per cent for the design conditions considered in this paper.

Neglect of irreversible effects leads to an overestimate of the maximum ground displacement at the boundary between the inelastic and elastic layers. This situation is illustrated in Figure 4.13. In Part (a), where inelasticity is considered, the maximum displacement at X = 1.667 is $(0.30)\ (\Delta\sigma_s\ c_o/M_o)\ (1.33)\ (t_o) = 0.40\ (\Delta\sigma_s\ c_o y_o/M_o)$. In Part (b), where inelasticity of the upper layer is ignored, the maximum displacement is $0.571\ (\Delta\sigma_s\ c_o t_o/M_o)$. On the basis of a few such examples, it appears that this error is also no greater than 20 per cent for typical design conditions, assuming $r \geq 0.8$.

The maximum particle velocity at ground surface is unaffected by the recovery ratio. The ratio

$$\frac{\text{maximum particle velocity at depth x}}{\text{maximum particle velocity at surface}}$$

is the same as the ratio $\Delta\sigma / \Delta\sigma_s$. Thus, if the actual stress-strain relation of the soil is irreversible, equation (1.1) will overestimate the maximum particle velocity. The magnitude of the error is indicated by the numbers in the table of section 4.2.1.

The irreversible model, with straight-line loading and unloading branches, leads to infinite particle accelerations at all depths if the input wave front is sharp. This model is not of use for explaining

the attenuation of peak acceleration as observed in field tests.

4.3 Wave propagation effects within non-linear material

A non-linear stress-strain curve in itself does not give rise to stress attenuation; other phenomena such as time-dependency or irreversibility must be coupled to the non-linearily to produce such effects. However, non-linear behavior in itself is capable of modifying the shape of the stress-time curve of a wave as the wave travels through the ground.

If the stress-strain curve of a soil is concave toward the stress axis (see Figure 3.10(a)), a shock wave must then form in the soil. That is, a sharp fronted wave, with corresponding large accelerations, must form regardless of whether or not the input stress wave has a sharp front. Shock waves are not observed to develop in soils, at least for stress levels less than 1000 lb/in^2. Hence it may be inferred that the stress-strain curves for soils are <u>not</u> simply concave to the stress axis.

If, on the other hand, the stress-strain curve is concave to the strain axis, a sharp fronted stress wave will be spread cut in time as it passes a distant station. A decrease in peak acceleration with distance is associated with this process. Thus, the type of stress-strain behavior shown in Figures 3.10(b) and 3.13 would readily explain the attenuation of peak acceleration which is observed in field tests in situations where essentially one-dimensional strain conditions exist.

As yet, no quantitative study of acceleration attenuation has been attempted. Prior to such a study, the stress-strain behavior at small strains must be identified more accurately.

REFERENCES

HEIERLI, W., "Inelastic Wave Propagation in Soil Columns," Proc. A.S.C.E., Vol. 88, No. SM6, pp 33-63, 1962

LAI, W., and SAUER, F. M., "Propagation of Stress Pulses in Standard Linear Visco-elastic Materials", Report by Stanford Research Institute to Defense Atomic Support Agency, DASA 1266-1, 1961

LEE, E. H., and KANTNER, I., "Wave Propagation in Finite Rods of Visco-elastic Material," J. Appl. Phys., Vol. 24, No. 9, p 1115, 1963

LEONARDS, G. A., "Laboratory Experiments on the Response of Soils to Shock Loadings," Interim Report to Air Force Special Weapons Center TDR 62-90 by Purdue University School of Civil Engineering, 1962

MORRISON, J. A., "Wave Propagation in Rods of Voigt Material and Visco-elastic Materials with Three-Parameter Models," Quart. J. App. Math., Vol. 14, No. 2, p 153, 1956

SALVADORI, M. G., SKALAK, R., and WEIDLINGER, P., "Waves and Shocks in Locking and Dissipative Media," Proc. A.S.C.E., Vol. 86, No. EM2, pp 77-105, 1960

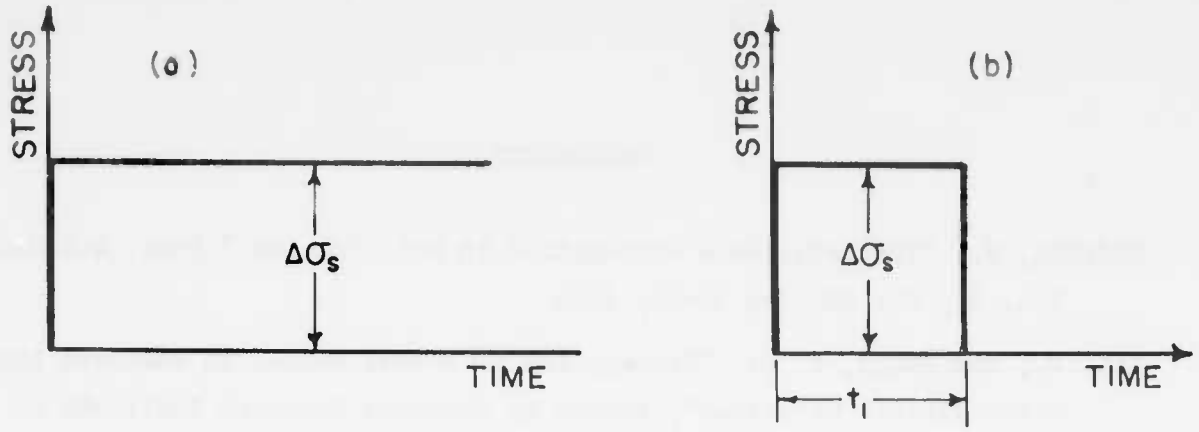

Step of stress

Pulse of finite duration

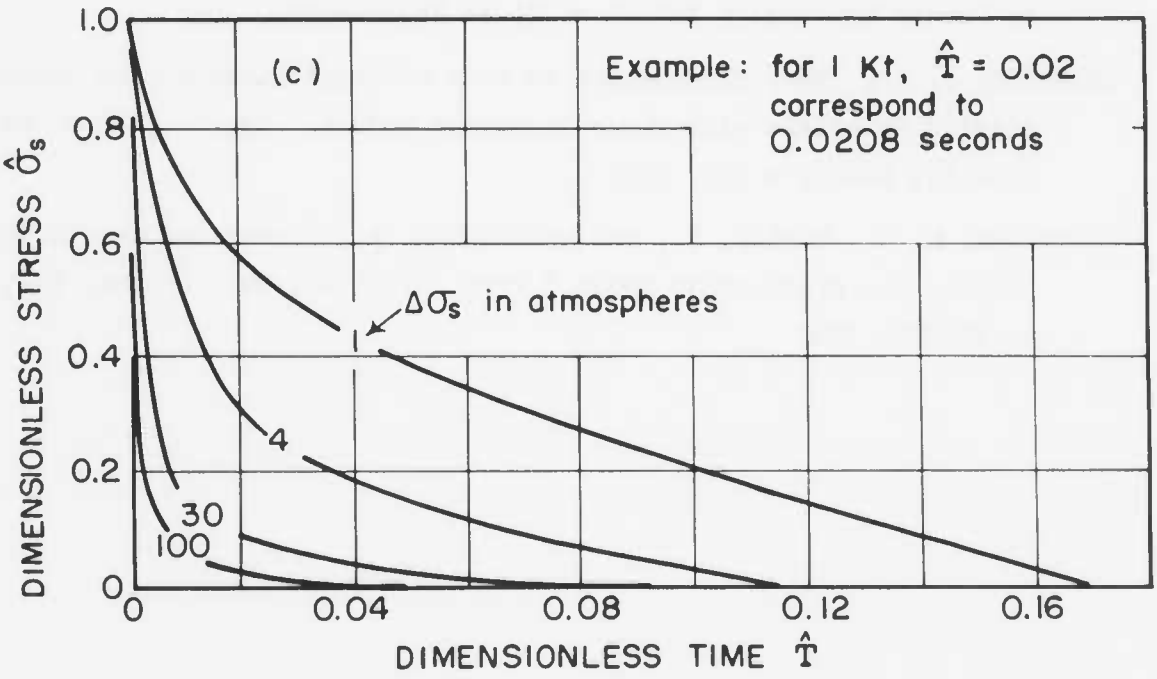

Blast stress

FIGURE 4.1 PATTERNS OF APPLIED STRESS FOR VISCO-ELASTIC MODEL

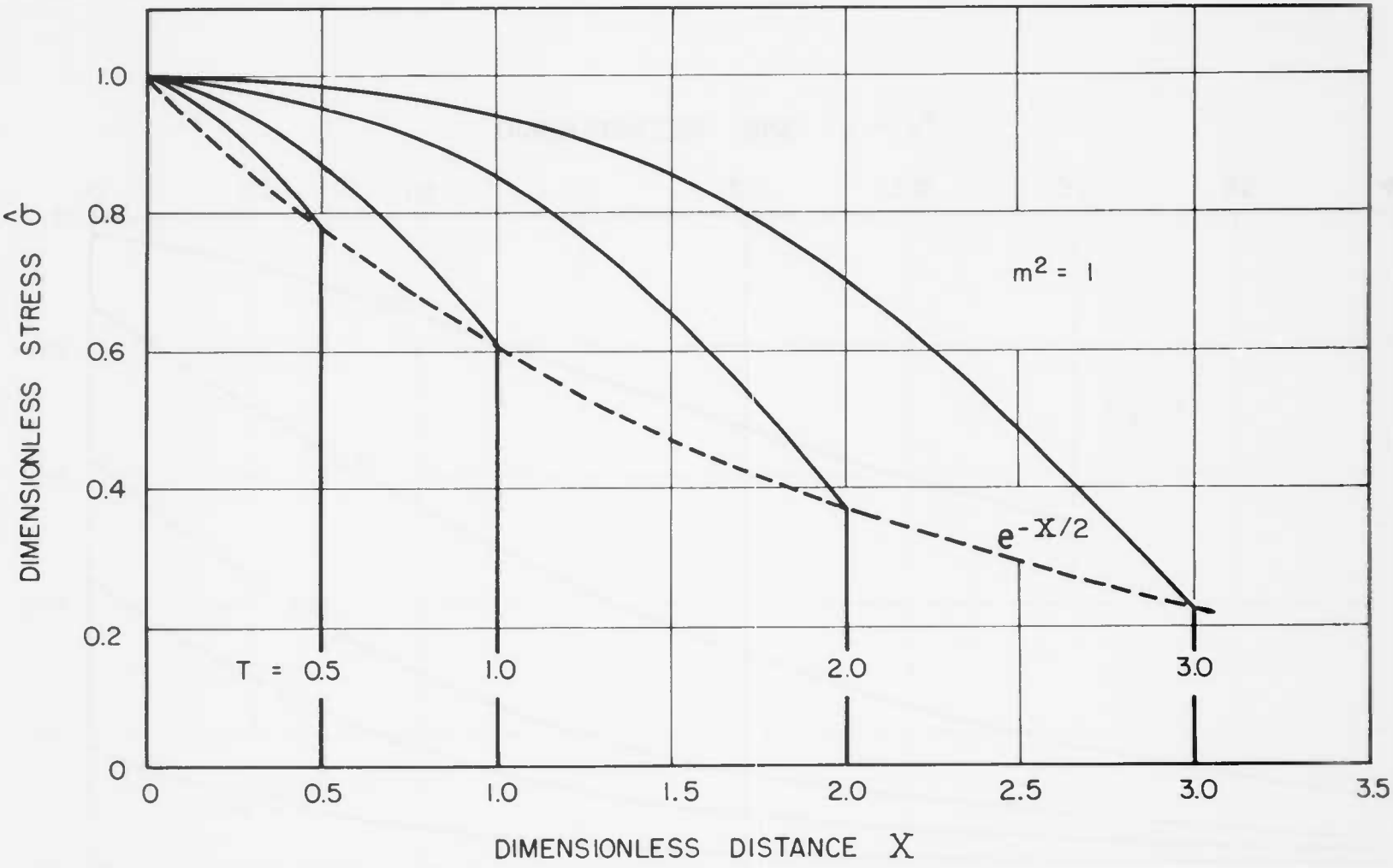

FIGURE 4.2 DISTRIBUTOIN OF STRESS ALONG VISCO ELASTIC COLUMN AT SEVERAL TIMES – STEP OF STRESS

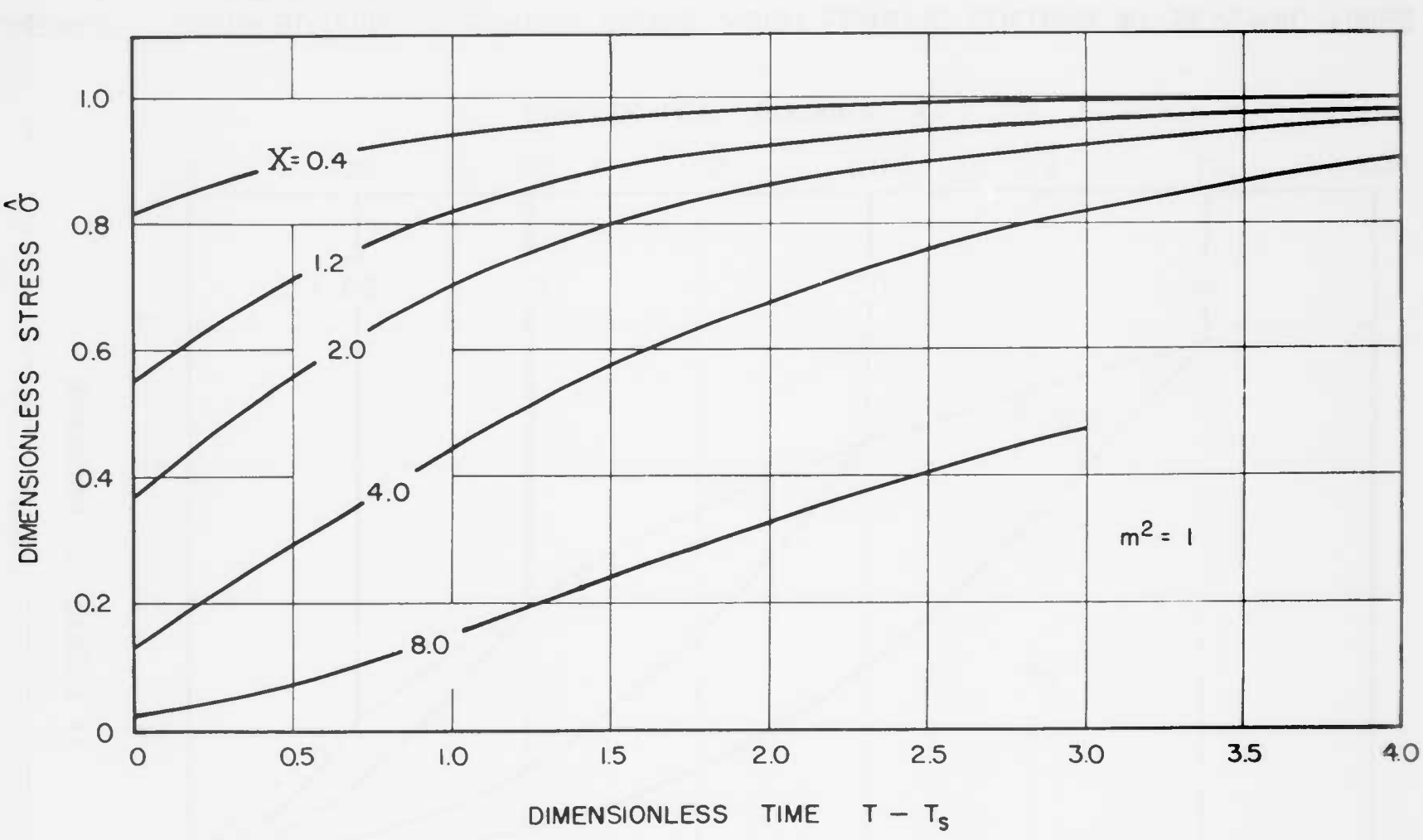

FIGURE 4.3 STRESS vs TIME AT SEVERAL POINTS ALONG VISCO-ELASTIC COLUMN — STEP OF STRESS

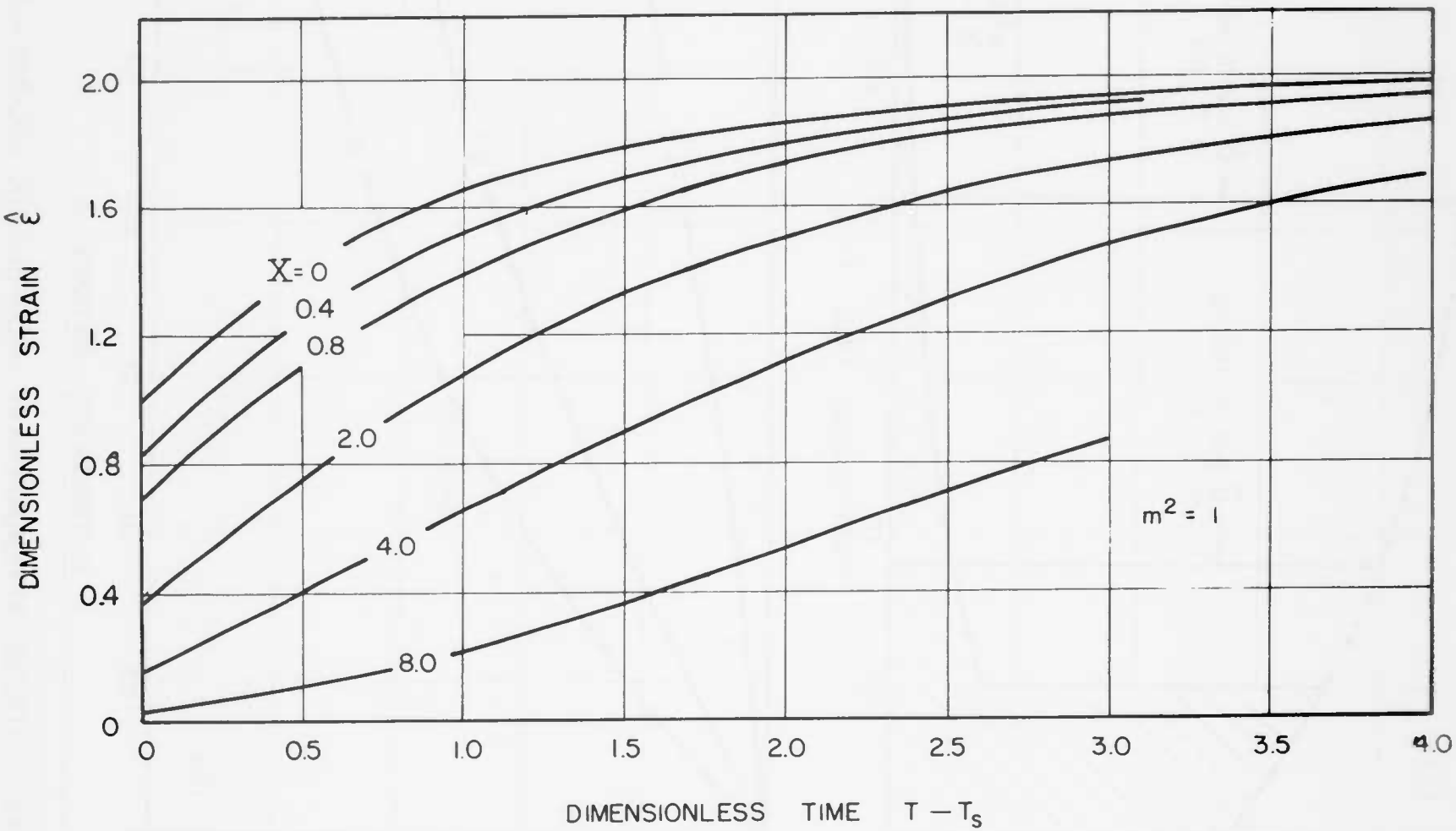

FIGURE 4.4 STRAIN vs TIME AT SEVERAL POINTS ALONG VISCO-ELASTIC COLUMN - STEP OF STRESS

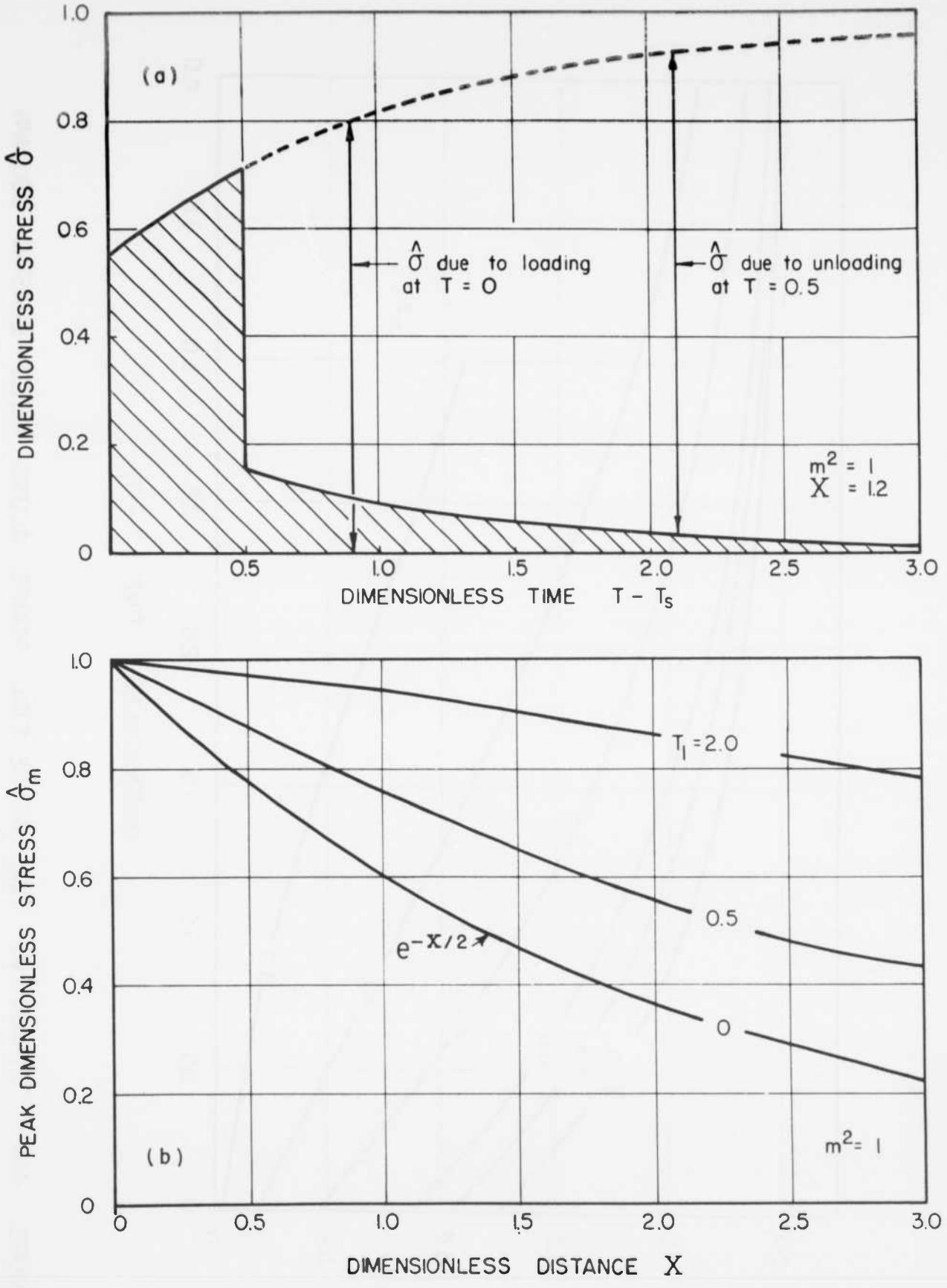

FIGURE 4.5 STRESS ATTENUATION IN VISCO-ELASTIC COLUMN — STRESS PULSE OF FINITE DURATION

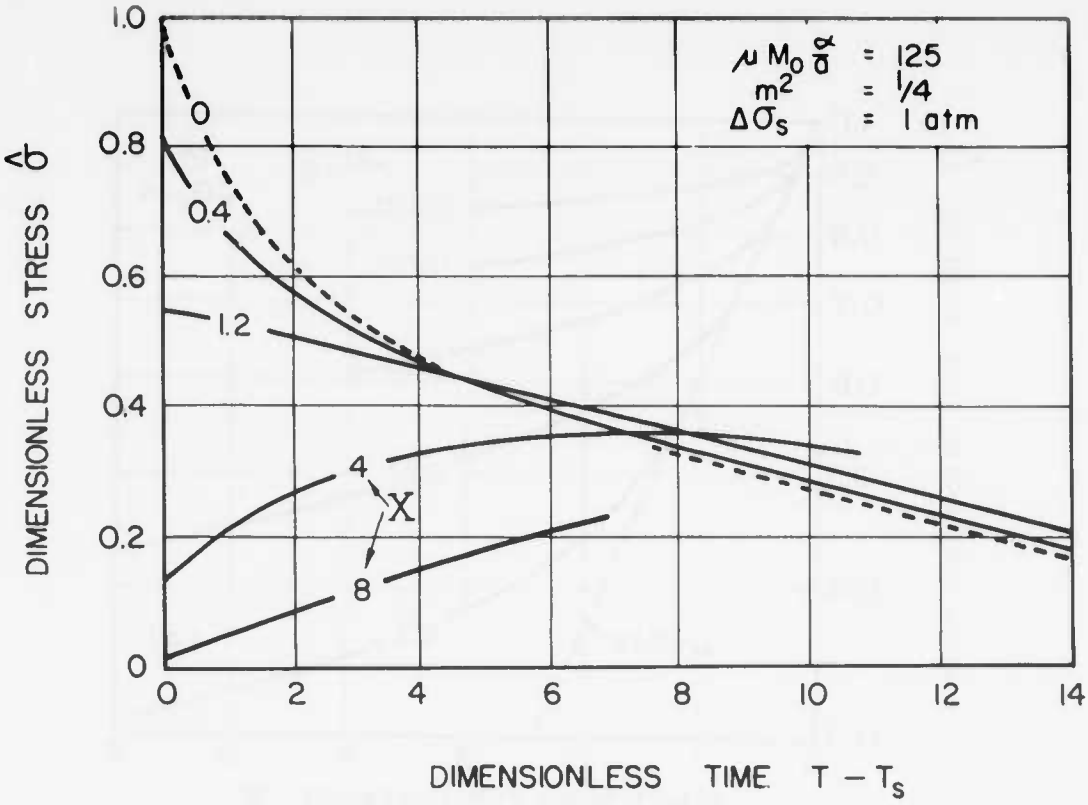

FIGURE 4.6 STRESS VS. TIME AT SEVERAL POINTS ALONG COLUMN – BLAST STRESS

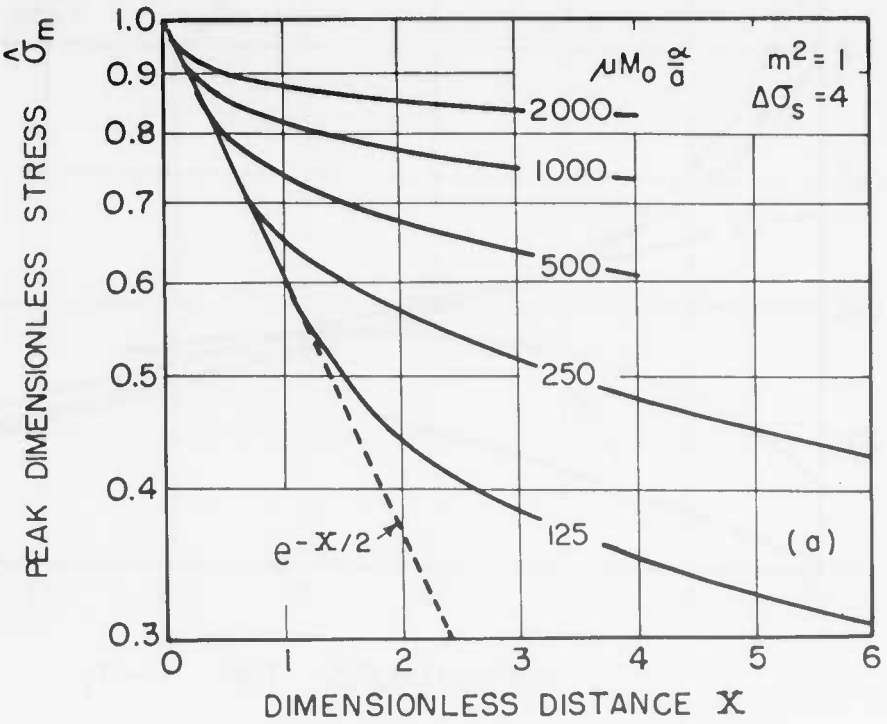

FIGURE 4.7 STRESS ATTENUATION IN VISCO-ELASTIC COLUMN — BLAST STRESS

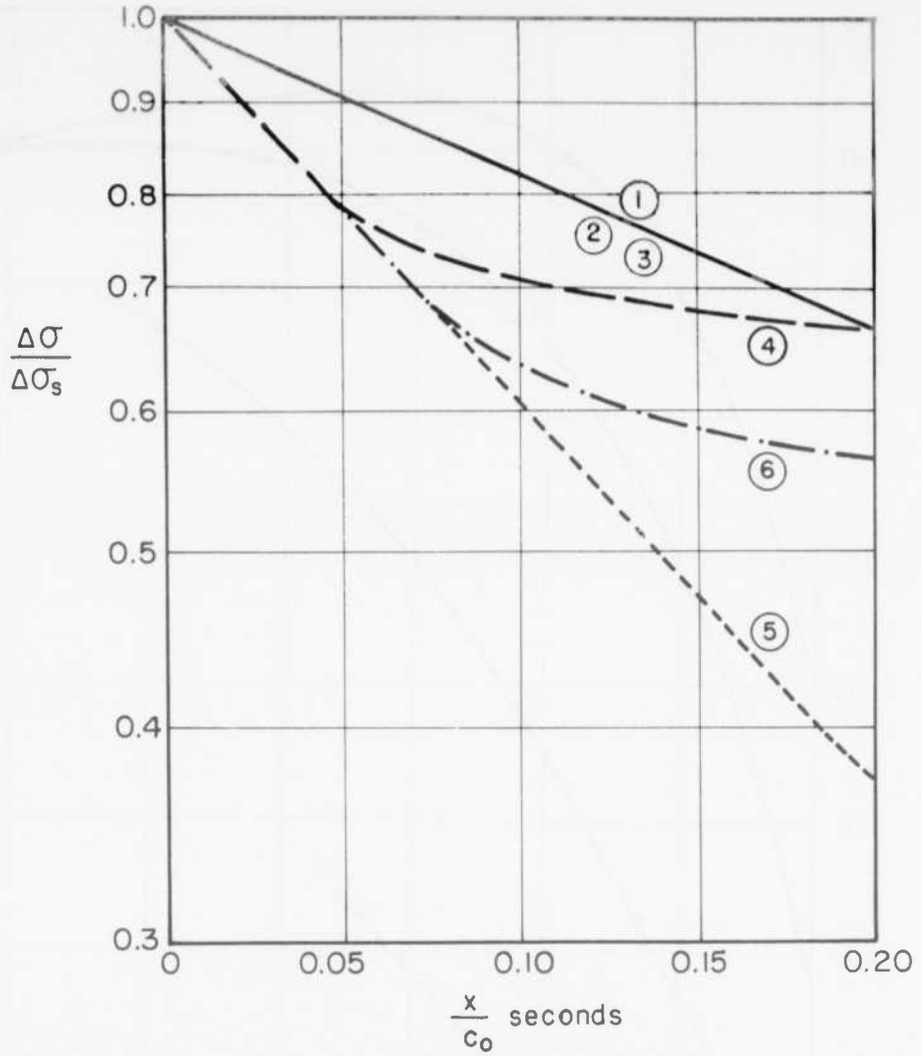

EXPLOSION megations	m^2	$1/\mu$ M_o seconds	$\Delta\sigma_s$ lb/in^2	CURVE	REMARKS
30	1	1/4	60	1	Properties typicol for undisturbed soils
30	1	1/4	450	2	
1	1	1/4	450	3	
30	1	1/10	60	4	Extreme properties for compacted fat cloy
30	1	1/10	450	5	
30	4	1/10	450	6	Prop. of Ottawa sand

FIGURE 4.8 STRESS ATTENUATION IN VISCOELASTIC COLUMN BLAST STRESS FROM LARGE EXPLOSIONS

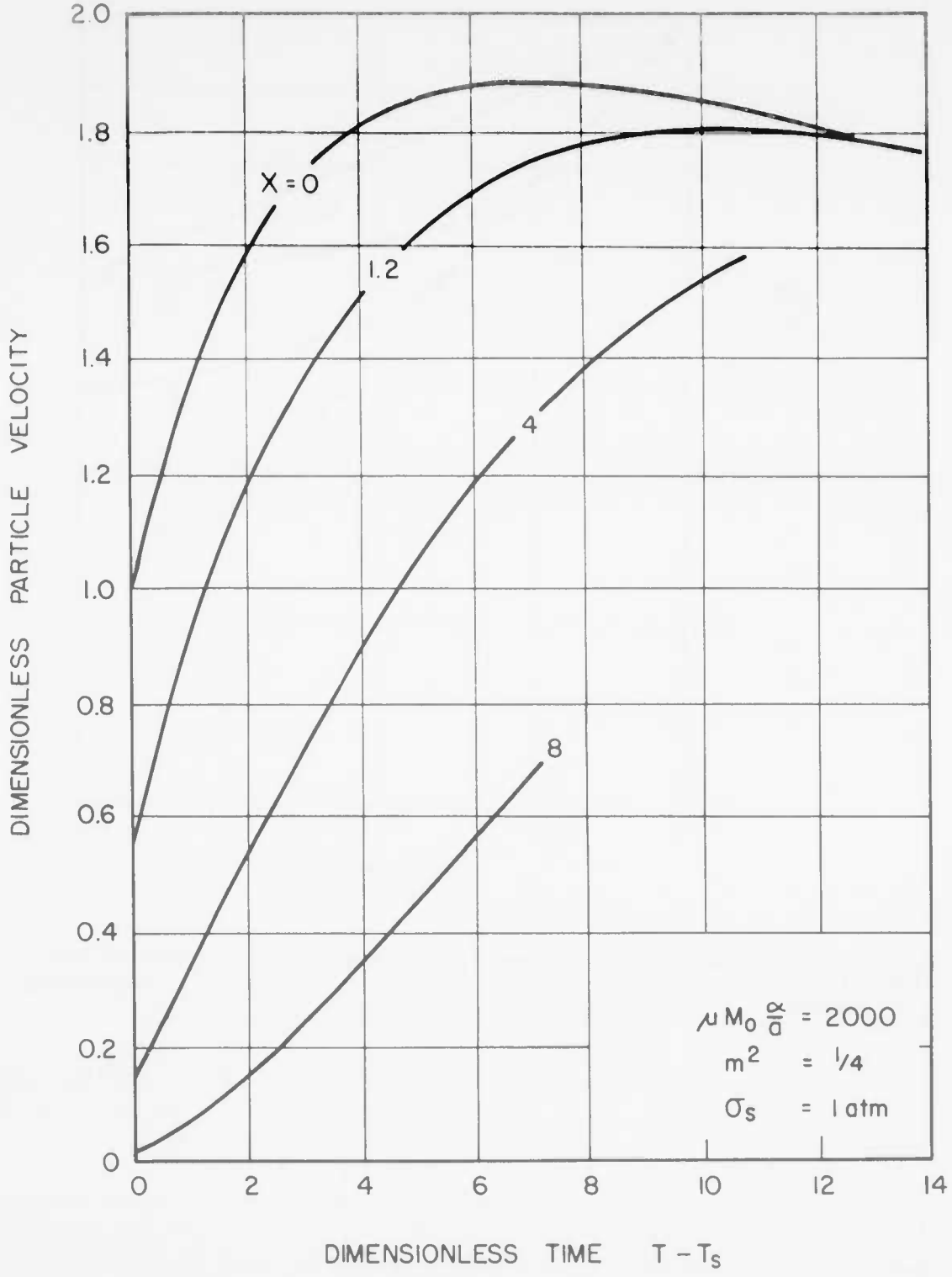

FIGURE 4.9 PARTICLE VELOCITY vs TIME AT SEVERAL POINTS ALONG VISCO-ELASTIC COLUMN - BLAST STRESS

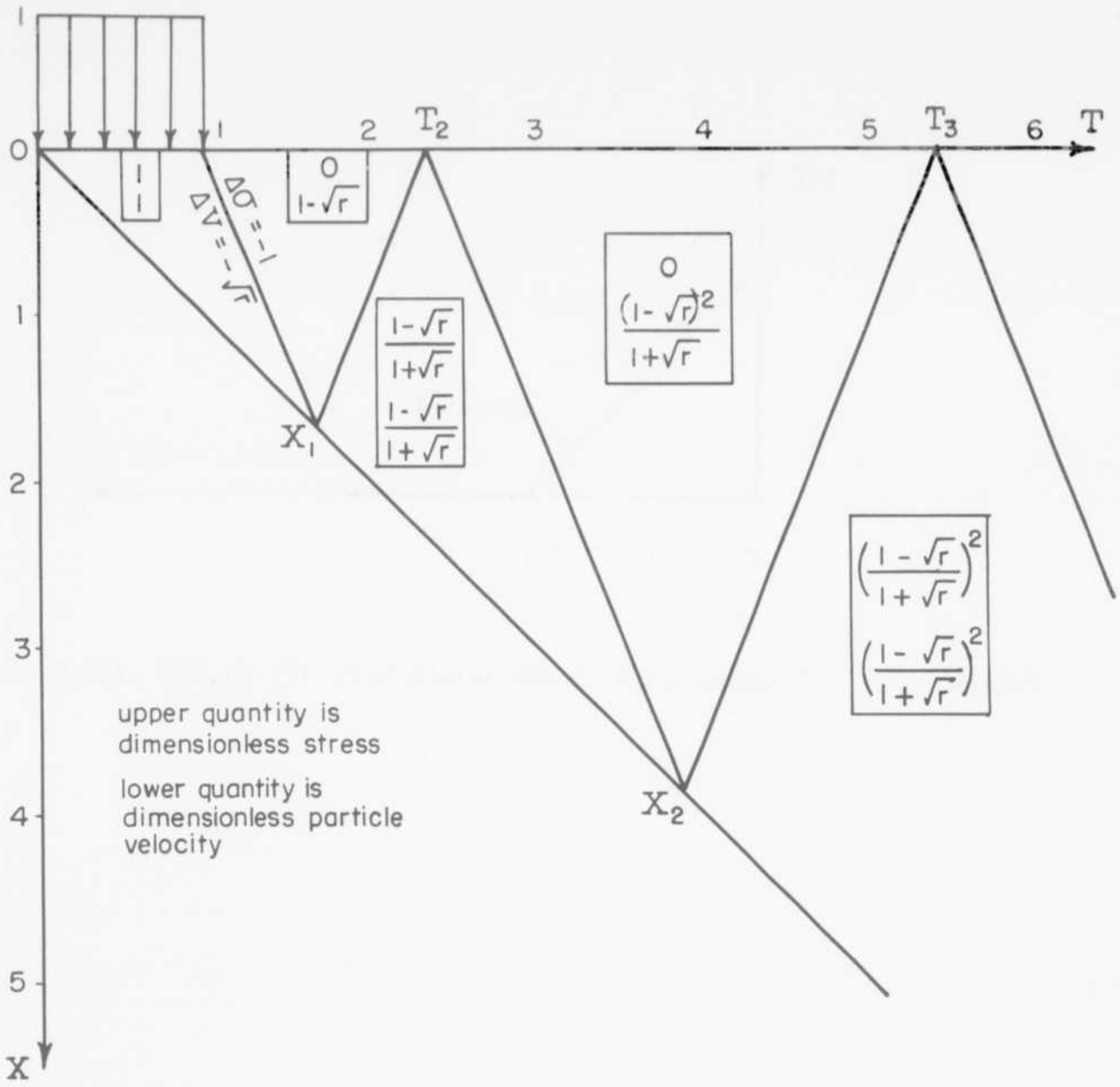

FIGURE 4.10 CHARACTERISTIC DIAGRAM FOR STUDY OF WAVE PROPAGATION THROUGH IRREVERSIBLE MATERIAL

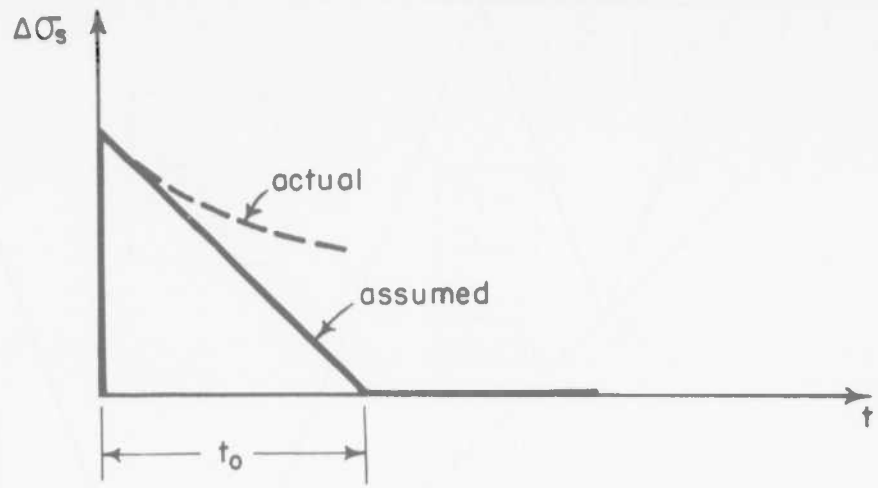

FIGURE 4.11 TRIANGULAR APPROXIMATION TO BLAST WAVE

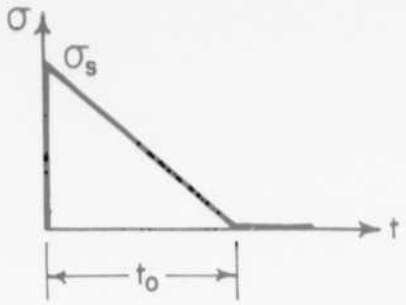

$$u_{max} = \left(\frac{3-r}{2}\right)\left(\frac{1}{2}\,\frac{\sigma_s\, t_o}{\rho c_o}\right) \qquad u_{mox} = \frac{1}{2}\,\frac{\sigma_s\, t_o}{\rho c_o}$$

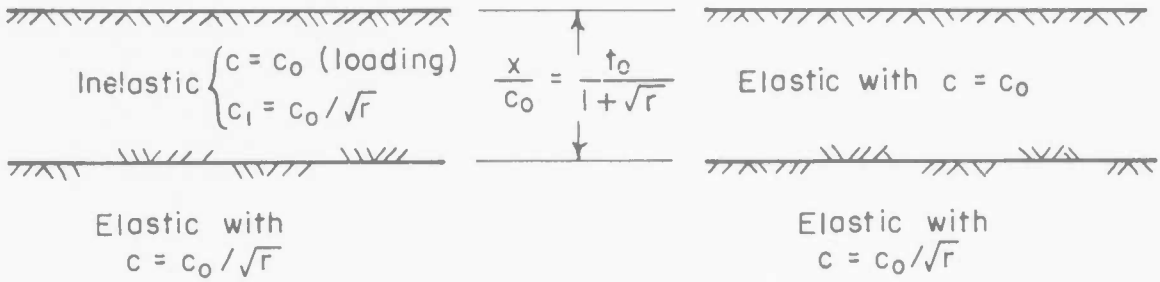

Part (a) Part (b)

FIGURE 4.12 EXAMPLE TO STUDY EFFECT OF IRREVERSIBILITY UPON SURFACE DISPLACEMENTS

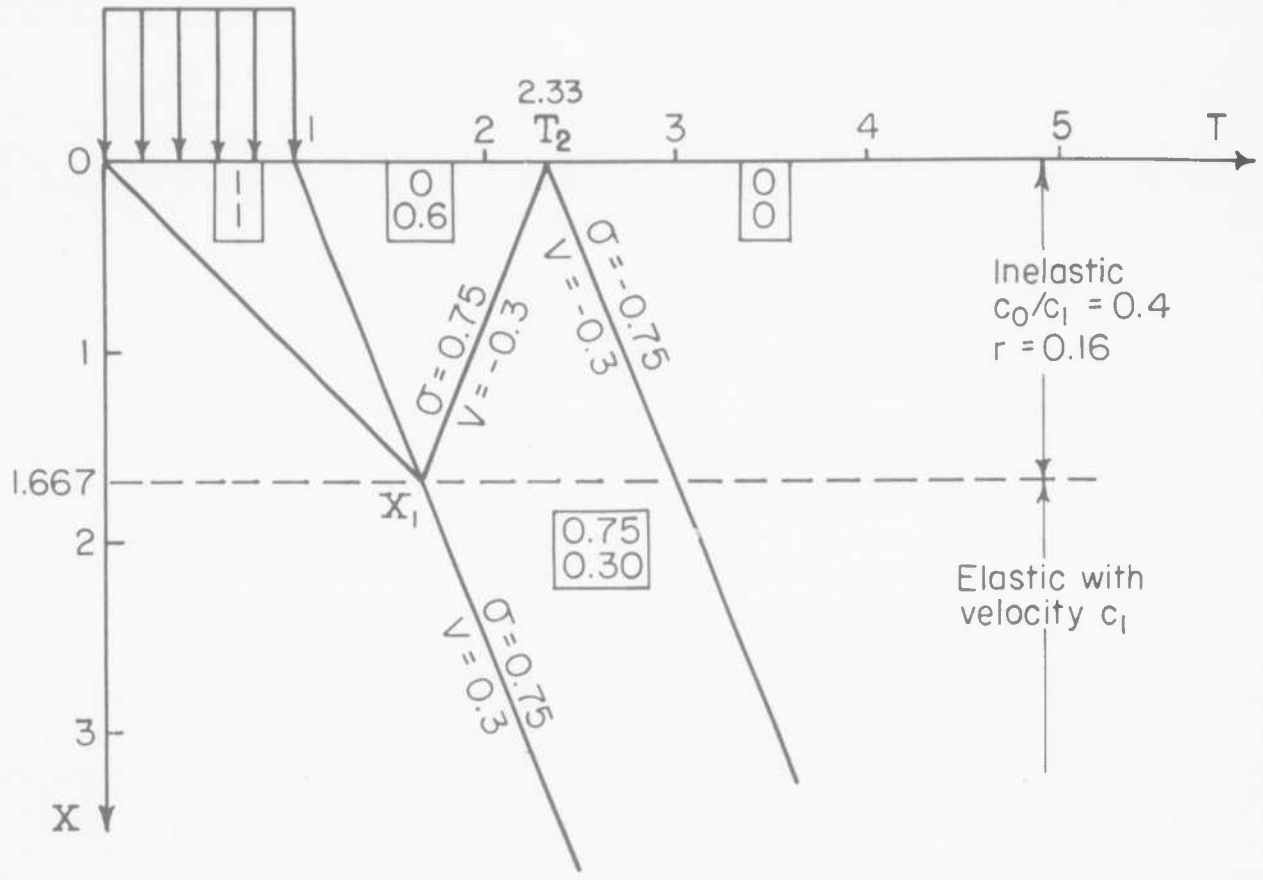

(a)

FIGURE 4.13 EXAMPLE TO ILLUSTRATE E
UPON DISPLACEMENTS AT D

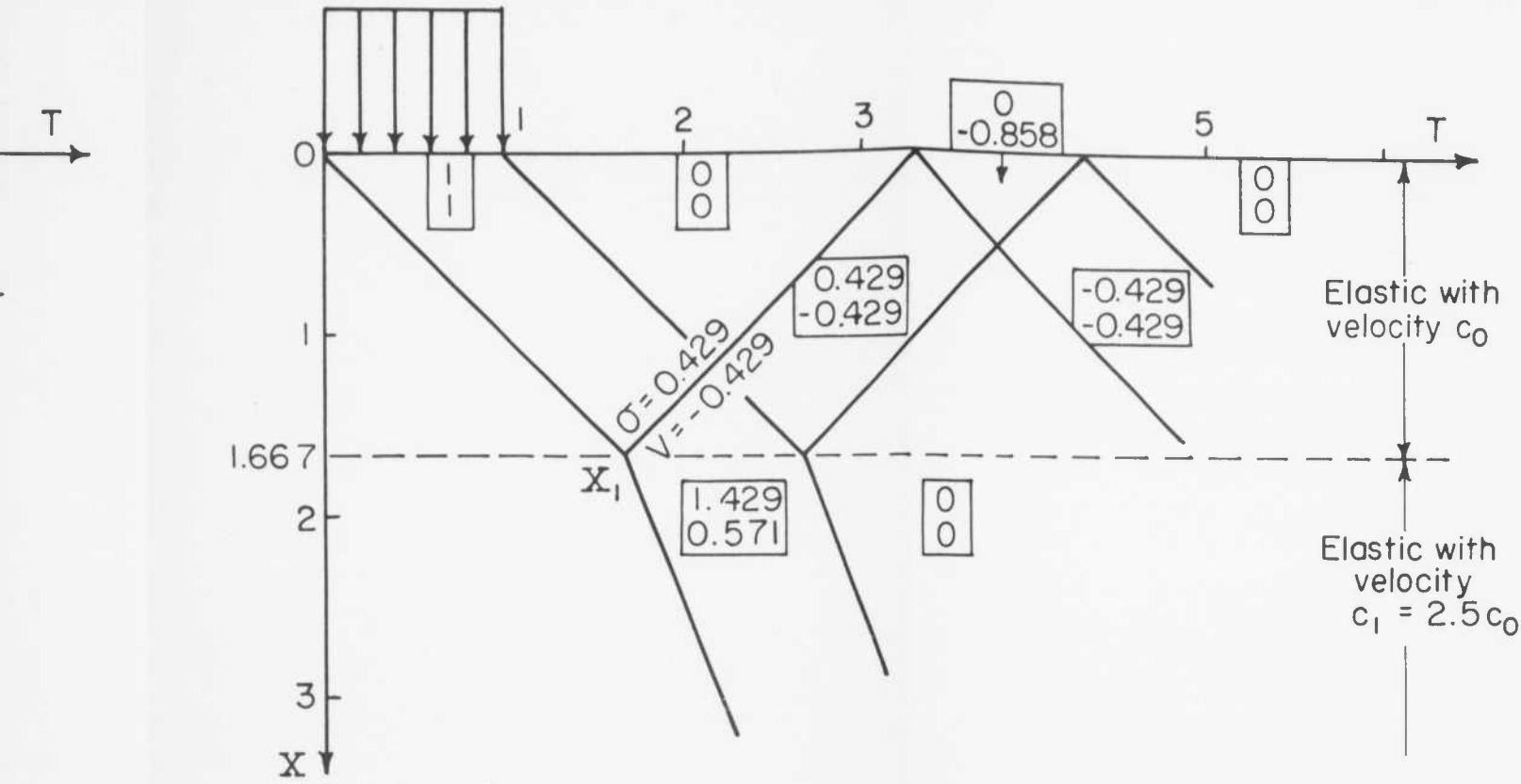

(b)

TRATE EFFECT OF IRREVERSIBILITY
TS AT DEPTH

Chapter 5

SUMMARY AND FINAL REMARKS

This report has summarized the available data regarding time-dependent, irreversible and non-linear effects during rapid one-dimensional compression of natural and reconstituted soils. Hopefully these data will be of use for future research into the problem of wave propagation through soils.

In addition, this report represents a first attempt to assess the possible importance of these non-elastic effects. The method used to analyze the data are relatively crude, and so too are the procedures used to evaluate the significant aspects of wave propagation behavior. A considerable amount of intuition and judgment has been used throughout, based in large measure upon the writer's experience while evaluating sites for ICBM bases. Nonetheless, it is believed that this study has helped focus attention upon the truly important aspects of soil behavior.

5.1 Predicting free field effects from explosion of megaton size

5.1.1 Stress attenuation

Irreversible or time-dependent stress-strain behavior causes attenuation of peak stress with distance. Using the data presented in this report, this attenuation was found to be of no practical significance for the type of design problem under consideration.

The tests described in this report do not preclude the presence of very short relaxation times; e.g. less than 1 millisecond. If such effects are actually present in soils, stress attenuation might begin to be of practical significance, especially for the higher overpressure levels.

The following patterns of behavior have been deduced for those cases where it makes sense to assume that a column of soil is essentially in a one-dimensional state of strain.

5.1.2 Ground motion predictions

In any ground motion prediction scheme, it is necessary to choose a "design propagation velocity". A value of c is needed when using Equations (1.1) and (1.2); a value of c_o is needed when using equations based upon visco-elasticity or irreversibility. The problem is to choose between the seismic wave propagation velocity and the "effective" propagation velocity deduced from the results of laboratory compression tests. If results from the first rapid loading of a compression test are used, the ratio between these two velocities ranges between about 2 and about 7 for typical undisturbed soils (see Table 3.3). In order to minimize the effects of sampling distrubance and testing errors, it is often suggested that the "effective" velocity should be based upon the second or subsequent loading. Again using results in Table 3.3 the ratio of the two velocities still ranges from 2 to about 5.

If time-dependent and irreversible phenomena are present, certain errors will arise from the use of Equations (1.1) and (1.2). The analyses in the preceding sections, however crude and inexact, provide a basis for estimating the probable magnitude of these errors.

Percentage Error at Ground Surface

	Max. Disp.	Max. Part. Vel.
Time-dependency	10	10
Irreversibility	10	0

Percentage Error at $^{x}/c$ = 0.1 Second

	Max. Disp.	Max. Part. Vel.
Time-dependency	10	20
Irreversibility	20	10

These errors are all less than the basic uncertainty as to the "design propagation velocity". Hence, at the present time, an engineer can properly use the simple Equations (1.1) and (1.2), and focus his attention upon the choice of the "design velocity".

The data presented in this report suggest one mechanism which may contribute importantly to the magnitude of the peak particle acceleration: the shape of the stress-strain curve, as shown in Figure 3.13. As yet, however, it is not possible, on the basis of laboratory data, to make quantitative statements regarding peak acceleration.

5.1.3 Selection of "Design Velocity"

On one hand, there is a sound reason to believe that the "design velocity" should be less than the seismic velocity; i.e. when large stresses are applied, the mineral skeleton of a soil breaks down as shown in Figure 3.13. On the other hand, the velocity deduced from laboratory compression tests is probably too small, as the result of testing and sampling errors. If the engineer judges that the mineral skeleton is well cemented so that the earth is rock-like, he should select a "design velocity" which is close to the seismic velocity. Otherwise, the engineer should select a "design velocity" closer to that deduced from laboratory tests.

5.2 Analysis of free field effects measured during explosion of kiloton size

In the case of small explosions, time-dependent and irreversible effects, especially the latter, can cause significant stress attenuation over depths such as 50 to 100 feet. It would seem that such effects must be considered when analyzing and interpreting the results from typical field test programs, especially since many of these tests involve relatively compressible soils. In so doing, it will be necessary to learn more concerning the presence or absence of relaxation times of less than 1 millisecond. It is, of course, also necessary to take cognizance of deviations from the condition of one-dimensional strain.

5.3 Problems for further study

One problem area stands out from this study: the discrepancy between seismic velocity and the "effective" propagation velocity back-figures from laboratory compression tests. The engineer must understand the causes of this discrepancy in order to select a "design velocity" on which to base ground motion predictions. The scientist must resolve this discrepancy before it will be possible to improve prediction techniques.

There would seem to be three possible explanations for this discrepancy.

(a) The stress-strain curve for soil during a very rapid loading has the shape indicated in Figure 3.13. Research to clarify this point is now underway under the present contract.

(b) There are very short relaxation times (less than one millisecond). Even if Figure 3.13 is a correct representation of stress-strain behavior, the extent of the first section of this curve (the part that is concave to the strain axis) may increase as the rise-time decreases. Tests to clarify this point must take due account of wave propagation phenomena within the test specimen.

(c) The discrepancy arises from errors inherent in laboratory tests, especially the disturbance of the soil during sampling. For an in situ soil, the first part of the stress-strain curve (that concave to the strain axis) may extend further than indicated by laboratory tests upon a sample of this soil. This possibility can be examined only by in situ dynamic loading tests.

5.4 Conclusions

When predicting ground motions caused by an explosion, the major problem is the selection of a "design wave propagation" velocity for the soil. While the stress-strain relation of soils is time-dependent and irreversible, the typical influence of these effects is less (on the basis of data now available) than the uncertainties in the selection of the "design velocity".

To reduce these uncertainties, further research must include field loading tests and laboratory tests involving rise-times less than 1 millisecond.

Appendix A

FIRST SERIES OF CYCLIC LOADING TESTS

PREFACE

The material in this appendix is based upon a thesis "A Study of Hysteresis in Granular Soils" submitted in May 1961 by James M. Roberts in partial fulfillment of the degree of Master of Science. Mr. Roberts was a full-time student, but was subsidized by the Dynamics Research Project to a minor degree; i.e. instrumentation and apparatus, additional parts, etc.

LIST OF FIGURES

1 Specimen Container
2 Details of Teflon Sleeve
3 Calibration for Apparatus Deformation
4 Various Forms of Hysteresis Loop
5 Change in Loop with Number of Cycles
6 Illustration of Terminology
7 Loops for Series 1
8 Loops for Series A
9 Loops for Series B
10 Loops for Series C
11 Loops for Series D
12 Loops for Series E
13 Loops for Series F
14 Modulus and Energy Loss vs. Minimum Pressure
15 Interpolated Curves for Modulus and Energy Retention
16 Energy Loss vs. Average Pressure

LIST OF TABLES

I Properties of Loop vs. Number of Cycles
II Results of Hysteresis Tests

1. Scope

This report covers a series of one-dimensional compression tests upon standard Ottawa sand (20-30 mesh) at a void ratio of 0.51. The axial stress was applied to the specimen at the rate of 10 cycles per minute, using a stress-time variation which was approximately sinusoidal. A minimum of several hundred cycles of stress was applied for each test condition; sometimes there were several thousand cycles. Stress and strain were recorded continuously and simultaneously, during both the loading and unloading portions of the cycle, in such a way as to show the size and shape of the hysteresis loops.

2. Objectives

The primary objective of these tests was to determine the energy loss per cycle of loading. Information regarding the magnitude of this energy loss is important in foundation vibration problems, such as the design of foundations for precision tracking radars, and is also of interest in wave propagation problems. A secondary objective was to determine the one-dimensional modulus following many cycles of loading, so as to compare the modulus thus measured with that backfigured from seismic velocity determinations.

The loading rates used in these tests were not within the dynamic range. However, all previous research has indicated that there is no dramatic change in the compressive behavior of sands as one moves from slow to very rapid rates of loading (for example, see Report No. 3). The test conditions used herein were selected to provide useful information regarding energy loss and modulus while avoiding the complications which arise from the use of very rapid loading rates. The one-dimensional test configuration was chosen so as to emphasize the behavior during compression and to minimize the effects associated with shearing action.

3. Apparatus

The general configuration of the apparatus is shown in Figure 1. The steel "pot" is the same piece of equipment used in the work described in Reports 3 and 4. The well in which the specimen is contained is 3.50 inches in diameter and 1 inch deep. Stress is applied by air pressure acting against a piston which covers the

full face of the specimen. The piston is 1/8 inch thick, leaving a specimen thickness of 0.875 inch. The piston fits "loosely" within the walls of the well, and a rubber membrane covering the piston prevents air pressure from reaching the void spaces of the specimen.

A crude but rather ingenious system was rigged for controlling the pressure applied to the specimen. Compressed air was supplied to this system at a constant pressure. A flap valve moved by a cam arrangement allowed varying amounts of air to leak from the system, thus establishing the desired sinusoidal pressure-time pattern. The pressure actually supplied to the specimen container was measured by a Dynisco pressure transducer.

The general arrangement of the strain measuring system is shown in Figure 1. A thin rod attached to the underside of the piston passes through a teflon sleeve to a displacement transducer (linear variable differential transformer manufactured by the Schaevitz Co.) located beneath the specimen holder. The details of the teflon sleeve are shown in Figure 2. It was found from preliminary experiments that such a sleeve was essential to minimize the effect of frictional forces acting against the thin metal rod. Schaevitz transducers with 0.020 and 0.040 inch linear ranges were used in these experiments. A rectifier circuit was built to convert the output of the Schaevitz transducer into a D.C. signal.

Stress and strain were displayed against each other on the Mosley "autograph" X-Y recorder. This recorder has a mechanical response time of about one second, and thus the recording system would accurately trace the stress-strain patterns (the hysteresis loop) during the 6 second period of the loading cycle.

4. Preliminary Tests and Final Procedures

In order to check for possible deformations within the test apparatus itself, a steel slug approximately 1-1/2 inches in diameter was loaded within the apparatus, as shown in Figure 3.* A typical hysteresis loop observed during this calibration test has been shown in the figure. The apparent modulus of the steel slug as calculated from the tests results was on the order of 10^6 lbs/in^2. This low result might indicate either that the steel slug seated imperfectly or that there was some measurable deformation of the test apparatus. In

*See addendum to this appendix.

either event, however, the measured modulus far exceeds that of the sand to be tested, and any errors resulting from apparatus deformability are of no consequence in the modulus determination. On the other hand, the energy loss per cycle during this calibration test was of significant magnitude (5-10%) with regard to the interpretation of the test results for sand.

Although the ratio of specimen thickness to diameter was chosen so as to minimize the possible effects of side friction, there was still some concern regarding side friction. Moreover, it was possible that friction forces between the piston and the walls of the specimen container, and between the thin rod and the teflon sleeve, might affect the results. A number of preliminary tests were conducted, and several treatments for the walls of the specimen container were investigated. The hysteresis loops obtained from these tests are compared with a "good" loop in Figure 4. Part (c) of this illustrates the result obtained when the piston did bind against the walls of the container. When this type of result was encountered during the test program, the apparatus would be dismantled and the piston rotated to re-establish a loose fit. Part (d) of the figure illustrates the type of result obtained when a sand grain would become trapped within the teflon sleeve, thus impeding the movement of the rod leading to the transducer. When this type of result was obtained, the apparatus would again be dismantled and the sand cleaned from the sleeve. The extreme loop illustrated in Part (b) of the figure was obtained from tests when a 1/8 inch thick rubber lining was used around the wall of the specimen container. A number of effects, including bearing of the piston against this liner, lead to this rather startling loop; needless to say, this scheme was abandoned. The use of a synthetic rubber membrane lining only 0.05 inch thick was also investigated, but the results with this wall treatment were no different from those with no wall treatment.

The procedure as finally used in the test program was as follows: the teflon sleeve was screwed into the container base leaving the tip approximately 1/4 inch above the proposed elevation of the specimen top. The sand was then placed in the container, the thin rod inserted into the sleeve, and the piston lowered to the top of the sleeve. Working from below the container, the sleeve was then lowered about 1/4 inch below the top surface of the specimen. The specimen was vibrated until

the piston top was flush with the top of the container, thus giving a known and reproducible volume of sand. The lid of the apparatus was then placed in position and loading commenced. After the loading had been carried to the point of apparent stabilization of the hysteresis loop, the entire load was removed and the sleeve screwed up to contact the piston, then lowered approximately 0.010 inch. The repeated loading sequence was then resumed with the thin rod well protected from frictional effects.

This procedure of allowing the specimen to stabilize under repeated loading before attempting to remove all of the frictional drag on the wire was found necessary, since the specimen accumulated some permanent strain during the process of initial stabilization. If the piston came to rest directly upon the top of the teflon sleeve, as a result of this cumulative strain, errors would be introduced into the measurement of strain within the specimen.

Once the test program described below was commenced, the sand was never removed from the apparatus. As described above, it was necessary upon occasion to remove the pressure acting against the specimen, and to disassemble the apparatus so as to free the piston or to clean the teflon sleeve. Since data regarding the hysteresis loops were taken only after many cycles of stress application, it was felt that the exact history of previous stress applications was of little consequence.

5. Results

During the first test, the hysteresis loop was recorded at a number of different times during the loading process in order to observe the process of stabilization. The results of this test are shown in Figure 5. As the loading process proceeded, the loops became noticeably "slimmer" and inclined more steeply. Thus the energy loss decreased and the average slope increased as the final stabilized condition was approached. The results in Table I illustrate this process of stabilization (the definition of energy retention and modulus are shown in Figure 6). In this test the process of stabilization was essentially complete at the end of 280 cycles.

The hysteresis loops observed during the regular test program have been reporduced in Figures 7 through 13. Note that these figures show direct reproductions of the loops as actually traced on the X-Y recorder. By manimpulating the controls of the X-Y recorder, the loop could be located at a spot on the graph paper which was convenient for recording, and the spacings between the loops is of no physical significance. Values of modulus and energy retention as calculated from these measured loops (a planimeter was used to obtain the areas for the energy retention calculation) have been listed in Table II. The hysteresis loops in Series I were recorded after approximately 4,000 cycles of stress application; the loops of the remaining series were recorded after approximately 200 cycles.

During analysis of the test results, it appeared that perhpas some of the tests had not been carried to the point of stabilization; i.e. some of the modulus values appeared to be too low while some of the energy retention values appeared to be too large. These questionable values were corrected as follows: Figure 14 shows plots of modulus and energy retention versus the minimum pressure for the tests in Series I (all of which were carried to at least 4,000 cycles of load application). All of the tests in Series I involved a stress change of approximately 1/2 atmosphere to either side of the average pressure. Each subsequent series of tests contained one test with $P_{variant}$ of approximately 1/2 atmosphere. The modulus and energy retention results for these "comparison" tests were adjusted until they fell on the curves of Figure 14, and all other test results for the same series were then adjusted in the same ratios.

6. Analysis of Data

In general, the test results showed just the trends which might be expected. An increase in the average stress, or a decrease in the variant stress, led to an increase in the modulus and a decrease in the energy retention.

The trends regarding the modulus are illustrated by the contours (based upon the corrected modulus values) shown in Figure 15. Note that there is a marked difference in the modulus for a minimum pressure of 0 and for a minimum pressure of, say, 3 lbs/in^2. Apparently, the mineral skeleton can spring apart when the minimum pressure

drops to within a few pounds per square inch of zero gauge pressure, thus leading to a greatly reduced modulus upon reloading. The effect of the last few pounds per square inch of unloading appears quite clearly in the shape of the hysteresis loops.

The data regarding energy loss have been plotted in Figure 16. The effect of the average pressure upon the energy loss is fairly clear. The effect of the magnitude of the stress excursion at fixed average pressure is not so clear, but can nonetheless be detected. It must be remarked that the numerical accuracy of the recorded energy loss values is rather low (the tabulation of these values to three significant figures is certainly misleading in this regard). This is especially true when the energy loss drops below 10 percent. Where values of less than 5 percent are recorded one can really only say that the energy loss is small. Indeed, it may be noticed from Figure 3 that a significant magnitude of energy loss was apparently encountered during the calibration test upon a steel slug.

Addendum

An independent check upon the stiffness of the apparatus was made in 1963. For this check, the thin rod leading to the transducer was glued to the inside of the sleeve (by now the sleeve was made of brass rather than Teflon) using an epoxy resin, and the tip of the sleeve was sealed with solder. Air pressure was then applied directly against the bottom of the container. The resulting deflection as measured by the displacement transducer indicated the presence of some bending distortion in the bottom of the specimen holder.

This test resulted in a substantially linear relationship between pressure and deflection, with the deflection reaching about 0.0002 inch under a pressure of 100 lbs/in^2. For a specimen of 1 inch thickness, this deflection would be equivalent to a modulus of 500,000 lbs/in^2. This new measurement of apparatus compressibility is within the range of uncertainty of the value quoted in Section 4 of this appendix, and is believed to be a more representative value. In the light of subsequent developments, it cannot be said that this amount of apparatus compressibility is always negligible. The results given in Appendices A and B have <u>not</u> been corrected for apparatus compressibility.

Table I

PROPERTIES OF LOOP VS. NUMBER OF CYCLES

Cycle	Modulus $lb/in^2 \times 10^{-4}$	Energy Loss %
10	2.88	19.7
25	3.02	17.0
50	3.10	13.5
100	3.12	12.5
280	3.16	10.5
580	3.07	10.3
1300	3.18	10.5
1520	3.12	10.4

Table II

RESULTS OF HYSTERESIS TESTS

	$P_{(average)}$ lb/in^2	$P_{(variant)}$ lb/in^2	$P_{(minimum)}$ lb/in^2	M_{II} lb/in^2 x 10^{-4}	E_R Percent
I	8.87	7.62	1.25	1.88	20.6
	9.62	8.12	1.50	2.31	20.7
	9.50	7.25	2.25	2.81	16.0
	11.00	7.50	3.50	3.20	11.6
	12.38	7.38	5.00	4.08	8.3
	13.88	7.38	6.50	4.26	7.2
	16.00	7.25	8.75	5.00	5.9
	18.38	7.88	10.50	5.39	4.4
	21.00	7.50	13.50	5.80	5.2
	23.62	7.62	16.00	6.15	3.2
	25.75	7.75	18.00	6.50	2.6
A	15.37	0.25	15.12	5.69(5.44)	Small
	15.82	0.70	15.12	5.60(5.36)	"
	16.00	0.88	15.12	5.56(5.32)	"
	17.00	1.88	15.12	5.66(5.42)	"
	17.50	2.50	15.00	5.64(5.40)	"
	18.12	3.12	15.00	5.64(5.40)	"
	18.75	3.75	15.00	5.70(5.45)	2.3
	19.37	4.37	15.00	5.83(5.58)	1.7
	20.12	5.12	15.00	5.83(5.58)	2.1
	20.62	5.62	15.00	5.83(5.58)	3.0
	21.25	6.25	15.00	5.83(5.58)	3.9
	22.25	7.75	15.00	6.05(5.79)	2.7
	22.88	7.88	15.00	6.05(5.79)	2.2
	23.37	8.25	15.12	6.10(5.84)	3.1
	23.88	8.88	15.00	6.01(5.75)	4.5
	24.63	9.75	14.88	6.10(5.84)	4.2
B	9.00	1.50	7.50	4.42(4.13)	Small
	10.00	2.50	7.50	4.47(4.19)	"
	11.00	3.50	7.50	4.46(4.18)	7.3(8.9)
	12.30	4.80	7.50	4.69(4.30)	6.8(8.3)
	13.38	6.00	7.38	4.73(4.43)	6.7(8.1)
	15.00	7.62	7.38	4.75(4.45)	6.0(7.3)
	15.88	8.50	7.38	4.81(4.51)	7.6(9.3)
	17.88	10.0	7.38	4.86(4.55)	8.4(10.2)
	18.63	11.25	7.38	4.87(4.56)	7.6(9.2)
	19.88	12.50	7.38	5.09(4.77)	9.0(10.9)

	$P_{(average)}$ lb/in^2	$P_{(variant)}$ lb/in^2	$P_{(minimum)}$ lb/in^2	M_H lb/in^2 x 10^{-4}	E_R Percent
C	5.25	1.50	3.75	3.10	Small
	6.00	2.25	3.75	3.12	7.5(9.3)
	7.00	3.25	3.75	3.08	8.3(10.2)
	8.00	4.25	3.75	3.08	13.0(16.0)
	9.00	5.25	3.75	3.12	14.0(17.3)
	10.75	7.00	3.75	3.32	10.2(12.5)
	12.13	8.38	3.75	3.51	11.5(14.2)
	13.00	9.25	3.75	3.54	12.2(15.0)
	14.37	10.62	3.75	3.73	11.6(14.3)
D	0.88	0.88	0.00	0.71	31.2
	2.30	2.30	0.00	0.88	21.8
	3.50	3.50	0.00	1.01	21.0
	4.75	4.75	0.00	1.30	20.4
	7.65	7.40	0.50	1.82	19.5
E	14.75	1.00	13.75	5.45(5.09)	Small
	15.00	2.00	13.00	5.45(5.09)	"
	14.75	3.75	11.00	5.10(4.92)	"
	15.12	5.12	10.00	5.00(4.74)	2.4(4.9)
	15.00	6.00	9.00	4.90(4.38)	4.5(9.0)
	14.88	7.38	7.50	4.75(4.17)	6.4(12.8)
	14.75	8.75	6.00	4.33(3.80)	8.0(16.0)
	15.00	10.00	5.00	4.00(3.73)	7.6(15.3)
	14.75	11.25	3.50	3.50(2.61)	8.0(16.0)
	14.50	12.25	2.25	3.05(2.29)	7.8(15.5)
F	10.62	7.62	3.00	3.11	9.7
	10.88	7.38	3.50	3.28	8.7
	9.12	6.12	3.00	3.06	8.0
	8.75	5.75	3.00	3.03	7.4
	7.50	5.00	2.50	2.71	7.9
	7.25	4.75	2.50	2.63	7.6
	5.75	3.75	2.00	2.32	7.8
	13.75	10.00	3.75	3.72	7.0
	13.50	11.50	2.00	2.85	10.3

Note: Where two values are listed, the one in parentheses are the original uncorrected value. Where only one value is shown, it is the uncorrected value.

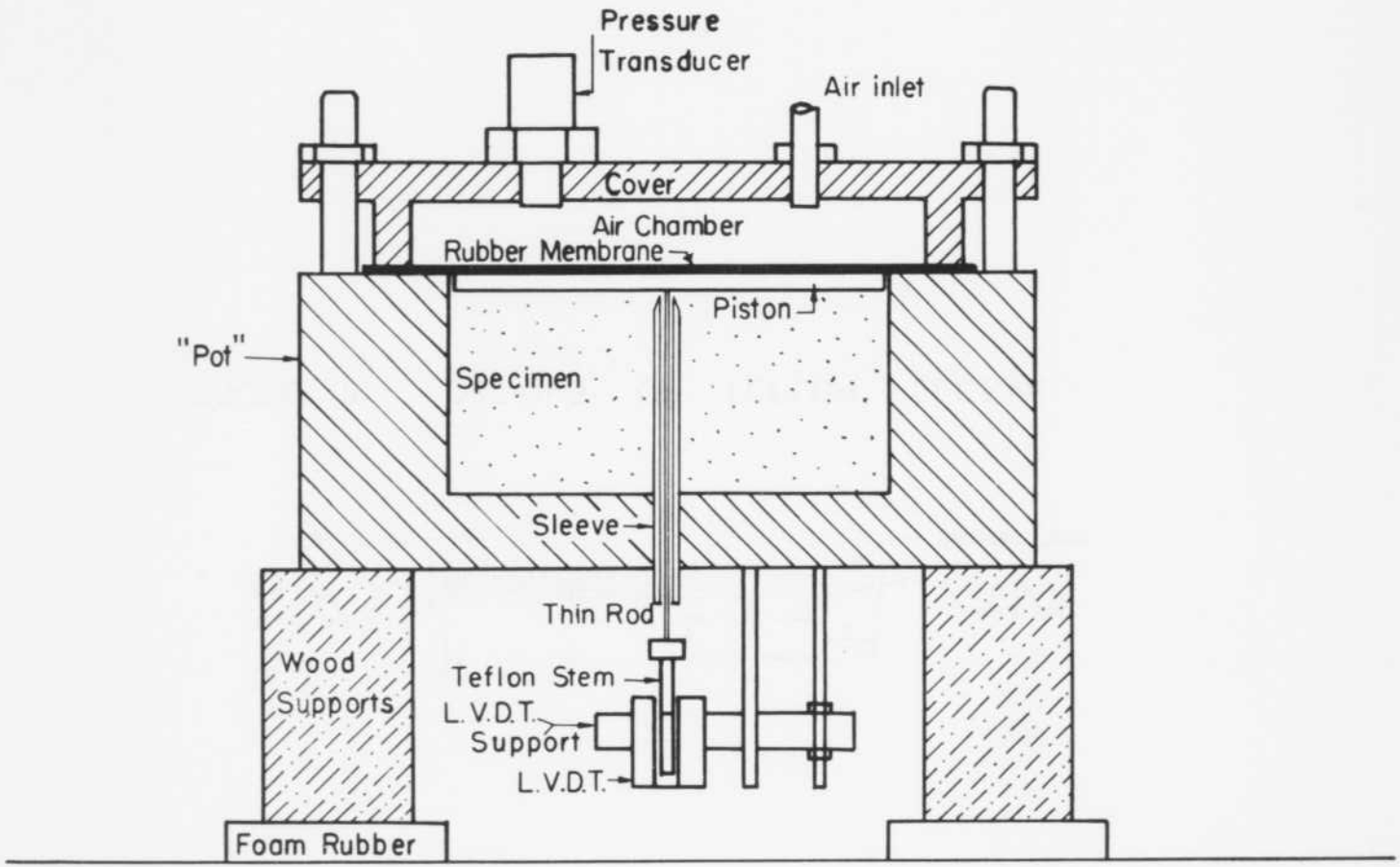

FIGURE 1 SPECIMEN CONTAINER

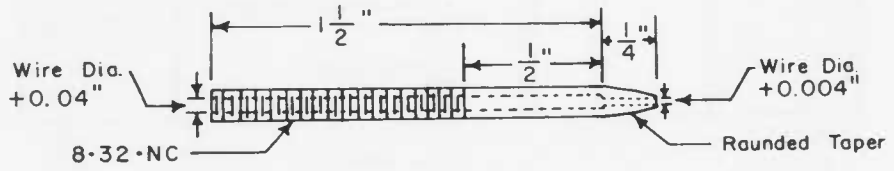

FIGURE 2 DETAILS OF TEFLON SLEEVE

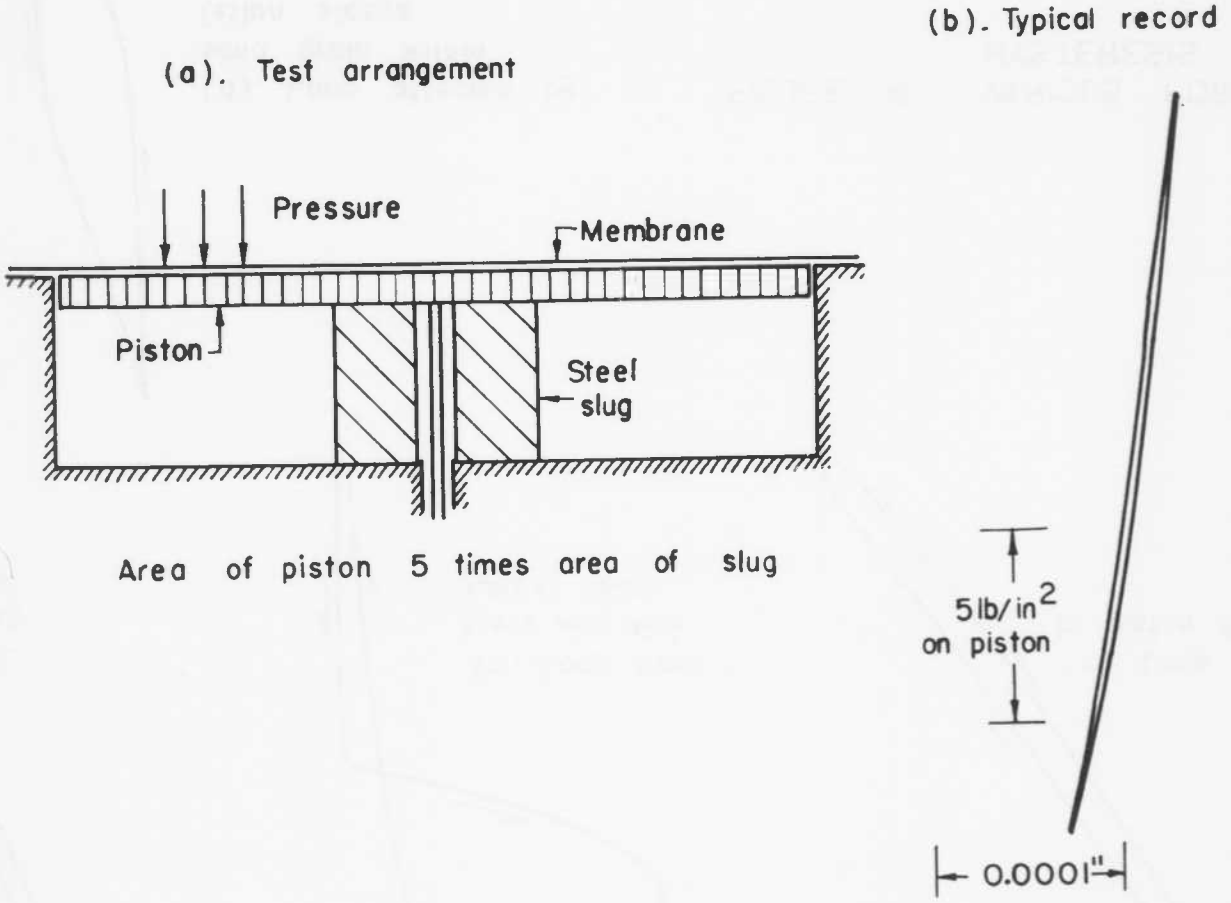

FIGURE 3 CALIBRATION FOR APPARATUS DEFORMATION

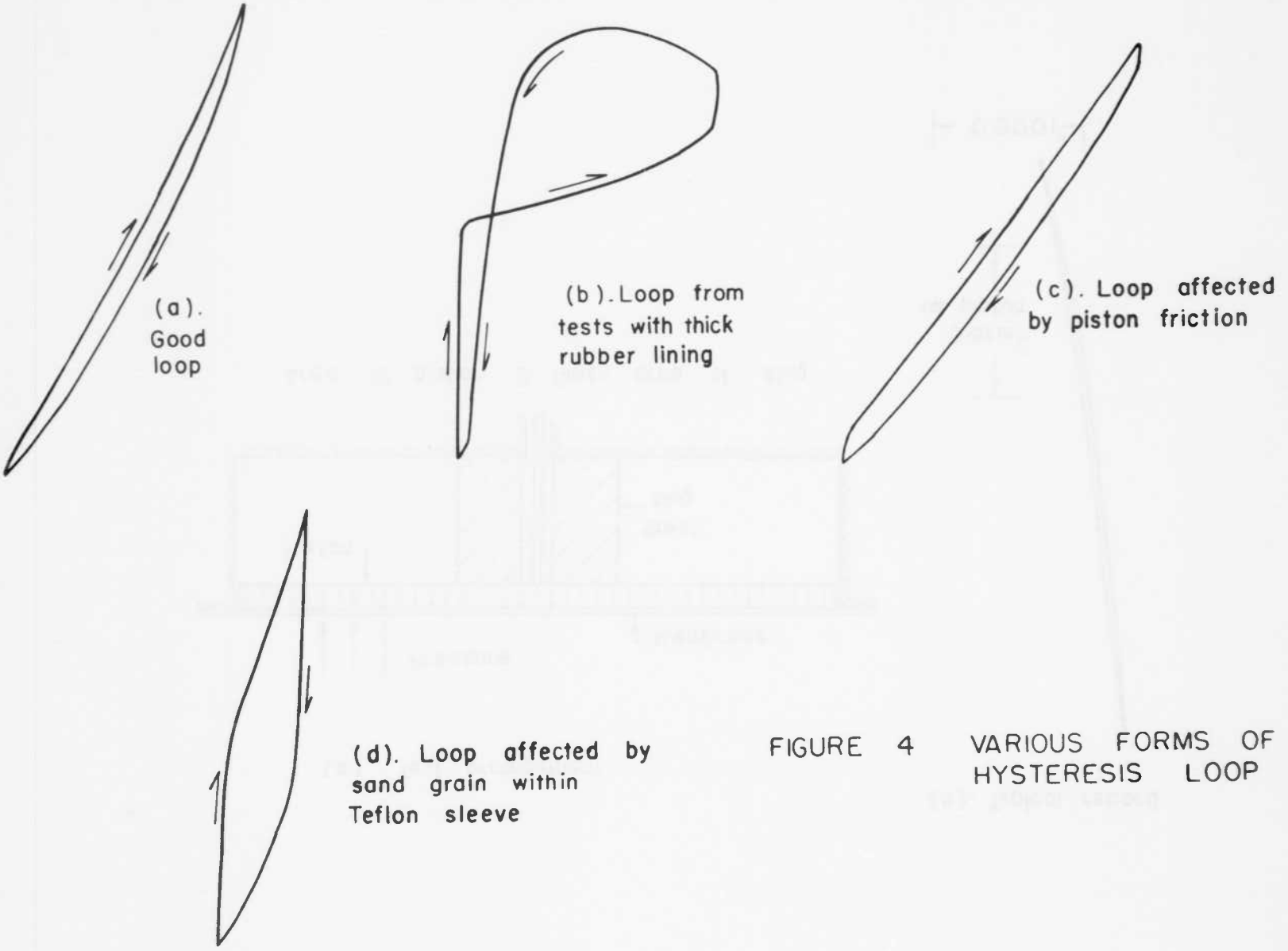

FIGURE 4 VARIOUS FORMS OF HYSTERESIS LOOP

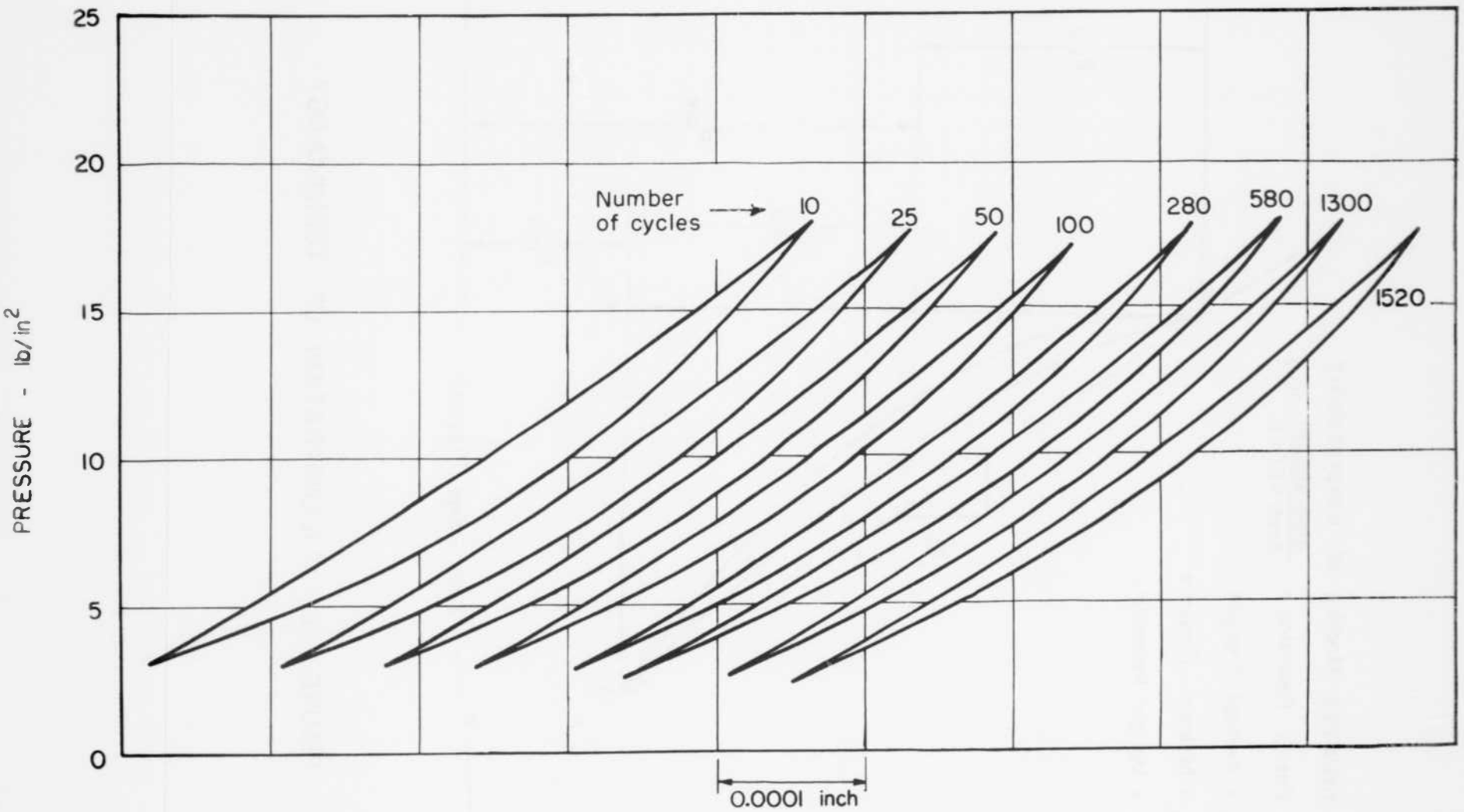

FIGURE 5 CHANGE IN LOOP WITH NUMBER OF CYCLES

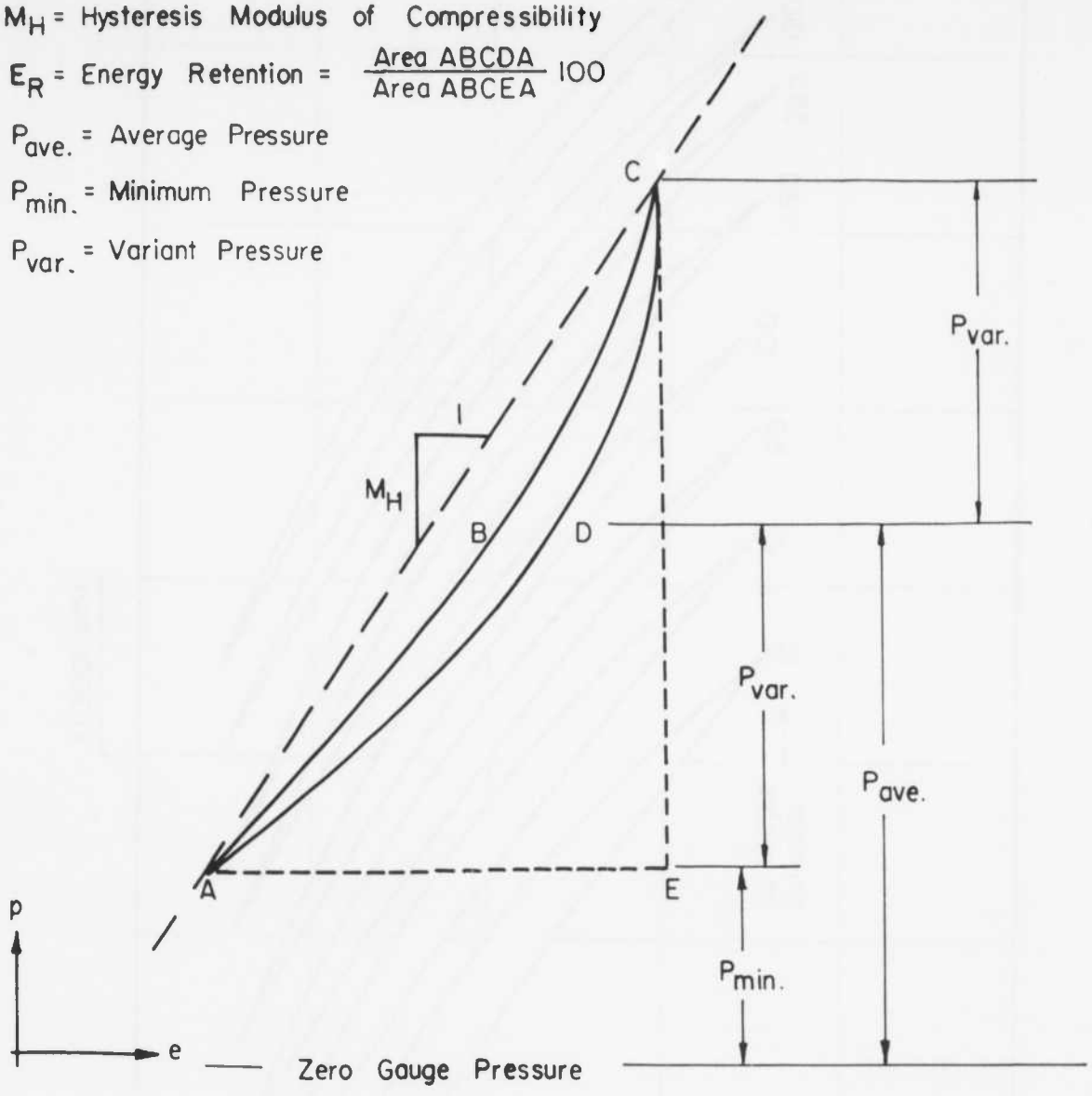

FIGURE 6 ILLUSTRATION OF TERMINOLOGY

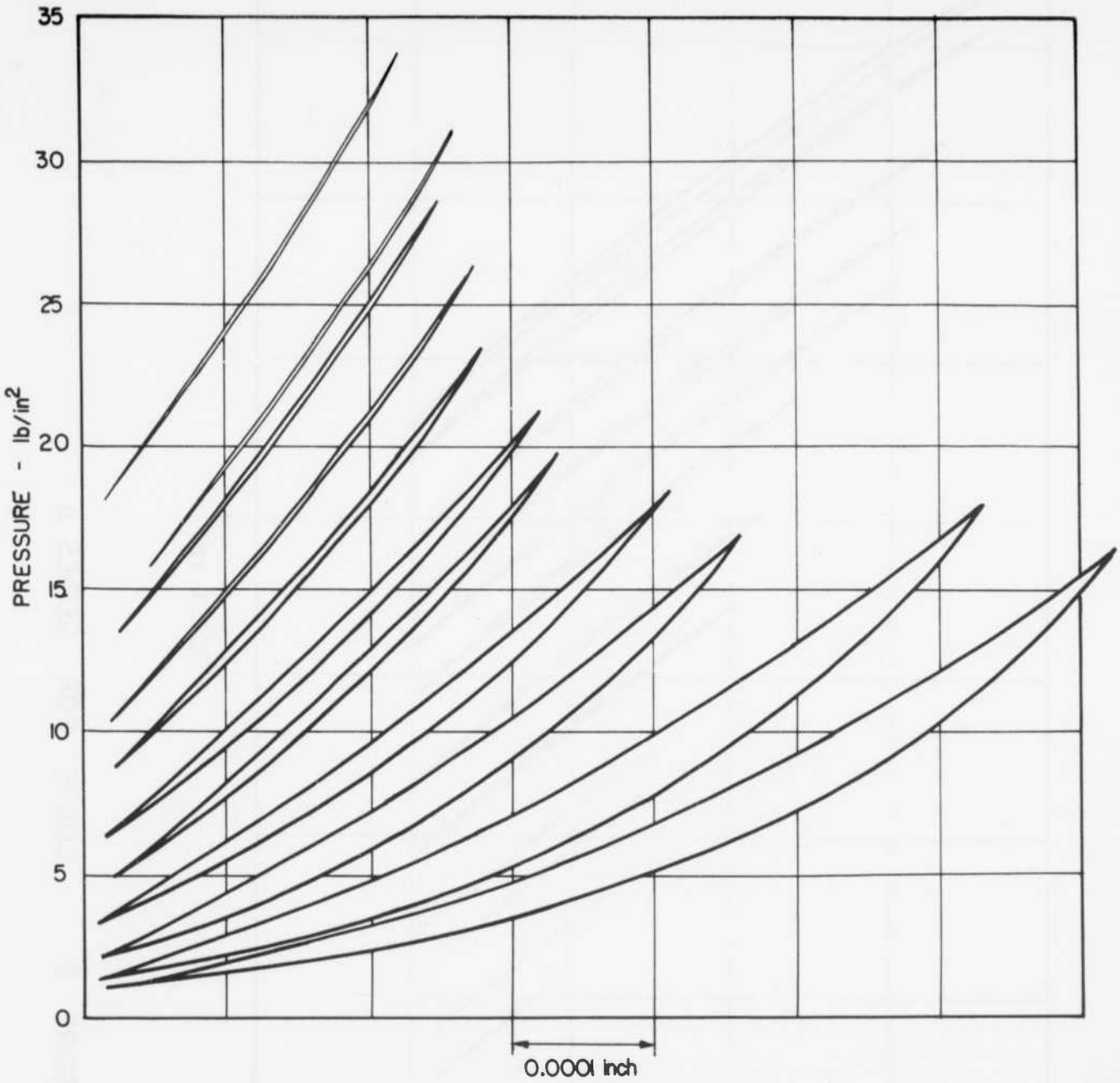

FIGURE 7 LOOPS FOR SERIES I

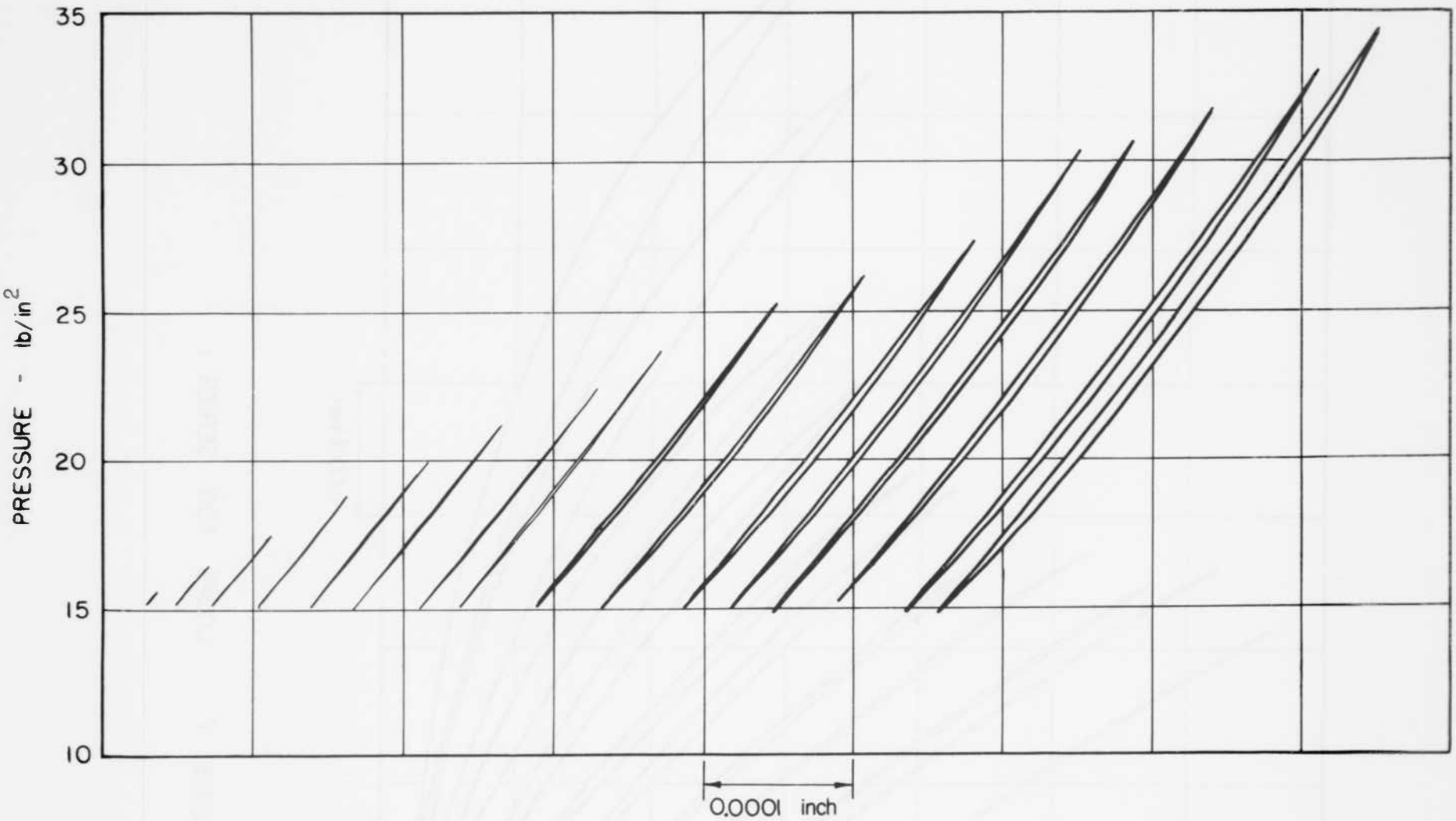

FIGURE 8 LOOPS FOR SERIES A

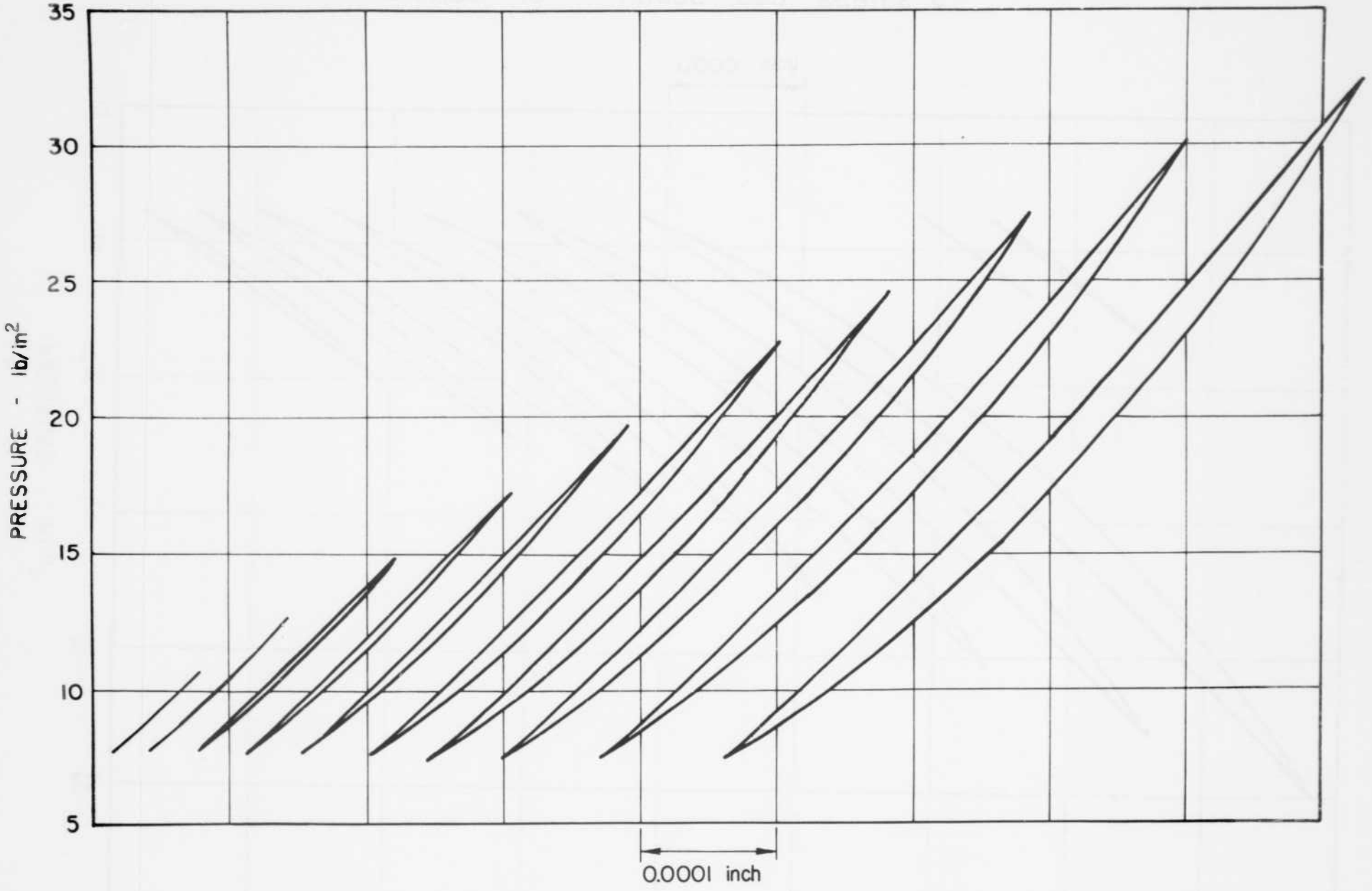

FIGURE 9 LOOPS FOR SERIES B

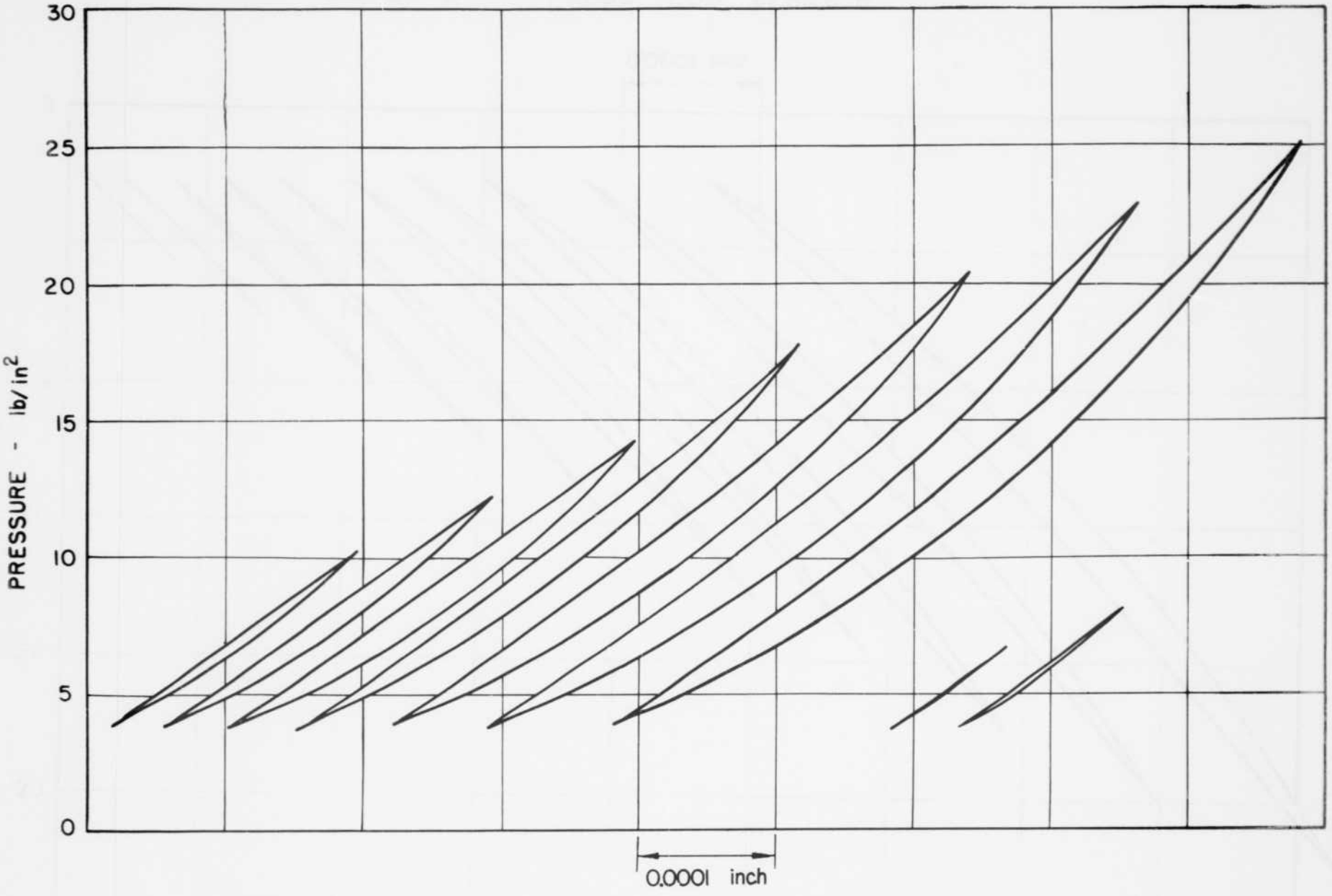

FIGURE 10 LOOPS FOR SERIES C

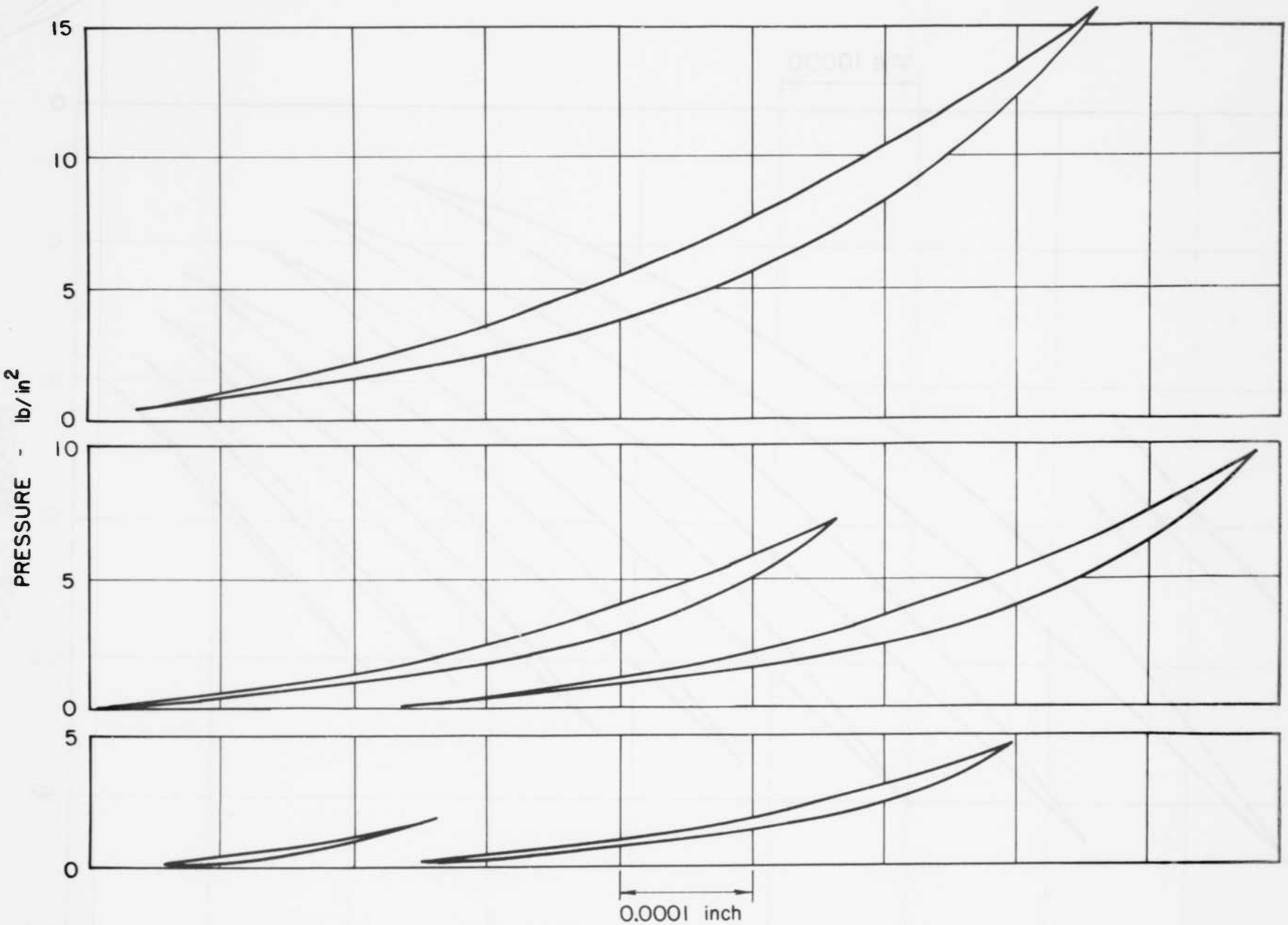

FIGURE 11 LOOPS FOR SERIES D

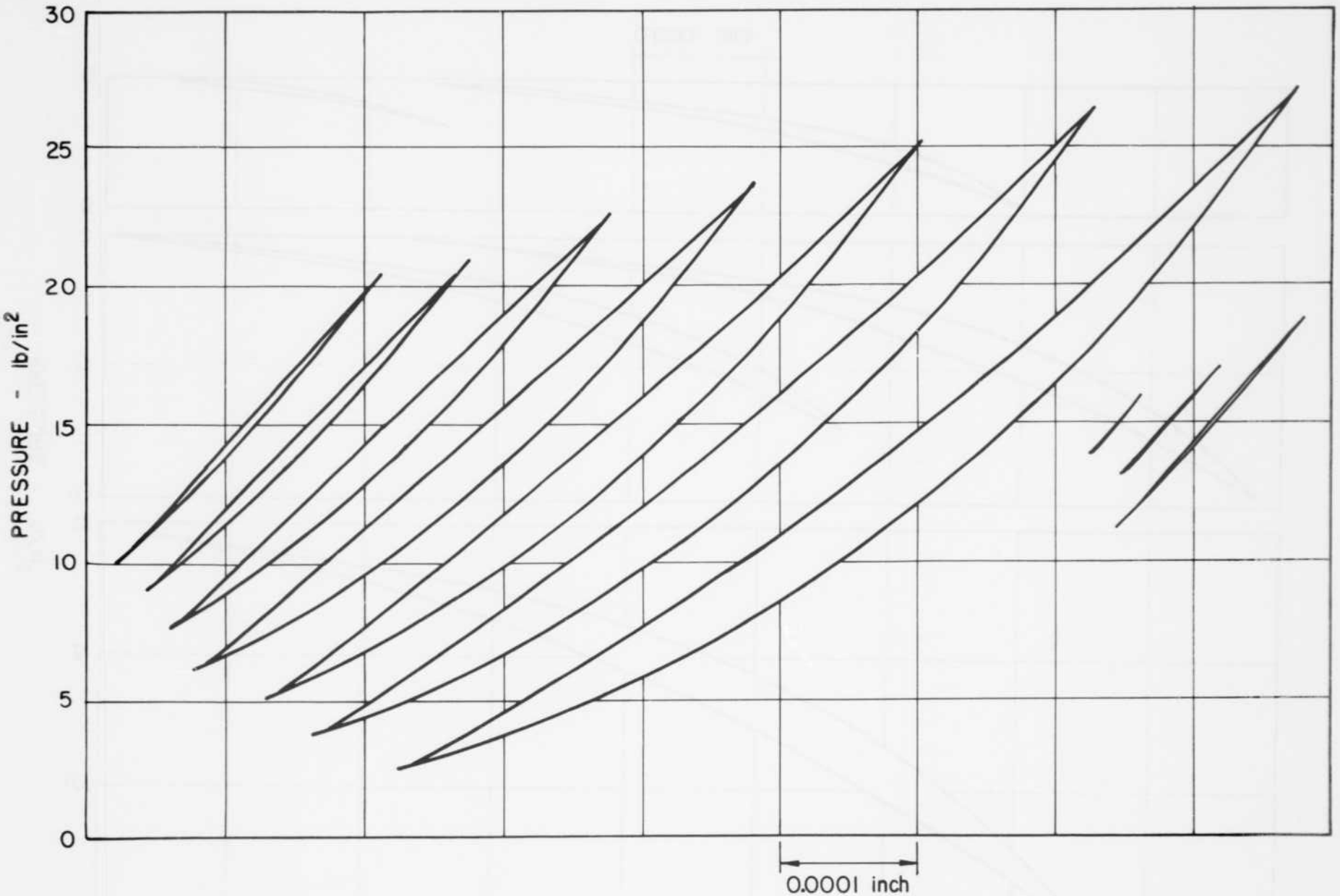

FIGURE 12 LOOPS FOR SERIES E

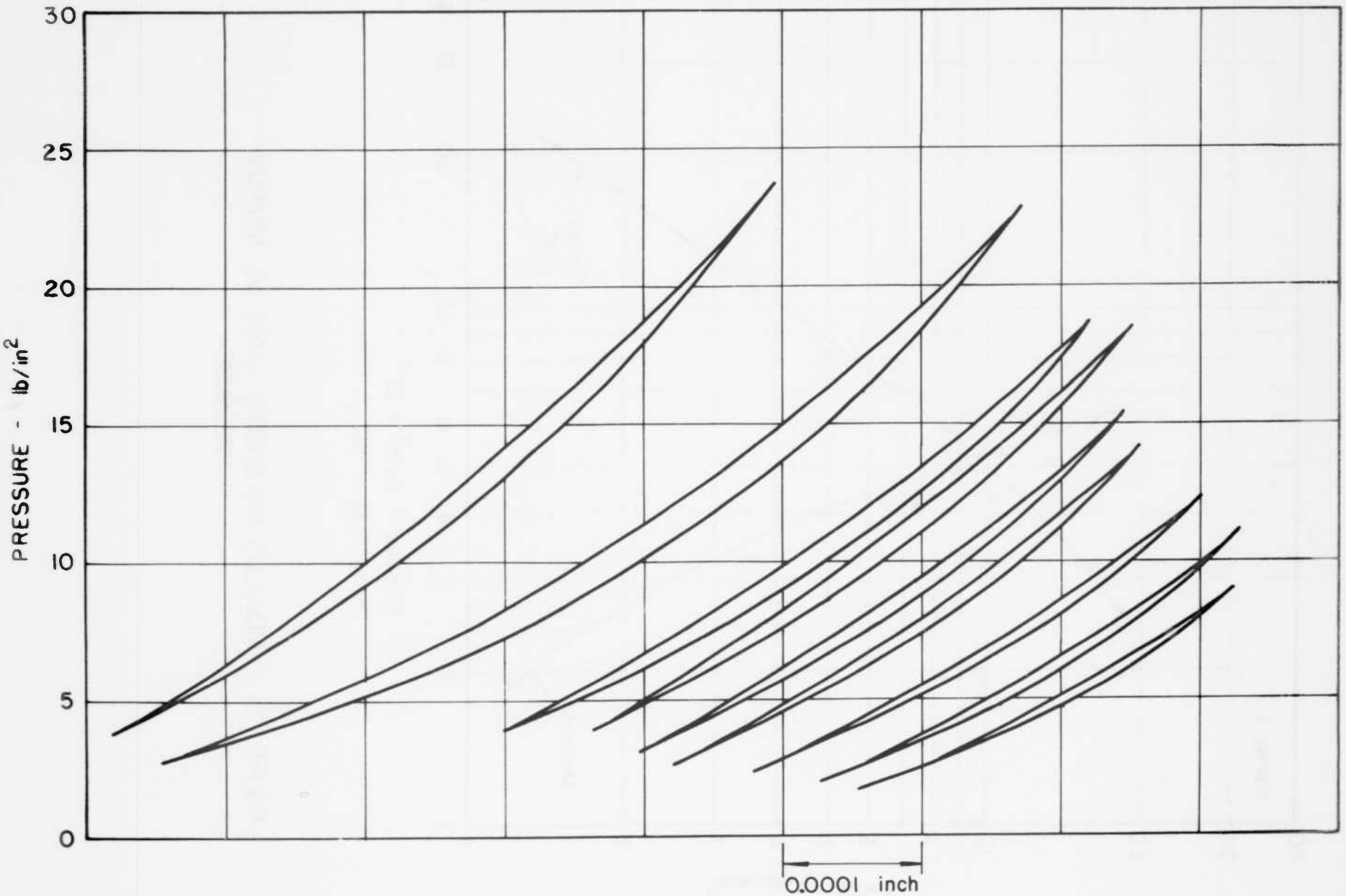

FIGURE 13 LOOPS FOR SERIES F

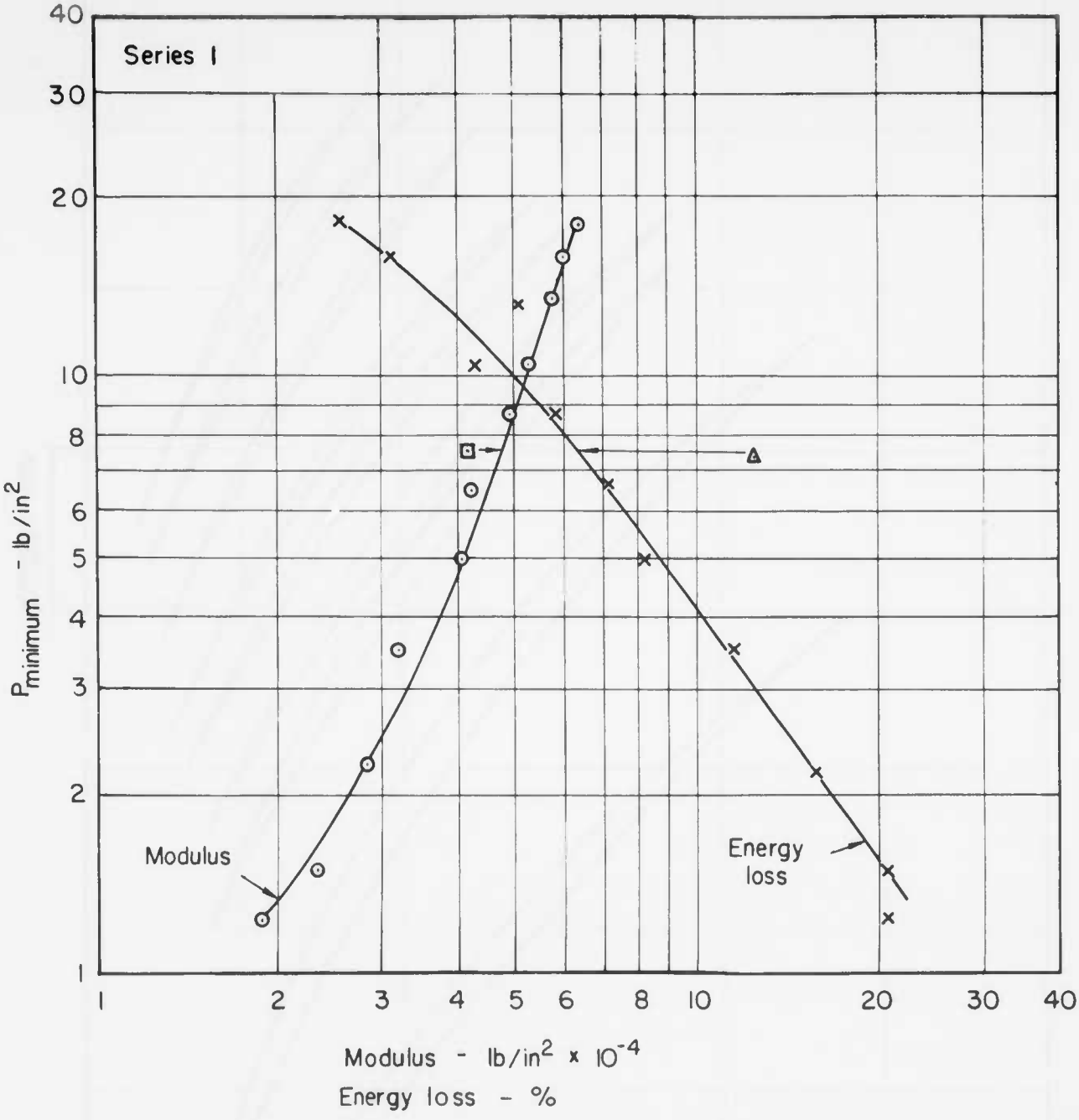

FIGURE 14 MODULUS AND ENERGY LOSS VS. MINIMUM PRESSURE

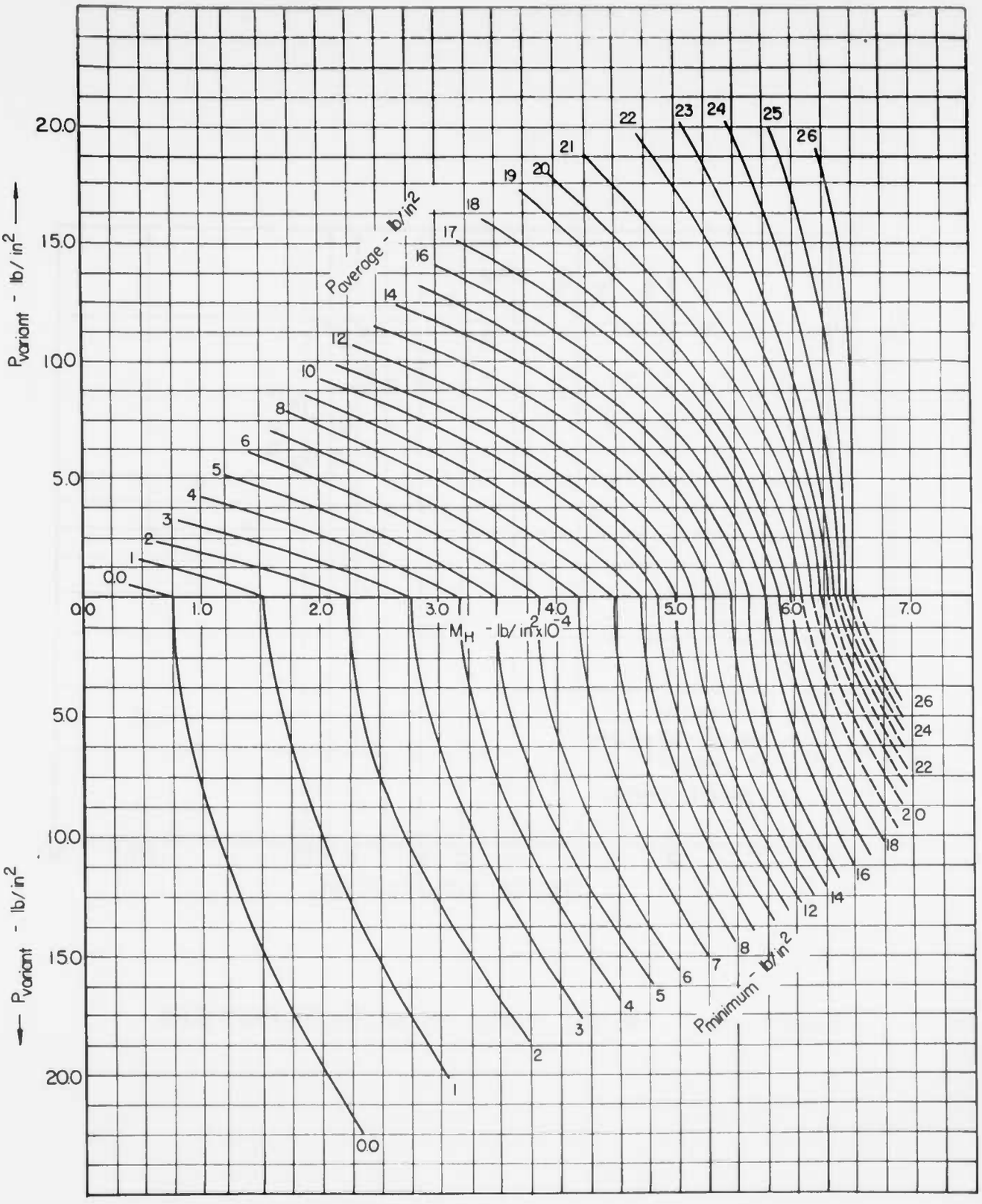

FIGURE 15 INTERPOLATED CURVES FOR MODULUS AND ENERGY RETENTION

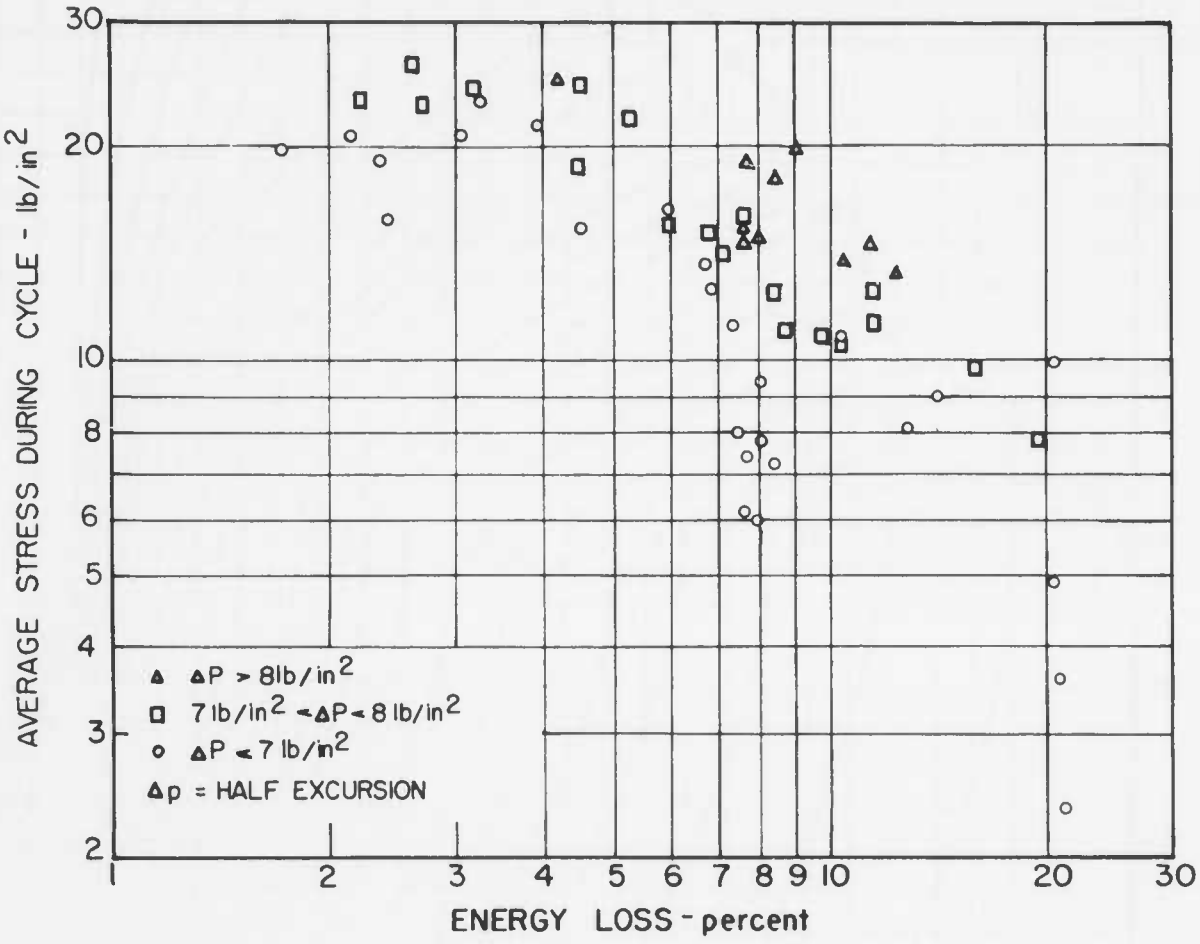

FIGURE 16 ENERGY LOSS VS AVERAGE PRESSURE

Appendix B

SECOND SERIES OF CYCLIC LOADING TESTS

PREFACE

The results described in this appendix represent the combined efforts of Messrs. Richard L. Ladd and Dennis J. Leary. During the time when this work was performed (fall and winter of 1961) Messrs. Ladd and Leary were students at Northeastern University and worked in the Soil Laboratory at M.I.T. during their co-operative work periods. Mr. Ladd initiated design and construction of the pressure control system used in this work. Mr. Leary completed the construction of this system, and devoted much time and painstaking effort to eliminating the "bugs" from the entire test apparatus. Mr. Ladd obtained the test results described herein, and this appendix is based upon a report "Measurement of Constrained Modulus and Hysteresis in Ottawa Sand under Repeated Loading" which he submitted to Northeastern University in January 1962 in fulfillment of his work period requirements.

LIST OF FIGURES

1 Pressure Regulating Device
2 Illustration of Terminology
3 Results for Series 1
4 Results for Series 2
5 Results for Series 3
6 Results for Series 4
7 Results for Series 5
8 Results for Series 6
9 Hypothetical Hysteresis Loop
10 Modulus from Tests with Constant Average Stress
11 Modulus from Tests with Constant Minimum Stress
12 Data Concerning Energy Retention

LIST OF TABLES

I Data for Modulus and Energy Retention

1. Introduction

The testing program described herein represents a follow-up to the earlier work of Roberts (Appendix A). A prime objective of the new testing effort was to ascertain the extent to which Roberts results could be reproduced. The focus of the work was however just reversed from that which guided Roberts work. In the new effort, the primary emphasis was upon the magnitude of the one-dimensional modulus and the factors which affected it, especially the size of the stress increment, and secondary emphasis was given to the determination of the energy retention factor.

These tests involved Ottawa standard sand at a void ratio of 0.53. Actually, both investigators (Roberts and Ladd) used extreme efforts to get their sand in as dense a condition as possible. Although the discrepancy between the void ratio in the present and in the past work can not now be resolved, it seems likely that this discrepancy resulted either/both from use of different specific gravities in the void ratio calculations or from use of different batches of sand with slightly different surface angularities.

2. Apparatus

There were only two modifications in the apparatus used earlier by Roberts. The rectifier circuit was rebuilt in such a way that a given strain would produce a larger motion on the X-Y recorder. Also, a new device was constructed for regulating the sinusoidally-varying pressure applied to the soil specimen.

The new system for controlling the pressure is shown in Figure 1. This new system permitted larger pressures to be applied, and also made possible the use of smaller stress increments. The minimum possible stress increment (ΔP) was 1 lb/in^2, while the largest possible increment was 30 lbs/in^2. The maximum over-all pressure that could be applied was 125 lbs/in^2.

3. Procedure

The test procedure was similar to that used by Roberts, save that the sand was generally replaced before the start of a test series, and in some tests great care was taken to record the modulus during the first cycle of loading. The sand was compacted into the well of the specimen container by tapping the piston into place with

with some small object such as a screw driver handle. The constant void ratio of 0.53 was obtained by adding a standard weight of sand and compacting until the top surface of the piston was flush with the corresponding surface of the specimen container.

After compaction, the piston was removed and the sand grains next to the top of the teflon sleeve pushed aside so that they would not be caught between the piston and sleeve during testing. The teflon sleeve was adjusted at this time to give a clearance of about 0.010 inches between the sleeve and the piston. The piston was returned to position, and the displacement transducer adjusted to give zero voltage output. Finally, the rubber membrane and apparatus cover were put into place and the air chamber filled with water (to minimize the volume of air flowing to the chamber) before the pressure transducer was attached. The pressure was cycled at 10 cpm. Between each test of a series, while the pressure was being adjusted for the next test, it was necessary to reduce the applied pressure all the way to zero.

4. Results

The terminology in this appendix is shown in Figure 2. The pressure increment ΔP here refers to the change between minimum and maximum pressure, whereas $P_{variant}$ as used by Roberts was the change in stress on either side of the average stress.

Most of the hysteresis loops recorded during this testing effort have been reproduced in Figures 3 through 8. On the basis of some preliminary tests by Leary, these loops were obtained after 500 cycles of loading. The strain axis runs the long way of these figures while the pressure axis extends along the short length of the paper. The loops in these figures have been traced directly from the loops actually recorded by the X-Y recorder. The position of the loop on the paper, and the scale along the pressure axis, have been arbitrarily selected for convenience. The scale along the strain axis is the same for all figures (see Figure 3).

Table I contains a complete listing of all modulus values and energy retention factors calculated from the recorded hysteresis loops. The energy retention was obtained by measuring the length and average thickness of the loops, rather than by use of a planimeter as done by Roberts.

5. Discussion of Results

The general shape of the hysteresis loops recorded during this renewed testing effort is shown in Figure 9. The loops typically exhibited steep portions at the beginning of both the loading and unloading curves. These steep portions were more-or-less prominent depending upon the size of the stress increment and the scale to which the loops were recorded. The loop shown in Figure 9 is similar to that which Roberts attributed to the effects of piston friction, and the "good" loops in Roberts thesis generally showed sharp tips. However, Ladd (and especially Leary during the preparatory work) found that these steep initial portions could be made to appear or disappear by adjusting the controls on the X-Y recorder which supressed higher frequency signals. As indicated by the comments on Figure 9, it is possible to rationalize the existence of these steep initial portions on the grounds of the physical behavior of sand. It is still an open question whether these steep initial portions represented a real aspect of the behavior of the sand, or are the result of some shortcoming in the testing apparatus and procedure.

Figures 10 and 11 show the modulus as a function of the stress increment. With constant average stress, an increase in the stress increment led to a decreasing modulus. Naturally, increasing the average stress level gave a higher value of modulus for any stress increment. On the other hand, with constant minimum pressure, the modulus was more-or-less constant with increasing stress increment, but with some interesting deviations from this "constant" value at very small stress increments. In the tests with a constant minimum pressure, the average pressure level increased with increasing stress increment. Using the data shown in Figure 10 and taking into account the effect of changing both average pressure and pressure increment, it proved possible to predict the general magnitude and trend of the curves in Figure 11. As discussed above, it is possible that the high values of modulus at very low stress increments were influenced by piston friction, especially since some of these values were greater than those backfigured from seismic velocity determinations for this sand (see Number 14 project report by Lawrence). In general, the agreement between modulus values shown in Figures 10 and 11 and those obtained earlier by Roberts was quite satisfactory.

During the tests run with a constant minimum

pressure, modulus values were obtained for the first application of loading. These modulus values were about 2/3 of the final value and generally followed the same trends as did the final modulus values. It should be recalled that the pressure against the sand was decreased to zero between successive tests of a given series. As noted in Appendix A, and as confirmed by the present results, the sand can undergo a significant expansion when the pressure is released all the way to zero. This circumstance undoubtedly accounts for the fact that the initial modulus for any test was always less than the final modulus during the previous test of the series.

Figure 12 shows the results for energy retention factor as a function of the average pressure level. The values shown in this figure are generally greater than those obtained by Roberts, although the agreement is not bad for the lower average stress values. This discrepancy is tied in with the difference in the shape of the hysteresis loop as noted above.

Table 1

DATA FOR MODULUS AND ENERGY RETENTION

Series	P_{ave} lb/in^2	Δp lb/in^2	$P_{min.}$ lb/in^2	Modulus 1st Cycle lb/in^2	Modulus Final lb/in^2	E_r Percent
1	*14.97	1.24	14.35		9.45	
	14.91	5.07	12.37		5.16	26.4
	14.80	10.52	11.54		4.45	
	*14.98	1.03	14.47		8.69	
	14.92	4.91	12.46		4.575	
	15.03	10.17	9.95		4.03	
	*15.00	1.12	14.34		8.64	
	15.00	2.06	13.97		5.59	
	15.14	5.03	12.63		4.56	22.0
	15.00	10.11	9.94		4.45	5.2
	15.00	15.00	7.50		4.13	9.85
	15.09	19.83	5.18		3.90	13.2
	***15.00	30.00	0.00		2.49	
	15.00	30.00	0.00		2.31**	
	*15.00	20.00	5.00		3.605	13.7
	14.88	20.00	4.88		3.70	12.8
	*15.00	30.00	0.00		2.38	31.6
	15.00	30.00	0.00		2.27**	
2	*30.00	1.52	29.2		8.25	
	30.1	5.16	27.5		6.67	
	29.9	9.95	25.0		6.07	12.2
	30.0	15.54	22.2		5.59	12.7
	30.0	20.0	20.0		5.61	10.2
	30.0	30.30	14.8		5.34	10.9
	30.0	15.34	22.34		5.97	10.8
	30.1	1.02	29.6		6.51	
3	*50.0	1.60	49.2		12.2	
	50.0	5.16	47.4		10.46	
	50.0	10.10	44.9		9.62	
	50.0	14.99	42.5		8.44	
	50.0	20.64	39.7		7.88	
	50.0	29.80	35.1		7.57	
	*50.0	29.80	35.1		7.165	8.90
	50.0	20.64	39.7		7.88	8.75
	50.0	15.54	42.2		8.45	9.90
	50.0	10.19	45.1		8.605	6.41
	50.0	5.10	47.4		9.045	6.75
	50.0	1.91	49.0		9.70	
	50.0	1.12	49.5		14.40	

Table I - Continued

Series	Pave lb/in^2	Δp lb/in^2	P_{min}, lb/in^2	Modulus 1st Cycle lb/in^2	Modulus Final lb/in^2	E_r Percent
4	*100.0	1.68	99.2		12.81	
	100.0	5.08	97.5		13.37	
	99.8	10.4	94.6		12.80	8.12
	99.6	15.5	91.8		11.60	7.78
	99.8	20.1	89.7		11.77	8.50
	98.8	29.5	84.1		10.33	6.94
5	*15.15	16.19	2.08		6.61	
	15.15	17.67	5.03	2.45	5.92	
	14.78	19.95	10.34	2.81	5.59	
	14.85	24.74	19.79	2.74	5.52	
	15.00	30.15	30.30	3.30	5.94	9.45
	15.00	24.92	19.85	3.14	5.60	10.3
	15.70	20.68	9.97	2.12	5.44	9.75
	*14.97	19.97	10.00		5.27	
	14.85	17.32	4.94	3.09	5.38	9.34
	*15.03	17.53	5.00		5.30	
	15.15	16.10	1.90	3.73	6.30	
	*15.00	16.15	2.30	3.29	5.84	
	Previously cycled at a lower pressure					
6	51.5	52.6	2.22	5.70	16.01	
	50.0	52.5	4.92	5.58	12.50	
	50.0	55.2	10.38	5.30	9.43	
	50.0	60.1	20.1	4.64	9.35	
	50.0	65.0	30.0	4.85	9.59	
	50.0	60.0	19.9	5.20	9.05	
	50.0	55.0	10.0	5.03	9.19	
	50.0	52.5	5.04	6.34	11.0	
	50.0	51.0	2.00	7.70	12.8	
7	*50.0	51.0	2.03		9.39	
	50.0	52.8	5.15	5.25	8.72	
	49.8	54.9	10.17	4.85	9.31	
	50.0	60.0	20.0	5.04	9.65	
	50.0	65.8	30.6	5.61	9.71	
	49.7	59.9	20.4		10.18	
	50.2	55.0	10.0	6.21	10.44	
	50.0	52.6	5.20	6.21	10.44	
	50.0	51.3	1.93	6.55	17.3	

Table I - Continued

Series	Pave lb/in^2	Δp lb/in^2	$P_{min.}$ lb/in^2	Modulus 1st Cycle lb/in^2	Modulus Final lb/in^2	E_r Percent
8	*50.3	51.3	2.00		10.5	
	50.3	52.8	5.00	6.74	10.37	
	49.9	55.0	10.21	5.40	9,48	
	49.8	59.8	20.1	5.25	9.98	
	49.5	64.5	30.0	5.86	9.95	6.26
	49.6	59.7	20.2	6.43	10.02	5.30
	50.4	55.1	9.45	6.74	9.98	6.84
	50.1	52.5	4.81	6.95	9.64	
	50.2	51.2	2.06		9.81	

* Denotes fresh specimen
** Tests at approximately 3 cycles per minute
***New specimen, but precycled at 20 lb/in^2

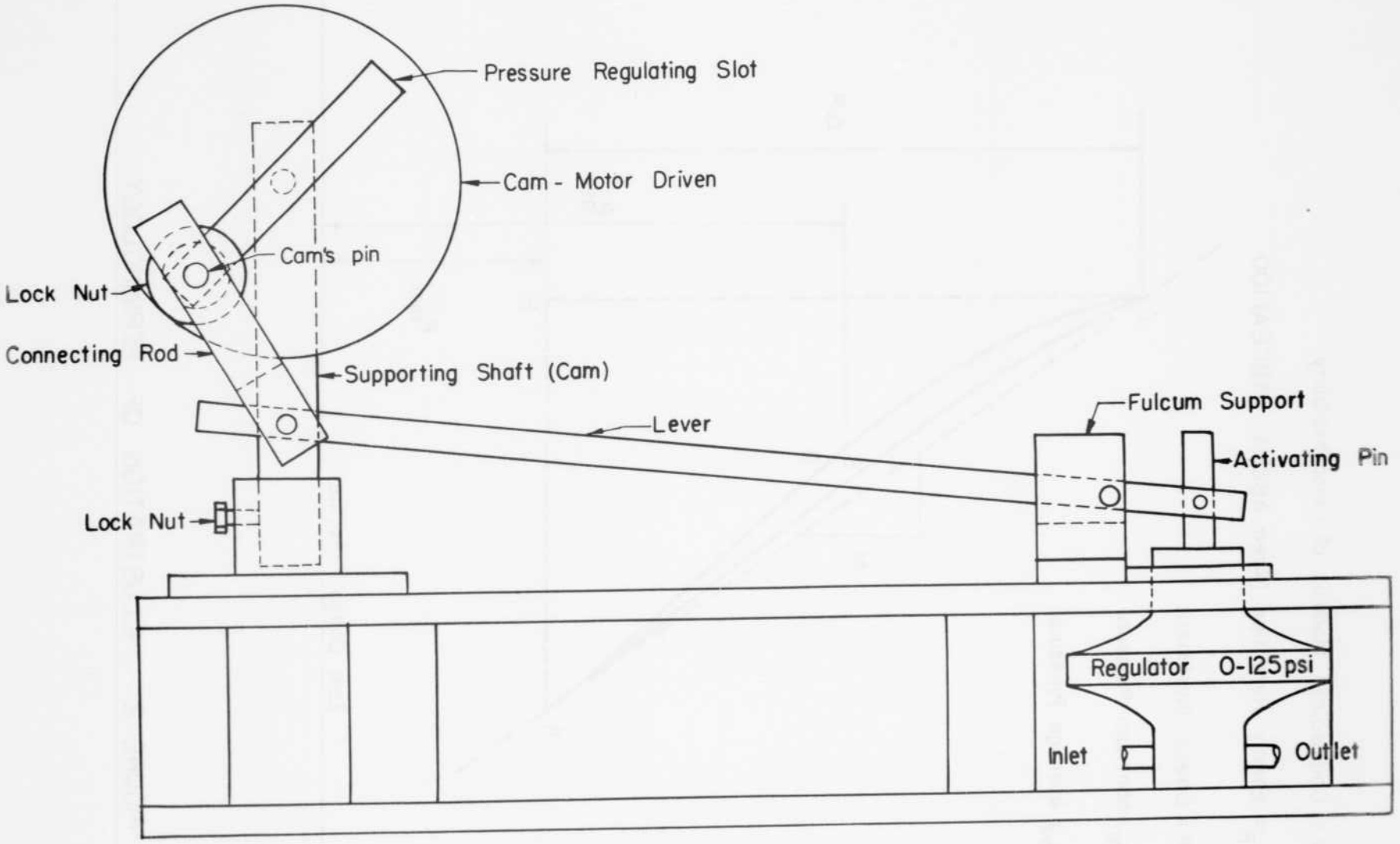

FIGURE 1 PRESSURE REGULATING DEVICE

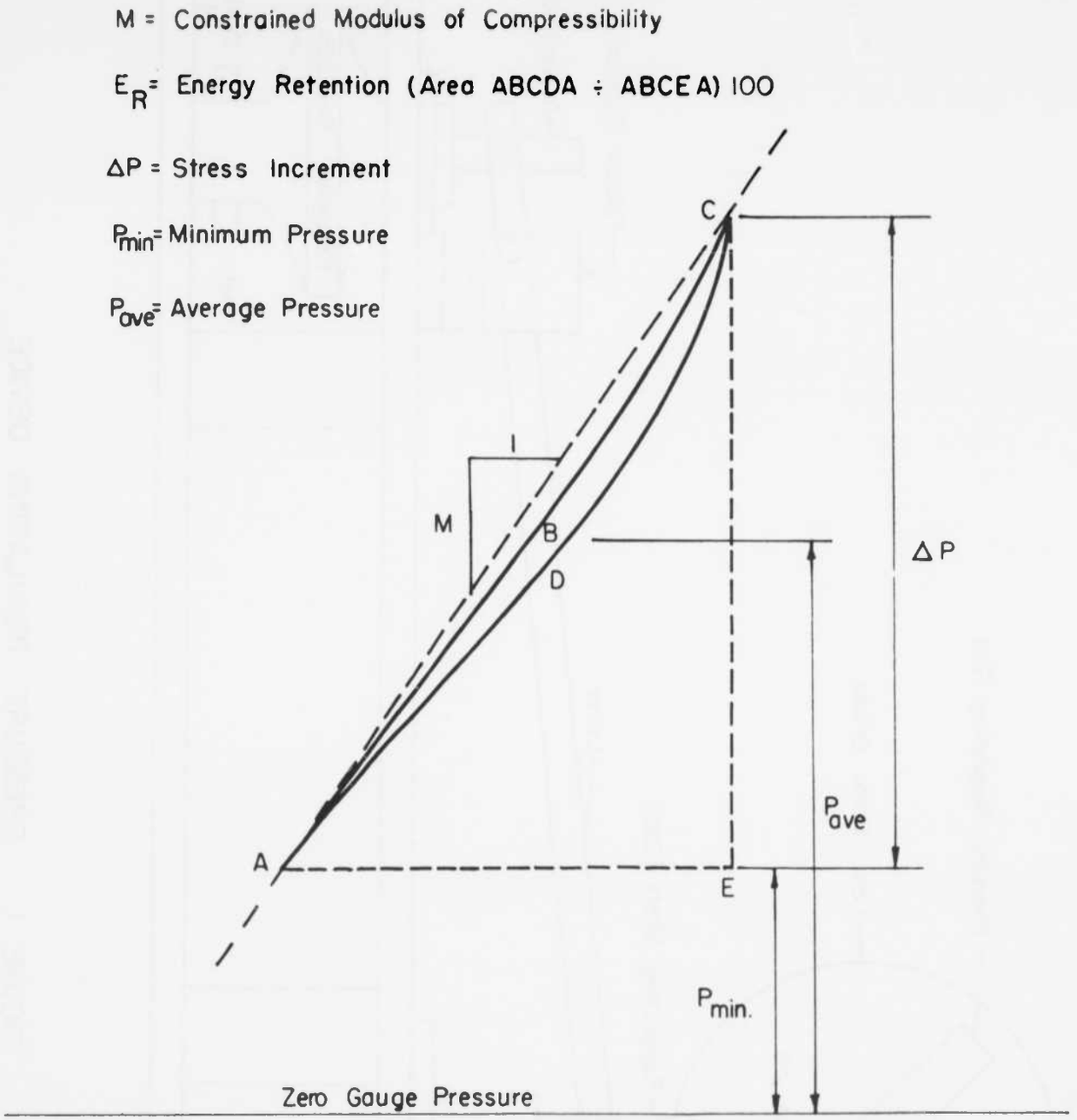

FIGURE 2 ILLUSTRATION OF TERMINOLOGY

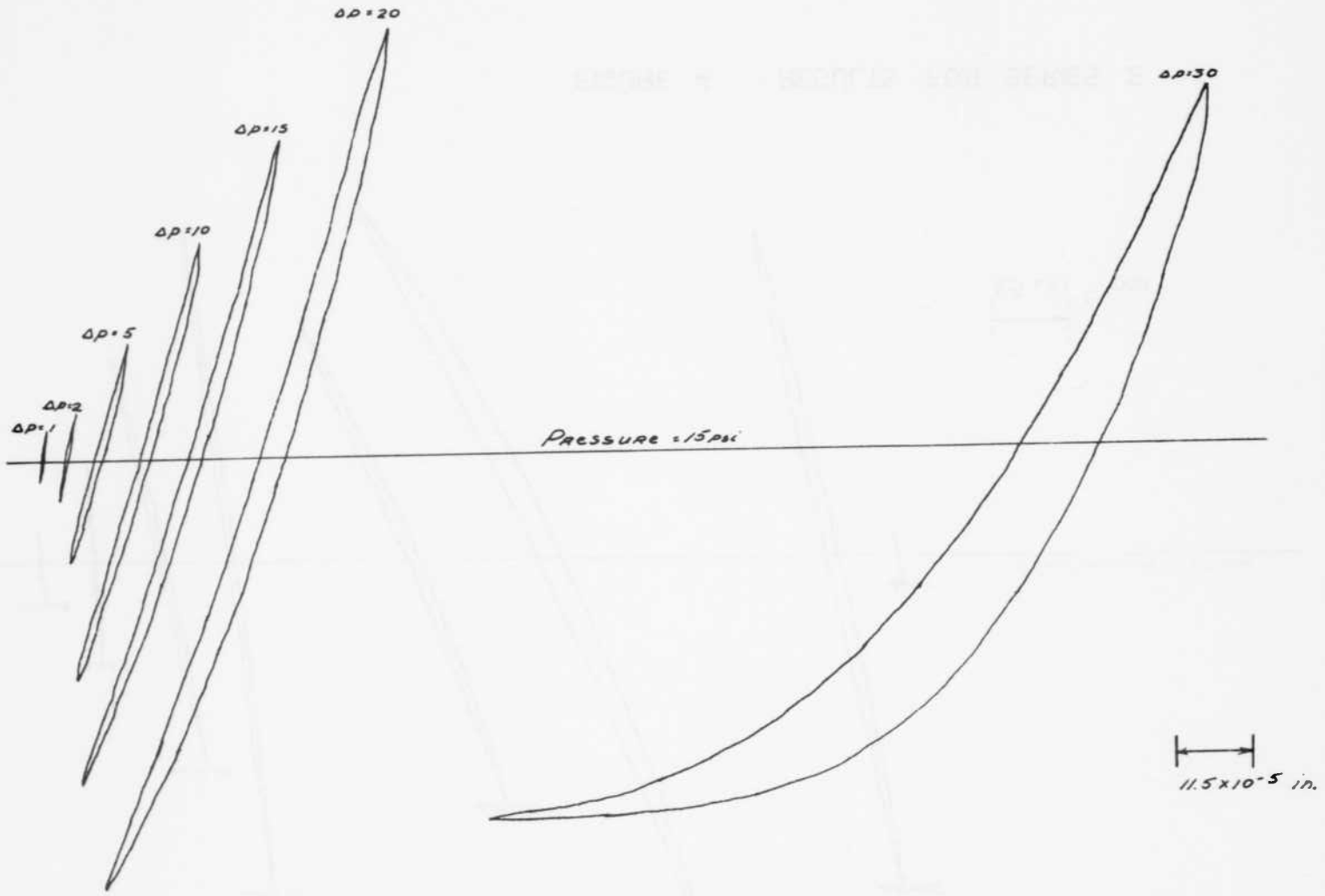

FIGURE 3 RESULTS FOR SERIES I

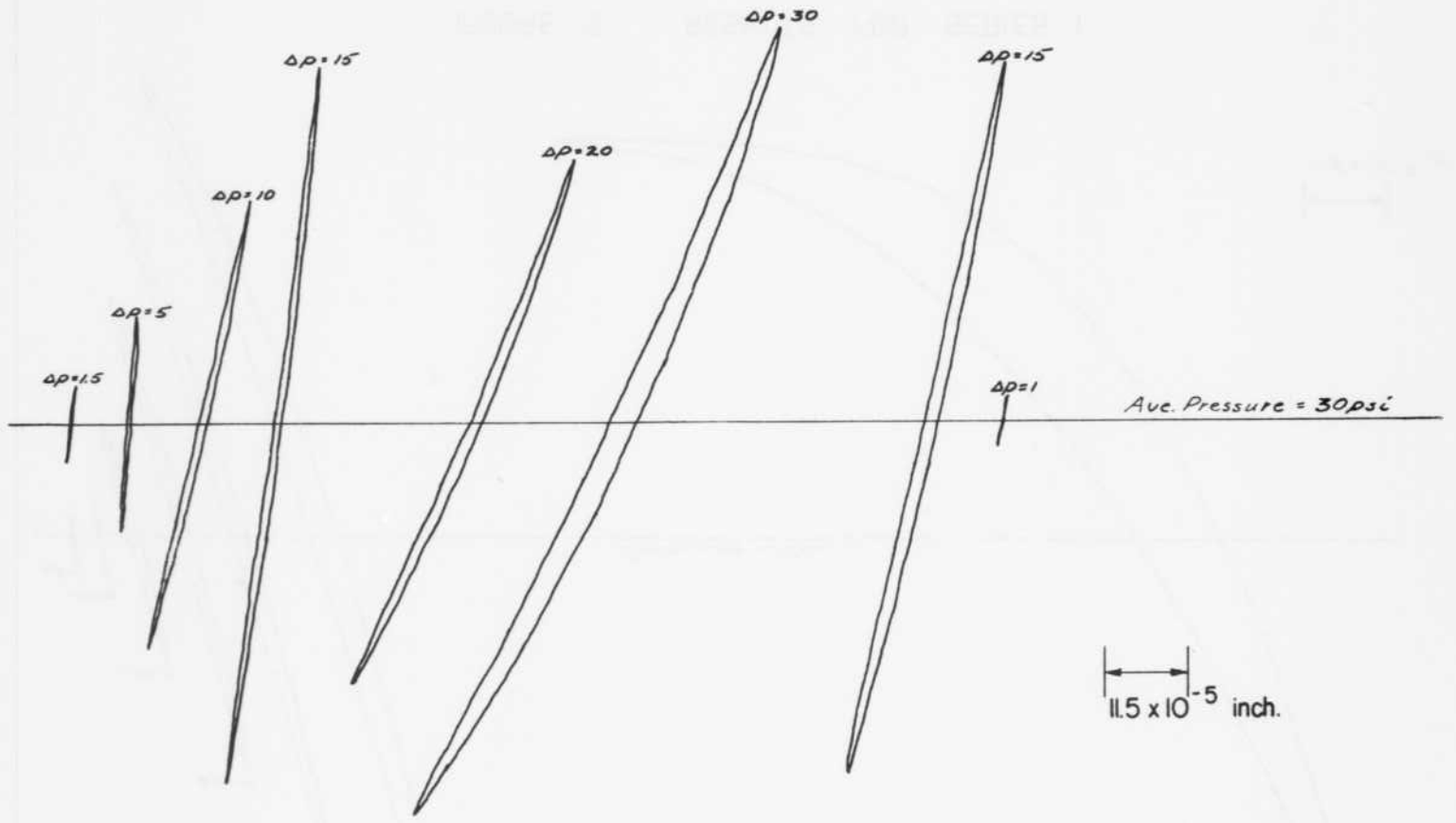

FIGURE 4 RESULTS FOR SERIES 2

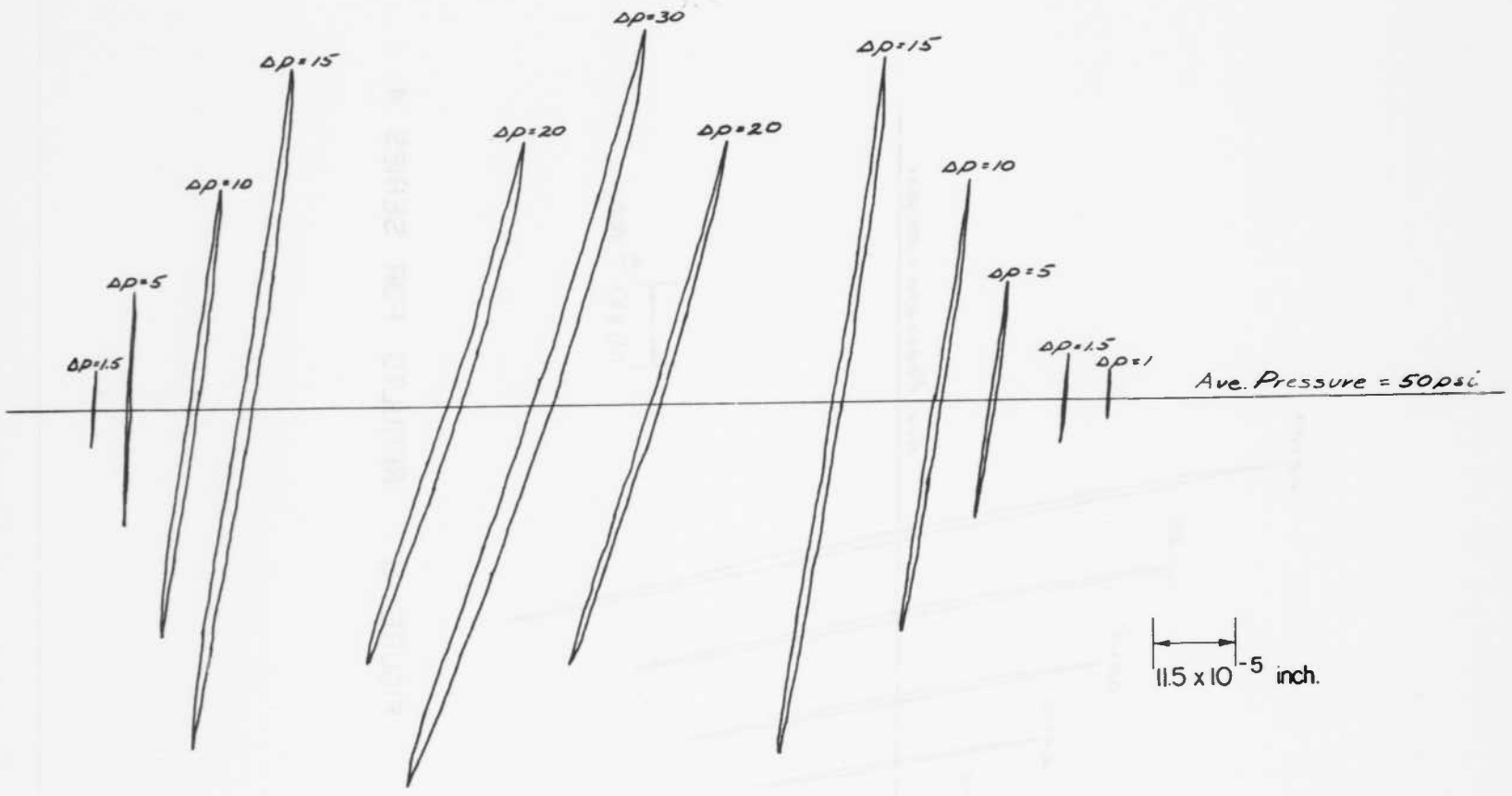

FIGURE 5 RESULTS FOR SERIES 3

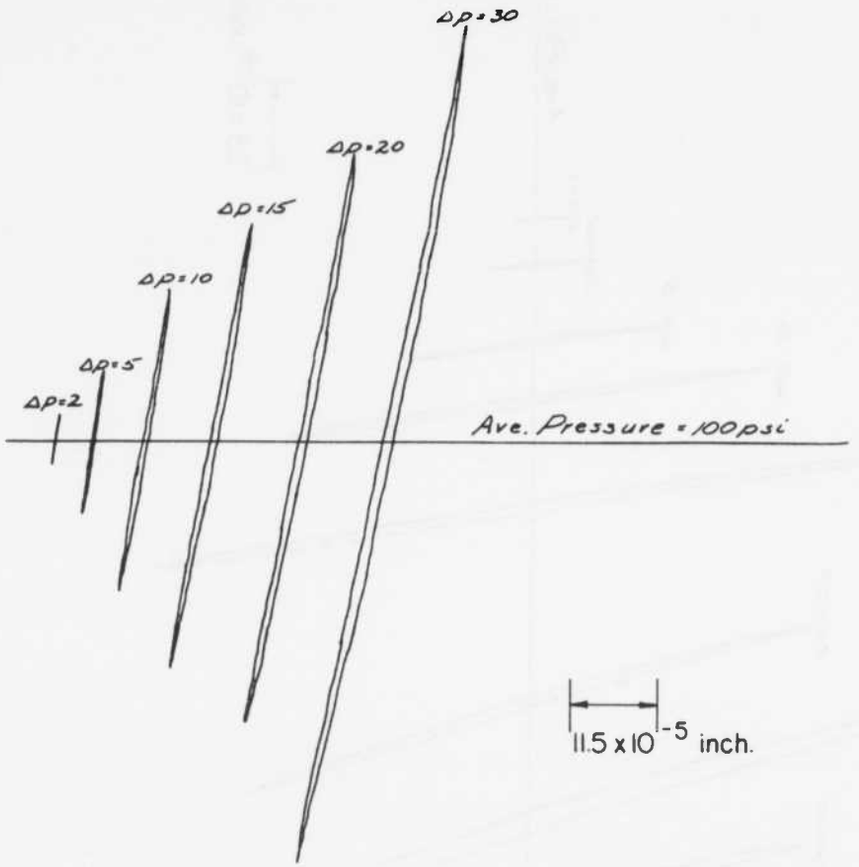

FIGURE 6 RESULTS FOR SERIES 4

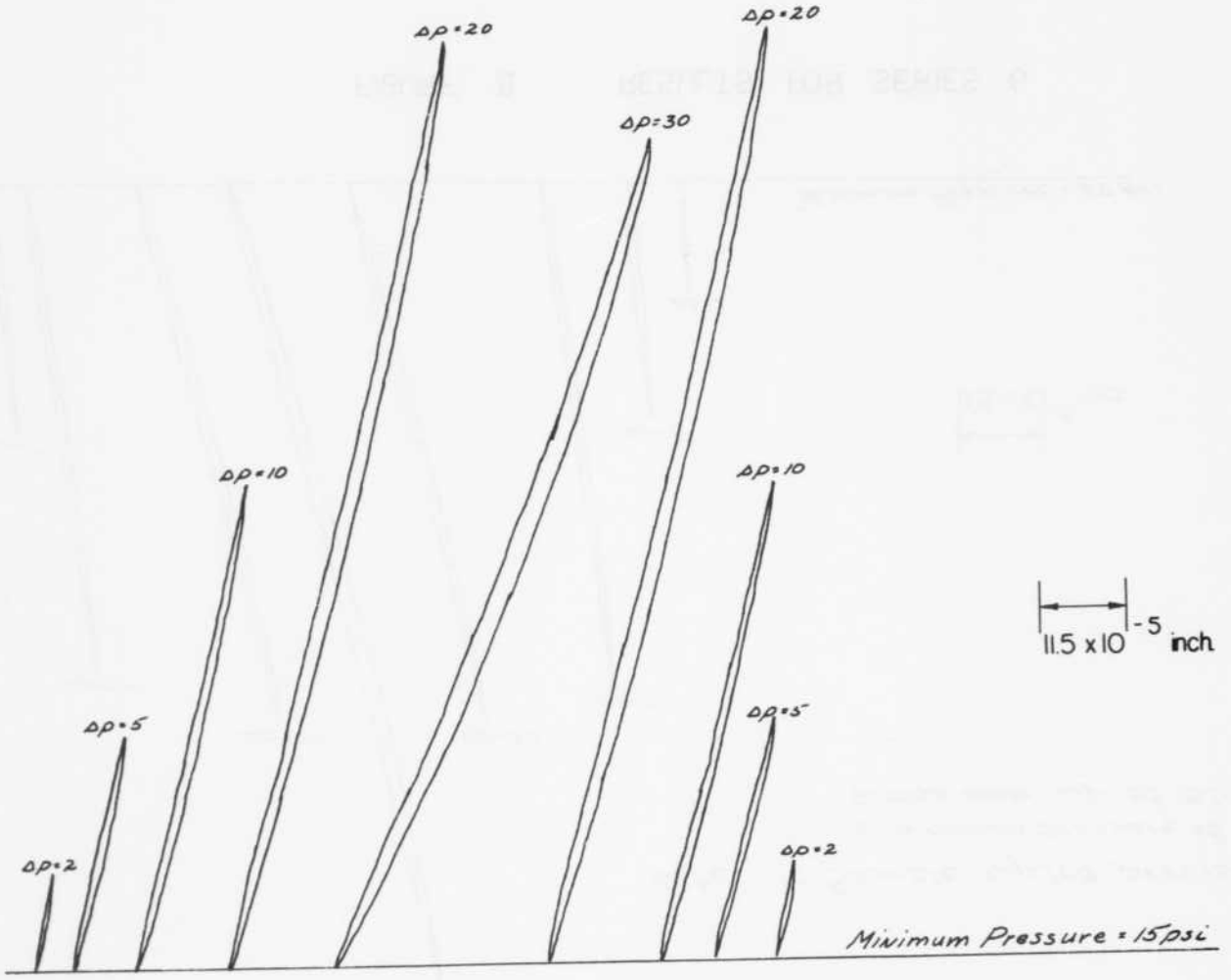

FIGURE 7 RESULTS FOR SERIES 5

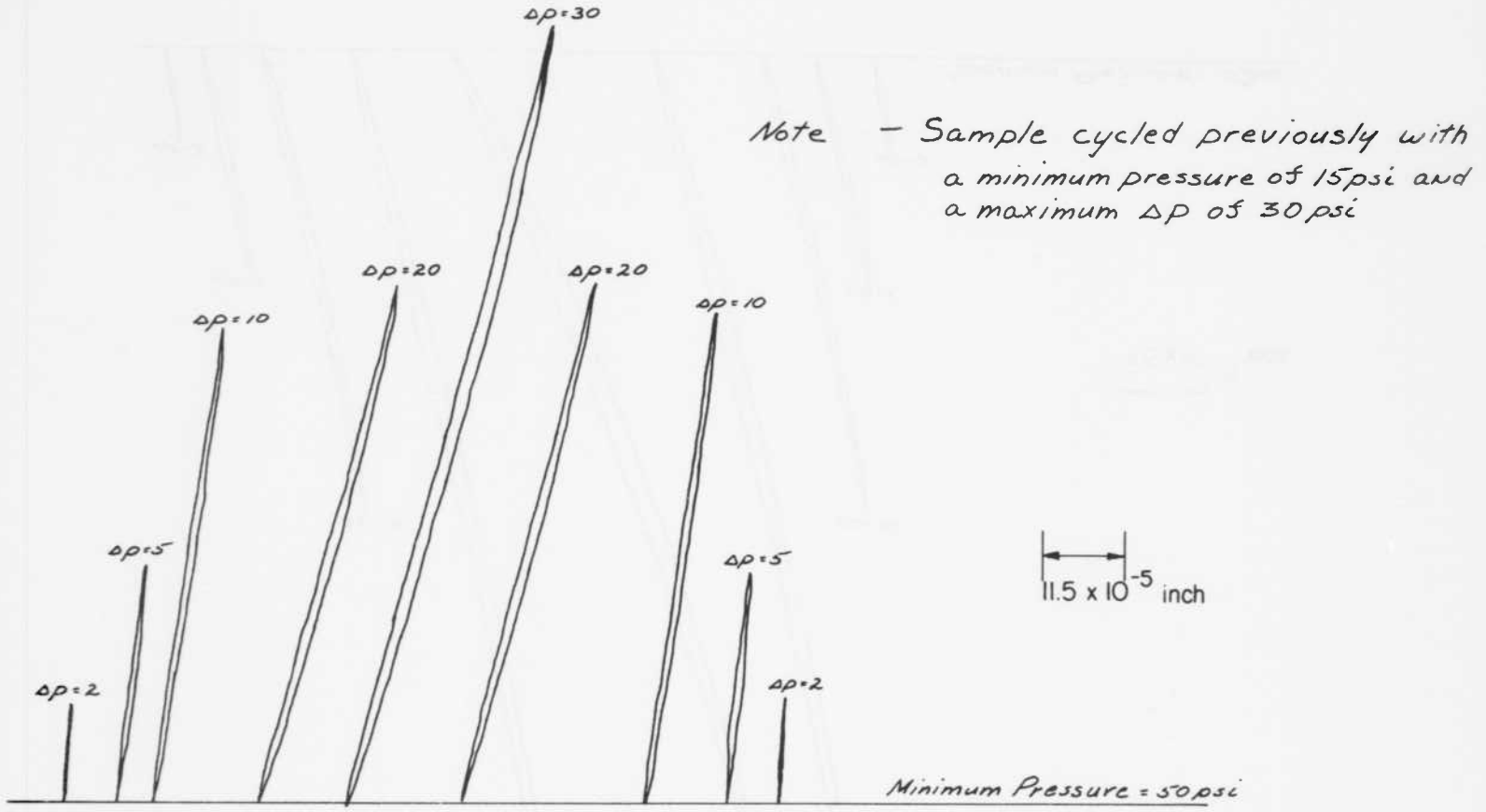

FIGURE 8 RESULTS FOR SERIES 6

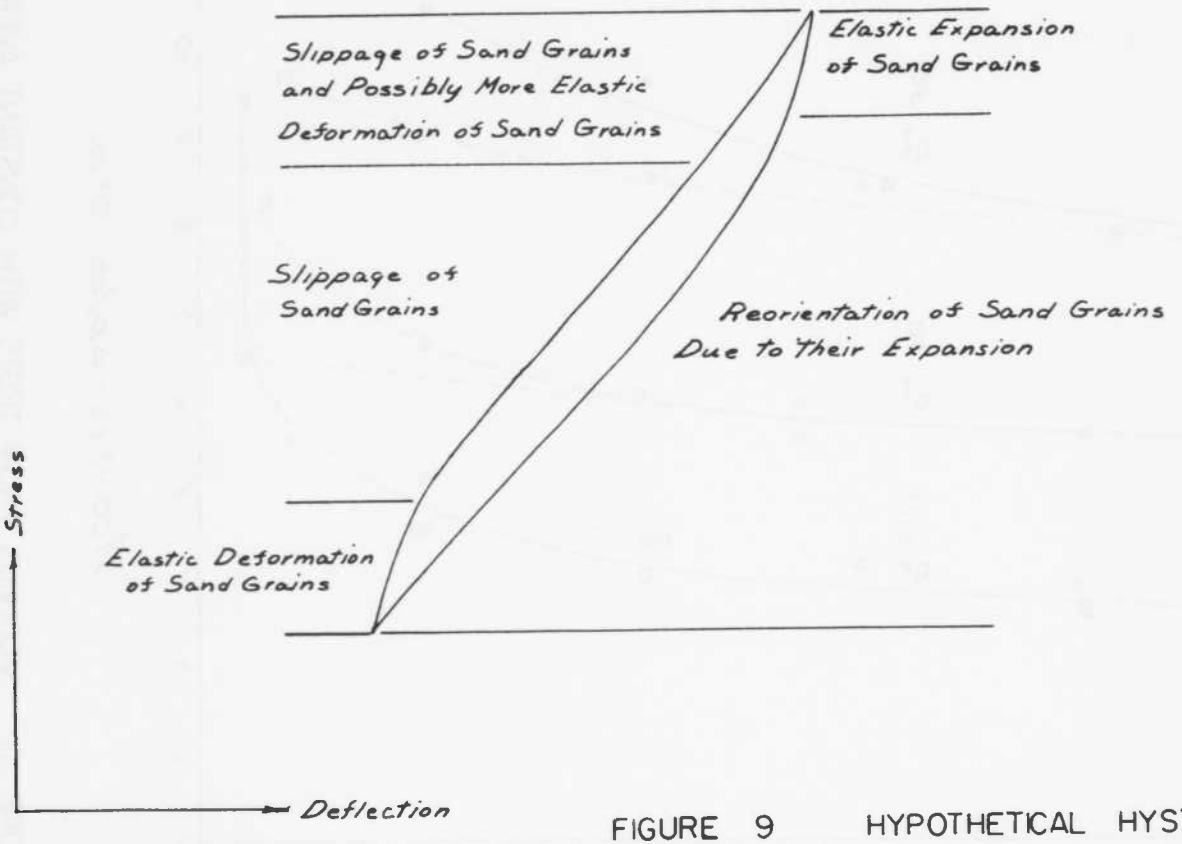

FIGURE 9 HYPOTHETICAL HYSTERESIS LOOP

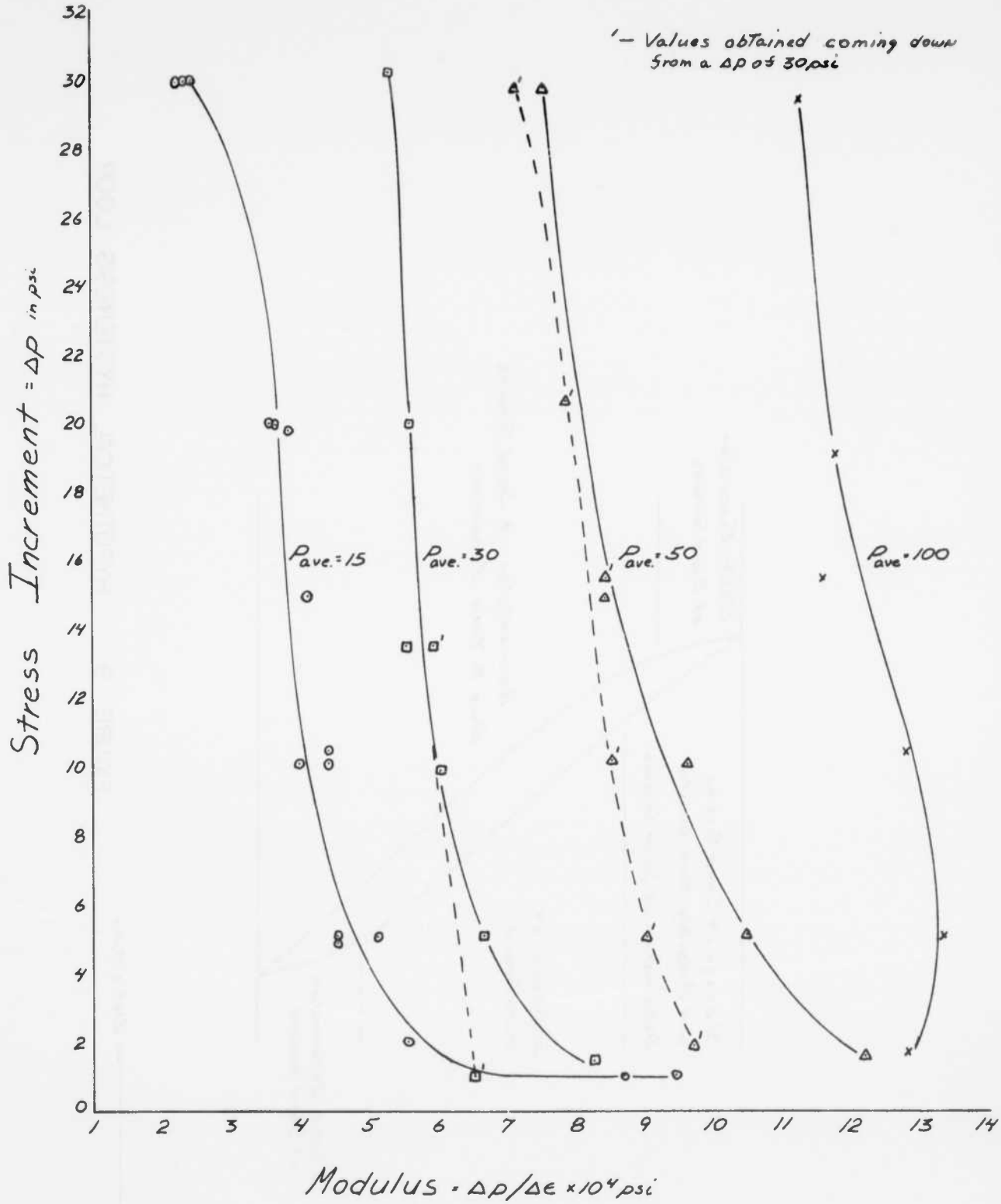

FIGURE 10 MODULUS FROM TESTS WITH CONSTANT AVERAGE STRESS

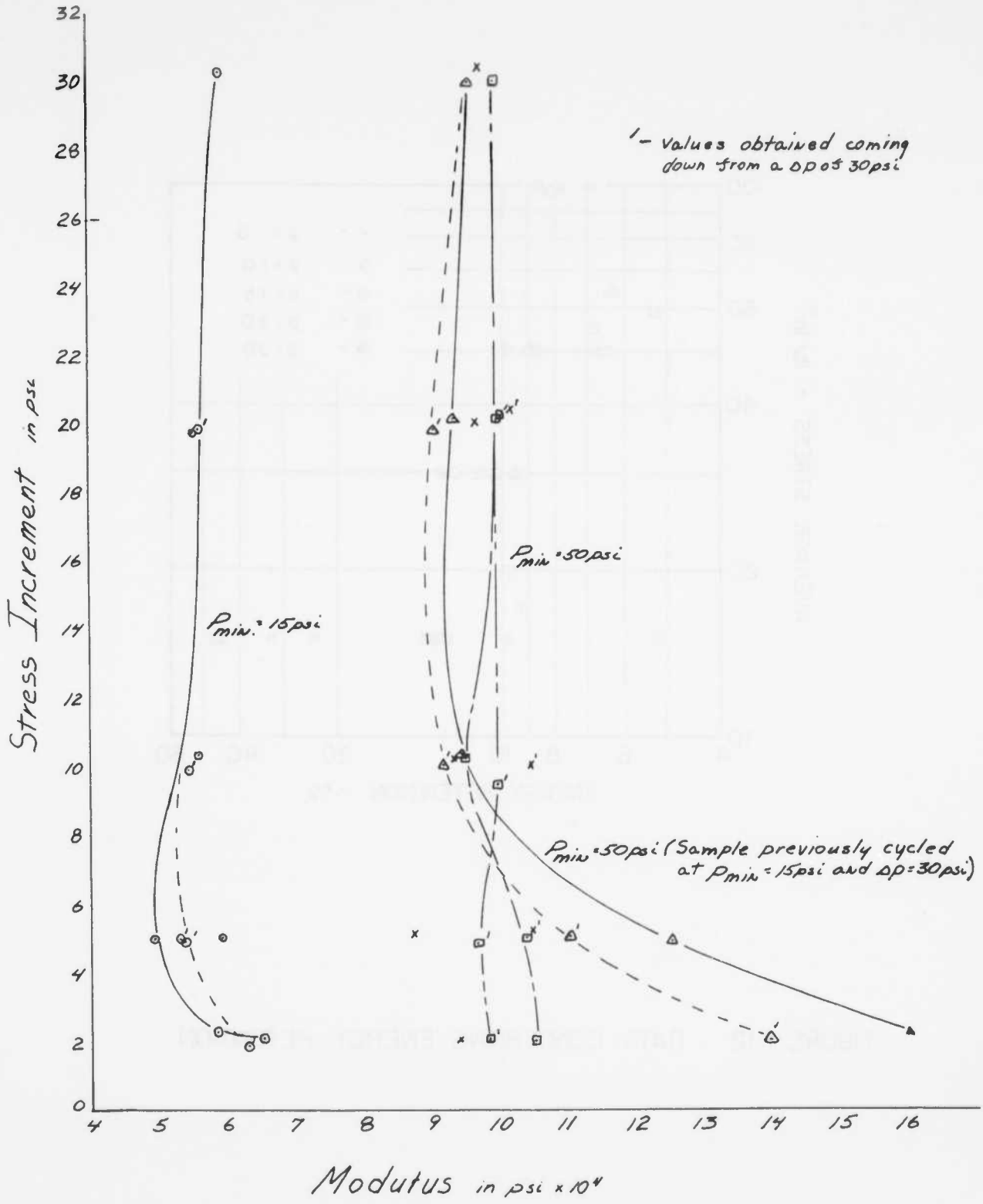

FIGURE II MODULUS FROM TESTS WITH CONSTANT MINIMUM STRESS

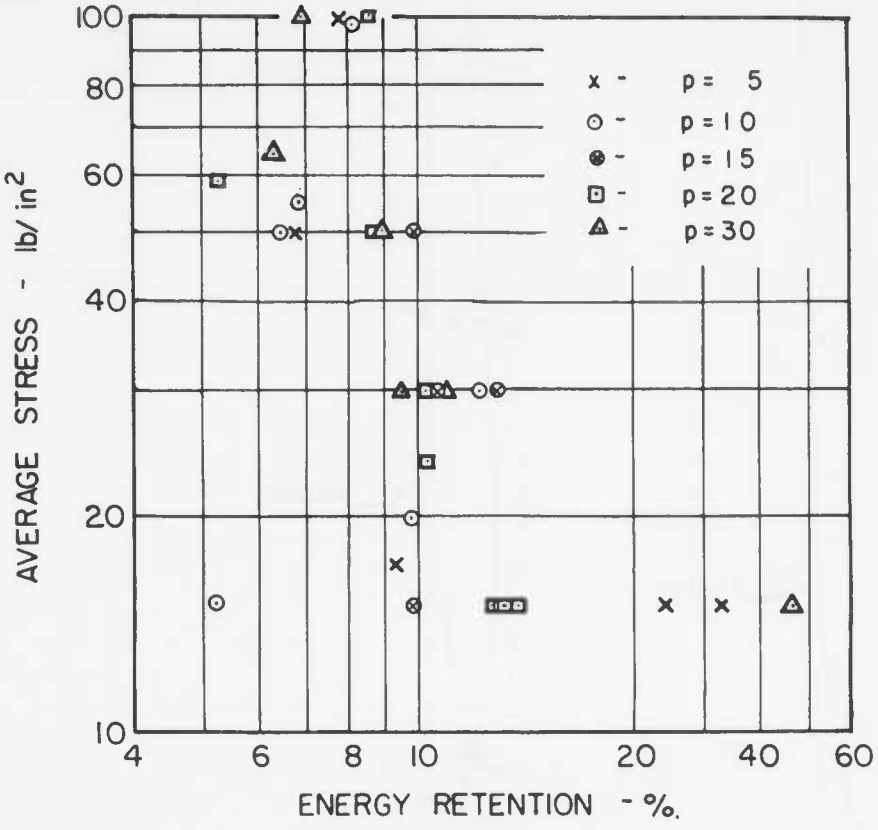

FIGURE 12 DATA CONCERNING ENERGY RETENTION

APPENDIX C

IMPROVEMENT OF ONE-DIMENSIONAL COMPRESSION TEST APPARATUS

PREFACE

This appendix describes the development of a series of test devices. Messers. Kent Healy, Jerome York, Edmond Miller and Dennis Leary all contributed to this effort. The work began in the spring of 1961 and continued through the spring of 1962.

LIST OF FIGURES

1 Cross-Section through Oedometer II

2 Apparatus for Compression Tests

3 Oedometer II

4 Pressure-Time Displays

5 Effect of Disc Size on Measured Compression

6 Apparatus Deflection Test

7 Cross-Section through Oedometer III

8 Valving System, Oedometer III

9 Cross-Section through Large Oedometer

10 Failure of Lucite Base

11 Pressure Supply System

12 Typical Cycle in Large Oedometer

13 Display of Electro-Mechanical Coupling Effect

14 Strain Trace Oscillations

15 Wave Propagation During Hypothetical Test Upon Linear Elastic Material

16 Apparent Stress-Strain Curves from Hypothetical Test Upon Linear Elastic Material

1. General Objectives

The equipment discussed in this appendix was developed to permit study into the behavior of the one-dimensional modulus during and subsequent to rapidly applied stresses. In particular the objectives were: (1) to obtain measurements of the modulus immediately following the rapid application of stress, and (2) to study the accumulation of creep strain during a subsequent interval of essentially constant stress. As the program progressed additional objectives were added: (3) comparison of the moduli during loading and subsequent unloading, i.e. the development of permanent strains, and (4) study of the shape of the stress-strain curve during the rapid application of stress.

It is, of course, necessary to be specific as to the meaning of "rapid application of stress". In those instances when the stress waves induced in the ground by nuclear explosions have been observed, the rise time to peak stress has been on the order of 1 to 5 milliseconds. Ideally, rise times of this same magnitude should be obtained in laboratory tests. Such short rise times are difficult to achieve. Hence, in this test program we have settled for those rise times which could be obtained by quite simple hydro-pneumatic loading systems. These rise times generally fell within the range from 15 milliseconds to 40 milliseconds, although, upon occasion, even shorter rise times were achieved. It would, furthermore, have been ideal to have the applied stress decay with time in a manner similar to the decay of overpressure from a nuclear explosion. The ideal decay time is not a fixed quantity, but would vary with the size of the explosion and overpressure range being modeled in the laboratory tests. Again, for reasons of expediency, very little attention has been paid in this test program to controlling the unloading time.

Early during the development of the test systems to be described in this appendix, a pattern of data acquisition was established, and this pattern has subsequently been followed without modification.

Each test was started with the application of a static pressure supposedly equivalent to some overburden pressure within the ground, and the soil specimen was allowed to sit for a matter of minutes so as to come to equilibrium under this static pressure. Then the "dynamic" stress increment was applied, and held constant for 3 minutes. The selection of the 3-minute duration stemed solely from the requirement of conducting a satisfactory test. During the interval of constant stress, the operator had to perform numerous functions, such as recording data on a sheet of paper, changing the film in the Polaroid-Land camera, etc. Three minutes was initially selected as the minimum period of time required for smooth performance of these functions; it proved to be a convenient operating interval and was followed thereafter. At the end of this 3-minute interval, the pressure being applied to the soil specimen was allowed to decay back to the initial "overburden" stress level. Another 3 minutes was allotted for this unloading phase of the test. Then the cycle of loading and unloading was repeated over again, usually through either 5 or 10 cycles.

The history of the applied pressure and the resultant strains during and immediately following the rapid application of stress or the decay of stress were recorded by photographing the screen of a dual beam oscilloscope. Visual readings as to the position of the pressure and strain traces on the oscilloscope screen were also taken at intervals such as 1 minute, 2 minutes, and 3 minutes following the start of a loading or unloading cycle. Obviously, if photographs were taken of both the loading and unloading portions for each cycle of each test, there would have been a tremendous expenditure of photographic film. Consequently, the use of photographic recording varied from test to test in accordance with the specific objectives of the test.

2. Development of Oedometer II

Figure 1 depicts the device which will hereafter be referred to as Oedometer II -- as contrasted to the apparatus described in Appendices A and B. The development of this particular oedometer was first undertaken during the spring of 1961. The history of this development is recorded in a series of reports: (1) Evaluation of Constrained Modulus of Glacial Till from the Vicinity of Minot, North Dakota" for the Ralph M. Parsons Co. in June 1961; and the following reports for the firm of Shannon & Wilson; (2) "Compressibility of Silt from Frenchman's Flat, Nevada," August 1961; (3) "Compressibility of Glacial Till from Above Water Table, Minot, North Dakota," September 1961; and (4) "Special Compression Studies, Lubbock, Texas," February 1962.

When the requirement for this testing system first arose, Oedometer I was in use by Roberts for the work described in Appendix A. Hence, use was made of another already available unit; the test cell which had been constructed for checking the response time of pore pressure measuring systems, as described in Report 5 of this dynamics series.

2.1 Specimen Container

The design of Oedometer II followed the basic ideas developed early in the recent soil dynamics research program, as reported in Reports Nos. 3 and 4. The disk, which was in contact with the top surface of the soil and which formed part of the strain measuring system, covered only a portion of the upper surface of the soil specimen. Thus, the applied pressure pressed directly against the soil through a rubber membrane over at least a portion of the surface of the soil.

When using specimens of a granular material, or when using laboratory compacted specimens of a clay, the specimen was formed directly into the well in the bottom portion of the oedometer.

Oedometer II provided for a specimen thickness of 1.57 inches and a specimen volume of 388 cubic centimeters, and a diameter thickness ratio of 2.8.

Oedometer II has also been used for testing undisturbed specimens. For such tests, the specimen was left in the sampling tube, and the specimen plus tube were set into the well as shown in Figure 1. The remaining portion of the well was packed with sand so as to support for that portion of the membrane outside of the test specimen itself.

The oedometer, as originally developed for the pore pressure studies (Report 5), had a porous stone extending over a portion of the bottom surface. For most of the present tests, the line leading from this porous stone was closed by a plug. In some tests on undisturbed specimens it became desirable to backpressure the pore spaces of the specimen, and the connection to the porous stone was used for this purpose.

2.2 Application of Stress

In Oedometer II, the confining pressure (or initial pressure) and the pressure increment (or high pressure) were supplied through two separate openings in the cover of the oedometer, as shown in Figure 1. Each of these pressures was supplied from a separate container of compressed nitrogen, regulated to the desired pressure.

Initially, a solenoid valve located at the outer end of a rubber tube was used to control the application of the stress increment, but this arrangement proved to have two serious drawbacks. First, the rise times were longer than were desired and, second, severe oscillation of the pressure in the cell occurred as the wave of pressure was reflected in the cell and in the tube. This arrangement was used only a few times and was abandoned in favor of a rotating plug valve.

In this second system, a plug valve was rotated to the open position by striking a handle attached to the rotating plug. A pressure accumulator consisting of a short piece of 1" pipe was inserted into the

pressure line adjacent to and upstream from the rotating valve. By filling the cell and the pressure lines with water up to the bottom of the valve, rise times as fast as 2 milliseconds could be obtained. This system, however, permitted leaks of pressure past the plug, and an upward creep of pressure before stress was applied by opening the valve itself.

This valving system was replaced by that shown in Figure 2. The valve was attached to the top of the cell as shown in Figure 2 and in Figure 3. The new system was held closed by the action of the high pressure in the accumulator on the top of the poppet valve. Then, as the poppet valve was opened, high pressure would begin to act immediately upon the valve face, thus reducing the force needed to complete the opening of the valve. Some "ringing" in the pressure trace was noted, and these oscillations were considerably reduced by the inclusion of a check valve in the system downstream from the poppet valve which acted as a throttling device. The shape of the stress-time traces obtained before and after insertion of the check valve are shown in Figure 4.

After the initial application of the stress increment, the pressure in the accumulator was reduced, and the regulator in the line caused the pressure in the accumulator to be restored to the pre-set value. Since the accumulator was now open to the cell, the cell pressure also was slowly increased for a period of several seconds. This produced an upward trend in the pressure trace of nearly all of the tests using this valve.

When the loading valve was closed, the pressure began to decay within the cell because of leaks inherent in the design of the cell. As shown in Figure 1, the 1/8" brass rod supporting the LVDT core passes out through the cover of the device. In order for free motion of this rod to take place, the fit of the rod to the hole through which it passes must be rather loose. Of course, this arrangement permits an annular ring around the rod, through which the fluid inside the cell may escape. In the operation of Oedometer II, the practice was to allow the leak thus created to control the rate of decay of the overpressure. Full decay of this overpressure took approximately 5 to 10 seconds, depending on the overpressure level and on the quantity of water remaining in the cell.

2.3 Measurement of Strain

The strain in the sample was measured as the deflection of the top surface of the sample under the application of the stress increment. Actual measurement of this displacement was accomplished through the use of a Shaevitz 040MSL Linear Variable Displacement Transformer (LVDT). This device was suspended over the cover of the cell, rather than beneath, as was the practice with Oedometer I, in order to eliminate the necessity of passing the shaft that positions the LVDT core through the sample itself. This feature enabled easier handling of the sample, and greatly simplified the testing of undisturbed samples. The rod supporting the core of the LVDT now passed through the cover of the cell as shown in Figure 1, and a pressure leak was thus created as described in Section 2.2.

The lower end of the shaft was attached to a disc that covered a portion of the sample surface. Tests were performed to determine the optimum size of this disc. It was found that the larger discs produced lower strain measurements under identical test conditions, but that strain measurements were essentially constant for the smaller disc sizes after cycles of loading. The strain measurements decreased quite rapidly as the disc diameter approached the diameter of the cell. The results of these tests are shown in Figure 5. As can be seen, less strain is recorded in each case using the 3.75" diameter disc. From cycle 2 on, each of the three smaller discs showed approximately the same strain. The difference between the large disc and the smaller discs is due to the influence of wall friction near the sides of the cell. On the basis of these tests, a disc size of 2.1" diameter was selected and used for all the tests performed with this oedometer and with Oedometer III.

2.4 Recording Arrangements

The output from the LVDT and the Dynisco pressure transducer were displayed on an oscilloscope as described earlier in this report. The oscilloscope was triggered by the closure of a switch in a 6 volt d.c. triggering circuit. An early switch consisted merely of a strip

of brass that completed the electrical circuit when touched by the brass operating lever of the valve. This brass strip, however, was bent out of the path of the operating lever on every loading cycle, and thus had to be reset for each load application. Later, this strip was replaced by a normally closed microswitch positioned above the operating lever as shown in Figure 8.

Since the LVDT is supported upon the top cap, and the pressure in the cell causes some movement of the top cap, there is certainly some false strain included in the measurements made by the LVDT due to deflection of the device. In order to obtain a quantitative measure of this deflection, a brass rod was extended to the bottom of the cell from the LVDT core, as shown in Figure 6. Then pressure was applied to the inside of the cell, and the deflections measured. This calibration resulted in the curve of deflection versus pressure that also appears in Figure 6.

3. Development of Oedometer III

Oedometer II has fairly obvious built-in disadvantages which prompted the design and construction of Oedometer III. The more obvious drawbacks in Oedometer II were corrected in the re-design, and the new design naturally developed unexpected troubles of its own.

Perhaps the most obvious disadvantage of the old design is connected with the LVDT support system. In the old design, the shaft to which the core of the LVDT is attached passes through the cover of the device. This creates an annular opening around the shaft permitting the loss of air or water from the loading system. The loss of fluid in itself is not of major consequence from the standpoint of compressed air use, although the reduction of air use is desirable. However, if this opening is the only escape route from the cell, the requirement of retention of pressure in the cell and the desired decay times on the release of the stress increment lead to different specifications regarding opening sizes. On the other hand, the opening should be kept as small as possible to avoid excessive air use and the general nuisance of leaking water, and to

facilitate the retention of pressure in the cell; while on the other hand, it should be as large as possible in order to allow rapid release of the stress increment when desired. Obviously, one or the other of these goals must suffer. If a second valve is employed to facilitate stress release, problems of syncronization arise which will be related in greater length in the discussion of the valving system to follow. Sealing the annular opening was not considered since this would introduce the effect of friction around the shaft into the analysis of the test data, and this extra variable should not be added if it could be avoided.

Since the LVDT was mounted over the top cover of Oedometer II, any movement of the top cover would be transferred to the LVDT. Although the thickness of the cover keeps these movements to a minimum, if they could be eliminated, it would be desirable to do so.

Other minor annoyances existing in the old design were considered as well when the plans for the new cell were prepared, and corrections were employed as follows.

The new device is shown in Figure 7. Since the LVDT is now supported within the device, the problems of motion and air leakage were both solved. The fact that the support for the LVDT now lies within the pressure field created difficulties of its own, however. In-rushing air from the loading valve strikes the plate supporting the LVDT, and causes vibrations to be set up in the plate. The resulting oscillations of the LVDT produce false indications of motion in the sample. This problem was largely eliminated by a throttling valve to slow down the in-rush of air. It was felt, however, that the design should be modified if possible to eliminate the problem source. The support was then increased in thickness from 1/4" to 1/2" and the support sleeve was made from brass rather than lucite to provide increased stiffness. However, no tests were ever performed using this modification, so its effectiveness has yet to be assessed.

Other difficulties, more serious from an operational standpoint, arose which caused the temporary abandonment of Oedometer III. Because the LVDT is held within the device, it must be positioned before the confining pressure is applied. It is desirable to maintain all movement of the core during the actual testing on one side of "null" because of the shape of the output curve obtained from the LVDT. Since some soil surface displacement occurs during the application of the confining pressure to the sample, a guess must be made as to the proper positioning of the LVDT prior to the application of the confining pressure so that the core is in the proper position after this operation is complete. Ideally, the core should be very close to and slightly below the "null" position.

In practice, it is relatively simple to get the core positioned on the proper side of "null", but it is extremely difficult to get the core positioned close enough to the "null" position. If the core is too far from "null", the base voltage output from the LVDT is large in comparison with the voltage change during the test. Therefore, a relatively insensitive scale must be used in order that the trace may be brought within the range of the oscilloscope, and small additional displacements become impossible to measure with sufficient accuracy.

From these points, it became apparent that some means of bringing the LVDT to "null" after the confining pressure is applied must be devised.

3.2 Valving System

The valving system shown in Figure 8 was devised for Oedometer III and works satisfactorily. This arrangement, of course, leaves unchanged the problem of upward drift in pressure following the initial rapid rise, and some improvements are needed to make the operation of the system simpler and more foolproof. As can be seen in Figure 8, the loading portion of the control valving is manually operated, and the unloading portion is solenoid operated. Unloading through the use of a solenoid valve works quite well, and further attempts should be made to include a solenoid operator in the loading valve.

At the beginning of a test, the loading valve is in the closed position, and the exhaust valve is in the open position, allowing the confining pressure to be applied to the sample. In order to load the sample, two operations must be performed nearly simultaneously: the exhaust valve must be closed and the loading valve then opened. If the cell is airtight, the exact syncronization of the two operations is not of major importance. Triggering of the oscilloscope is accomplished through the use of the microswitch shown as the handle of the loading valve is moved down. If this operation of opening the loading valve can be automated through the use of a solenoid operator, triggering could be accomplished through sensing the closure of the electrical circuit that actuates the valve, and both solenoids could be operated by action of the same switch. This would eliminate the need for setting the microswitch before each loading, thus eliminating one major source of error. Also, it would eliminate one human operation in the loading sequence, making correct operation more certain.

The reverse of these operations is followed on unloading. First the loading valve is closed and then the exhaust valve is opened. Again, as long as the system is airtight, exact syncronization of these movements is not of major importance. The solenoid circuit is wired through one side of a double pole - single throw switch. The unloading triggering circuit is wired through the other side of this same switch, so that closing the switch operates the valve and triggers the oscilloscope simultaneously. Here again, the operation of the loading valve through the use of a solenoid would reduce the chance for human error through the elimination of one manual operation.

Rise times possible with this valving system, since the same loading valve is incorporated in this system that was used with Oedometer II, are the same as those described in Section 1 of this appendix, and generally lie in the range of 15 to 40 milliseconds. Decay times, since the excess pressure sink is designed to absorb 99% of the pressure excess in the cell "instantaneously", are controlled by the size of the effective

orifice in the exhaust valve. The decay times actually recorded are almost constant and generally lie in the range of 50 to 70 milliseconds.

Attempts to automate the application of the stress increment took two directions. First, an attempt was made to electrify the loading valve shown in Figure 8. However, due to the large forces necessary to operate the valve under large stress increments, no solenoid could be found that was strong enough to open the valve consistently. Second, commercially available solenoid operated poppet valves similar to the exhaust valve were investigated, but it was found that use of this type of valve would limit the minimum rise time to approximately 50 milliseconds, the same time that was available for decay times.

When this valving system was applied to Oedometer II, the importance of automating the loading cycle increased. Because of the leak around the LVDT shaft described earlier, a loss of pressure between the closing of one valve and the opening of the other was unavoidable. Thus, there was an opportunity for the pressure in the cell to drift lower during the brief interval between the end of one cycle and the beginning of the next. The magnitude of the pressure change during these intervals was so great that use of this valving system with Oedometer II had to be abandoned entirely.

4. Development of a Large Oedometer

There are many possible sources of error in the experiments carried out in Oedometers I, II and III. Bedding and seating errors may still be significant because of the small thickness of the specimen. Side friction may be important owing to the relatively small diameter/thickness ratio. Unfortunately, it is difficult to imagine field tests that will provide a satisfactory check upon the results of tests in small oedometers, and yet some form of independent check is needed. As one step in this direction, an oedometer with a much larger diameter was constructed.*

*Use of an oedometer with a diameter of 3 ft. has been suggested by T. K. Chaplin, "Some Mechanical Properties of Granular Materials at Law Strains," Proc. Midland Soil Mech. and Found. Eng. Society, Vol. 4, 1961, pp 19-36.

The dimensions chosen for this large oedometer were 11 inches diameter, and 1 inch deep. The basic concepts of the design of this oedometer were the same as those employed in Oedometer III. That is, the LVDT was supported internally, and the stress increment was applied and removed through solenoid valves. In the large oedometer, however, the application and the release of stress were completely automated. Details of the oedometer are shown in Figure 9.

Out of a desire to expedite the construction of the large oedometer, the decision was made to construct the base from lucite. The base was designed to withstand bending and tensile stresses from an internal pressure of 130 psi. Realizing that lucite would be relatively flexible, the cell had to be calibrated to allow correction for its own deformation. During the calibration procedure, a deflection of the base of 0.05" was noted at an internal pressure of 80 psi. This is far larger than the strains expected in the soil specimen, and pointed up the necessity of making the base more rigid in a later re-design of the equipment.

When the internal pressure was increased to 100 psi during an attempt to determine the deflections under the full design pressure, the lucite base failed around the periphery of the cell cavity. Analysis of the failure indicates that the stresses in the lucite were concentrated in the sharp corners produced in the intersection of the walls and the base of the cell cavity, causing a locally overstressed zone that failed. Characteristics of this failure can be seen in Figure 10. In light of the overly high deflections, the idea of a lucite base was abandoned after the failure, and the decision was made to construct the base out of a more rigid material, possibly steel plate with stiffening plates perpendicular to the base plate, in any subsequent re-design of this equipment. As of this date, no further attempt has been made to construct such a large oedometer.

4.1 Valving System

The valving system for the large oedometer is shown schematically in Figure 11. This system was fully automated in the manner

suggested in Section 3.2 of this appendix by inclusion of a solenoid valve in both the loading and unloading circuits. The valves were wired in parallel so that one valve opened as the other closed. Both valves were wired to a timing device which could be set to permit a wide range of combinations of time periods of high and low pressures. Several of the traces of pressure versus time obtained with this system are shown in Figure 12. A photograph of both a pressure increase and decay is shown in Figure 13. As shown in this figure, the rise and decay times are approximately equal, and approximately 80 milliseconds. The excursions at the beginning of each trace are due to electrical and mechanical coupling between the valve operation circuit of the pressure transducer circuit.

5. Strain Measurement Difficulties

Figure 14 shows four photographs of stress and strain versus time traces obtained with Oedometer II. The strain trace shows oscillations that do not reflect a corresponding change in stress. The complete reason for these oscillations has not yet been determined, but continued use and refinement of the equipment has reduced or eliminated most of them. In Photo D, a small dip in the curve may be seen approximately 35 milliseconds after the beginning of the pressure increase. This dip appeared in several tests, each time at 35 milliseconds after the beginning of the pressure increase. This appears to be produced electrically and uniformly in each test, perhaps as a characteristic of the LVDT used. During the period when most of the difficulty was experienced in the strain measurement, the LVDT wiring was damaged and "homemade" repairs were made on the device. Since that time, a new LVDT has been obtained as a replacement and the strain measuring difficulties were largely overcome at the same time. In interpreting the tests using the old LVDT, however, the most reasonable smooth curve was drawn through the oscillating trace, and this smooth curve was used in interpreting the strain data

5. Wave Propagation During Compression Tests

When stress is applied suddenly to the upper surface of a test specimen, a stress wave starts through the specimen. The presence of such stress waves will, in general, mean that stress and strain are not uniform over the thickness of the specimen.

To illustrate this point, let us assume that we perform an experiment upon a linear elastic specimen; i.e., a straight line. A ramp loading is applied; that is, the stress increases linearly to its maximum value. The time to achieve the maximum applied stress is assumed to be 4 times the time required for a stress wave to transit the thickness of the specimen.

The stress wave patterns within this specimen are analyzed in Figure 15. For this analysis, the ramp loading has been replaced by a series of step loadings. Part (b) of this figure is a form of characteristics diagram (for example, see Crandall, S. H., "Engineering Analysis," McGraw-Hill Book Co., Inc. (1956) chapter 6). The lines in part (b) show the wave fronts. The diagram in (b) may be thought of as a three dimensional plot, with time and distance measured in the plane of the diagram and stress and particle velocity shown by elevations normal to the plane. This "topographic map" consists of plateaus separated by vertical escarpments. The quantities written astride the wave fronts represent the changes in stress and particle velocity across the fronts. The quantities within boxes indicate the levels of stress and particle velocity which exist between successive wave fronts.

For example, at mid-depth of the specimen at time $7L/4C$:

$$\text{stress} = 4\sigma$$

$$\text{particle velocity} = 2\sigma c/M$$

where c: wave propagation velocity

M: modulus $= \rho c^2$

ρ: mass density

At this same time, the stress (and hence the strain) is less at both ends of the specimen than at mid-depth.

Part (c) shows the particle velocity at the top surface of the specimen: the dashed line is derived on the basis of the series of step loadings; for the ramp loading, the curve of particle velocity vs. time would be as shown by the solid line. Integrating the solid curve in part (c) gives the displacement of the top surface as a function of time, as shown in part (d). With the experimental system used in this study, the curve of measured strain vs. time would be as in (d).

Figure 16 shows the stress-strain curve that would be deduced from our hypothetical experiment. Because of wave propagation effects, the apparent stress-strain curve is non-linear even though the actual stress-strain curve is linear.

Apparent stress-strain curves have also been deduced for hypothetical experiments in which the times to peak stress are 2L/c and 8L/c. These stress-strain curves are also shown in Figure 16. As the loading time becomes very long compared to the transit time for a wave, the observed stress-strain curve approaches the actual stress-strain curve.

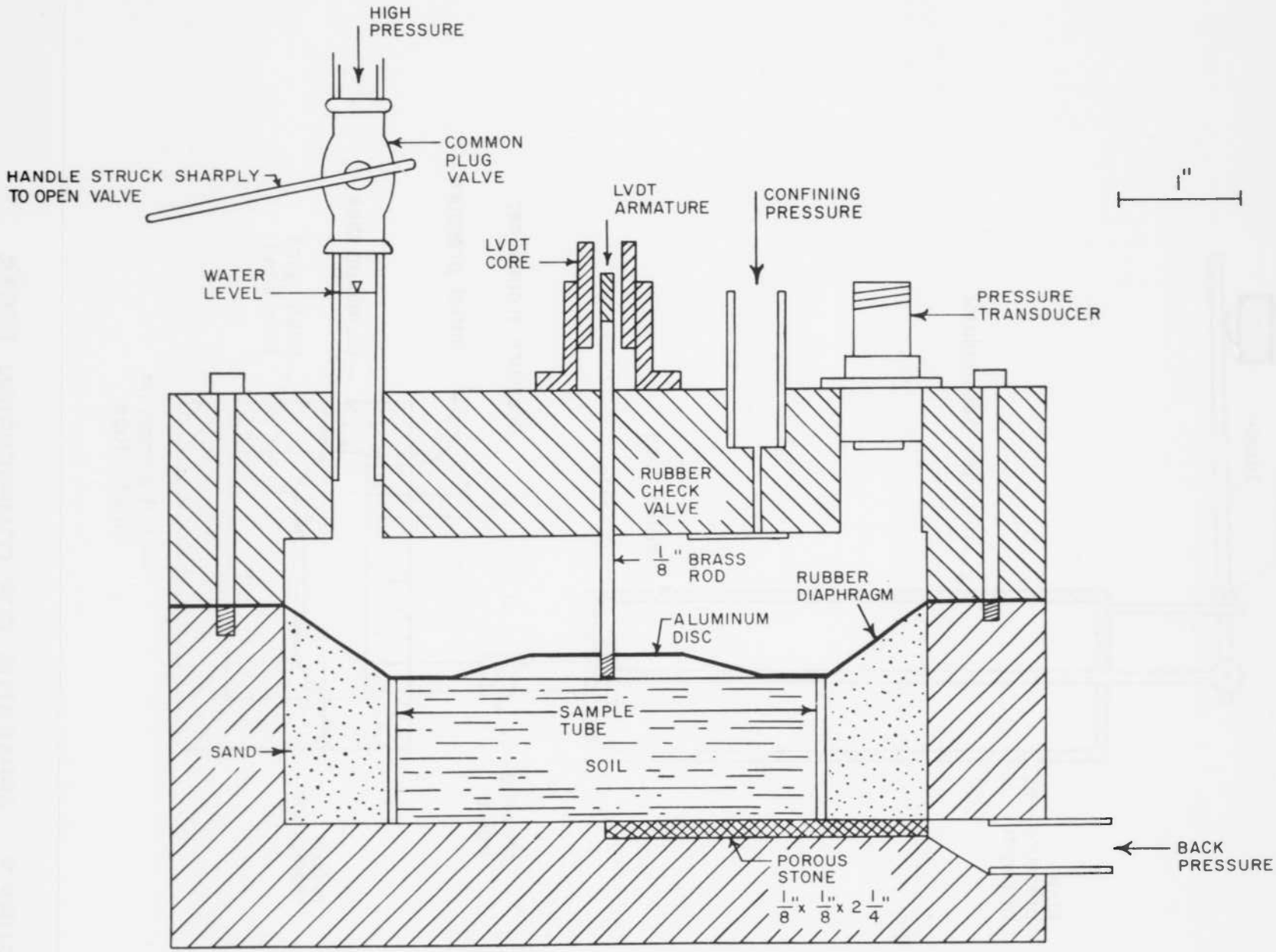

FIGURE I CROSS-SECTION THROUGH OEDOMETER II

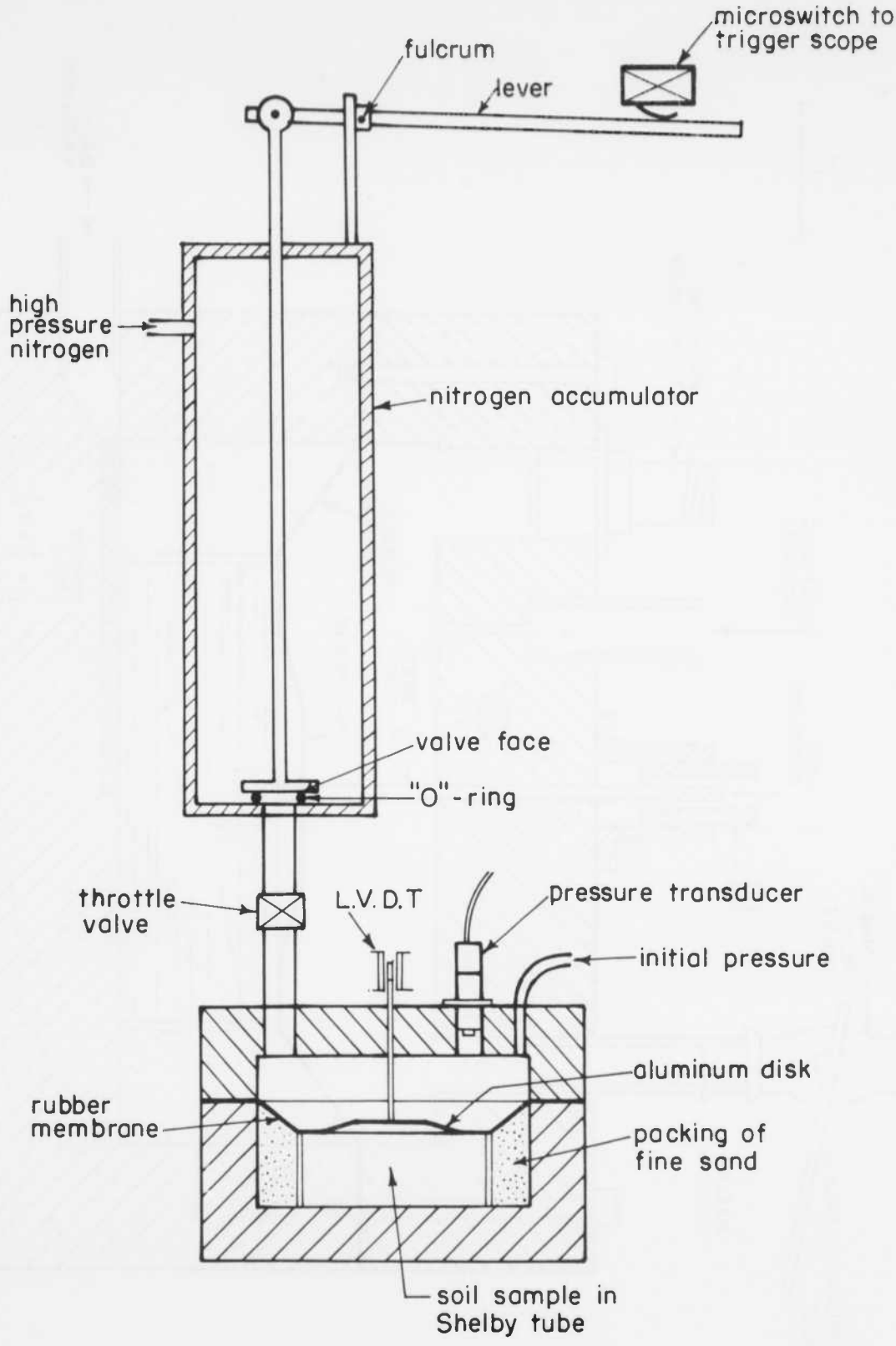

FIGURE 2 APPARATUS FOR COMPRESSION TESTS

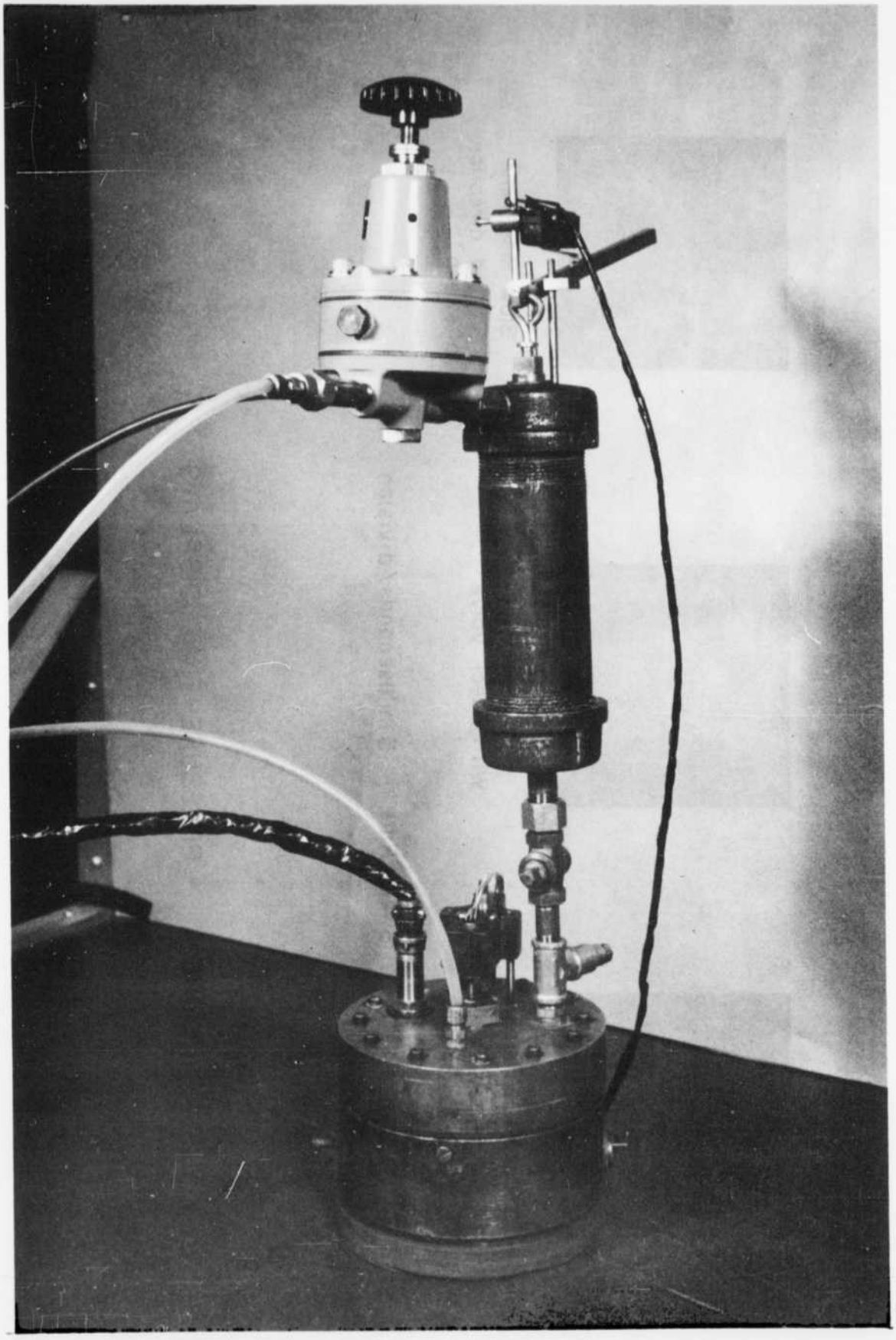

FIGURE 3 OEDOMETER II

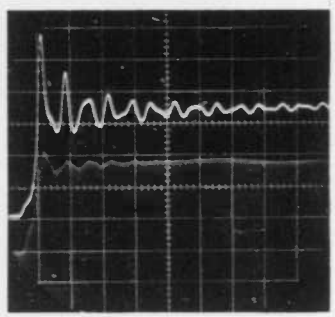

Fast Rise Time
Without Check Valve

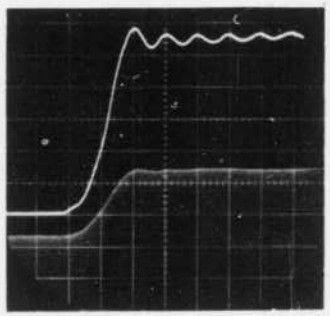

Fast Rise Time
With Check Valve

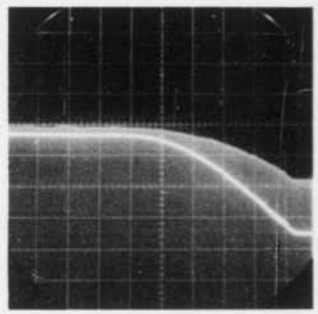

Slow Rise Time
(reversed direction
of sweep)

Sweep Rate - 5 milliseconds/division

FIGURE 4 PRESSURE-TIME DISPLAYS

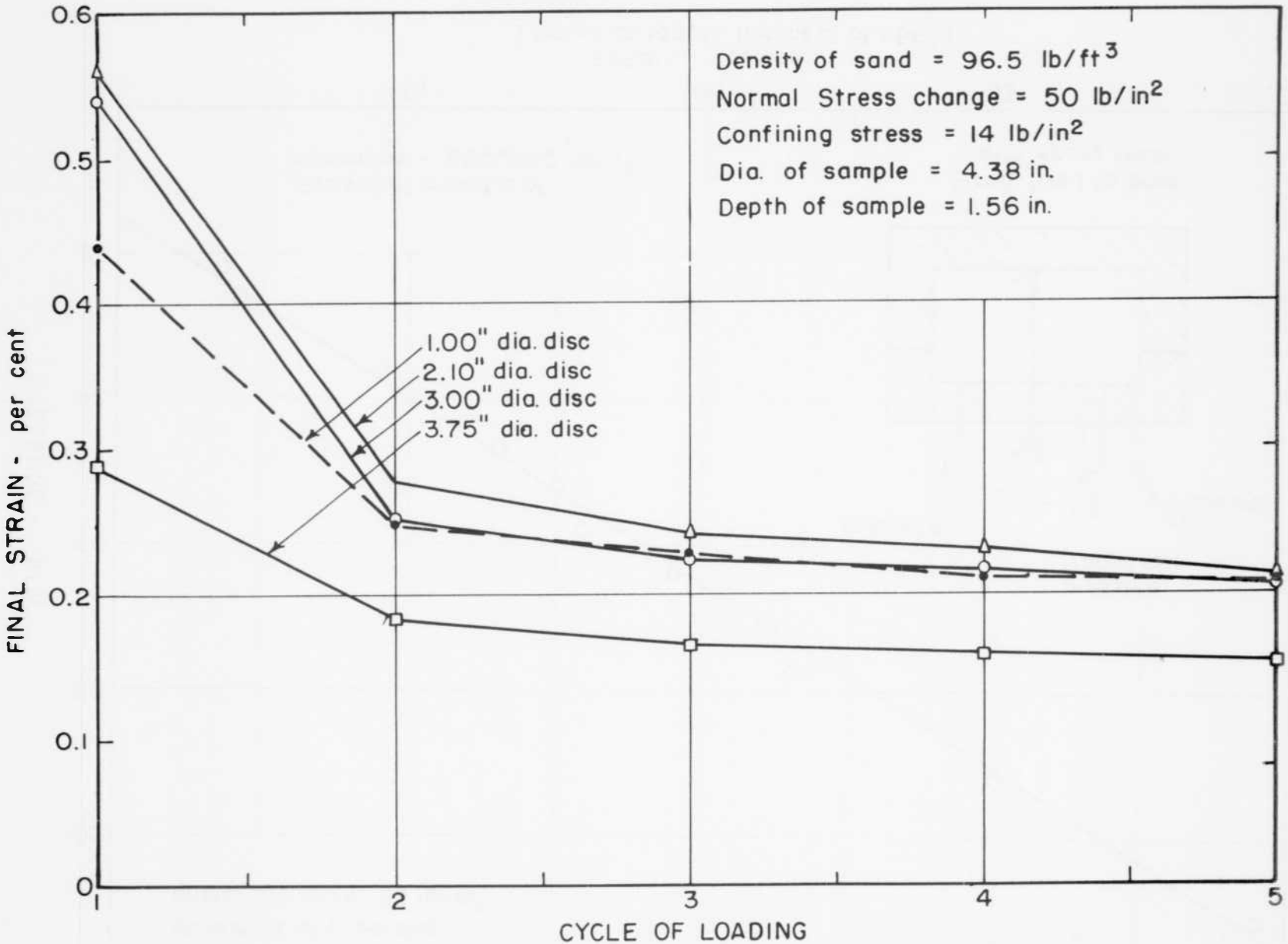

FIGURE 5 EFFECT OF DISC SIZE ON MEASURED COMPRESSION

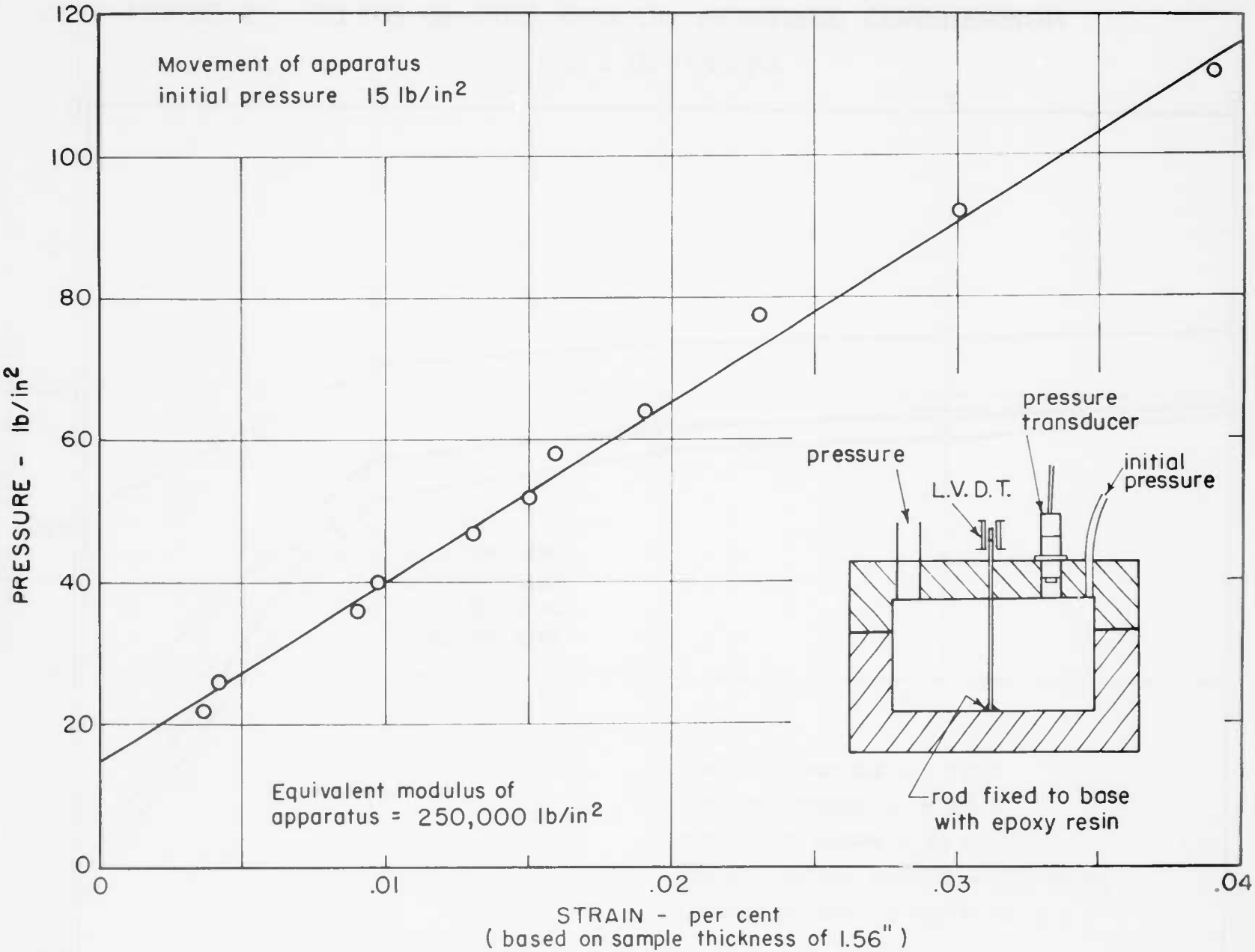

FIGURE 6 APPARATUS DEFLECTION TEST

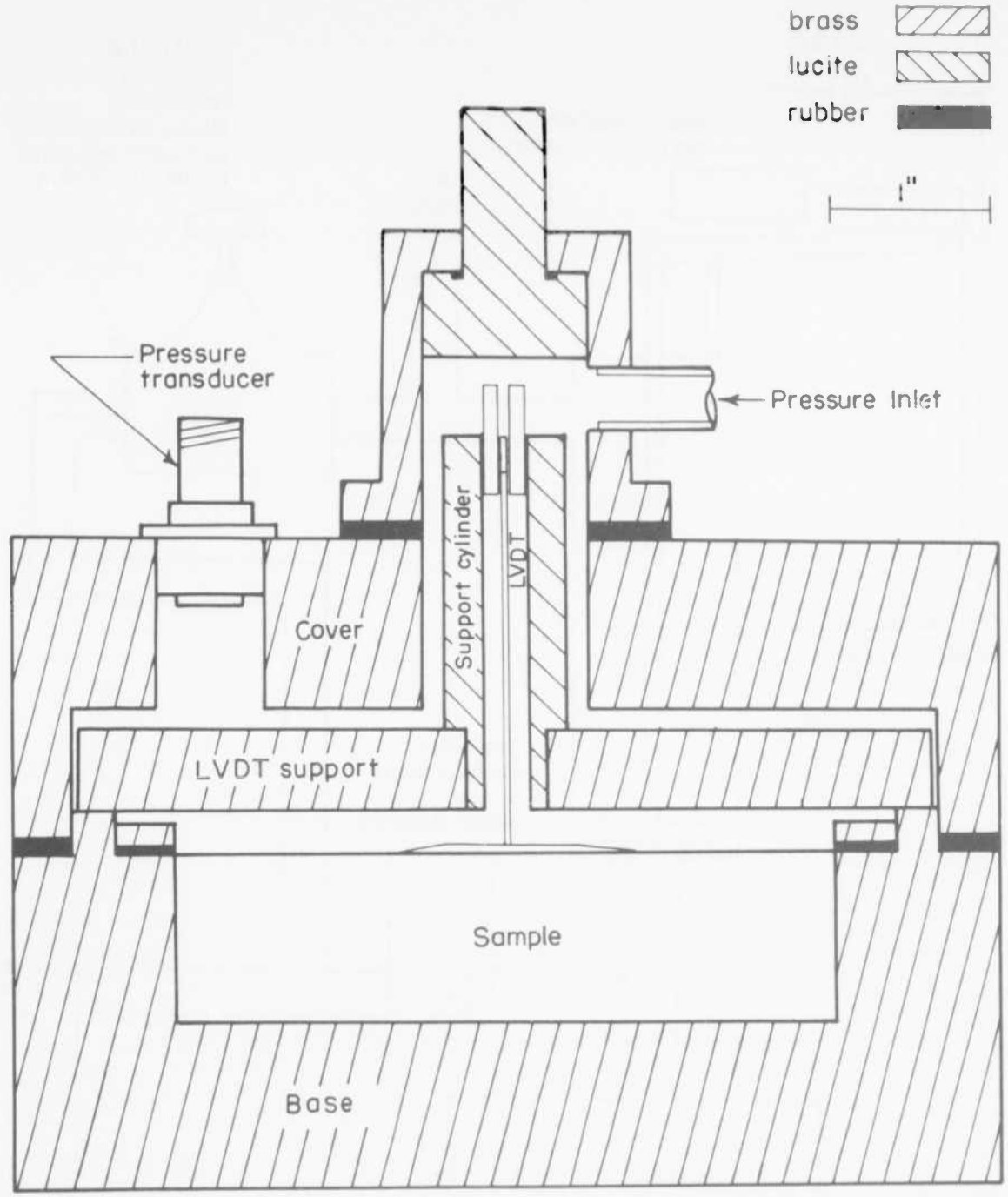

FIGURE 7 CROSS-SECTION THROUGH OEDOMETER III

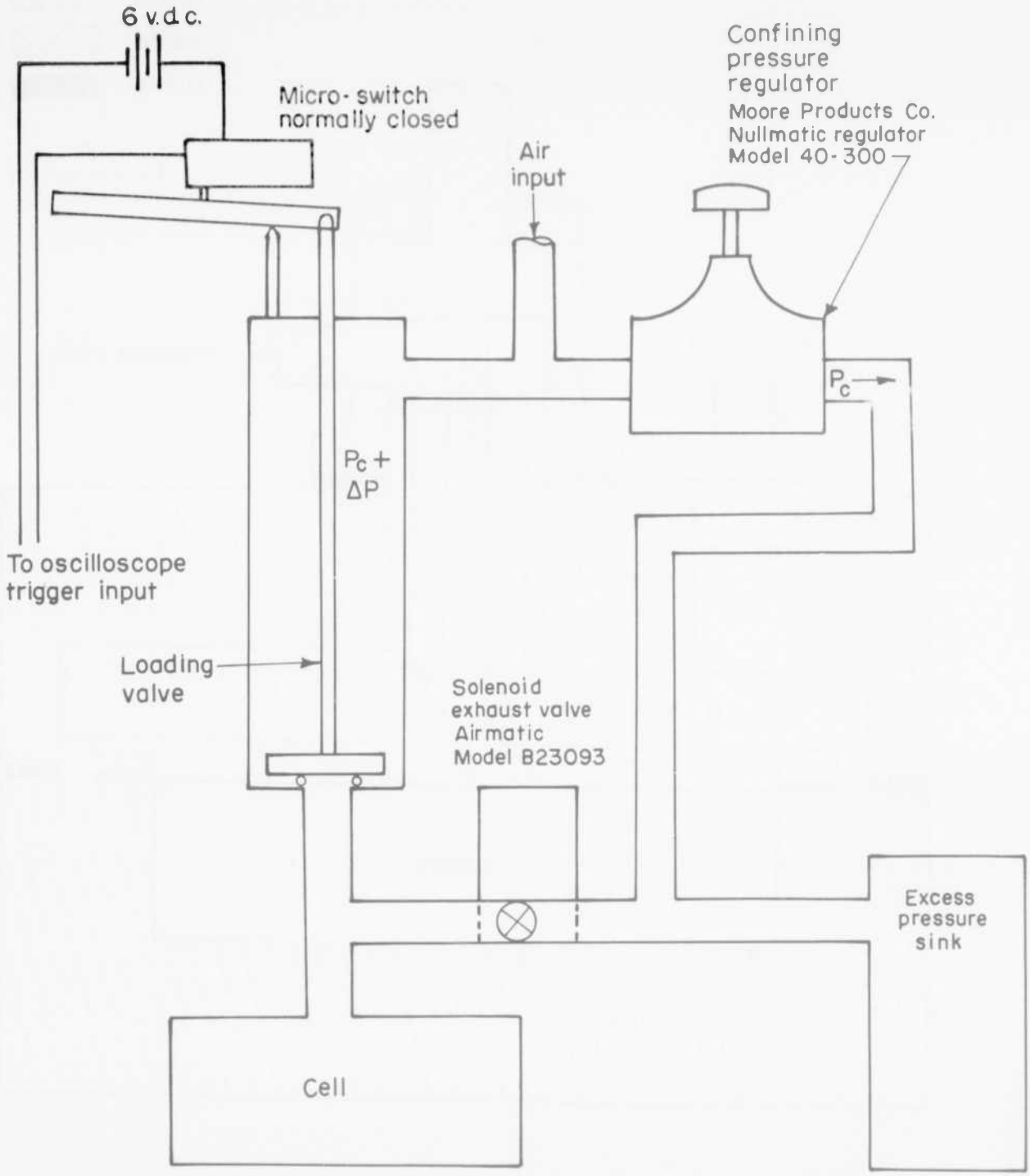

FIGURE 8 VALVING SYSTEM, OEDOMETER III

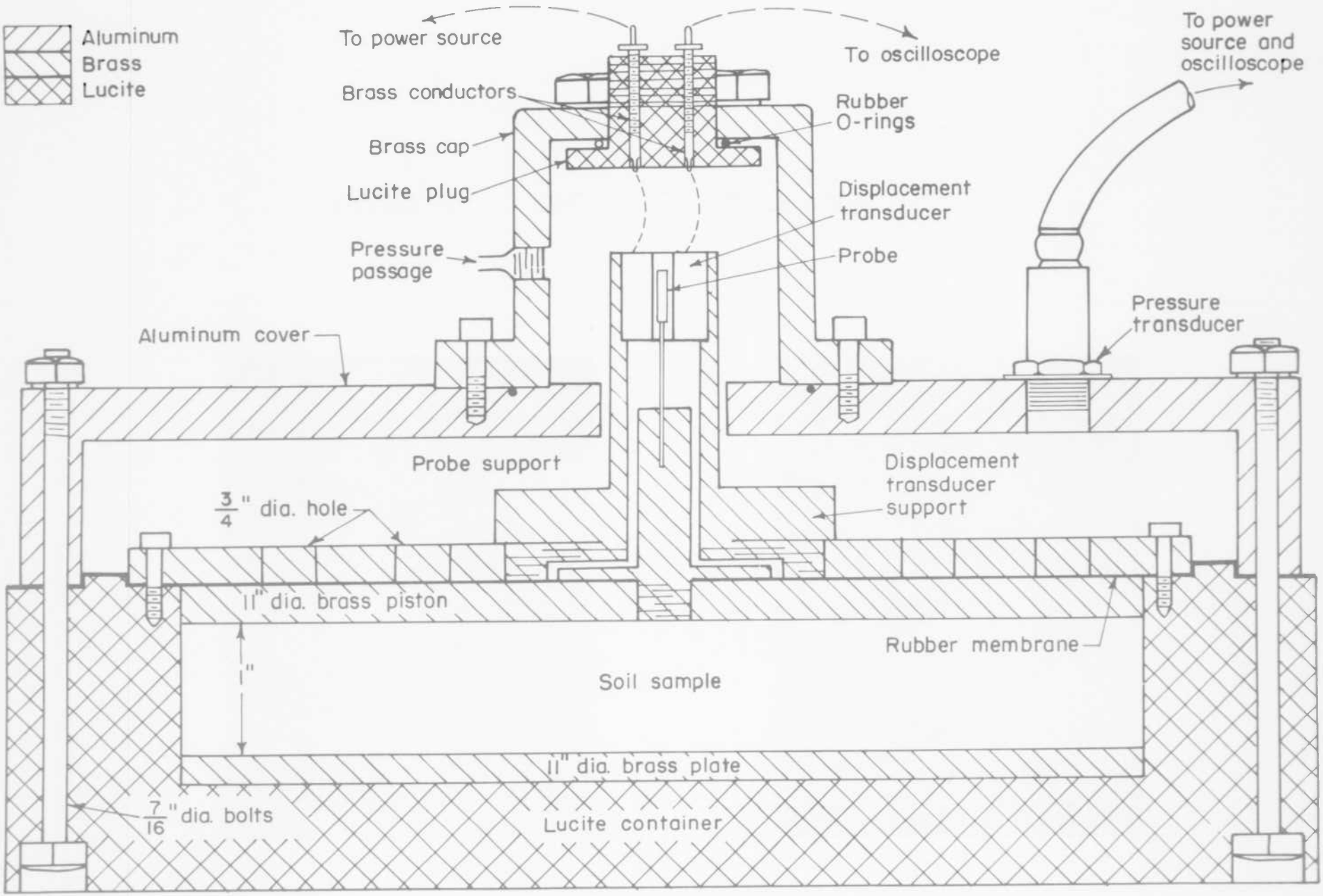

FIGURE 9 CROSS-SECTION THROUGH LARGE OEDOMETER

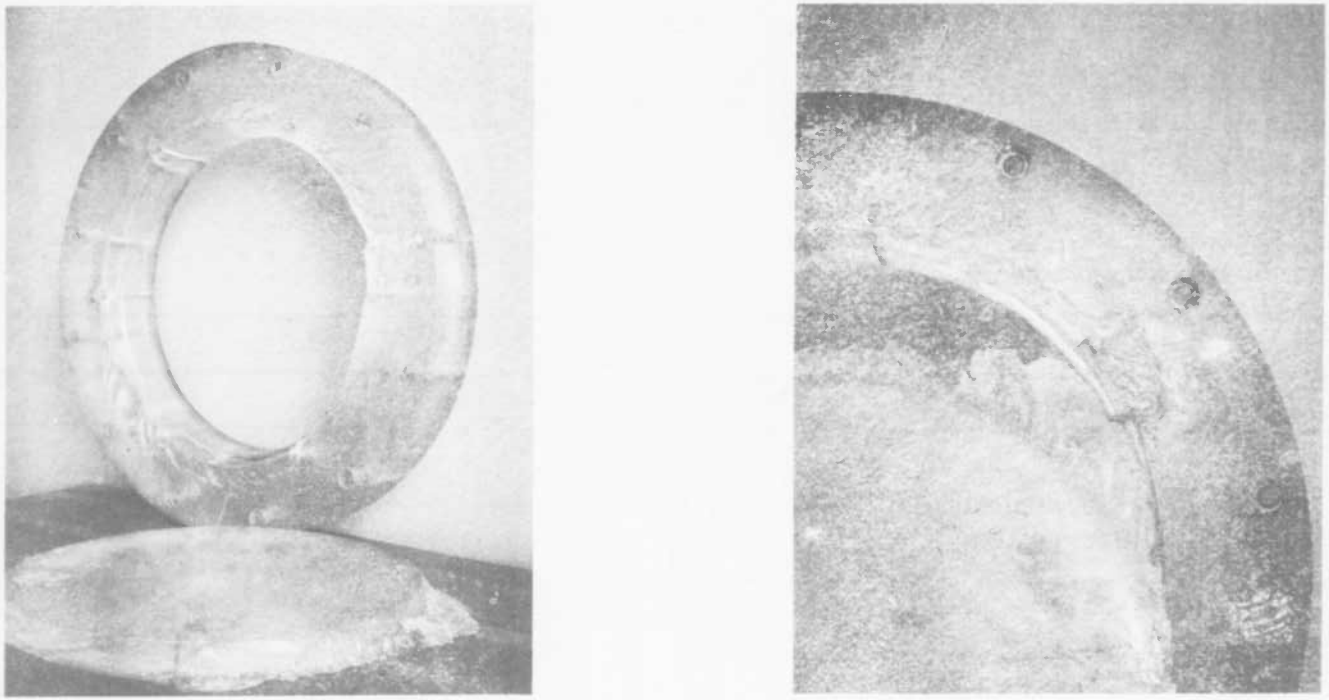

FIGURE 10 FAILURE OF LUCITE BASE

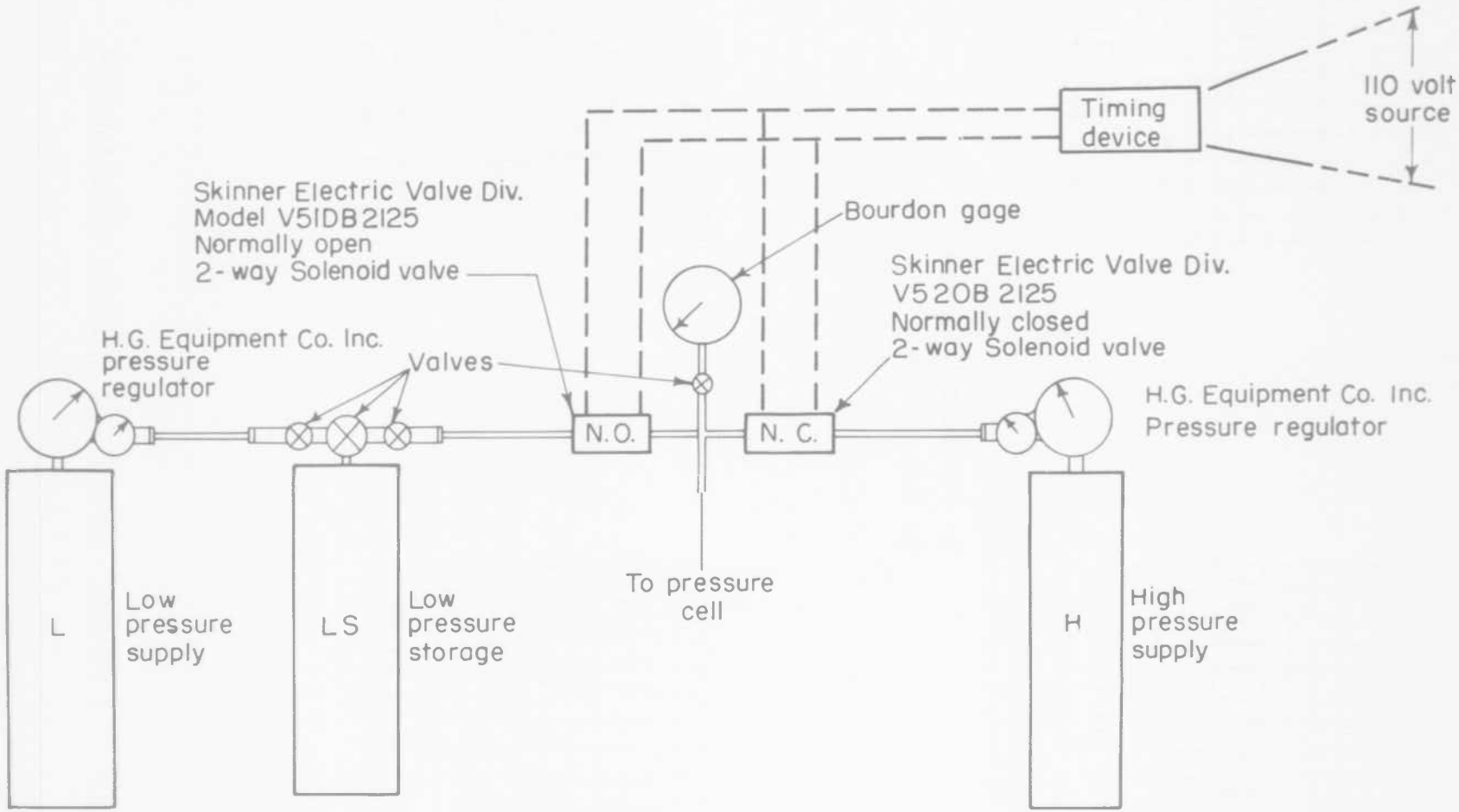

FIGURE 11 PRESSURE SUPPLY SYSTEM

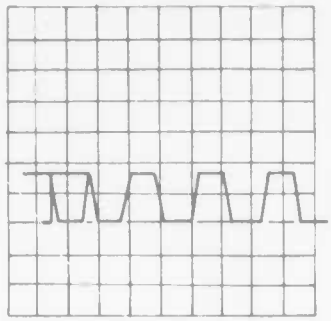

I = 20 → 30 psi
S = 5 sec/cm

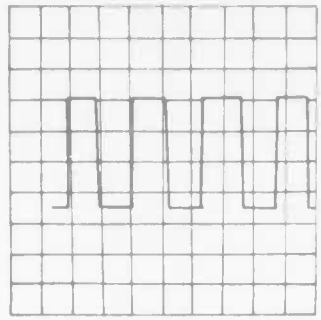

I = 30 → 40 psi
S = 2 sec/cm

I - Pressure Increment
S - Sweep rate

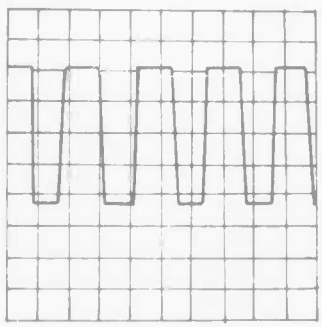

I = 0 → 50 psi
S = 5 sec/cm

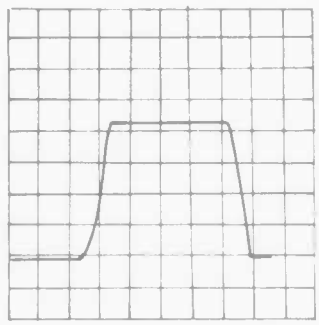

I = 0 → 50 psi
S = 1 sec/cm

FIGURE 12 TYPICAL CYCLE IN LARGE OEDOMETER

Oscillations (widening) of early portion of traces caused by Electrical and/or Mechanical coupling of solenoid valve operation and stress transducer circuit

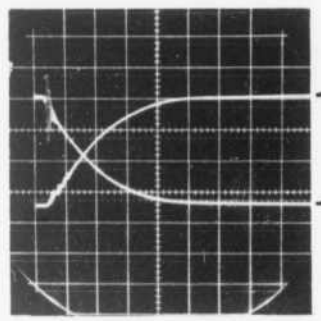

Stress Increment = 40 psi
Sweep rate = 20 milliseconds / division

FIGURE 13 DISPLAY OF ELECTRO-MECHANICAL COUPLING EFFECT

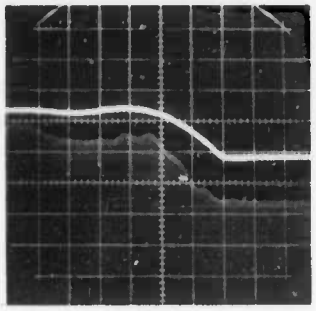

(a)

Sweep 5 milliseconds /cm

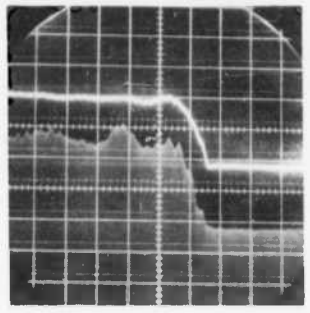

(b)

Sweep 5 milliseconds/c

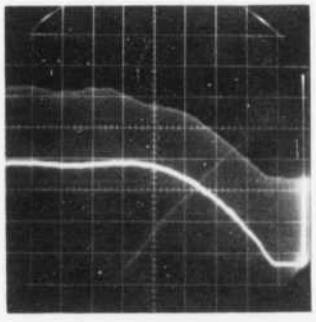

(c)

Sweep - 2 milliseconds/ cm

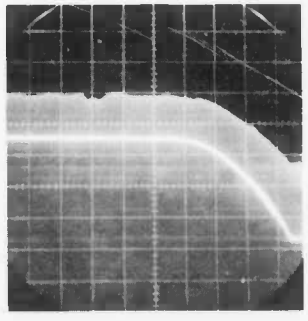

(d)

Sweep - 5 milliseconds / cm

FIGURE 14 STRAIN TRACE OSCILLATIONS

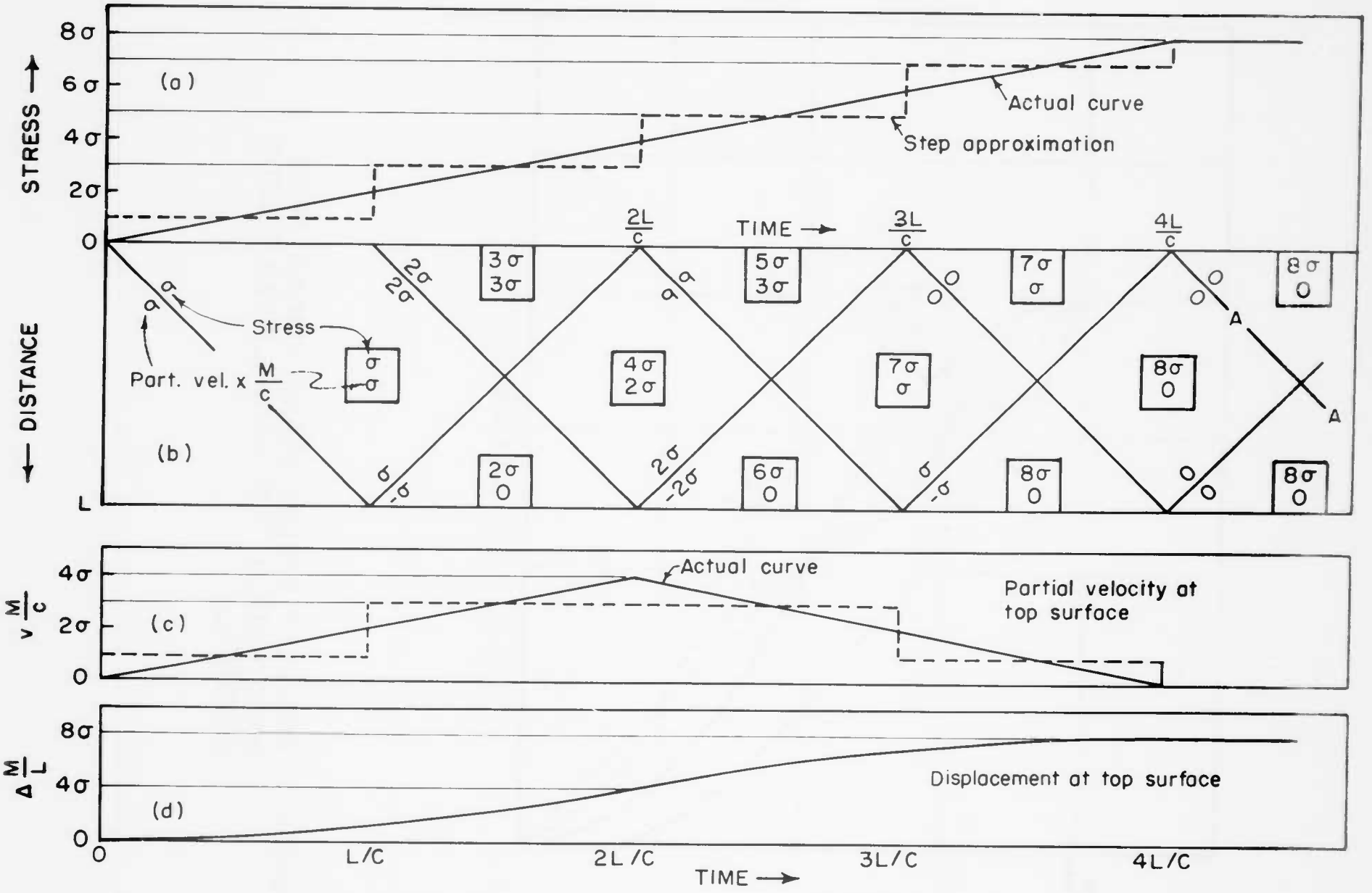

FIGURE 15 WAVE PROPAGATION DURING HYPOTHETICAL TEST UPON LINEAR ELASTIC MATERIAL

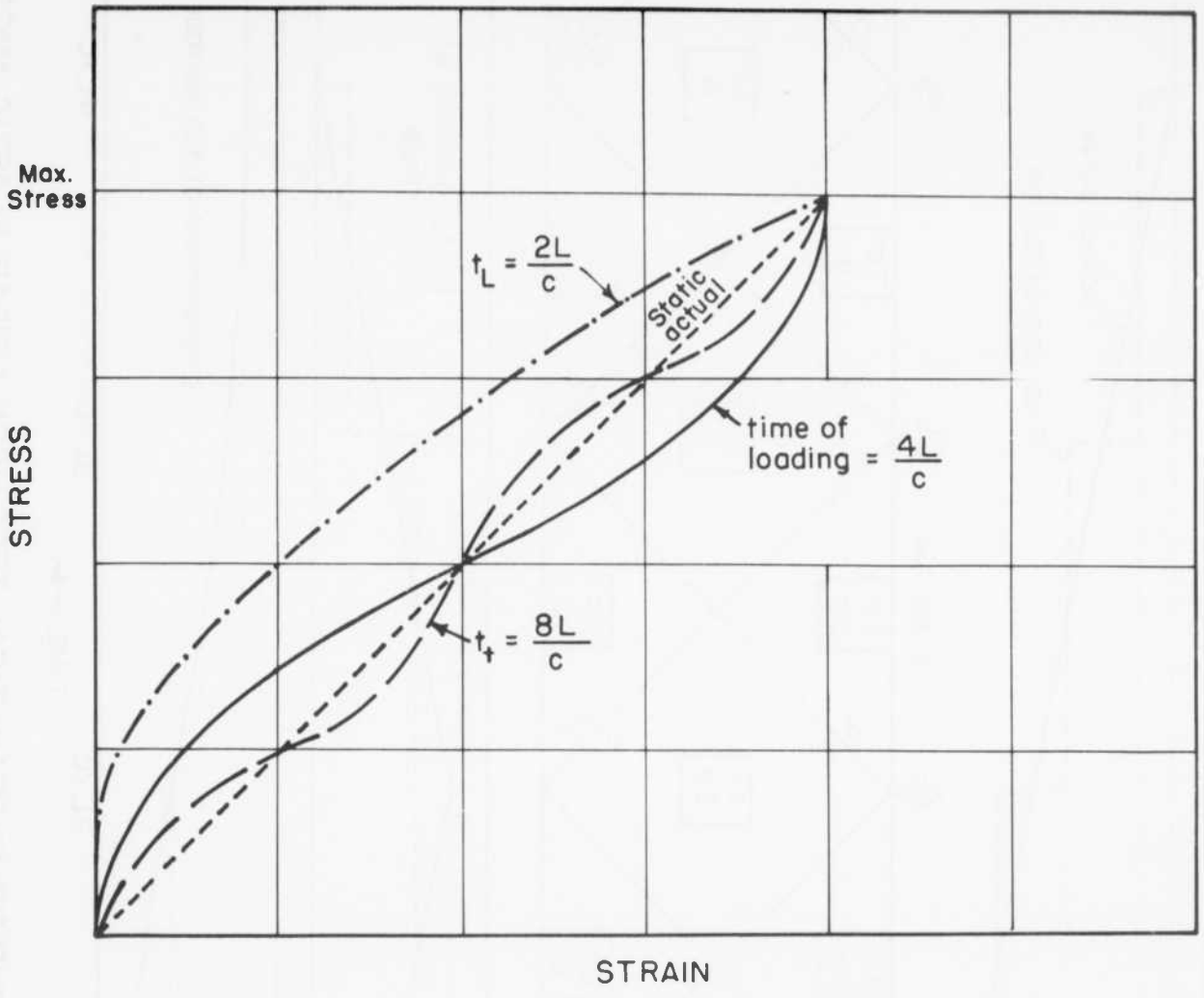

FIGURE 16 APPARENT STRESS-STRAIN CURVES FROM HYPOTHETICAL TEST UPON LINEAR ELASTIC MATERIAL

APPENDIX D

FIRST SERIES OF RAPID LOADING TESTS UPON GRANULAR MATERIALS

PREFACE

The tests reported in this appendix were carried out by Jerome York, a research assistant, employed by the Soil Dynamics Project during the period from September 1961 through January 1962. Edmond T. Miller and Peter J. Moore, both research assistants, have aided the writer in the reduction and interpretation of the data.

LIST OF FIGURES

1 Data from Test Y2 on Ottawa Sand

2 Data from Test Y6 on Ottawa Sand

3 Stress-Strain Data for Ottawa Sand: Initial Stress of 10 lb/in^2

4 Stress-Strain Data for Ottawa Sand: Initial Stress of 100 lb/in^2

5 Stress-Strain Data for Ottawa Sand: Small Stress Increments

6 Early Creep in Ottawa Sand

7 Stress-Strain for Glass Beads

8 Stress-Strain Data for Glass Beads

LIST OF TABLES

I Test Program for Ottawa Sand

II Uncorrected Data for Modulus of Ottawa Sand

III Corrected Data for Modulus of Ottawa Sand

IV Test Program for Glass Beads

V Constrained Moduli for Glass Beads

1. Test Program

This series of tests was designed to provide preliminary information concerning the effect of initial stress level and stress increment upon the strain-time response of granular materials to a rapidly applied one-dimensional loading. Two granular materials were studied: 20-30 mesh Ottawa sand, and glass beads having the following particle size distribution:

Fraction retained on U. S. Sieve No. 20: 0%
40: 70%
50: 25%
60: 5%

Each of these materials was tested at essentially 100% relative density.

Cedometer II, with value system A, was used for these tests. Each test involved the program of cyclic loading and unloading described at the end of Section 1, Appendix C.

An old oscillator was used to provide the input to the LVDT, and neither the frequency nor the voltage of the output of this oscillator could be set accurately. To get around these difficulties, the LVDT was calibrated immediately before each test, and the settings of the oscillator were then left untouched until the test was complete.

A dry-cell battery was used to provide the input for the pressure transducer, and the voltage of this battery tended to fluctuate rather rapidly and to degrade with use. This circumstance meant that the relationship between the output of the transducer and the applied pressure was changing all the time. Unfortunately, the exact value of the input voltage during each test was not recorded. Thus, even though the output of the pressure transducer was observed during each test with an oscilloscope, these observations could not be used to determine the pressure actually being applied to the soil. The pressure being applied as an initial stress and the pressure made available for the pressure increment were read with ordinary Bourdon gages. During the first reduction of the data, the "nominal pressure increment" determined from these Bourdon gage readings was used to compute the desired stress-strain ratios. It soon became apparent that the results of these

tests were inconsistent and, as will be described, an attempt was made to correct the pressure increment values.

2. Tests Upon Ottawa Sand

Sand was tamped into the specimen container so as to obtain essentially maximum density. The procedure employed ensured that the same void ratio was achieved in each test. The actual void ratio value was 0.53, which seems rather high, but it appears that the minimum void ratio of Ottawa sand varies from batch to batch.

Table I indicates the scope of the test program. A fresh specimen was used for all tests except Y1b and Y4b. The rise-time of stress varied as the applied pressures varied, as indicated in the table. The beams swept across the oscilloscope in 50 milliseconds: thus there was moderately good definition of the rising portions of the stress-time and strain-time curves, but only a short interval of time was available for the observation of creep strains.

Figures 1 and 2 show typical sets of data as they were recorded during the tests. The numbers in the tables on these figures are deflections of the strain beam measured in grid spacings. Thus, during the first cycle of loading for test Y2, the strain beam had deflected 2.6 spaces by the time that the first visual reading was made at 15 seconds following load application, and no further beam deflection occurred during the remaining 2-3/4 minutes of the load cycle. When the stress increment was removed, the first visual reading found the strain beam 0.8 spaces from its original position; i.e. the strain decreased by 1.8 spaces as the result of unloading. The next cycle of loading increased the strain by 1.9 spaces, etc.

The figures also contain typical photographs of the oscilloscope screen as taken to record the strains during and just after the sudden increase of applied pressure. There was a considerable overshoot when the pressure movement was only 10 lb./in.^{2}, but relatively little overshoot when the larger increments were used.

2.1 Analysis of data for modulus

Based upon such data, three different modulus values were computed: "fast modulus", equal to the nominal pressure increment divided by the change in strain immediately following the initial rise in the pressure increment; "slow modulus", equal to the nominal pressure increment divided by the change in strain at the end of the three minute loading interval; and "unloading modulus", equal to the nominal pressure increment divided by the change in strain at the end of the three minute interval of unloading. In all cases the change in strain was measured relative to the strain at the end of the preceding interval. "Slow" and "unloading" moduli were determined from each of the ten cycles of load application; the "fast" modulus was determined only for those load applications during which the oscilloscope was photographed.

Table II summarizes the modulus data for the various tests as determined by these procedures.* The precision with which the strain, and hence the modulus, can be determined from an oscilloscope picture is obviously rather low. This situation undoubtedly accounts for the fact that the moduli values sometimes decrease with increasing number of cycles instead of increasing as would be expected. The values of slow and unloading modulus for the 5th and 10th cycles are actually average values for the 4th, 5th, 6th and 8th, 9th, 10th cycles, respectively.

The test results given in Table II all seem reasonable, with the exception of those for test Y6. It had been expected that the modulus values from this test would be as large, if not larger, than those from tests Y4 through Y5. Concern about the results from this test led to a re-examination of the information concerning the actual magnitude of the pressure increment.

A calibration curve was established for the pressure transducer, and an estimate was made of the battery voltage which probably existed during the test program. Then the probable magnitude of the immediate pressure increment (that existing just after the initial rapid rise in pressure) was computed from the photographs of pressure traces such as those in Figures 1 and 2. These studies led to the "estimated immediate increment" values

*These results have not been corrected for apparatus compressibility.

listed in Table I. Unfortunately, the position of the pressure trace was not recorded during visual readings. Thus there is no real way of knowing just how much the pressure increased above the immediate value (see Section 2.2, Appendix C). Based upon other studies, an estimate was made as to how much this increase might be, and the "estimated final increment" values listed in Table I were thus established. The modulus data of Table II were then recomputed, and the values given in Table III are based upon "estimated actual pressure increments".

It is hard to be sure that the corrected values are really any more accurate than the uncorrected modulus values. The only really large change was in the results for test Y6, and these results were brought more into line with the rest of the results. The difference between the fast and slow modulus values was reduced as the result of the correction; it certainly was too large in the uncorrected data, but it is not certain that the difference is really correct in the corrected data. The correction has not changed the ratio of slow to unloading modulus.

Despite the scarcity of the data and the uncertainties regarding the data, a few conclusions may be drawn from the information presented in Table III.

(a) The slow modulus increases considerably between the first and second cycles. By the fifth cycle of loading this modulus has essentially arrived at a stabilized value, and increases only slightly as the result of further loading cycles. The rate of stabilization is somewhat slower when the initial pressure is low.

(b) After the first two cycles of loading the slow and unloading moduli are essentially the same; that is, there is a substantially complete (although not quite complete) recovery of strain as the result of one cycle of loading and unloading.

(c) The modulus values increase with an increase in the initial stress level.

(d) To the extent that it is possible to draw any conclusion regarding the effect of the stress increment, it would appear that:

(1) with a low initial stress level, an increase in the size of the stress increment leads to an increase in the stabilized slow and unloading moduli; while (2) at high initial pressure, an increase in the size of the stress increment leads to a decrease in the magnitude of the stabilized slow and unloading moduli.

2.2 Stress-Strain Curves

Starting from photographs such as those in Figures 1 and 2, it is possible to construct diagrams which show the stress-strain relation during the interval of rapid pressure rise. Figures 3, 4 and 5 show some of the results of this data take-off. Each of the data points plotted in Figures 4 and 5 represents an individual take-off of stress and strain from a pair of stress-time and strain-time curves.

When the initial stress level was low and the stress increment large, the stress-strain curves proved to be concave toward the stress axis, as is commonly found for granular materials (see Figure 3).

When the initial stress level was high and the stress increment large (see Figure 4) the apparent stress-strain relation was substantially linear over the major portion of its length. However, if the straight line relation is extended back toward zero strain, there would apparently be a stress intercept. Apparently the stress-strain curve starts off with a steeper slope. At high pressures, the stress-strain curve shown in Figure 4 tends to bend over, presumably as the result of a creep phenomenon.

Figure 5 shows the results from tests with a small stress increment. The results in this figure would suggest that the stress-strain relation is actually concave toward the strain axis, especially when the initial stress level is large.

The trends noted in Figures 3 through 5 would tend to confirm the tentative conclusions set forth in Item (d) of the previous subsection. Obviously, however, the data are not sufficient to permit a firm conclusion.

2.3 Data Regarding Creep

From examination of photographs such as those in Figures 1 and 2, it was generally observed that the strain continued to rise following the initial rapid rise in pressure. Some of this continued increase in strain resulted from the continued increase in pressure. Figure 6 was constructed in an attempt to tell whether any creep phenomena was present. Time marks were laid off upon the photographs at 10, 20, etc. milliseconds intervals following the end of the initial rapid rise in pressure. At each of these time marks, the ratio of the excursion of the strain trace to the excursion of the stress trace was determined. This ratio was normalized by dividing by the ratio of strain trace excursion to stress trace excursion at the end of the initial rapid rise of pressure. Figure 6 thus shows the strain creep corrected for the fact that the stress is actually increased somewhat during the time intervals shown.

The wide scatter of the data points reflects the extreme difficulty inherent in taking off such data from the photographs. Averaging all points together, it would appear that a creep phenomena is present for approximately the first 20 milliseconds following the initial rapid rise in pressure. To the extent that it is possible to identify the effect of the test variables upon the amount of creep, it would seem that the creep was greatest when both the initial pressure and the stress increment were large, and was least when the initial pressure was small.

3. Tests Upon Glass Beads

Table IV indicates the scope of test program involving glass beads. The procedures involved in these tests were quite similar to those used for the tests upon Ottawa sand. The beads were placed in the specimen container at essentially the maximum density for this assortment of beads. The exact void ratio was not recorded during this test program, but based upon subsequent work it would appear that the void ratio was about 0.61. A sizeable fraction of the beads were not of spherical shape, and this fact accounts for the rather high value of minimum void ratio. With regard to both the general characteristics of the oscilloscope photographs and the visual strain readings, the data from the tests upon glass beads were entirely similar to the data obtained for Ottawa sand.

A tabulation of the modulus values obtained for several cycles for each of the four tests is shown in Table V. The definitions of fast modulus, slow modulus and unloading modulus are the same as in the case of the Ottawa sand tests. Since these moduli made use of the nominal stress increment, a set of corrected values has been placed in Table V beneath the uncorrected figures. This correction makes allowance for the fact that the nominal stress increment is not always the stress increment which is applied. Since the battery voltage was not measured and since measurements of stress changes were not made following the first 50m. seconds of the loading cycle, it was necessary to estimate the applied stresses. These estimates are shown in Table IV. By using oscilloscope photographs and by making a reasonable estimate of the battery voltage, an estimate of the immediate increment could be made with some confidence. For estimating the final increment a more uncertain basis had to be applied. From other test data which was obtained using a similar test set-up to that used for the glass beads, it was known that the ratio of the immediate to the final increment averaged around 0.75. Consequently this was the figure which was used to estimate the final increment for glass beads.

As indicated in Tables IV and V, the results of Test Y9 were particularly affected by this correction since here the applied stress

increment was vastly different from the nominal increment.

An examination of Table V indicates that fast, slow and unloading moduli are increased considerably by an increase in initial confining pressure. For both the 10 lb./in.^{2} and 100 lb./in.^{2} initial pressures, however, it appears that the effect of increasing the stress increment does not significantly change the three moduli. For all four tests the fast and slow moduli do not differ by a significant amount. For long term creep effects to be present the slow modulus would be expected to be significantly lower than the fast modulus. If anything the slow moduli obtained in these four tests seems to be slightly greater than the corresponding fast moduli. Therefore, it appears that no long term creep has taken place. This conclusion must be accepted conditionally since it must be remembered that it is based on adjusted results and not on directly measured values of stress.

Oscilloscope photographs were generally taken on the loading portion of cycles 2, 5 and 10 for each test. These photographs are similar in general appearance to those shown in Figures 1 and 2 for Ottawa sand. By reading off points on the photographs, the stress-strain curves for cycles 2 and 10 in Figures 7 and 8 were obtained. Tests Y7 and Y10 and Tests Y8 and Y9 have been plotted together since each pair had the same nominal stress increment.

The stress-strain characteristics of those tests with the same initial pressure are almost identical. This is really just another way of restating the comment above that increasing the stress increment does not greatly influence the modulus. The indication of any long term creep in these curves would be the bending over of the stress-strain curve to show a concavity to the strain axis. As this concavity is not observed, it again suggests that long term creep is not present.

Special mention should be made of the two final points on cycle 10 of Test Y9 shown in Figure 8. These two points show the same strain. The 23 lb./in.^{2} stress for the upper point was obtained by applying the ratio 4/3 to the immediate stress increment. Examination of the photograph for this cycle shows that for 50m.seconds after loading both stress and strain traces remained horizontal. So it appears likely that this is one case where

the final increment and immediate stress increment were equal.

3.1 Conclusions

(a) The fast, slow and unloading moduli increase noticeably with an increase in initial confining pressure.

(b) The three moduli are not significantly affected by changes in stress increment.

(c) There does not appear to be any long term creep effects present.

Table I

TEST PROGRAM FOR OTTAWA SAND

Test	Initial Pressure lb/in^2	Nominal Increment lb/in^2	Est. Immed. Increment lb/in^2	Est. Final Increment lb/in^2	Rise Time M Sec
Y1	10	100	75	85	18
Y1a	10	200	160	180	22
Y2	10	200	165	185	20
Y3	10	10	11	13	8
Y4	100	100	100	105	11
Y4a	100	200	195	205	15
Y5	100	200	175	185	16
Y6	100	10	24	25	5

TABLE II

UNCORRECTED DATA FOR MODULUS OF OTTAWA SAND

(thousands of lb./in.²)

Test No.	Initial p lb./in.²	Nominal Δp lb./in.²	Fast Modulus				Slow Modulus				Unloading Modulus			
			Cycle 1	Cycle 2	Cycle 5	Cycle 10	Cycle 1	Cycle 2	Cycle 5	Cycle 10	Cycle 1	Cycle 2	Cycle 5	Cycle 10
Y1	10	100		60	63	63	47	47	49	51	49	49	50	53
Y1a	10	200		71	66	66	40	54	56	57	57	57	57	58
Y2	10	100	42		61	66	35	48	51	55	51	51	54	57
Y3	10	10		27	32	31	26	23	27	27	26	26	27	27
Y4	100	100		87	94	94	44	66	75	75	66	75	75	77
Y4a	100	200		105	118	118	73	86	86	94	86	86	86	94
Y5	100	200		106	119	106	50	79	79	86	86	86	86	86
Y6	100	10		28	39	47	22	24	32	39	26	32	35	39

TABLE III

CORRECTED DATA FOR MODULUS OF OTTAWA SAND

(thousands of lb./in.^{2})

Test No.	Initial p lb./in.^{2}	Nominal Δp lb./in.^{2}	Fast Modulus				Slow Modulus				Unloading Modulus			
			Cycle 1	Cycle 2	Cycle 5	Cycle 10	Cycle 1	Cycle 2	Cycle 5	Cycle 10	Cycle 1	Cycle 2	Cycle 5	Cycle 10
Y1	10	100		45	47	47	40	40	42	43	42	42	43	45
Y1a	10	200		57	53	53	36	49	50	51	51	51	51	52
Y2	10	100	35		50	54	32	44	47	51	47	47	50	53
Y3	10	10		30	35	34	34	30	35	35	34	34	35	35
Y4	100	100		87	94	94	46	69	79	79	69	79	79	81
Y4a	100	200		102	115	115	75	88	88	95	88	88	88	95
Y5	100	200		93	104	93	46	73	73	80	80	80	80	80
Y6	100	10		67	94	113	55	60	80	98	65	80	90	98

Table IV

TEST PROGRAM FOR GLASS BEADS

Test	Initial Pressure lb/in^2	Nominal Increment lb/in^2	Est. Immed. Increment lb/in^2	Est. Final Increment lb/in^2	Rise Time M Sec
Y7	10	100	77	100	15
Y8	10	10	9	12	12
Y9	100	10	17	23	10
Y10	100	100	91	120	14

TABLE V CONSTRAINED MODULI FOR GLASS BEADS
(thousands of lb./in.^{2})

Test No.	Fast Modulus			Slow Modulus				Unloading Modulus			
	Cycle 2	Cycle 5	Cycle 10	Cycle 1	Cycle 2	Cycle 5	Cycle 10	Cycle 1	Cycle 2	Cycle 5	Cycle 10
Uncorrected											
Y 7	61	61	61	47	51	51	51	51	51	51	51
Y 8	45	45	50	26	34	34	37	34	37	34	37
Y 9	46	51	57	35	41	46	51	41	41	51	51
Y 10	94	102	102	56	77	82	88	77	82	88	88
Corrected											
Y 7	47	47	47	47	51	51	51	51	51	51	51
Y 8	40	40	44	31	41	41	44	41	44	41	44
Y 9	88	91	97	80	95	105	116	95	95	116	116
Y 10	86	93	93	67	92	98	105	92	98	105	105

Visual strain readings, in grid spaces

Time min.	Cycle 1		Cycle 2		Cycle 3		Cycle 4		Cycle 5		Cycle 6		Cycle 7		Cycle 8		Cycle 9		Cycle 10	
	Load	Unload	Load	Unload	Load	Unload	Load	Unload	Load	Unload	Load	Unload	Load	Unload	Load	Unload	Load	Unload	Load	Unload
1/4	2.6	0.8	2.7	0.9	2.8	1.0	2.8	1.1	2.9	1.2	2.9	1.2	2.9	1.3	3.0	1.3	3.0	1.4	3.0	1.4
1	2.6	0.8	2.7	0.9	2.8	1.0	2.8	1.1	2.9	1.2	2.9	1.2	3.0	1.3	3.0	1.3	3.0	1.4	3.0	1.4
2	2.6	0.8	2.7	0.9	2.8	1.0	2.8	1.1	2.9	1.2	2.9	1.2	3.0	1.3	3.0	1.3	3.0	1.4	3.0	1.4
3	2.6	0.8	2.7	0.9	2.8	1.0	2.8	1.1	2.9	1.2	2.9	1.2	3.0	1.3	3.0	1.3	3.0	1.4	3.0	1.4

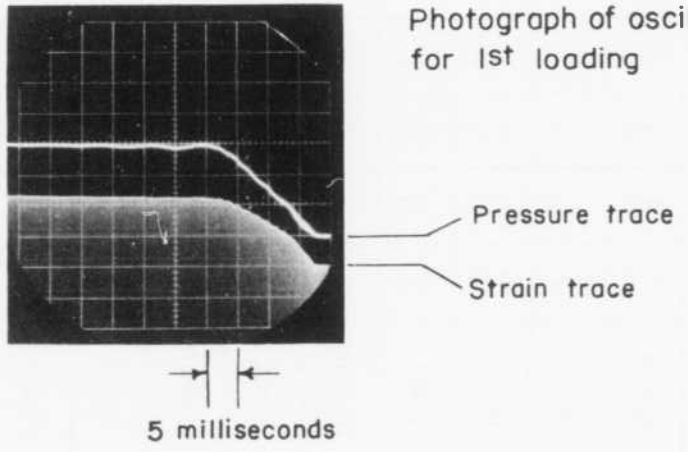

FIGURE 1 DATA FROM TEST Y2 ON OTTAWA SAND

Visual strain readings, in grid spaces

Time min.	Cycle 1		Cycle 2		Cycle 3		Cycle 4		Cycle 5		Cycle 6		Cycle 7		Cycle 8		Cycle 9		Cycle 10	
	Load	Unload	Load	Unload	Load	Unload	Load	Unload	Load	Unload	Load	Unload	Load	Unload	Load	Unload	Load	Unload	Load	Unload
1/4	4.6	0.8	4.7	1.8	4.9	2.0	5.0	2.1	5.1	2.3	5.1	2.5	5.2	2.7	5.2	2.8	5.2	2.8	5.2	2.8
1	4.6	0.8	4.8	1.8	4.9	1.9	5.0	2.0	5.1	2.2	5.1	2.4	5.2	2.6	5.2	2.7	5.2	2.7	5.2	2.7
2	4.7	0.7	4.8	1.7	5.0	1.9	5.0	1.9	5.1	2.2	5.1	2.4	5.2	2.6	5.2	2.6	5.2	2.6	5.2	2.6
3	4.7	0.7	4.9	1.7	5.0	1.9	5.1	1.8	5.1	2.2	5.1	2.4	5.2	2.6	5.2	2.6	5.2	2.6	5.2	2.6

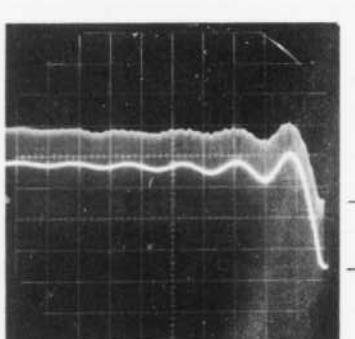

Photograph of oscilloscope for 10th loading

FIGURE 2 DATA FROM TEST Y6 ON OTTAWA SAND

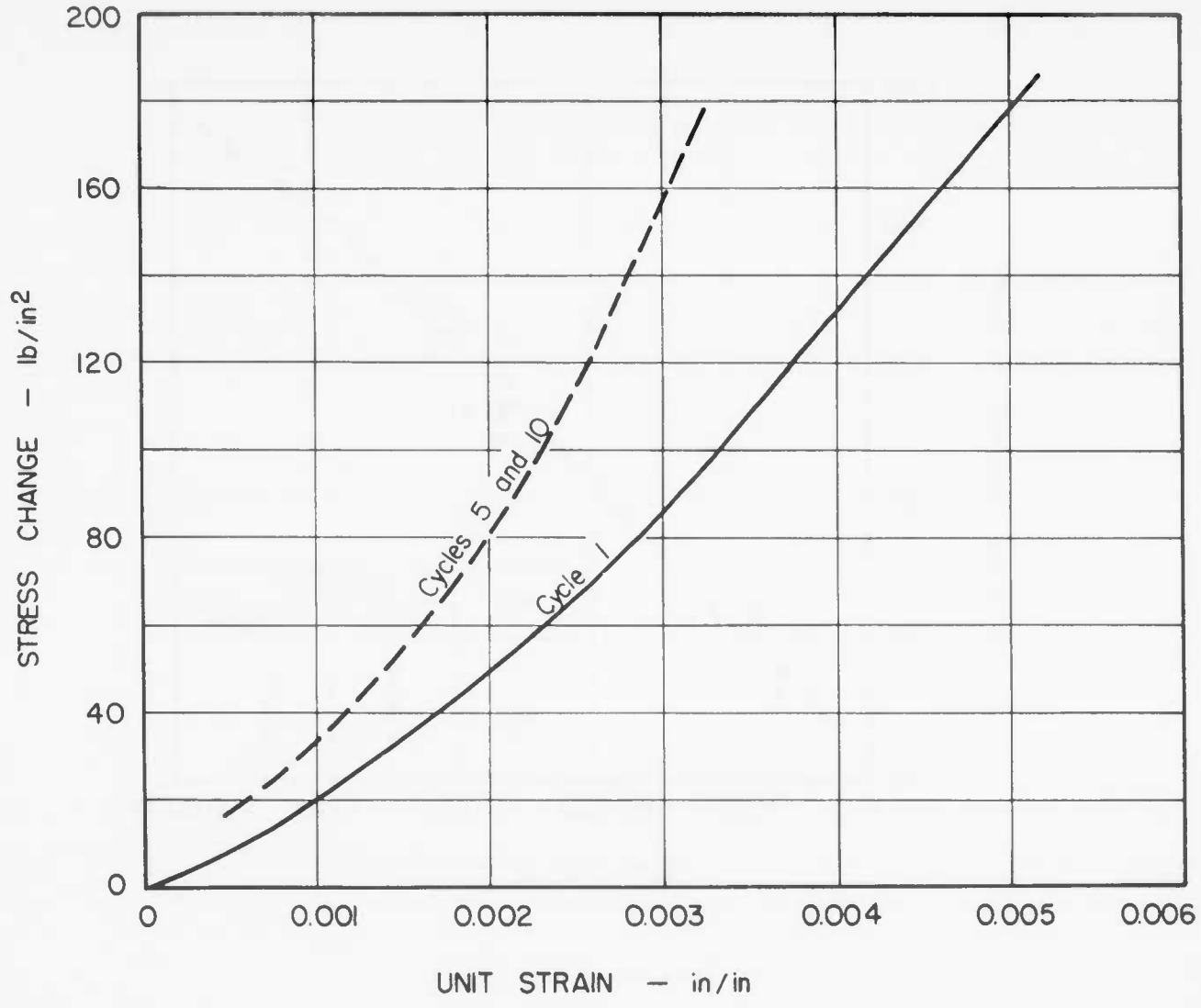

FIGURE 3 STRESS - STRAIN DATA FOR OTTAWA SAND: INITIAL STRESS OF 10 LB/IN^2

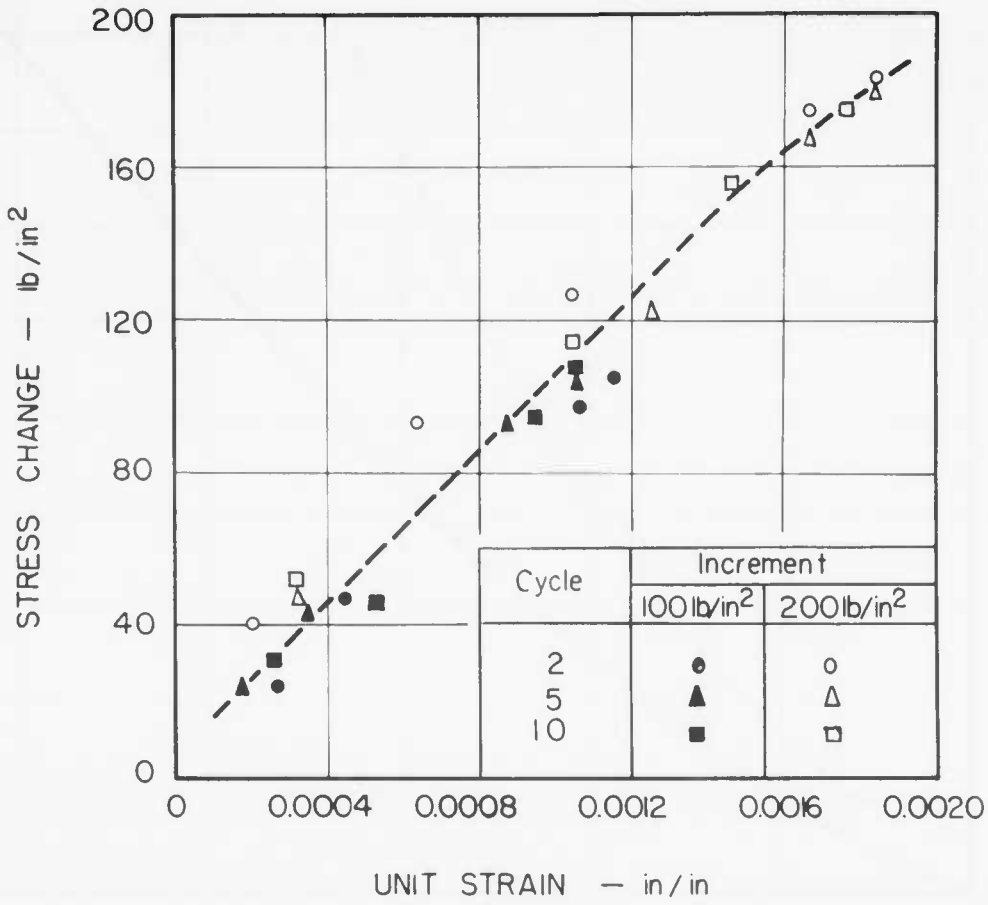

FIGURE 4 STRESS–STRAIN DATA FOR OTTAWA SAND
INITIAL STRESS OF 100 LB/IN^2

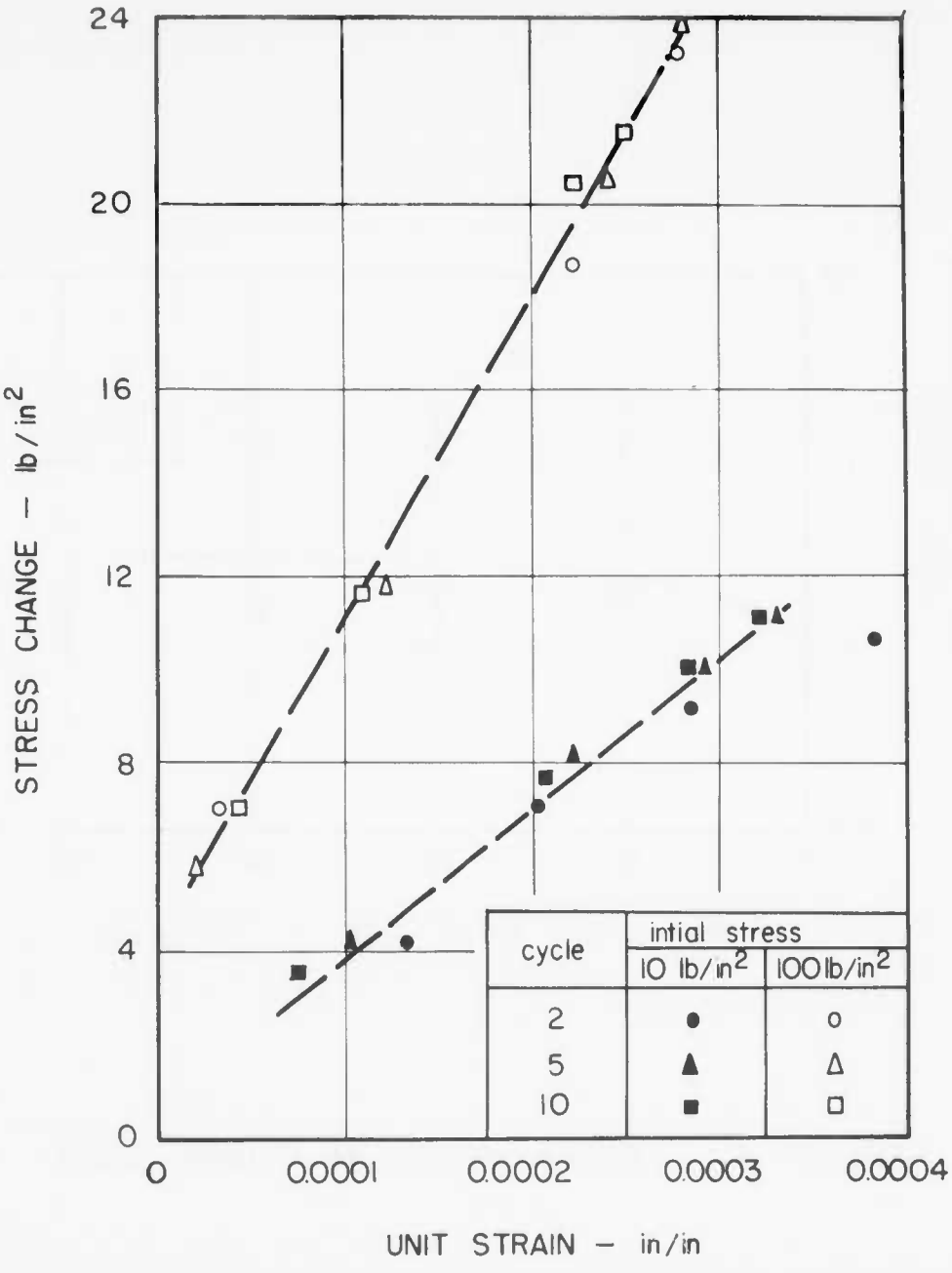

FIGURE 5 STRESS-STRAIN DATA FOR OTTAWA SAND: SMALL STRESS INCREMENTS

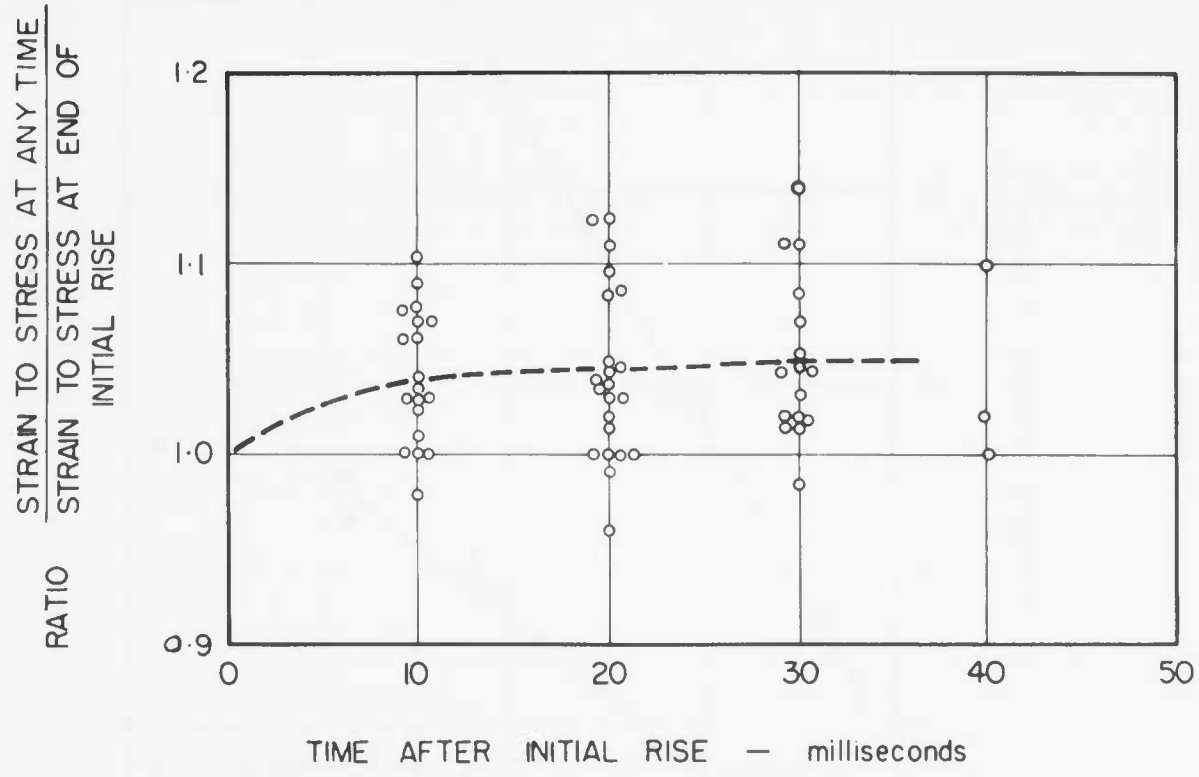

FIGURE 6 EARLY CREEP IN OTTAWA SAND

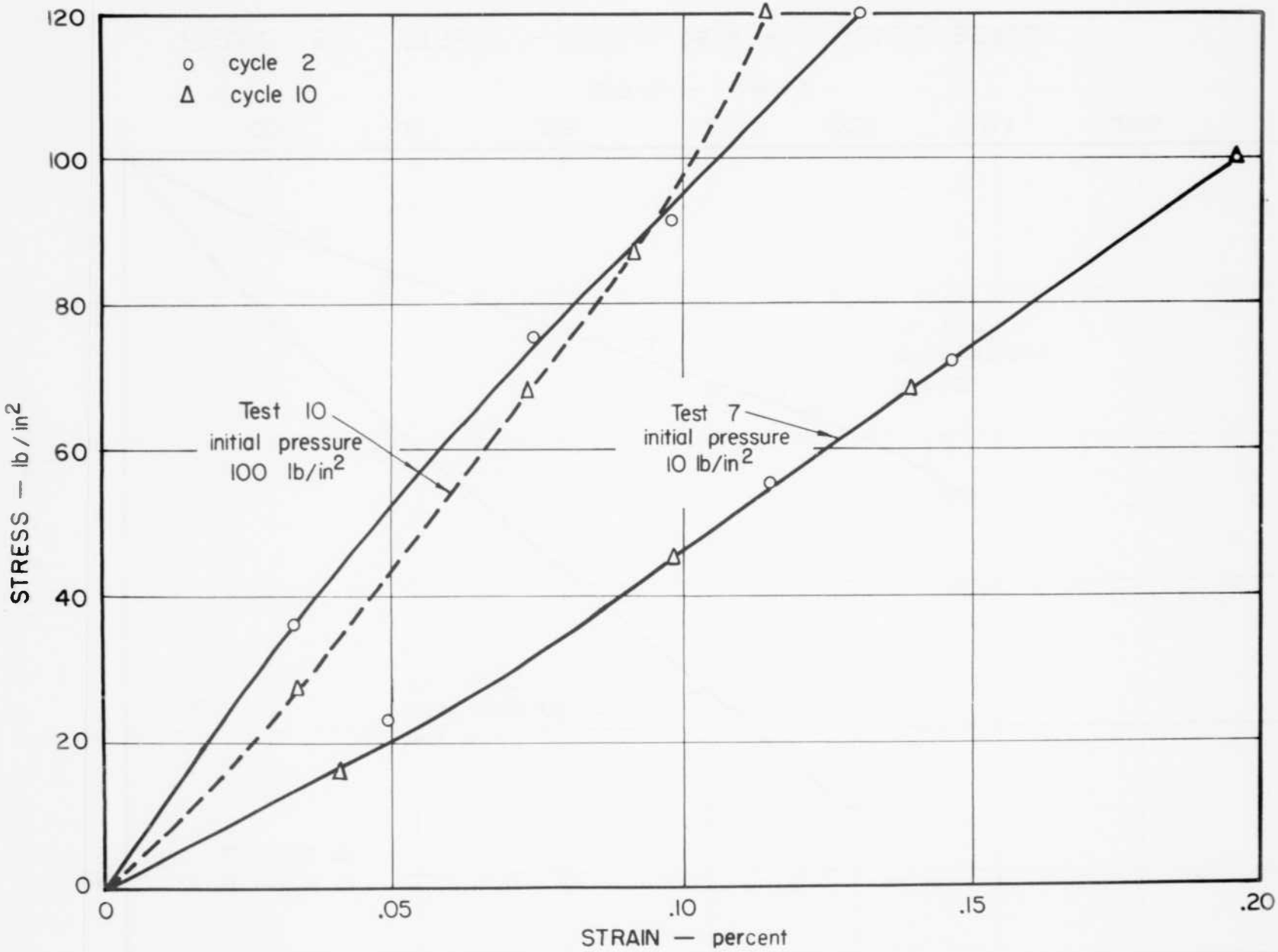

FIGURE 7 STRESS — STRAIN FOR GLASS BEADS

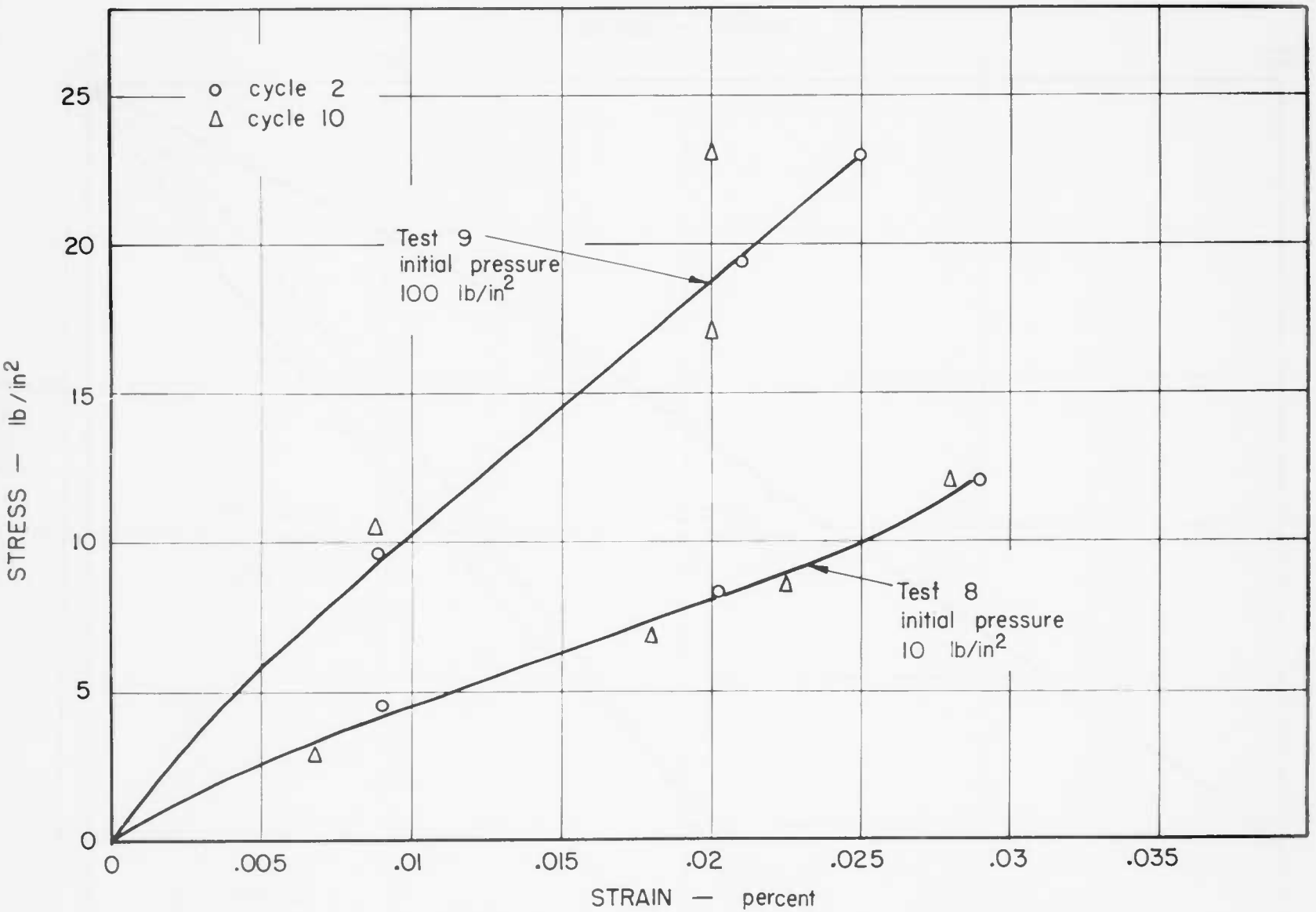

FIGURE 8 STRESS — STRAIN DATA FOR GLASS BEADS

APPENDIX E

SECOND SERIES OF RAPID LOADING TESTS UPON GRANULAR MATERIALS

PREFACE

The tests reported in this appendix were carried out during the period from January 1962 through May 1962 by Edmond T. Miller, a Research Assistant employed by the Soil Dynamics Project. Mr. Miller has also assisted the author in the reduction and interpretation of the data.

LIST OF FIGURES

1 Data from Test M 13 on Ottawa Sand
2 Data from Test M 24 on Glass Beads
3 Initial Creep in Ottawa Sand
4 Ottawa Sand - Fast Modulus - First Cycle
5 Ottawa Sand - Slow Modulus - First Cycle
6 Ottawa Sand - Slow Modulus - Fifth Cycle
7 Ottawa Sand, Stress - Change vs. Strain
8 Ottawa Sand, Stress - Change vs. Strain
9 Glass Beads, Fast Modulus - First Cycle
10 Glass Beads, Slow Modulus - First Cycle
11 Glass Beads, Slow Modulus - Fifth Cycle
12 Glass Beads Stress - Change vs. Strain in Small Increment Tests
13 Glass Beads, Stress - Change vs. Strain in Small Increment Tests
14 Glass Beads, Stress - Change vs. Strain in Large Increment Tests
15 Glass Beads, Stress - Change vs. Strain in Large Increment Tests
16 Glass Beads, Stress - Change vs. Strain in Large Increment Tests

LIST OF TABLES

I Testing Program
II Miller Tests on Ottawa Sand
III Miller Tests on Glass Beads

1. Test Program

This series of tests was designed to give further information concerning the effect of initial stress level and stress increment on the strain-time response of granular materials to a rapidly applied, one-dimensional loading. The two granular materials used in this series were the same as those tested in the tests described in Appendix D.

Two oedometers were used in this series. Oedometer II was used as set up for the tests of Appendix D for the majority of the tests. Oedometer III was used for tests M7, M8, and M9, but was abandoned thereafter for the reasons outlined in Appendix C.

A newer oscillator was used for these tests to drive the LVDT so that the frequency and the voltage output could be set with a higher degree of accuracy. In addition, a simple calibration of the oscillator was performed at the beginning of each day's testing to insure uniformity of input to the LVDT. The oscillator was connected directly to the oscilloscope, and the output signal for the oscillator was adjusted to produce readings of 20,000 cps in frequency, and 20 volts amplitude on the oscilloscope. Once this was achieved, the LVDT was connected to the oscillator, and the settings were left unchanged for the day's testing.

Early in the program, a dry cell was used as a power source for the pressure transducer. However, recognizing the difficulties associated with maintaining a constant input with the dry cell, a change was later made to a wet cell. This provided a more constant source of 6 volt d.c. current, and as soon as a decay in the voltage became perceptible, the wet cell could be re-charged to maintain a constant calibration.

2. Tests Upon Ottawa Sand and Glass Beads

Sand or glass beads was tamped into the specimen container to duplicate as nearly as possible the test conditions in the tests presented in Appendix D. Table I shows the test conditions used in each test in the series. A fresh specimen was prepared for each of the tests in the

the series, but several of the tests were subjected to two different magnitudes of stress increment. In these tests, the lower increment was applied through enough cycles to establish approximate equilibrium, and then the second stress increment was applied for the remaining cycles of the test.

Tests M1 through M6 were made using a relatively slow sweep rate so that observations of the trace could be made after the initial increment of stress was applied. Therefore, creep could be observed for a short period of time. Remaining tests used a fast sweep so that the stress-strain characteristics could be observed. Figures 1 and 2 show typical sets of data as they were recorded during the tests. Numbers in the tables are deflections of the strain and stress beams measured in grid spacings. Interpretation of the data is the same as that described in Section 2 of Appendix D.

2.1 Analysis of Data for Modulus

Three modulus values were computed as described in Section 2 of Appendix D, and a fourth modulus was computed in this series only. These moduli are: "fast loading modulus," equal to the immediate pressure increment divided by the change in strain during the immediate pressure rise; "slow loading modulus," equal to the final stress increment divided by the final change in strain, both measured at the end of the three-minute loading interval; "fast unloading modulus," equal to the immediate pressure decrement divided by the initial change in strain during the pressure decline; and "slow unloading modulus," equal to the final stress decrement divided by the final change in strain, both measured at the end of the three-minute unloading cycle. The two "fast" moduli were measured only for those cycles which were photographed.

Tables II and III summarize the modulus data determined in these tests, uncorrected for apparatus compressibility. Those comments made in Appendix D, Section 2.1, concerning accuracy of modulus measurement, also apply to these tests.

Modulus values for test M16 appear to be far out of reason when viewed in relation to other data. No definite reason for the high values has been determined. However, it may be due to an error in the recording of the strain sensitivity of the oscilloscope. The test data has been included in the tabulations in the hope that it will become useful at some later date.

Certain observations were made regarding the results of the tests which should be regarded merely as observations at this time. The reasons for the specific form the results have taken are not yet clearly understood.

Modulus tends to increase with increasing initial pressure and generally tends to decrease or remain approximately constant with increasing stress increment. These tendencies are less pronounced after application of several cycles of loading. Trends are difficult to establish clearly because of the scarcity of data for higher stress increments.

Unloading modulus is initially much higher than the loading modulus. In some cases this modulus decreases and then again increases as the number of cycles increases. In any case, the general trend of the unloading modulus tends to approach the loading modulus as a limit. For various reasons, the unloading modulus is more erratic than the loading modulus and trends are harder to identify.

These modulus data for Ottawa sand have been shown in graphical form in Figures 4, 5 and 6, and for glass beads in Figures 9, 10 and 11.

2.2 Stress-Strain Curves

As in the tests described in Appendix D, the photographs of stress-time and strain-time curves were used as the source of information to produce stress-strain curves. The results of some of these tests are shown for Ottawa sand in Figures 7 through 8 and for glass beads in Figures 13 through 16.

Some of the tests show a very definite time lag between the application of load and the beginning of strain (up to approximately one millisecond). Some, if not all, of the effect can possibly be explained by a small inertial lag in the motion of the piston as load is applied.

In other tests, the opposite effect is seen. There are large strains produced with only a small increase in stress and then a more gradual increase in the latter portions of the stress rise. Where this effect was seen, it appeared only in the first cycle, and may be due to an initial looseness in the upper stratum of the soil sample.

Evidence may be obtained from the stress-strain plots that the stress-strain curve is actually (1) a straight line, (2) concave, or (3) convex, depending on the test observed. At this time, however, the evidence is still too sketchy to make a positive statement about which may be correct, or, assuming that each may be correct part of the time, what conditions control the shape of the curve. The curves seem to become straighter with increasing numbers of cycles of stress application.

2.3 Data Regarding Creep

Tests M1 through M6 were performed primarily to gain operator experience in the manipulation of the test equipment. In addition to this purpose, a check on the previous tests was provided, and valuable data on the creep experienced in the early stages following loading were obtained. Because of the relatively slow sweep rates employed in these tests, and the resulting very steep rise curves, it was not possible to obtain adequate data to produce stress-strain curves for these tests. The creep observations are shown in Figure 3.

Erratic data on creep and the crude methods used in the photo analysis make it difficult to make positive statements concerning creep. However, it seems fairly safe to state that creep occurs rather rapidly

for the first few milliseconds and then arrives at a much slower rate for several seconds. In most cases, very little creep appears to be taking place at the end of a three-minute period.

Table 1

TESTING PROGRAM

Test	Oedometer	Soil	Initial Pressure	Pressure Increment*	Rise Time
M1	II	Ottawa Sand	15	10	8
M2	II	Ottawa Sand	100	15	No picture
M3	II	Ottawa Sand	50	20	8
M4	II	Ottawa Sand	15	100	12
M5	II	Ottawa Sand	50	100	10
M6	II	Ottawa Sand	100	100	20
M7	III	Ottawa Sand	15	5	15
M8	III	Ottawa Sand	15	10 & 15**	10 & 13**
M9	III	Ottawa Sand	50	10	5
M10	II	Ottawa Sand	50	10 & 20	10 & 15
M11	II	Ottawa Sand	100	10	6
M12	II	Ottawa Sand	100	15	6
M13	II	Ottawa Sand	100	10 & 20	10 & 15
M14	II	Glass Beads	15	5	10
M15	II	Glass Beads	15	10 & 20	10 & 12
M16	II	Glass Beads	15	100	20
M17	II	Glass Beads	15	200	25
M18	II	Glass Beads	50	10	6
M19	II	Glass Beads	50	10 & 20	6 & 8
M20	II	Glass Beads	50	100	18
M21	II	Glass Beads	50	200	23
M22	II	Glass Beads	100	5	5
M23	II	Glass Beads	100	10 & 20	6 & 8
M24	II	Glass Beads	100	100	15
M25	II	Glass Beads	100	200	18

*These pressure increments are "nominal" values, or those that were attempted in each test. Actual pressures achieved in the tests were measures and vary somewhat from these nominal values.

**Where two values appear, the first value applies to the first portion of the test, and the second applies to the last portion of the test.

TABLE III. MILLER TESTS ON OTTAWA SAND

CONSTRAINED MODULI (thousands of lb/sq.in.)

TEST NO.	Initial Pressure	Stress Change	Fast Loading Modulus			Slow Loading Modulus			Fast Unloading Modulus			Slow Unloading Modulus		
			Cycle 1	Cycle 2	Cycle 5	Cycle 1	Cycle 2	Cycle 5	Cycle 1	Cycle 2	Cycle 5	Cycle 1	Cycle 2	Cycle 5
M-1	15	10			44	15	24	36		38		35	32	40
M-2	100	15	72			42	76	83	125			83	88	84
M-3	50	20	38			24	50	65	65			52	58	65
M-4	15	100	27	39		25	36	40		44		42	42	42
M-5	50	100	23			20	47	60		78		56	58	60
M-6	100	100	34			29	71	83				83	83	83
M-7	15	5		22		19	21	30	24	25		21	25	30
M-8	15	10	28			23	28	31	27			28	35	31
M-8a	15	15	30			22	25	28	30			31	30	30
M-9	50	10	65		101	39	69	93	106		90	100	93	93
M-10	50	10	50	73		32	58	62	76			71	62	62
M-10a	50	20		58	56	62	50	56	62		58	55	58	56
M-11	100	10	115		106	56	76	79	107		92	89	84	79
M-12	100	15	95	116	112	76	86	90			120	97	91	95
M-13	100	10	92		95	59	73	82	96		91	82	78	89
M-13a	100	20	96		107	75	84	87	102		97	84	87	86

TABLE III MILLER TESTS ON GLASS BEADS

CONSTRAINED MODULI (thousands of lb/sq.in.)

TEST NO.	Initial Pressure	Stress Change	Fast Loading Modulus			Slow Loading Modulus			Fast Unloading Modulus			Slow Unloading Modulus		
			Cycle 1	Cycle 2	Cycle 5	Cycle 1	Cycle 2	Cycle 5	Cycle 1	Cycle 2	Cycle 5	Cycle 1	Cycle 2	Cycle 5
M-14	15	5	46		57	32	42	41	50		46	53	42	41
M-15	15	10	44			31	40	42		47		42	42	42
M-15a	15	20	52		49	39	42	43	46		48	42	43	43
M-16	15	100	194			175	193	208	266			196	212	218
M-17	15	200	25			24	45	47	66			50	50	50
M-18	50	10		91		33	46	49	70			53	49	49
M-19	50	10	76			54	64	58	67			66	64	63
M-19a	50	20			70	60	50	58	71	63	64	63	63	58
M-20	50	100	39	65	65	30	52	56	58		64	54	58	57
M-21	50	200	29		69	27	54	58	60		64	58	58	62
M-22	100	5	114			80	91	91	95			91	106	100
M-23	100	10	84		89	24	57	55	82			73	77	69
M-23a	100	20	90		81	46	57	62	83		76	65	69	65
M-24	100	100	59			47	70	70	74			66	71	71
M-25	100	200	37		87	34	66	72	80		79	71	71	74

Visual strain readings in grid spaces

Time min.	Cycle 1		Cycle 2		Cycle 3		Cycle 4		Cycle 5		Cycle 6		Cycle 7		Cycle 8		Cycle 9		Cycle 10	
	Load	Unload	Load	Unload	Load	Unload	Load	Unload	Load	Unload	Load	Unload	Load	Unload	Load	Unload	Load	Unload	Load	Unload
1/4	2.2	0.8	2.3	1.2	2.5	1.1	2.4	1.0	2.4	1.1	4.0	1.5	4.0	1.6	4.0	1.6	4.0	1.6	4.1	1.6
1	2.3	0.8	2.4	1.1	2.5	1.0	2.4	0.9	2.5	1.0	4.0	1.4	4.0	1.6	4.1	1.6	4.1	1.6	4.1	1.6
2	2.3	0.8	2.5	1.0	2.5	1.0	2.4	0.9	2.5	1.1	4.0	1.4	4.0	1.5	4.1	1.6	4.1	1.6	4.1	1.6
3	2.4	0.8	2.6	1.0	2.5	1.0	2.4	0.9	2.5	1.1	4.0	1.4	4.0	1.5	4.1	1.6	4.1	1.6	4.1	1.6

Photographs of Oscilloscope

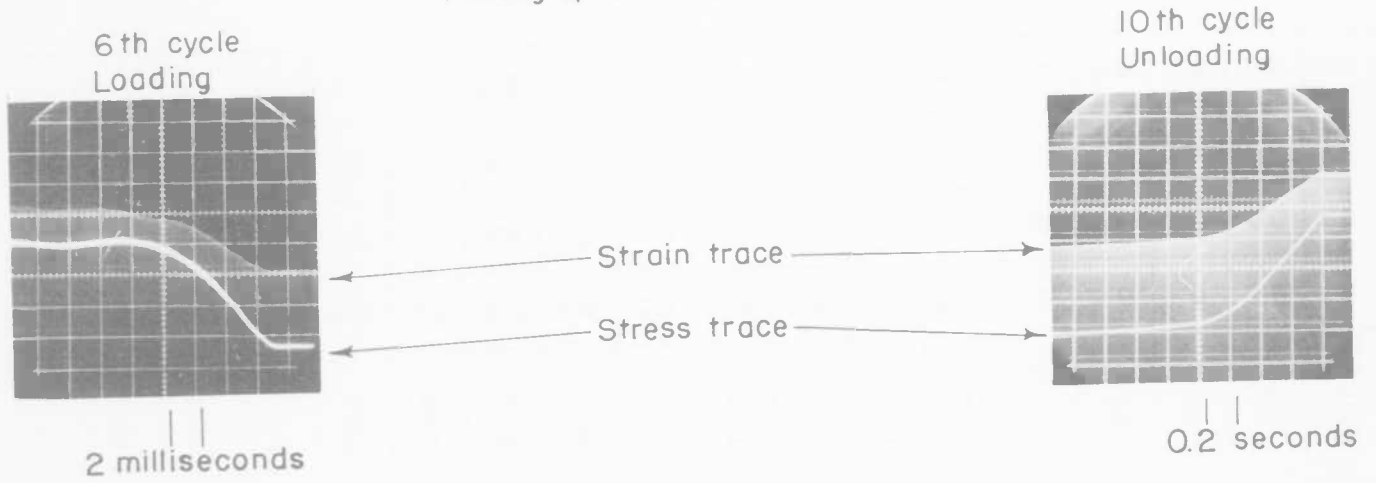

FIGURE 1 DATA FROM TEST M13 ON OTTAWA SAND

Visual strain readings in grid spaces

Time min.	Cycle 1		Cycle 2		Cycle 3		Cycle 4		Cycle 5		Cycle 6		Cycle 7		Cycle 8		Cycle 9		Cycle 10	
	Load	Unload	Load	Unload	Load	Unload	Load	Unload	Load	Unload	Load	Unload	Load	Unload	Load	Unload	Load	Unload	Load	Unload
1/4	5.4	1.6	5.6	1.7	5.6	1.8	5.7	1.8	5.8	1.8	5.8	1.8	5.8	1.8	5.8	1.8	5.8	1.9	5.8	1.9
1	5.5	1.5	5.6	1.6	5.7	1.7	5.8	1.7	5.8	1.8	5.8	1.8	5.8	1.8	5.8	1.8	5.8	1.9	5.8	1.9
2	5.6	1.5	5.6	1.6	5.7	1.7	5.8	1.7	5.8	1.8	5.8	1.8	5.8	1.8	5.8	1.8	5.8	1.9	5.8	1.9
3	5.6	1.5	5.6	1.6	5.7	1.7	5.8	1.7	5.8	1.8	5.8	1.8	5.8	1.8	5.8	1.8	5.8	1.9	5.8	1.9

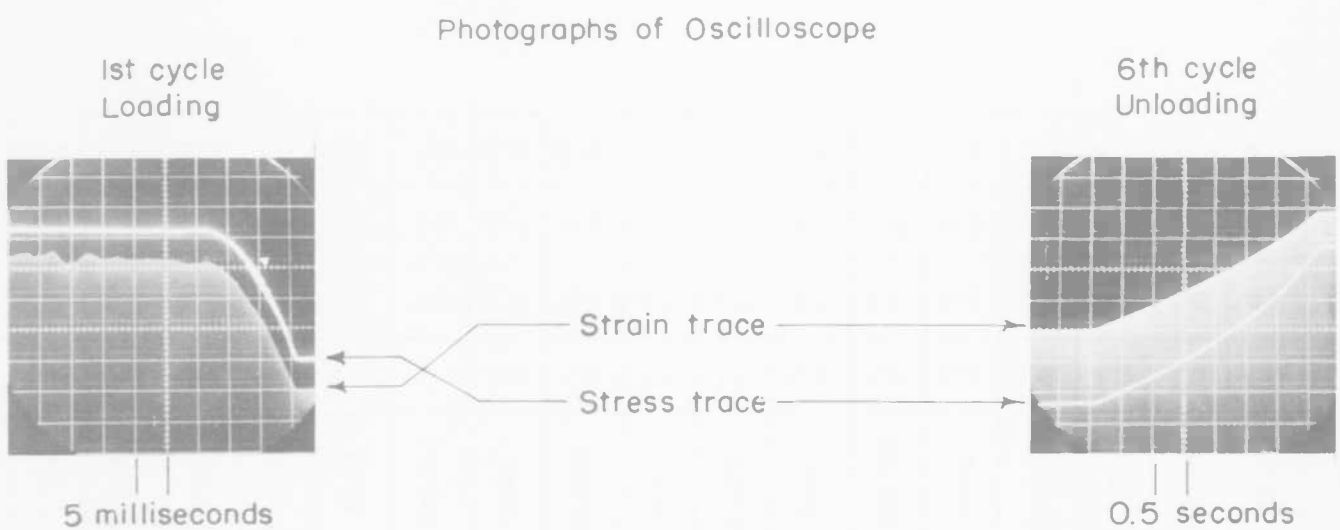

FIGURE 2 DATA FROM TEST M24 ON GLASS BEADS

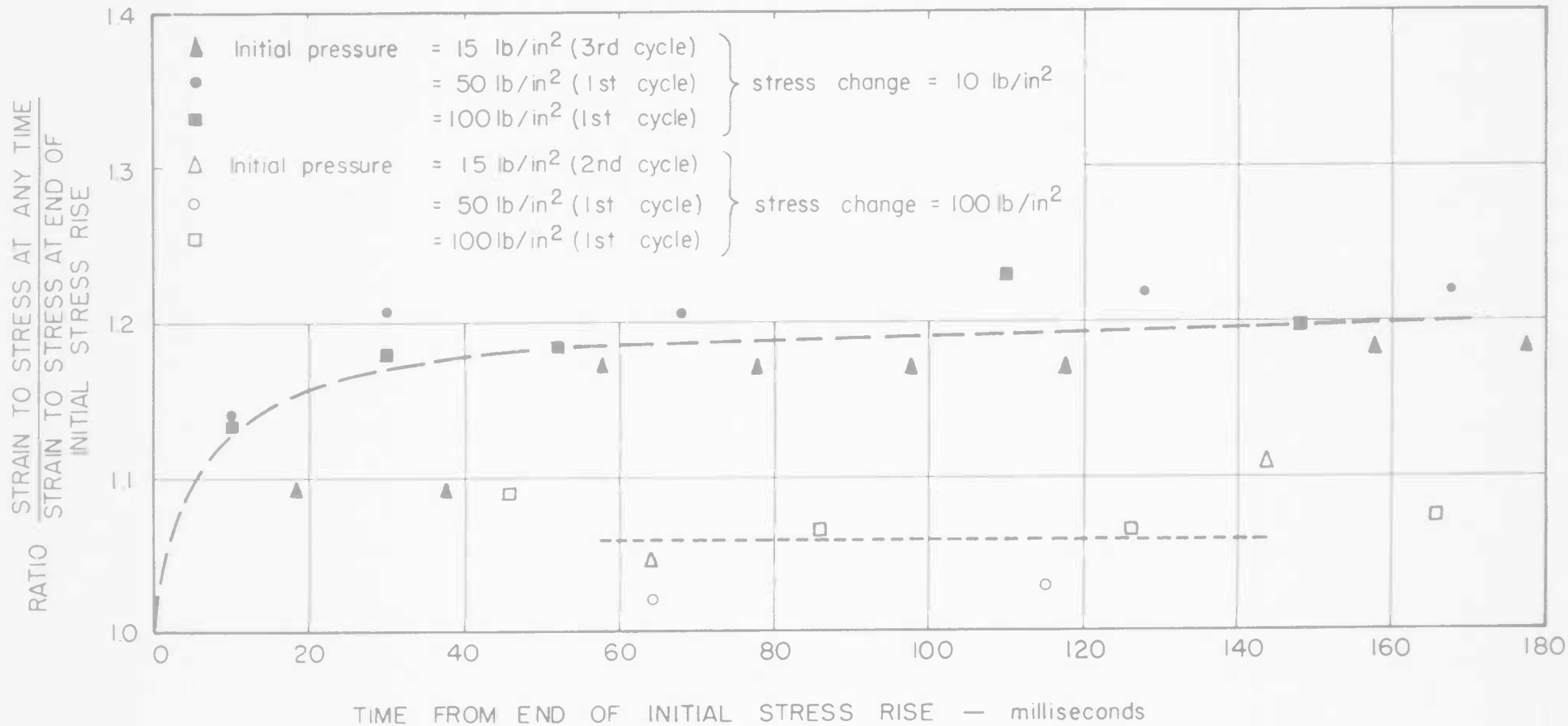

FIGURE 3 INITIAL CREEP IN OTTAWA SAND

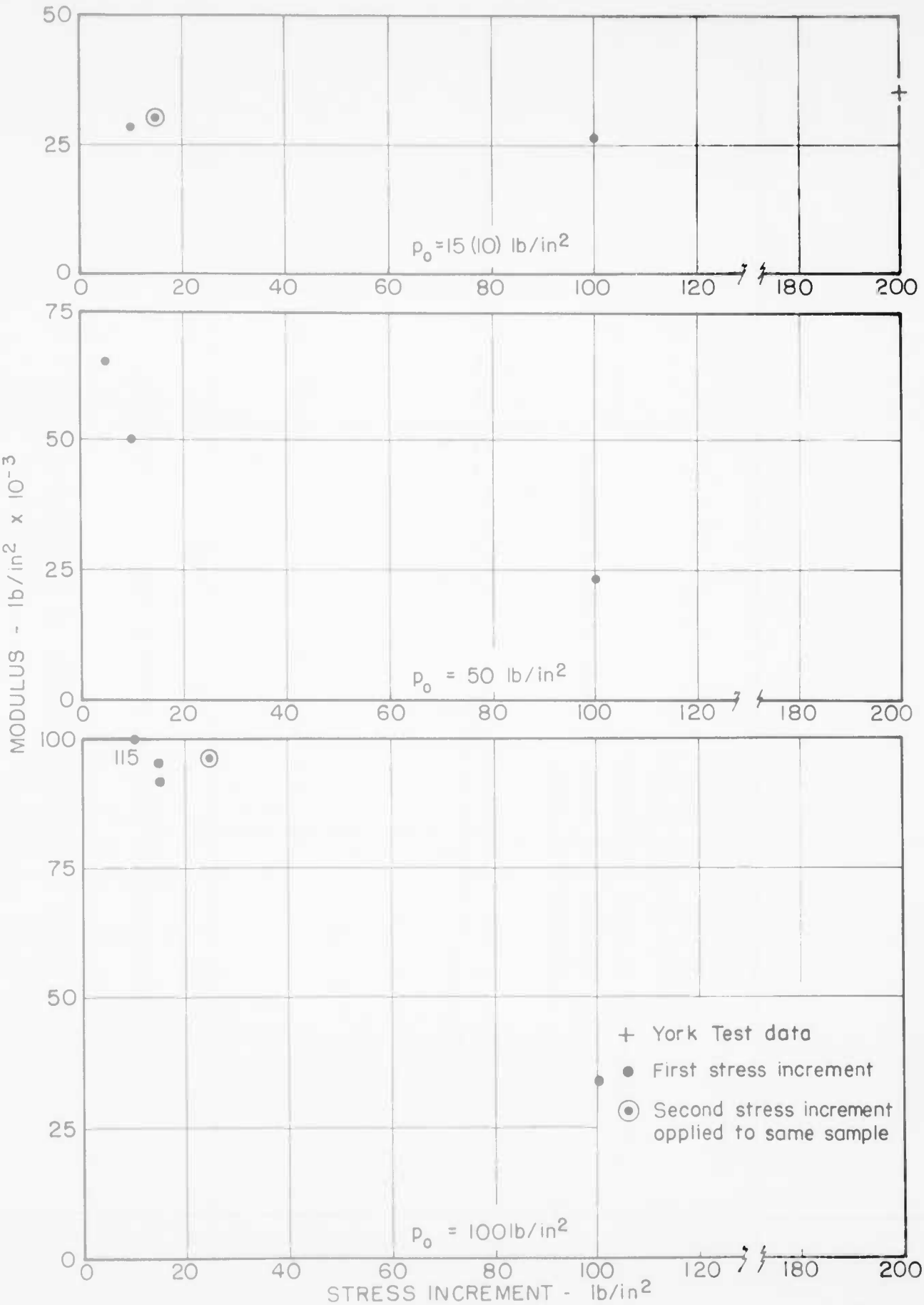

FIGURE 4 OTTAWA SAND - FAST MODULUS - FIRST CYCLE

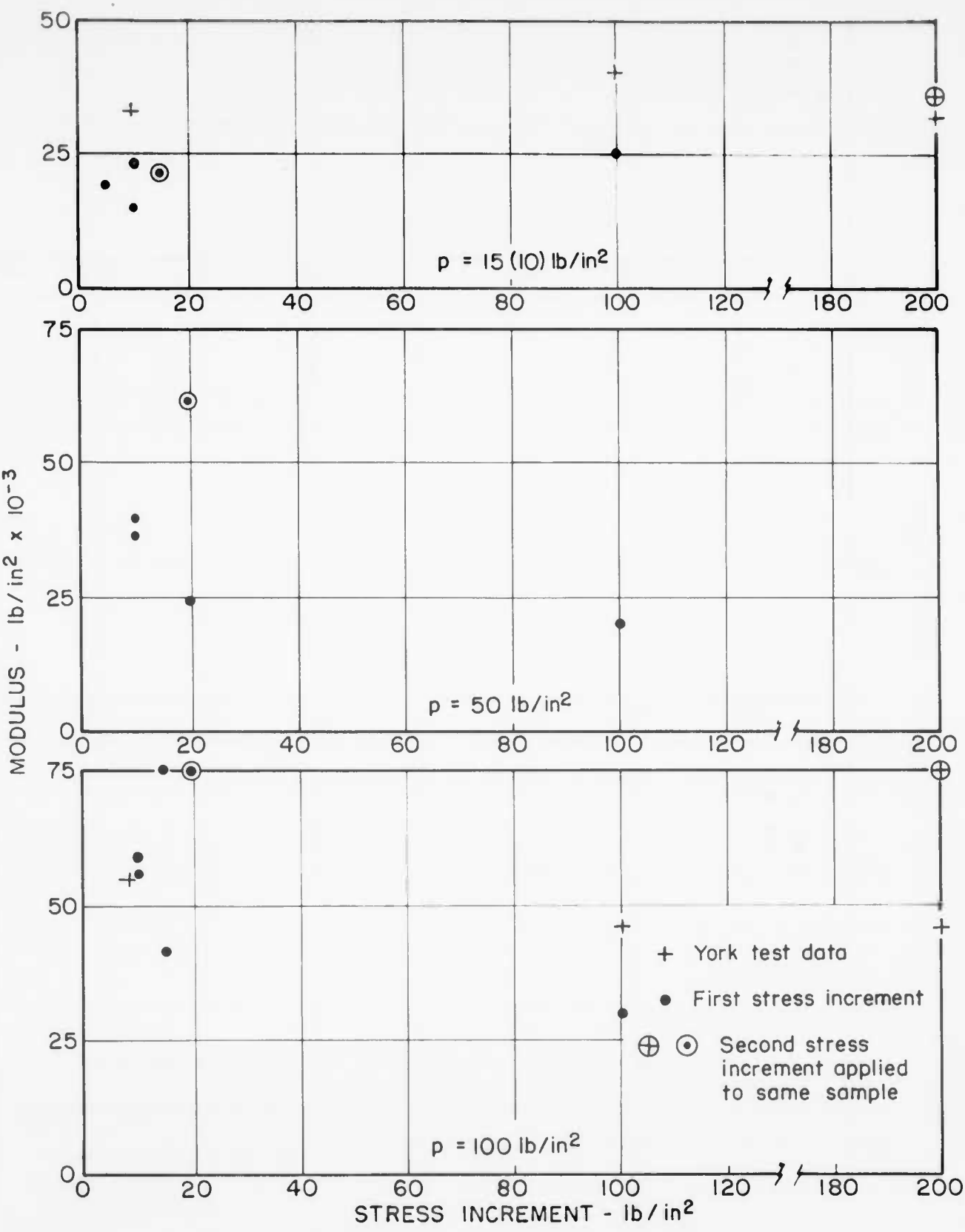

FIGURE 5 OTTAWA SAND - SLOW MODULUS - FIRST CYCLE

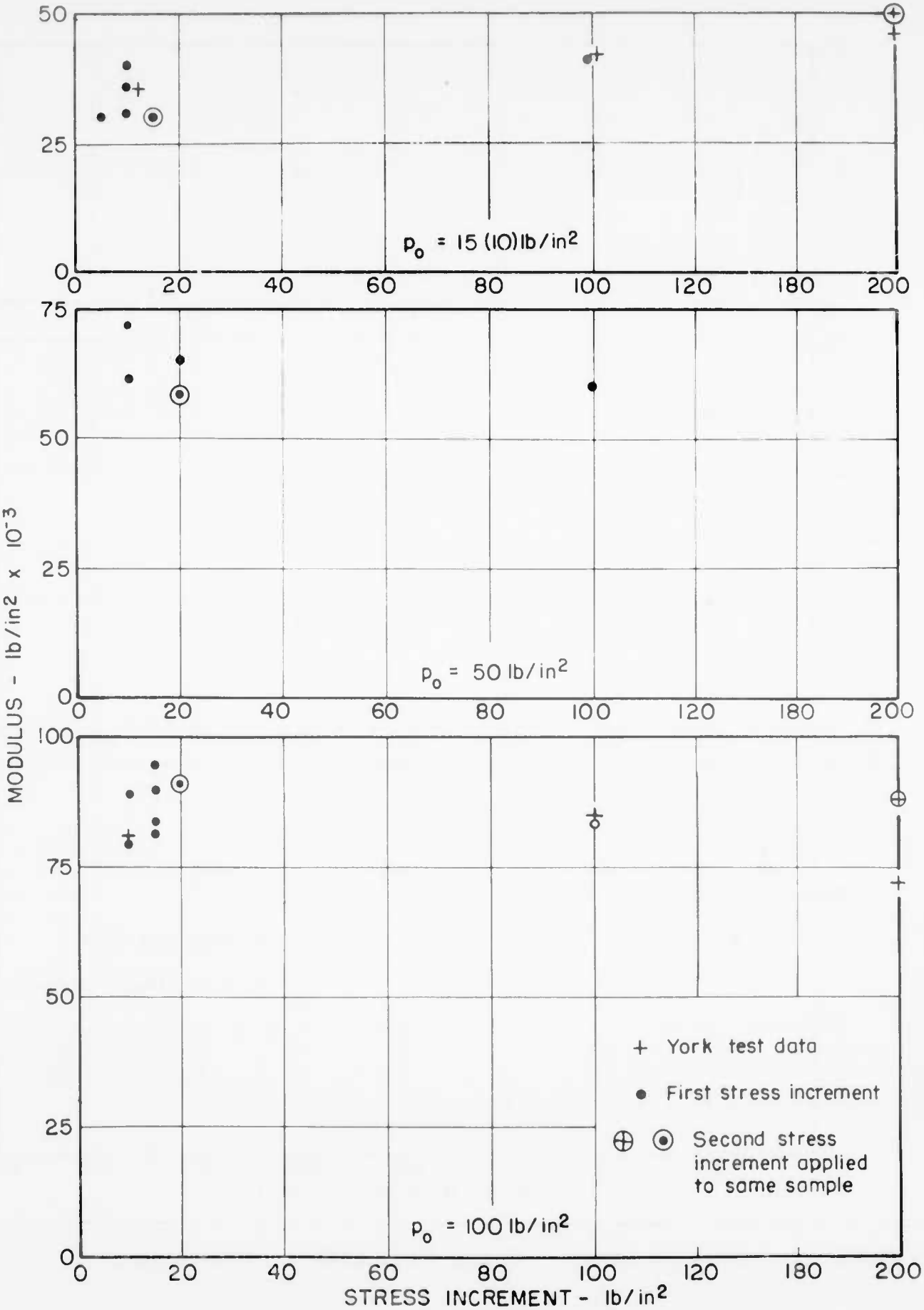

FIGURE 6 OTTAWA SAND - SLOW MODULUS - FIFTH CYCLE

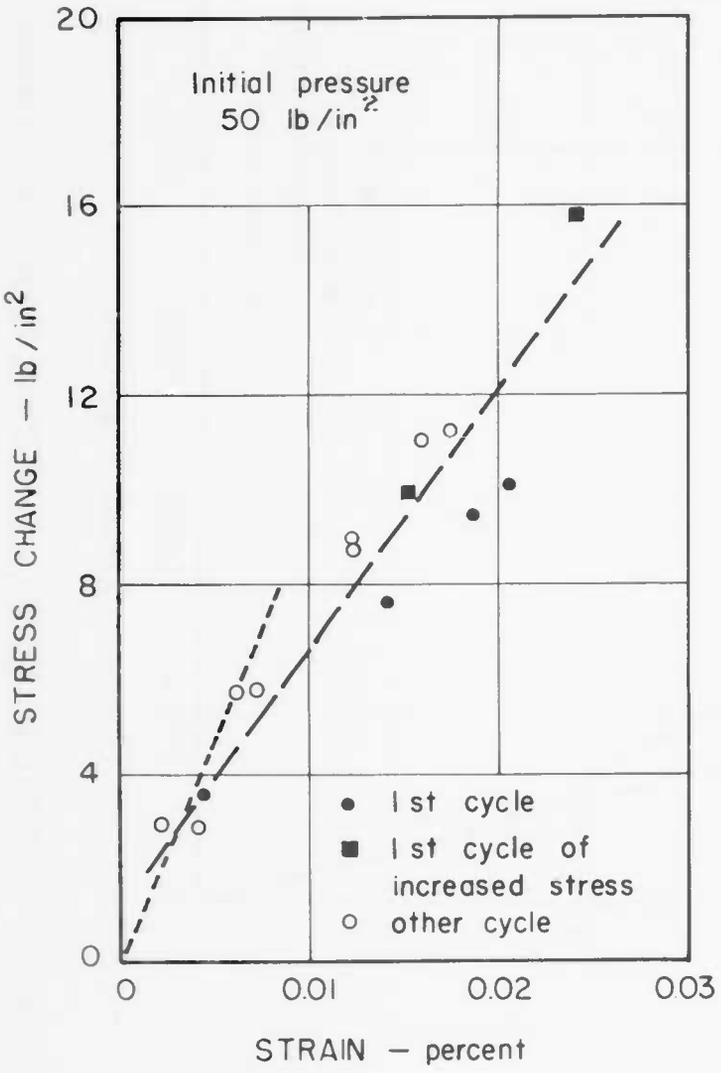

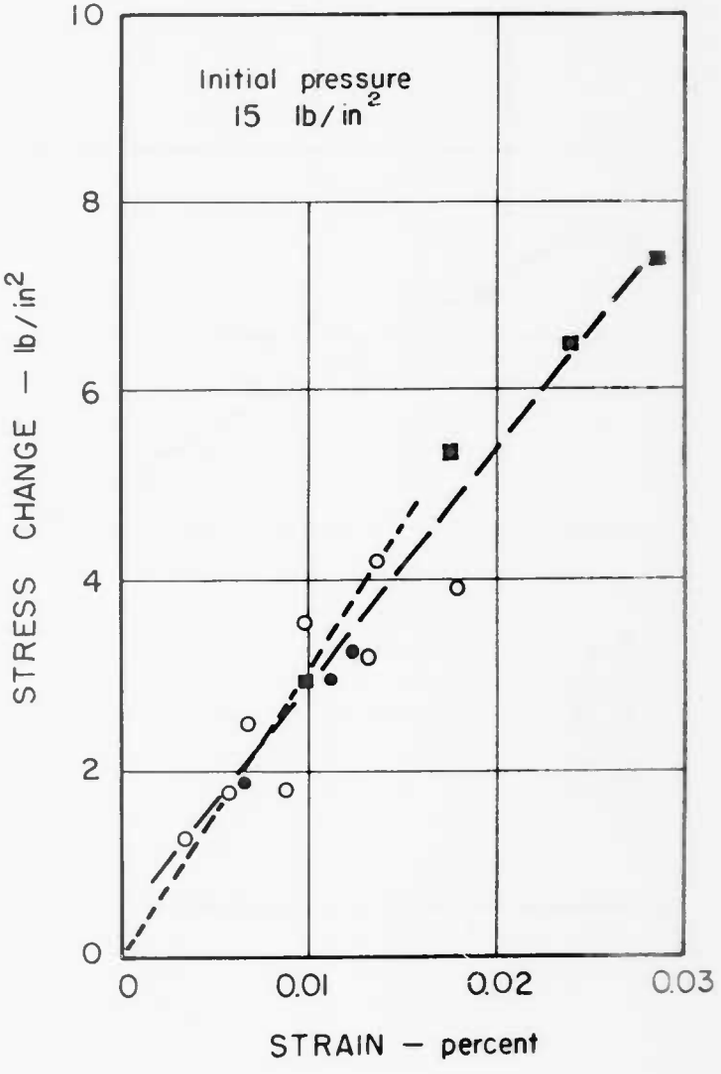

FIGURE 7 OTTAWA SAND, STRESS-CHANGE vs STRAIN

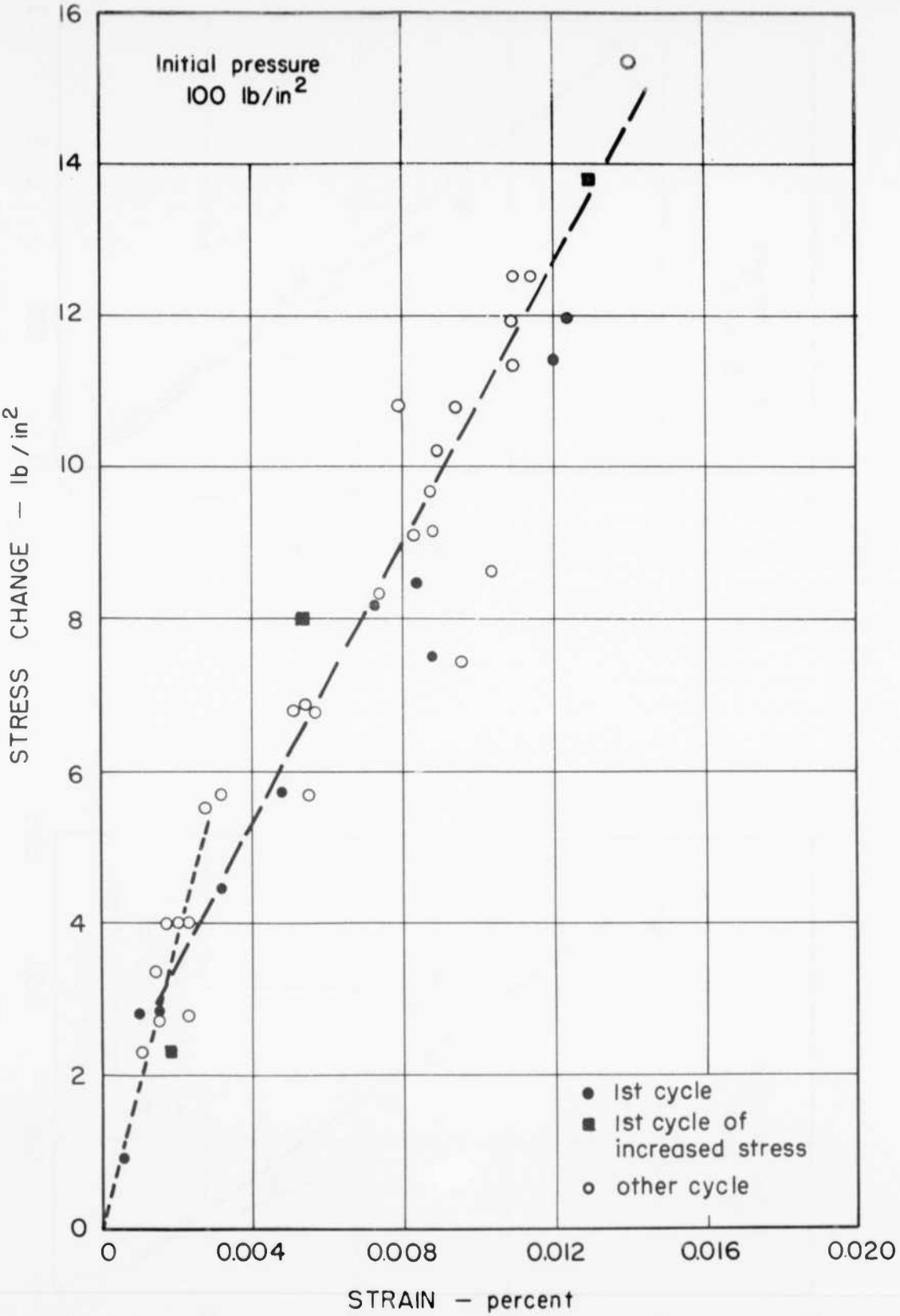

FIGURE 8 OTTAWA SAND, STRESS-CHANGE vs STRAIN

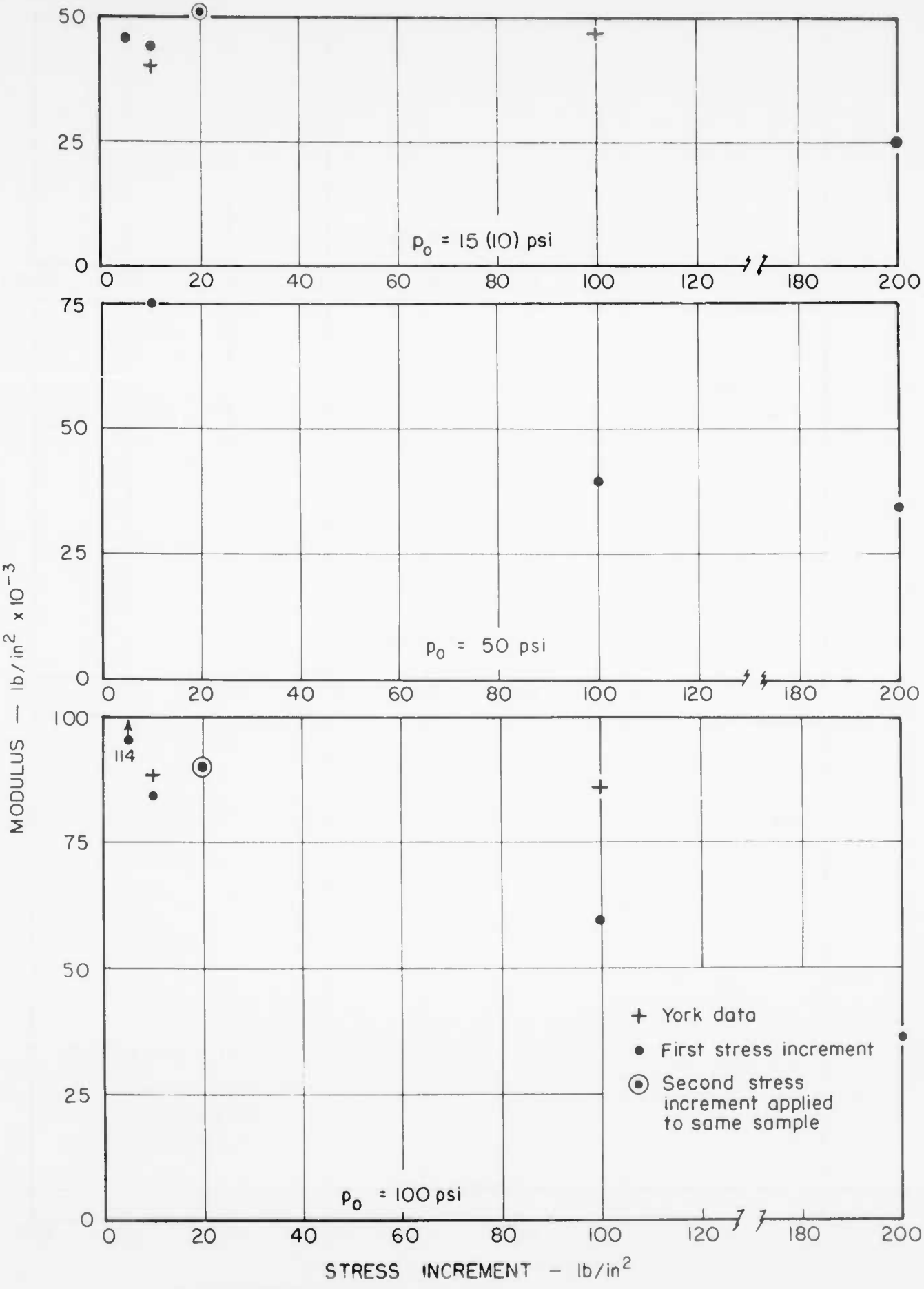

FIGURE 9 GLASS BEADS, FAST MODULUS FIRST CYCLE

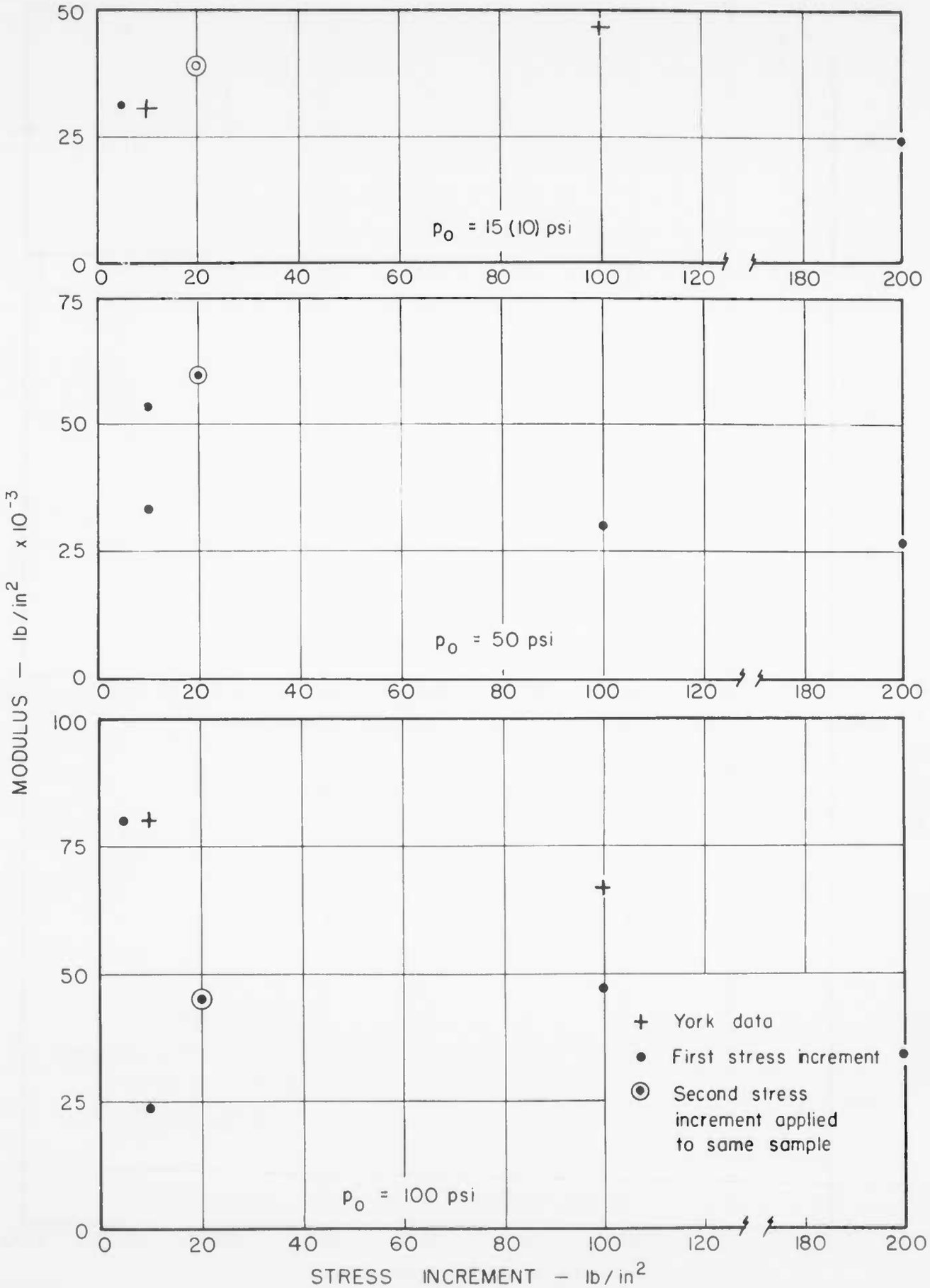

FIGURE 10 GLASS BEADS, SLOW MODULUS FIRST CYCLE

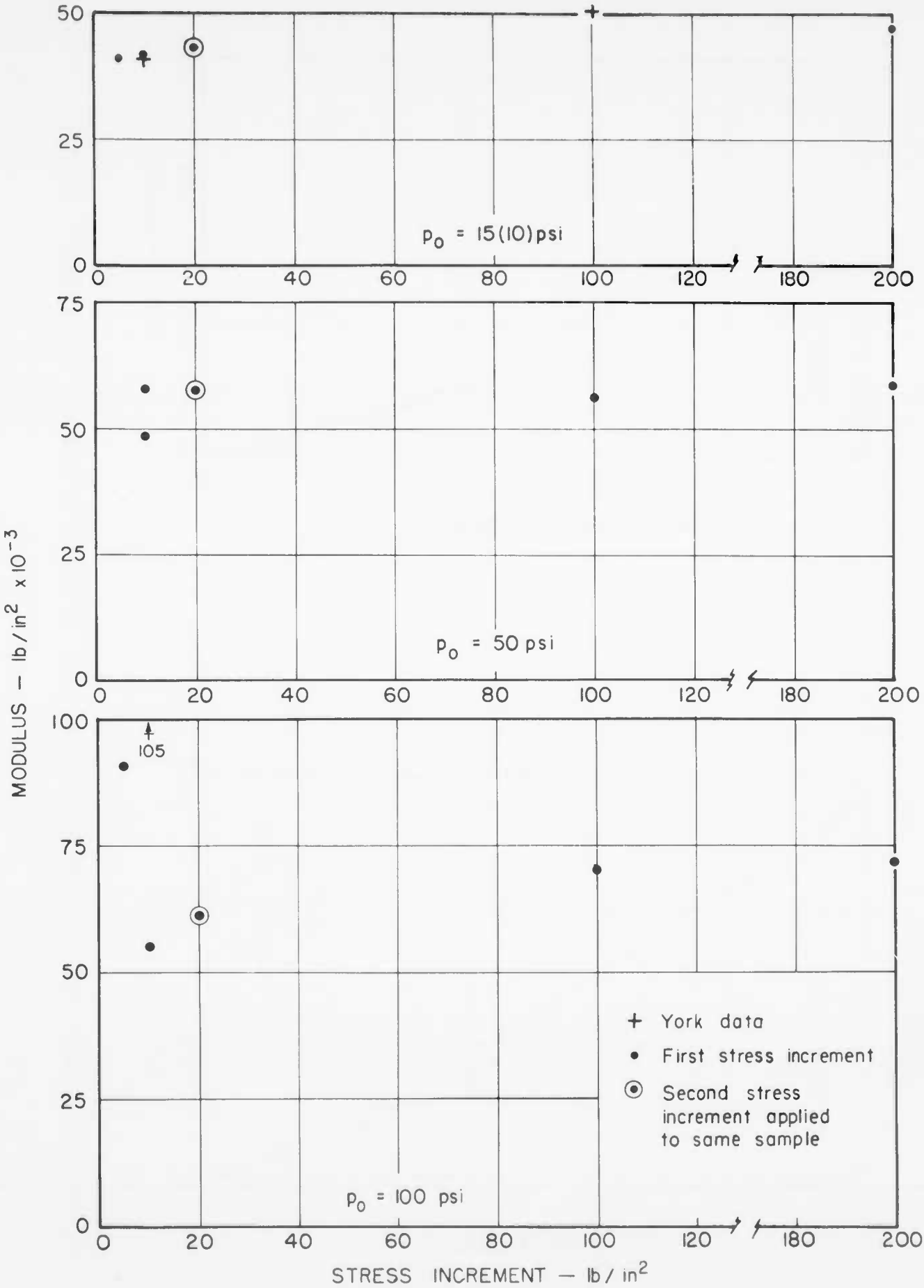

FIGURE 11 GLASS BEADS, SLOW MODULUS FIFTH CYCLE

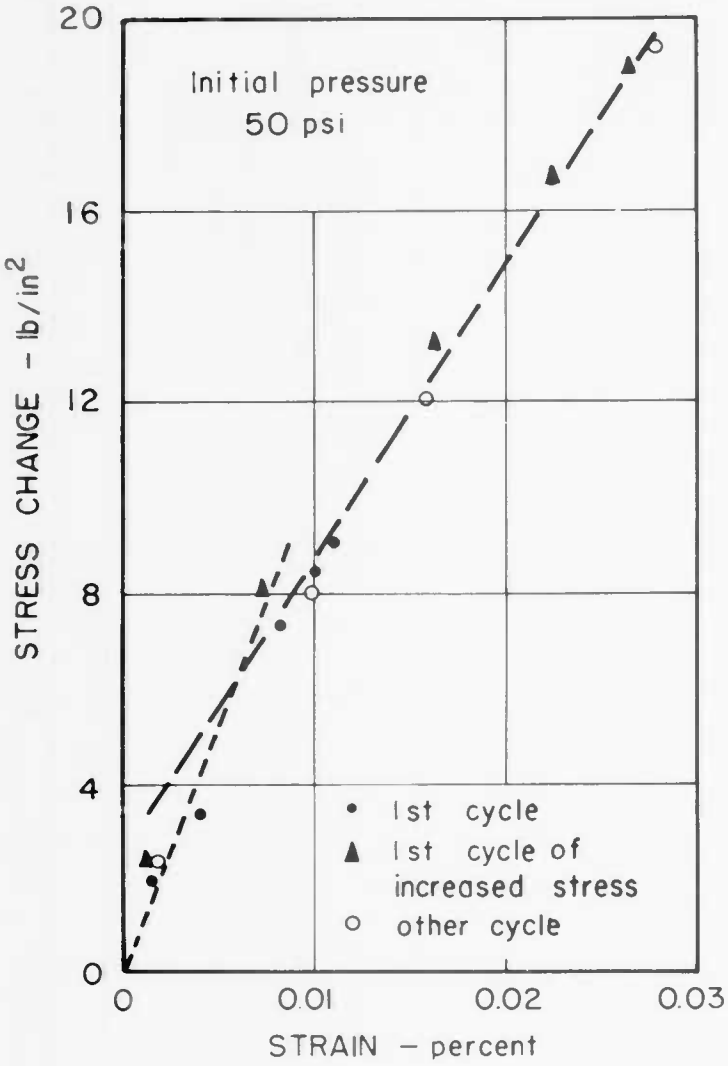

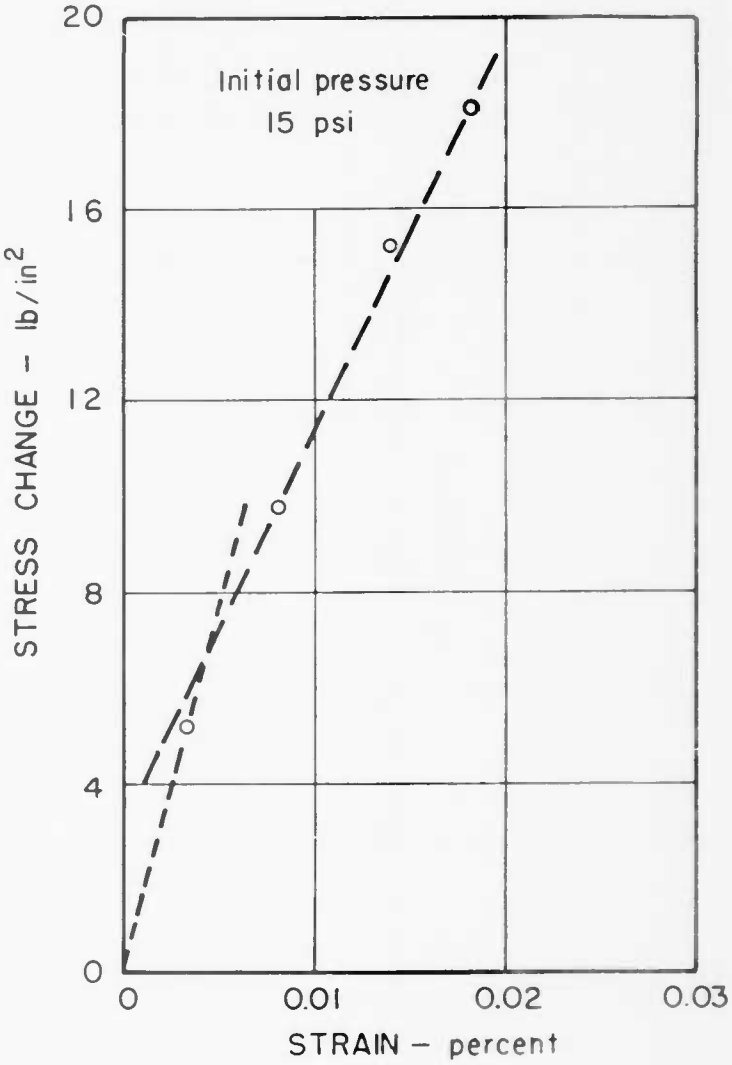

FIGURE 12 GLASS BEADS STRESS-CHANGE vs STRAIN IN SMALL INCREMENT TESTS

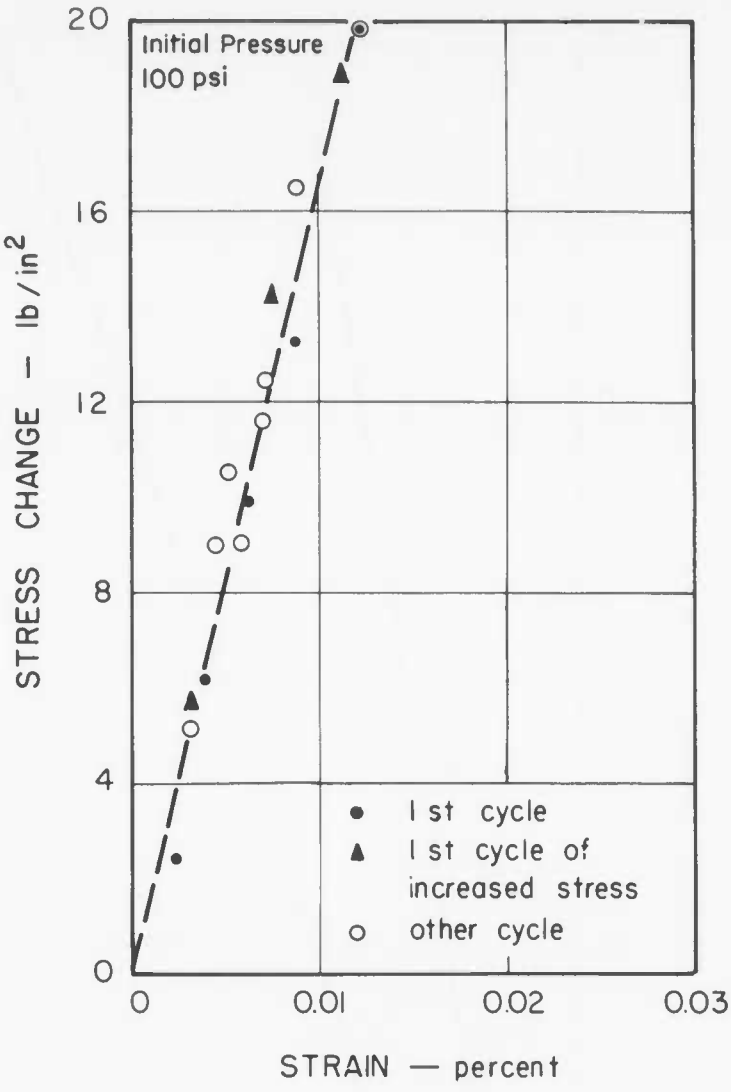

FIGURE 13 GLASS BEADS, STRESS-CHANGE vs STRAIN IN SMALL INCREMENT TESTS

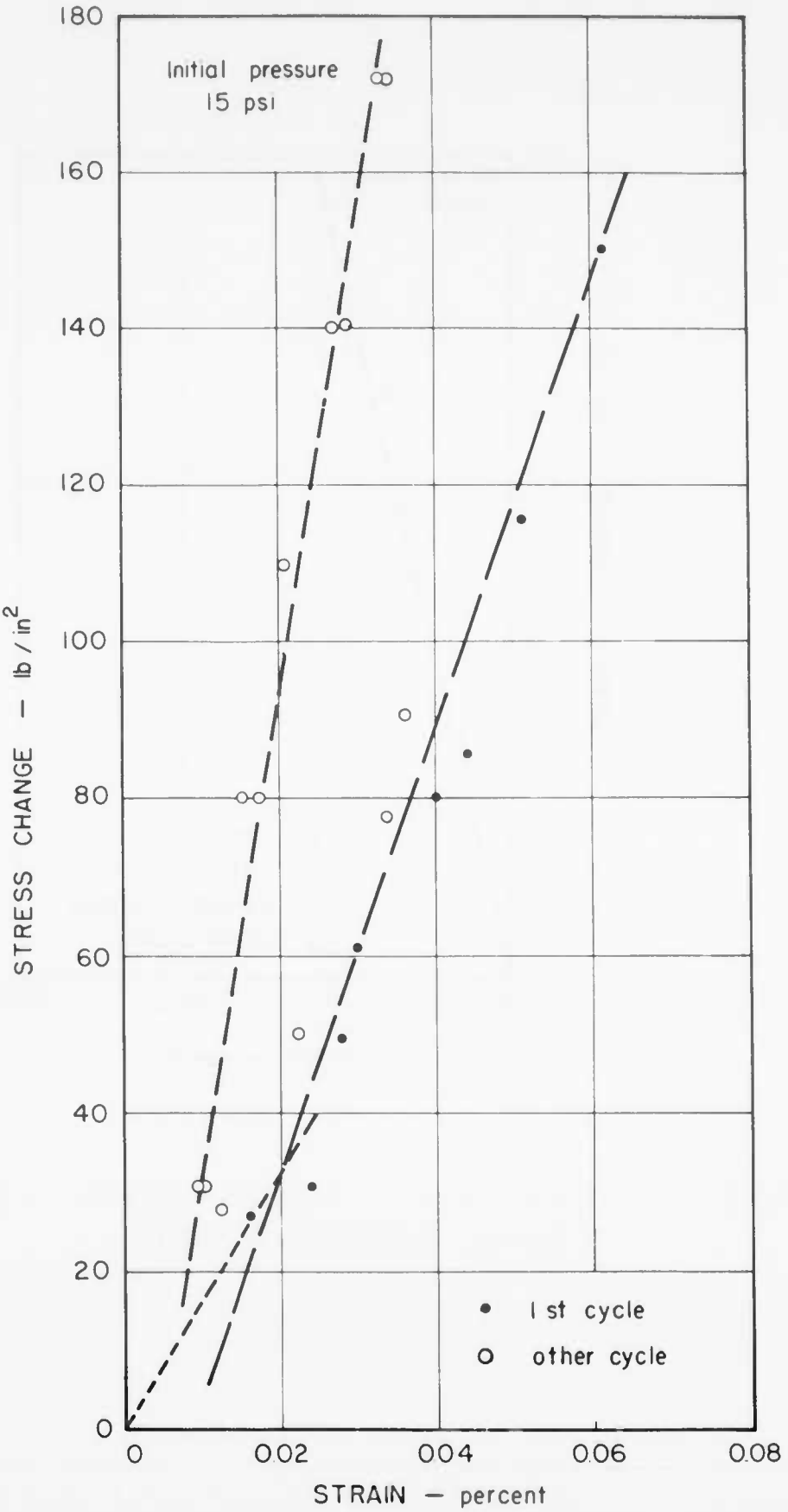

FIGURE 14 GLASS BEADS, STRESS-CHANGE vs STRAIN IN LARGE INCREMENT TESTS

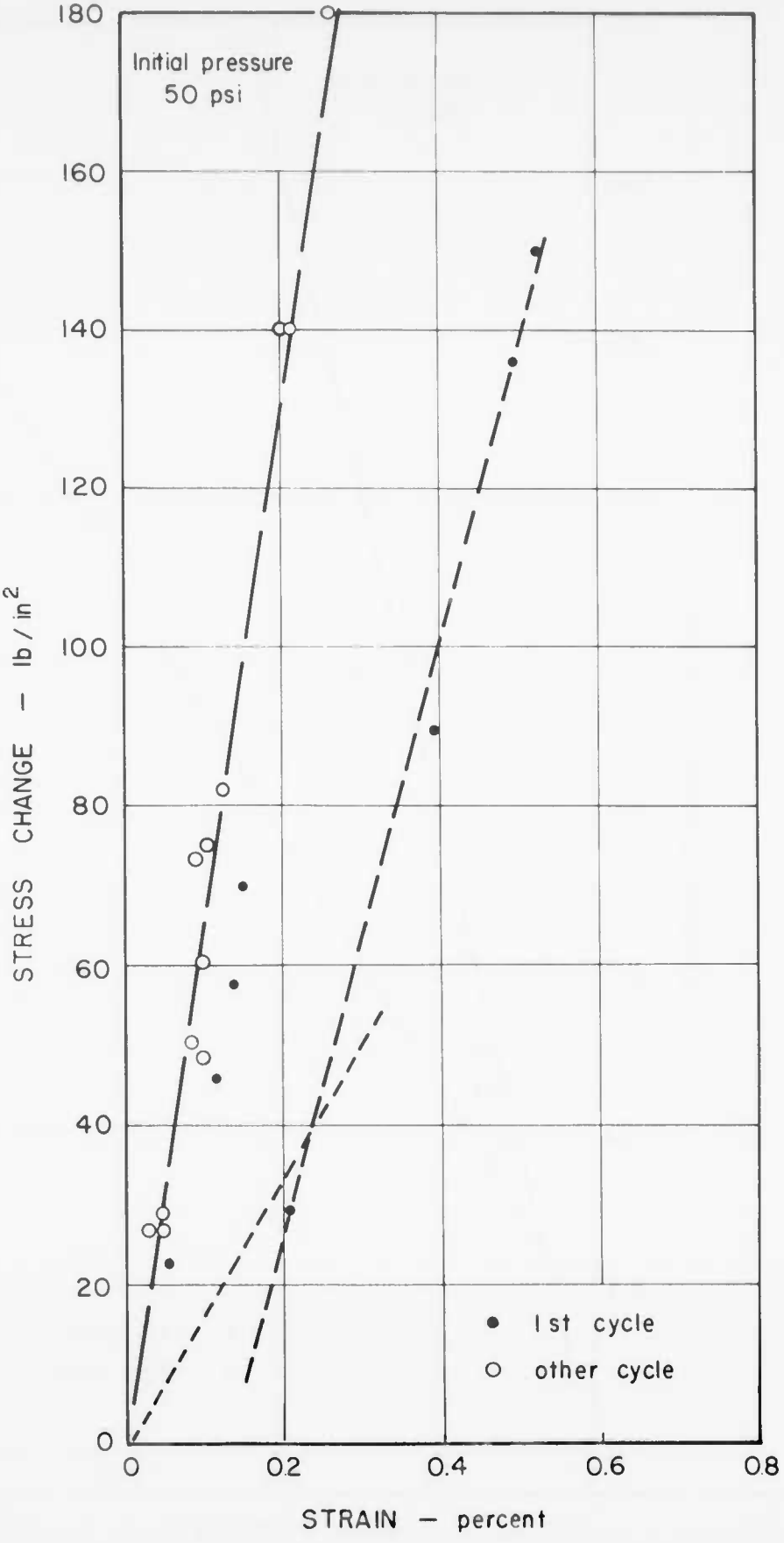

FIGURE 15 GLASS BEADS, STRESS-CHANGE vs STRAIN IN LARGE INCREMENT TESTS

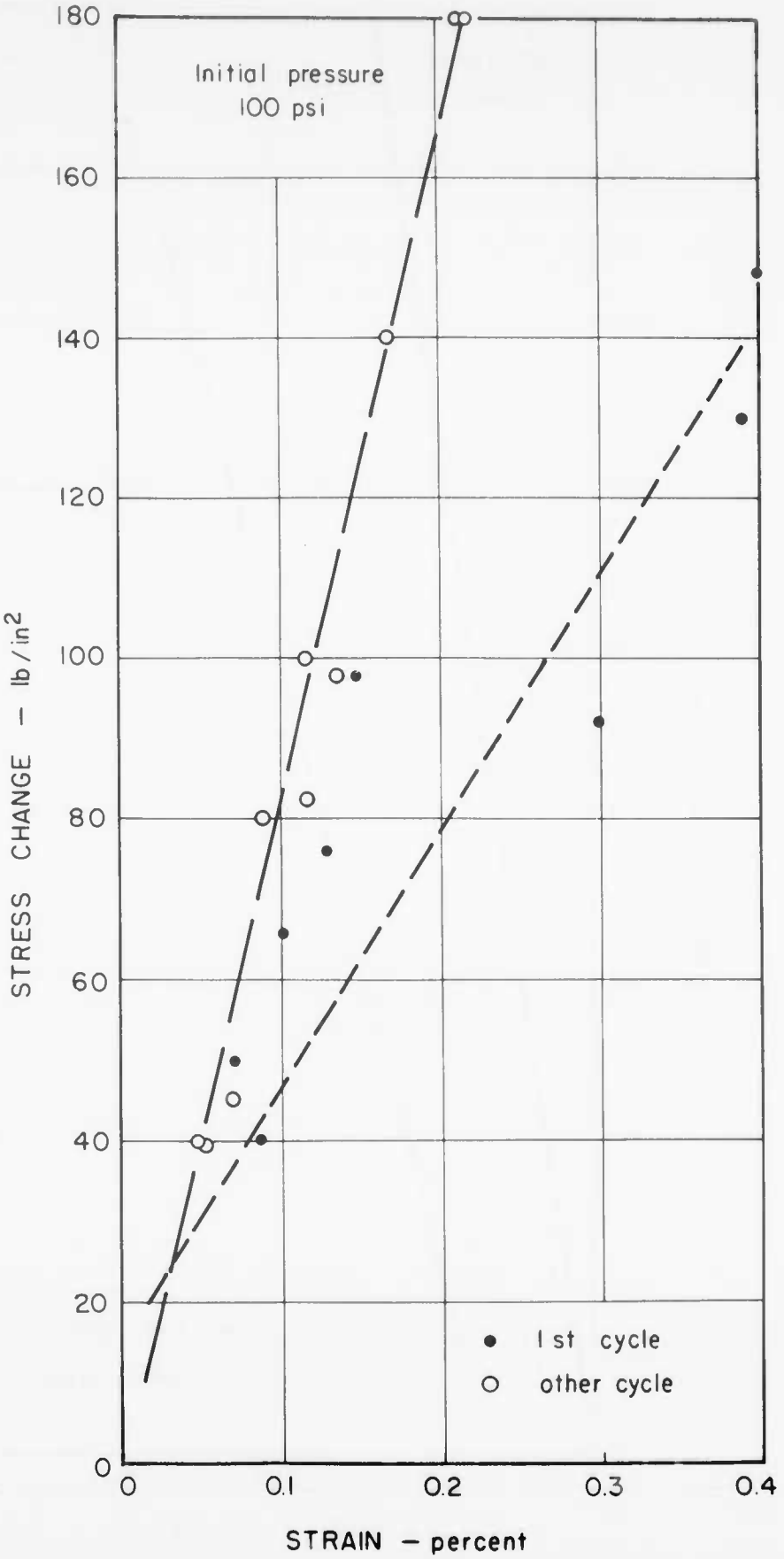

FIGURE 16 GLASS BEADS, STRESS-CHANGE vs STRAIN IN LARGE INCREMENT TESTS

APPENDIX F

TRIAXIAL TESTS USING CYCLIC LOADING

PREFACE

The results contained in this appendix were obtained by Mr. Peter J. Moore, Research Assistant. The work started in the fall of 1961 and ended in the spring of 1962.

These tests were part of a larger effort aimed at ascertaining the three-dimensional stress-strain behavior for granular soils. The tests reported herein were designed to secure very accurate data concerning the initial modulus during triaxial compression. The total test program was also to include measurement of lateral strains during triaxial compression tests and torsional loadings upon triaxial specimens. These various results were then to be compared with the results of one-dimensional compression tests.

It soon became apparent that the success of this total effort would depend upon considerable advances in testing appartus and procedures, especially with regard to the ability to measure very small displacements. Hence the decision was made to concentrate upon the one-dimensional compression tests.

The results from the triaxial compression tests are of interest with regard to the general magnitude of the measured modulus, and hence the results are included in this report.

LIST OF FIGURES

1 Test Procedure

2 Ottawa Sand - Grain Size Distribution

3 Eglin Field Sand - Grain Size Distribution

4 Glass Beads - Grain Size Distribution

5 Variations in Modulus Ratio with Cycles of Loading

6 Variations in Modulus with Cycles of Loading

7 Variations of First Cycles Modulus Ratio with Major Principal Stress

8 Modulus Determinations from Triaxial Test - Ottawa Sand

9 Modulus Determinations from Triaxial Test - Eglin Field Sand

10 Modulus Determinations from Triaxial Test - Glass Beads

11 Effect of Void Ratio on Modulus

12 Hysteresis Loops Obtained on Third Loading Cycle

13 Hysteresis Loops Obtained on Third Loading Cycle

14 Stress - Deflection Curves - Ottawa Sand

15 Stress - Deflection Curves - Ottawa Sand

LIST OF TABLES

1 Modulus for Ottawa Sand - Sample 6
2 Modulus for Ottawa Sand - Sample 7
3 Modulus for Ottawa Sand - Sample 8
4 Modulus for Ottawa Sand - Sample 9
5 Modulus for Ottawa Sand - Sample 10
6 Modulus for Ottawa Sand - Sample 11
7 Modulus for Elgin Field Sand - Sample 12
8 Modulus for Elgin Field Sand - Sample 13
9 Modulus for Elgin Field Sand - Sample 14
10 Modulus for Elgin Field Sand - Sample 15
11 Modulus for Elgin Field Sand - Sample 16
12 Modulus for Elgin Field Sand - Sample 17
13 Modulus for Elgin Field Sand - Sample 18
14 Modulus for Elgin Field Sand - Sample 19
15 Modulus for Glass Beads - Sample 20
16 Modulus for Glass Beads - Sample 21
17 Modulus for Glass Beads - Sample 22
18 Modulus for Glass Beads - Sample 24
19 Modulus for Glass Beads - Sample 25
20 Modulus for Glass Beads - Sample 26

1. Test Procedure

The tests described in this appendix have been conducted using vacuum triaxial techniques. Samples were prepared by tamping the dry soil in a membrane held in a 4-inch diameter compaction mold. This produced samples approximately 8-3/4 inches long. The metal top cap was placed in position and the vacuum was applied before the compaction mold was removed. The membrane was held in position by means of two rubber rings at each end. The sample was supported on the regular 4-inch triaxial cell base. Instead of using the regular top of the 4-inch triaxial cell, a special top was made so that frictional resistance on the loading ram could be minimized. This was done by provision of a ball bearing guide for the loading ram.

The vacuum was applied with a Cenco Hyvac vacuum pump, the amount of suction being measured on a mercury manometer. A confining pressure of less than one atmosphere could be provided by permitting a controlled leak in the line between the vacuum pump and the sample.

The samples were tested in the large Wykeham and Farrence load frame, using a strain rate of 0.012 inches per minute. The proving ring which was used for vertical load measurement had a sensitivity of approximately 120 lbs. per 0.10 inches deflection. The deflection of the sample was measured by two diametrically opposite 0.0001 inch dial gauges, which registered the vertical movement of the metal top cap on the sample.

The test procedure is illustrated in Figure 1, which is self-explanatory. In most cases four cycles of loading were run, enabling determinations of loading modulus and unloading modulus to be made in each case. At the end of each loading cycle, the strain application was stopped and readings of creep as a function of time were taken. These readings were continued until all movement had apparently ceased. This frequently occurred around 10 to 20 minutes after cessation of load application, but with the higher values of major principal stress, some readings were taken up to two hours after the completion of load application. Creep is defined here as all the movement which occurs after load application is stopped. The amount of load relaxation accompanying this creep was also noted. It was appreciated that the amount of load relaxation was not a unique property of the soil, since it depended primarily on the stiffness of the proving ring.

2. Description of Soils

The tests described in this report were conducted on three sand-size materials, two of which were of very uniform grain size, the third material showing a somewhat wider gradation. The first sample tested was Ottawa sand, the grain size curve of which is shown in Figure 2. The second material tested was Eglin Field sand, a medium sand containing a trace of silt and which was obtained from Eglin Air Force Base in Florida. The grain size curve for this material is shown in Figure 3.

The last material tested consisted of uniform glass beads of medium sand size, the grain size curve of which is shown in Figure 4. These beads were supplied by the Minnesota Mining and Manufacturing Company, and the following information on physical properties was provided by the manufacturer:

3M "Superbrite" Glass Beads

a) Modulus of Elasticity of the glass = 11×10^6 lb./in.^{2}

b) Crushing Strength per bead ≠ 10 to 15 lb.

c) Shape - 3% to 10% of the glass spheres may not be accurate spheres

3. Test Results

The most obvious parameter which could be extracted from the test results was Young's modulus for the loading and unloading portions of each cycle. These results have been tabulated in Tables 1 through 6 for Ottawa sand, Tables 7 through 14 for Eglin Field sand, and Tables 15 through 20 for glass beads.

4. Discussion of Data

A glance at the tabulated data shows immediately the following features:

a) The unloading modulus shows relatively small variations from cycle to cycle compared with the loading modulus.

b) For the one atmosphere confining pressure the creep tends to cease after the first cycle, particularly for the lower stress increments.

c) For the one-third of an atmosphere confining pressure, the creep does not cease after the first cycle for the higher stress increments, although there is a significant decrease in the magnitude of the creep.

d) The loading modulus for the first cycle is usually quite low compared with the moduli for subsequent cycles.

e) By the end of the fourth cycle, the loading modulus appears to be levelling off to a constant value.

f) The loading modulus determined after permitting creep and relaxation to occur is only slightly lower than the original loading modulus.

Some of these features may be demonstrated by means of a graphical presentation. Figure 5 shows the variation in modulus ratio for various cycles of loading for all of the Ottawa sand samples. A modulus ratio of 1.0 corresponds to the final, apparently constant value of modulus for the loading portion of a cycle. On the Figure, boundaries, which enclose most of the test results, have been drawn. This plot shows the rapid rise in loading modulus and its levelling off at a "constant" value. It is also seen that the unloading moduli are higher than the loading moduli, and they do not show a great variation with cycle of loading.

For sample 10 these results have been plotted in Figure 6 in terms of actual modulus in lb./in.^{2}. Here the same general pattern described above is evident. This plot also shows a relationship not evident in Figure 5, namely that both loading and unloading moduli increase with stress level. It does appear, however, that for the first cycle the reverse relationship is true for the loading portion of the cycle.

This point is demonstrated in more detail in Figure 7. This plot shows that for a particular value of confining pressure the loading modulus ratio decreases with an increase in major principal stress (first loading cycle only). At the same time it appears that the unloading modulus ratio does not show any significant variation with major principal stress.

With the results so far available it seems that the modulus is more dependent on major principal stress than on confining pressure. Plots of modulus (levelled off "constant" value) against major principal stress has been made for all the Ottawa sand samples in Figure 8, for the Eglin Field sand in Figure 9, and for the glass beads in Figure 10. With the relatively few points available it is evident that tests at much higher confining pressures would be desirable to define the relationships more clearly. However, even with the information so far available some statements can be made from a comparison of Figures 8, 9 and 10.

In general, it appears that the Young's modulus decreases with an increase in the stress increment ($\Delta\sigma$). The modulus values for the glass beads are of the same order of magnitude as those for the Ottawa sand. But the rate of increase of modulus with respect to major principal stress is greater in the case of the glass beads. The modulus values for the Eglin Field sand are significantly less than for both the glass beads and the Ottawa sand. This difference may be explainable partly by the differences in void ratios, Eglin Field sand having a void ratio of 0.63, Ottawa sand 0.53, and the glass beads 0.59. The results of some tests on Eglin Field sand at different void ratios are presented in Figure 11. From this plot it seems not too unreasonable to state that the differences between the Ottawa sand and Eglin Field sand moduli can be explained in terms of void ratio differences. In the case of the glass beads however, there seems to be some other factor influencing the moduli. Conceivably, this factor may be surface roughness of the particles.

To gain an impression of the shape of the hysteresis loops, some typical stress-strain curves for the third cycle of loading have been plotted in Figures 12 and 13. It is noted that complete equilibrium has not been attained since none of the hysteresis loops fully close. The shapes of these loops are generally convex upwards for loading and concave upwards for unloading. This differs somewhat from the hysteresis loops obtained by Weissmann and Hart in "The Damping Capacity of Some Granular Soils", where the stress strain curves were concave upwards for both loading and

unloading. This is illustrated in the inset in Figure 12. Probably one should not expect agreement in the shape of the hystersis loops since the two sets of data are not strictly comparable. In addition to testing soils of larger grain size than has been described in this report, Weissmann and Hart kept cycling the load until a closed hysteresis loop was obtained. They have not stated how many cycles were required to do this.

If energy loss is defined as the area within the loop, it is seen that the energy loss for a lower confining pressure (5 lb./in.^{2}) is many times the energy loss for a higher confining pressure (14.7 lb./in.^{2}). It is of further interest to note the almost perfect elastic behavior of the glass beads under the higher confining pressure.

For an examination of creep behavior an initial plot of principal stress difference against deflection has been made in Figures 14 and 15. For the samples under the higher confining pressure the magnitude of creep deflection seems to be increasing at a similar rate as the total deflection. However, for the samples under the lower confining pressure the creep deflection appears to reach a maximum value while the total deflection still increases.

Table 1

MODULUS FOR OTTAWA SAND - SAMPLE 6

$e = 0.54$, $\sigma_c = 14.8$ p.s.i., $\Delta\sigma = 2.0$ p.s.i.

σ_a p.s.i.	First Cycle		Second Cycle		Third Cycle		Fourth Cycle
	Load	Unload	Load	Unload	Load	Unload	Load
2.0	30,000*	55,000	50,000	49,000	47,000	49,000	47,000
4.0	12,000 (10,300)⊗	60,000	50,000	52,000	52,000	52,000	52,000
6.0	5,400 (4,700)	67,000	52,000	56,000	47,000 (36,000)	53,000	49,000
8.0	2,700 (1,900)	53,000	33,000 (9,900)	55,000	49,000 (35,000)	56,000	50,000

* Units of modulus are lb./in.^{2}.

⊗ Numbers in brackets refer to modulus measurements made after permitting creep and relaxation to occur.

Table 2

MODULUS FOR OTTAWA SAND - SAMPLE 7

$e = 0.54$, $\sigma_c = 14.6$ p.s.i., $\Delta\sigma = 1.0$ p.s.i.

σ_a p.s.i.	First Cycle		Second Cycle		Third Cycle		Fourth Cycle
	Load	Unload	Load	Unload	Load	Unload	Load
2.0	31,000 (28,000)	52,000	49,000	52,000	52,000	52,000	52,000
4.0	18,000 (14,000)	59,000	55,000	68,000	59,000	63,000	59,000
6.0	8,300 (6,000)	72,000	55,000	68,000	68,000	89,000	59,000
8.0	4,100 (2,900)	64,000	55,000	81,000	59,000	74,000	59,000
10.0	2,000 (1,400)	88,000	68,000 (35,000)	89,000	63,000	81,000	59,000

Table 3

MODULUS FOR OTTAWA SAND - SAMPLE 8

e = 0.53, σ_c = 14.7 p.s.i., $\Delta\sigma$ = 4.0 p.s.i.

σ_a p.s.i.	First Cycle		Second Cycle		Third Cycle		Fourth Cycle
	Load	Unload	Load	Unload	Load	Unload	Load
4.0	18,000 (15,000)	52,000	51,000	51,000	53,000	52,000	50,000
6.0	14,000 (11,000)	54,000	50,000 (44,000)	54,000	52,000	55,000	52,000
8.0	7,100 (5,300)	60,000	53,000 (49,000)	56,000	53,000	56,000	52,000 (48,000)

Table 4

MODULUS FOR OTTAWA SAND - SAMPLE 9

e = 0.54 σ_c = 4.9 p.s.i., $\Delta\sigma$ = 1.0 p.s.i.

σ_a p.s.i.	First Cycle		Second Cycle		Third Cycle		Fourth Cycle
	Load	Unload	Load	Unload	Load	Unload	Load
2.0	7,700 (6,500)	35,000	34,000	35,000	34,000	35,000	34,000
4.0	800 (650)	42,000	35,000	47,000	37,000	44,000	39,000
6.0	280 (210)	48,000	47,000	49,000	42,000	52,000	42,000

Table 5

MODULUS FOR OTTAWA SAND - SAMPLE 10

$e = 0.54$, $\sigma_c = 4.9$ p.s.i., $\Delta\sigma = 2.0$ p.s.i.

σ_a p.s.i.	First Cycle		Second Cycle		Third Cycle		Fourth Cycle
	Load	Unload	Load	Unload	Load	Unload	Load
2.0	4,700 (3,900)	27,000	25,000 (21,000)	29,000	26,000 (25,000)	29,000	27,000
4.0	610 (540)	34,000	31,000 (21,000)	36,000	34,000 (32,000)	39,000	35,000
6.0	240 (220)	40,000	40,000	43,000	43,000		

Table 6

MODULUS FOR OTTAWA SAND - SAMPLE 11

$e = 0.52$, $\sigma_c = 5.0$ p.s.i., $\Delta\sigma = 4.0$ p.s.i.

σ_a p.s.i.	First Cycle		Second Cycle		Third Cycle		Fourth Cycle
	Load	Unload	Load	Unload	Load	Unload	Load
4.0	840 (780)	29,000	24,000 (20,000)	29,000	27,000 (23,000)	29,000	26,000
6.0	400 (370)	36,000	28,000 (23,000)	37,000	32,000 (25,000)	38,000	34,000 (28,000)

Table 7

MODULUS FOR EGLIN FIELD SAND - SAMPLE 12

$e = 0.64$, $\sigma_c = 14.2$ p.s.i., $\Delta\sigma = 2.0$ p.s.i.

σ_a	First Cycle		Second Cycle		Third Cycle		Fourth Cycle
p.s.i.	Load	Unload	Load	Unload	Load	Unload	Load
2.0	20,000 (13,500)	39,000	36,000	40,000	36,000	40,000	39,000
4.0	13,000 (7,500)	42,000	36,000 (32,000)	42,000	36,000 (31,000)	44,000	39,000
6.0	9,500 (4,000)	45,000	40,000 (36,000)	45,000	40,000	44,000	42,000
8.0	7,000 (3,300)	52,000	43,000 (40,000)	53,000	43,000	51,000	43,000

Table 8

MODULUS FOR EGLIN FIELD SAND - SAMPLE 13

$e = 0.63$, $\sigma_c = 14.4$ p.s.i., $\Delta\sigma = 1.0$ p.s.i.

σ_a	First Cycle		Second Cycle		Third Cycle		Fourth Cycle
p.s.i.	Load	Unload	Load	Unload	Load	Unload	Load
2.0	16,000 (6,600)	37,000	35,000	38,000	38,000	38,000	36,500
4.0	8,200 (3,100)	42,000	33,500	49,000	38,000	44,000	36,500
6.0	4,000 (1,600)	46,000	35,000	40,000	38,000	51,000	38,000
8.0	2,800 (1,000)	44,000	36,500	49,000	40,000	55,000	40,000
10.0	2,400 (950)	62,000	32,000	62,000	35,000	79,000	38,000

Table 9

MODULUS FOR EGLIN FIELD SAND - SAMPLE 14

$e = 0.62$, $\sigma_c = 14.7$ p.s.i., $\Delta\sigma = 4.0$ p.s.i.

σ_a	First Cycle		Second Cycle		Third Cycle		Fourth Cycle
p.s.i.	Load	Unload	Load	Unload	Load	Unload	Load
4.0	7,300 (5,000)	37,000	35,000 (28,000)	38,000	36,000 (33,000)	38,000	38,000
6.0	11,500 (6,400)	41,000	33,500 (26,000)	41,000	38,000	41,000	40,000
8.0	9,000 (4,900)	44,000	39,000	47,000	41,000 (34,000)	47,000	43,000 (38,000)

Table 10

MODULUS FOR EGLIN FIELD SAND - SAMPLE 15

$e = 0.61$, $\sigma_c = 5.0$ p.s.i., $\Delta\sigma = 4.0$ p.s.i.

σ_a	First Cycle		Second Cycle		Third Cycle		Fourth Cycle
p.s.i.	Load	Unload	Load	Unload	Load	Unload	Load
4.0	3,700 (2,900)	22,000	21,500 (17,000)	23,000	23,000 (20,000)	24,000	23,000
6.0	1,700 (1,400)	25,000	24,000 (19,000)	29,000	26,000 (22,000)	28,000	26,500

Table 11

MODULUS FOR EGLIN FIELD SAND - SAMPLE 16

$e = 0.58$, $\sigma_c = 4.9$ p.s.i., $\Delta\sigma = 1.0$ p.s.i.

σ_a	First Cycle		Second Cycle		Third Cycle		Fourth Cycle
p.s.i.	Load	Unload	Load	Unload	Load	Unload	Load
2.0	16,000 (13,000)	30,000	29,000	31,000	30,000	31,000	29,000
4.0	8,800 (5,800)	30,000	31,000 (19,000)	32,000	31,000	32,000	31,000
6.0	2,400 (1,600)	34,000	31,000	36,000	32,000	38,000	35,000
10.0	460 (290)	53,000	32,000 (22,000)	58,000	35,000	55,000	36,000

Table 12

MODULUS FOR EGLIN FIELD SAND - SAMPLE 17

$e = 0.63$, $\sigma_c = 4.8$ p.s.i., $\Delta\sigma = 1.0$ p.s.i.

σ_a	First Cycle		Second Cycle		Third Cycle		Fourth Cycle
p.s.i.	Load	Unload	Load	Unload	Load	Unload	Load
2.0	12,500 (10,000)	27,000	24,000	25,000	25,000	25,000	25,000
4.0	6,800 (4,000)	29,000	28,000	29,000	27,000	30,000	29,000
6.0	1,800 (1,000)	35,000	32,000	35,000	34,000	35,000	32,000
10.0	450 (260)	54,000	40,000	51,000	38,000	51,000	38,000

Table 13

MODULUS FOR EGLIN FIELD SAND - SAMPLE 18

e = 0.63, σ_c = 5.0 p.s.i., $\Delta\sigma$ = 2.0 p.s.i.

σ_a p.s.i.	First Cycle		Second Cycle		Third Cycle		Fourth Cycle
	Load	Unload	Load	Unload	Load	Unload	Load
2.0	13,000 (10,800)	23,000	22,000	23,000	23,000	24,000	23,000
4.0	6,700 (4,600)	25,000	25,000	26,000	24,000	26,000	25,000
6.0	1,600 (1,150)	30,000	27,000 (13,000)	32,000	30,000	34,000	30,000
14.5	290 (210)	61,000	50,000	60,000	51,000	62,000	50,000

Table 14

MODULUS FOR EGLIN FIELD SAND - SAMPLE 19

e = 0.78, σ_c = 5.0 p.s.i., $\Delta\sigma$ = 1.0 p.s.i.

σ_a p.s.i.	First Cycle		Second Cycle		Third Cycle		Fourth Cycle
	Load	Unload	Load	Unload	Load	Unload	Load
2.0	10,000 (7,400)	19,000	19,000	19,000	19,000	19,000	19,000
4.0	6,200 (3,800)	26,000	24,000	25,000	24,000	25,000	24,000
6.0	1,900 (1,100)	27,000	26,000 (8,400)	29,000	28,000	30,000	29,000
10.0	380 (200)	34,000		40,000	31,000	38,000	38,000*

* This modulus is for the fifth loading cycle, no readings being taken for the fourth and second loading cycles.

Table 15

MODULUS FOR GLASS BEADS - SAMPLE 20

$e = 0.59$, $\bar{\sigma_c} = 14.4$ p.s.i. $\Delta\sigma = 2.0$ p.s.i.

σ_a p.s.i.	First Cycle		Second Cycle		Third Cycle		Fourth Cycle
	Load	Unload	Load	Unload	Load	Unload	Load
2.0	35,000	53,000	49,000	55,000	53,000	55,000	50,000
4.0	35,000 (29,000)	58,000	55,000	56,000	55,000	56,000	56,000
6.0	27,000 (21,000)	60,000	60,000	60,000	58,000	65,000	60,000
8.0	20,000 (14,500)	56,000	63,000	63,000	63,000	63,000	60,000

Table 16

MODULUS FOR GLASS BEADS - SAMPLE 21

$e = 0.58$, $\bar{\sigma_c} = 14.6$ p.s.i., $\Delta\sigma = 4.0$ p.s.i.

σ_a p.s.i.	First Cycle		Second Cycle		Third Cycle		Fourth Cycle
	Load	Unload	Load	Unload	Load	Unload	Load
4.0	29,000 (27,000)	59,000	52,000	58,000	54,000	59,000	53,000
6.0	33,000 (27,000)	56,000	56,000	58,000	56,000	57.000	56,000
8.0	32,000 (26,000)	63,000	66,000	66,000	66,000	66,000	65,000

Table 17

MODULUS FOR GLASS BEADS - SAMPLE 22

$e = 0.59$, $\sigma_c = 14.5$ p.s.i. $\Delta\sigma = 1.0$ p.s.i.

σ_a p.s.i.	First Cycle		Second Cycle		Third Cycle		Fourth Cycle
	Load	Unload	Load	Unload	Load	Unload	Load
2.0	46,000 (42,000)	58,000	58,000	58,000	58,000	58,000	58,000
4.0	31,000 (27,000)	73,000	58,000	67,000	62,000	67,000	62,000
6.0	19,000 (13,000)	77,000	73,000	73,000	80,000	80,000	73,000
8.0	10,000 (7,200)	86,000	67,000	73,000	73,000	73,000	67,000
10.0	4,800 (3,400)	91,000	67,000	80,000	73,000	80,000	73,000

Testing of sample 23 was discontinued when it was found that the vacuum had been accidentally altered during the test.

Table 18

MODULUS FOR GLASS BEADS - SAMPLE 24

e = 0.59, σ_c = 5.4 p.s.i., $\Delta\sigma$ = 2.0 p.s.i.

σ_a	First Cycle		Second Cycle		Third Cycle		Fourth Cycle
p.s.i.	Load	Unload	Load	Unload	Load	Unload	Load
2.0	10,000 (9,400)	30,000	34,000 (31,000)	33,000	34,000	35,000	35,000
4.0	2,900 (2,500)	36,000	43,000	42,000	42,000	42,000	42,000
6.0	740 (680)	37,000	36,000 (31,000)	39,000	39,000	37,000	41,000
8.0	210 (200)	44,000	42,000 (33,000)	45,000	45,000	45,000	44,000

Table 19

MODULUS FOR GLASS BEADS - SAMPLE 25

e = 0.59, σ_c = 5.1 p.s.i., $\Delta\sigma$ = 1.0 p.s.i.

σ_a p.s.i.	First Cycle		Second Cycle		Third Cycle		Fourth Cycle
	Load	Unload	Load	Unload	Load	Unload	Load
2.0	5,100 (3,600)	35,000	36,000	36,000	36,000	38,000	38,000
4.0	530 (450)	40,000	44,000	44,000	44,000	44,000	44,000
6.0	160 (130)	42,000	40,000	46,000	42,000	49,000	40,000

Table 20

MODULUS FOR GLASS BEADS - SAMPLE 26

e = 0.59, σ_c = 4.9 p.s.i., $\Delta\sigma$ = 4.0 p.s.i.

σ_a p.s.i.	First Cycle		Second Cycle		Third Cycle		Fourth Cycle
	Load	Unload	Load	Unload	Load	Unload	Load
4.0	1,100 (1,030)	23,000	22,000 (18,000)	26,000	25,000 (23,000)	28,000	26,000
6.0	270 (260)	27,000	24,000 (20,000)	30,000	26,000	33,000	28,000

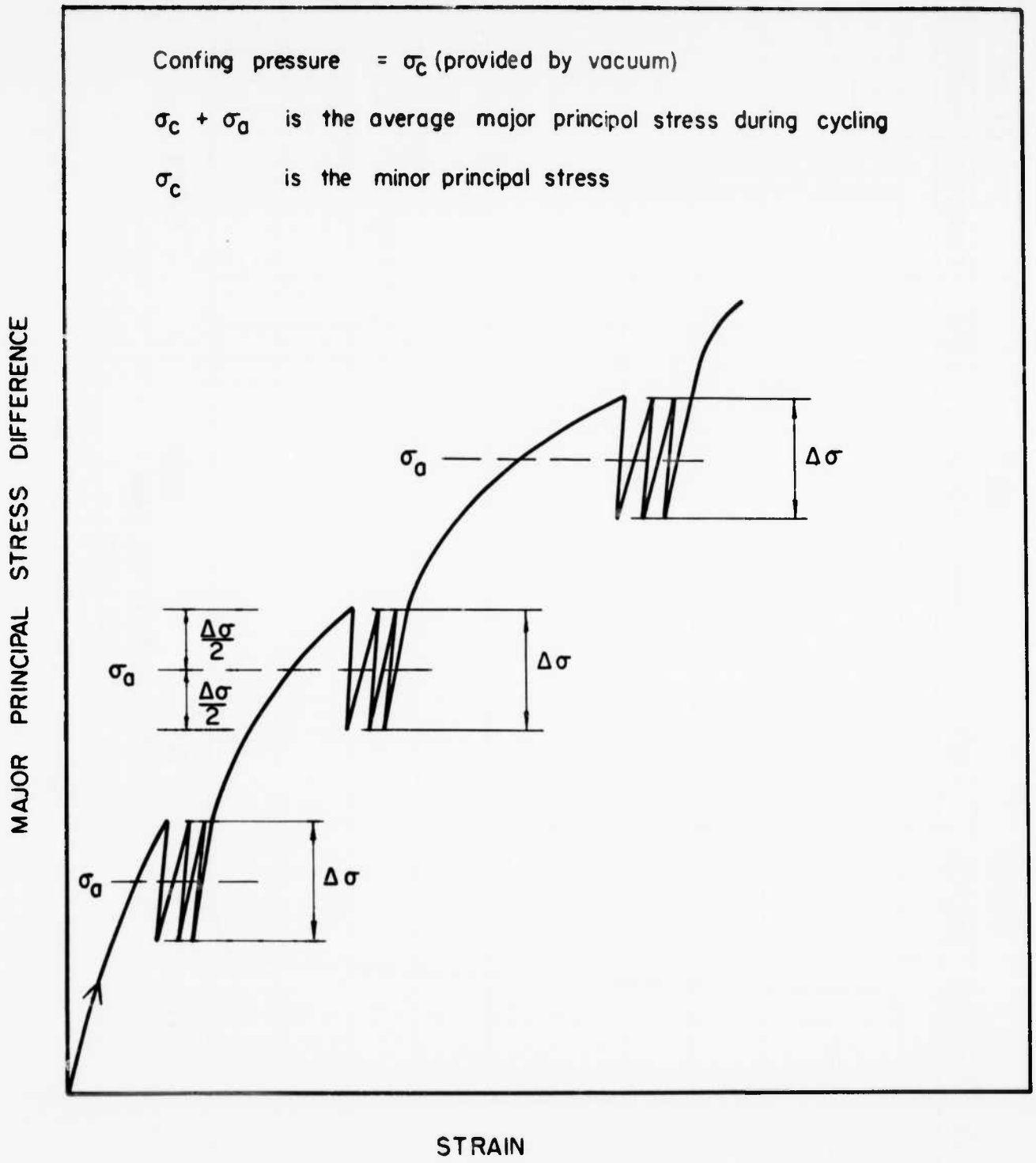

FIGURE 1 TEST PROCEDURE

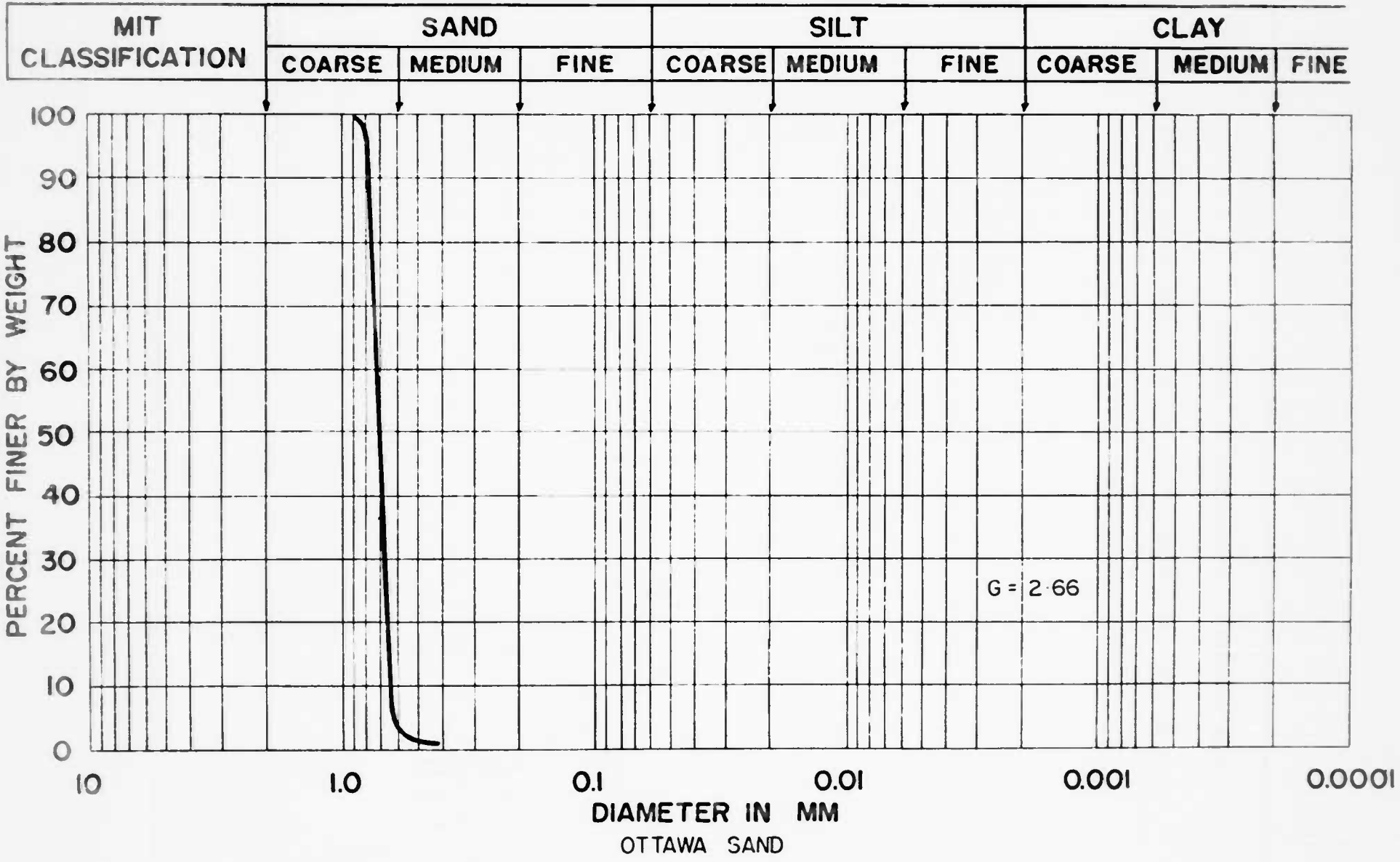

OTTAWA SAND

FIGURE 2 GRAIN SIZE DISTRIBUTION

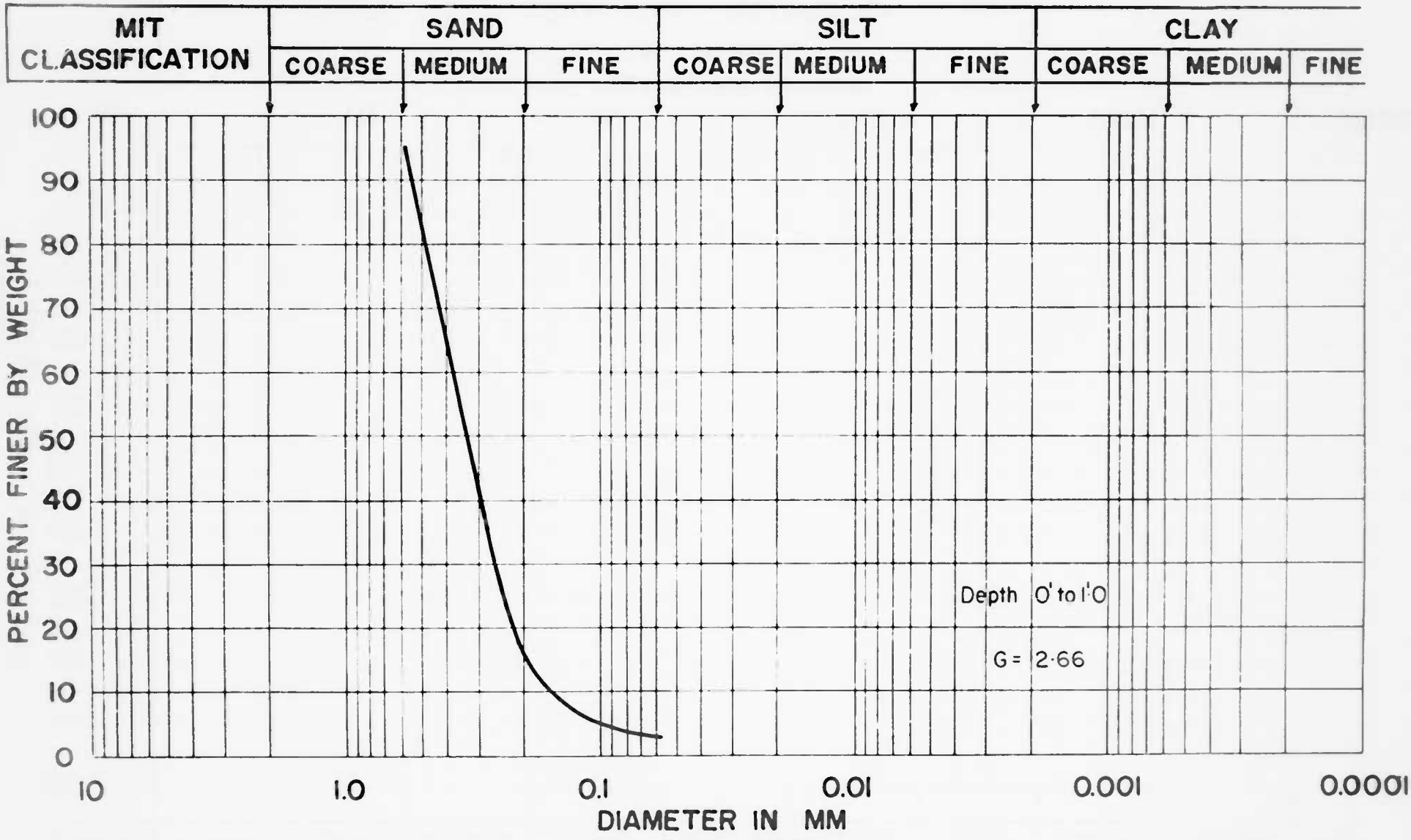

EGLIN FIELD SAND

FIGURE 3 GRAIN SIZE DISTRIBUTION

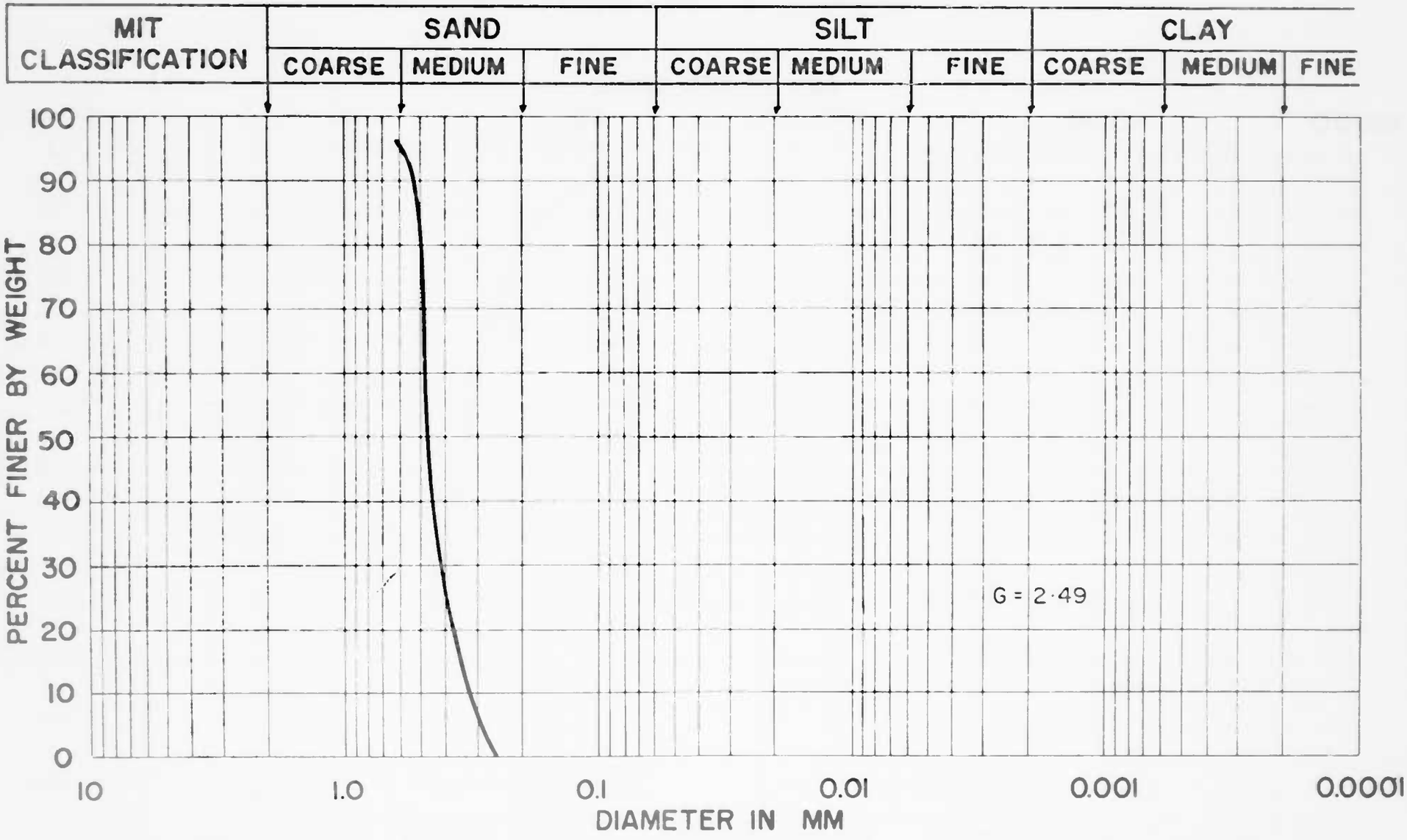

GLASS BEADS

FIGURE 4 GRAIN SIZE DISTRIBUTION

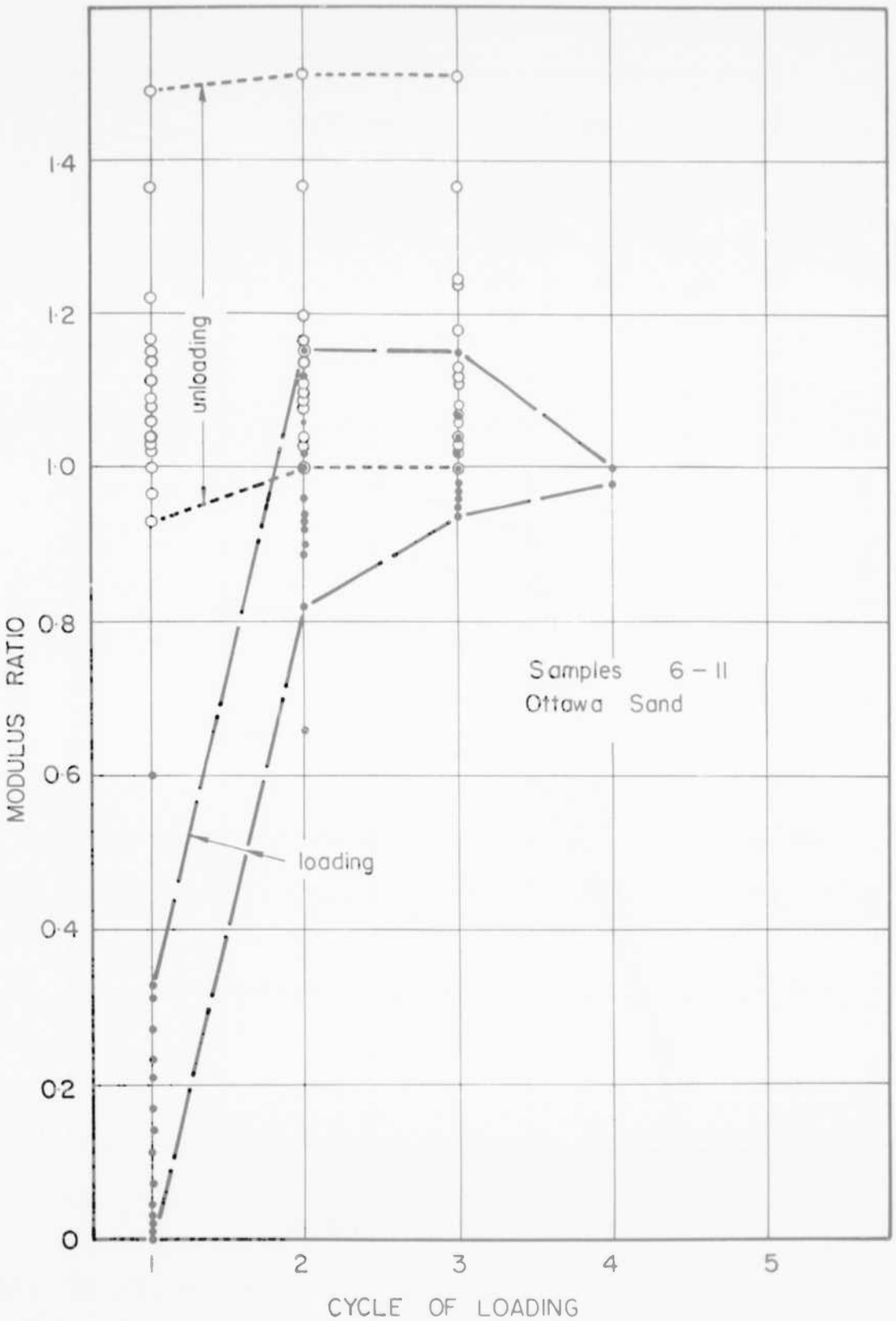

FIGURE 5 VARIATIONS IN MODULUS RATIO WITH CYCLES OF LOADING

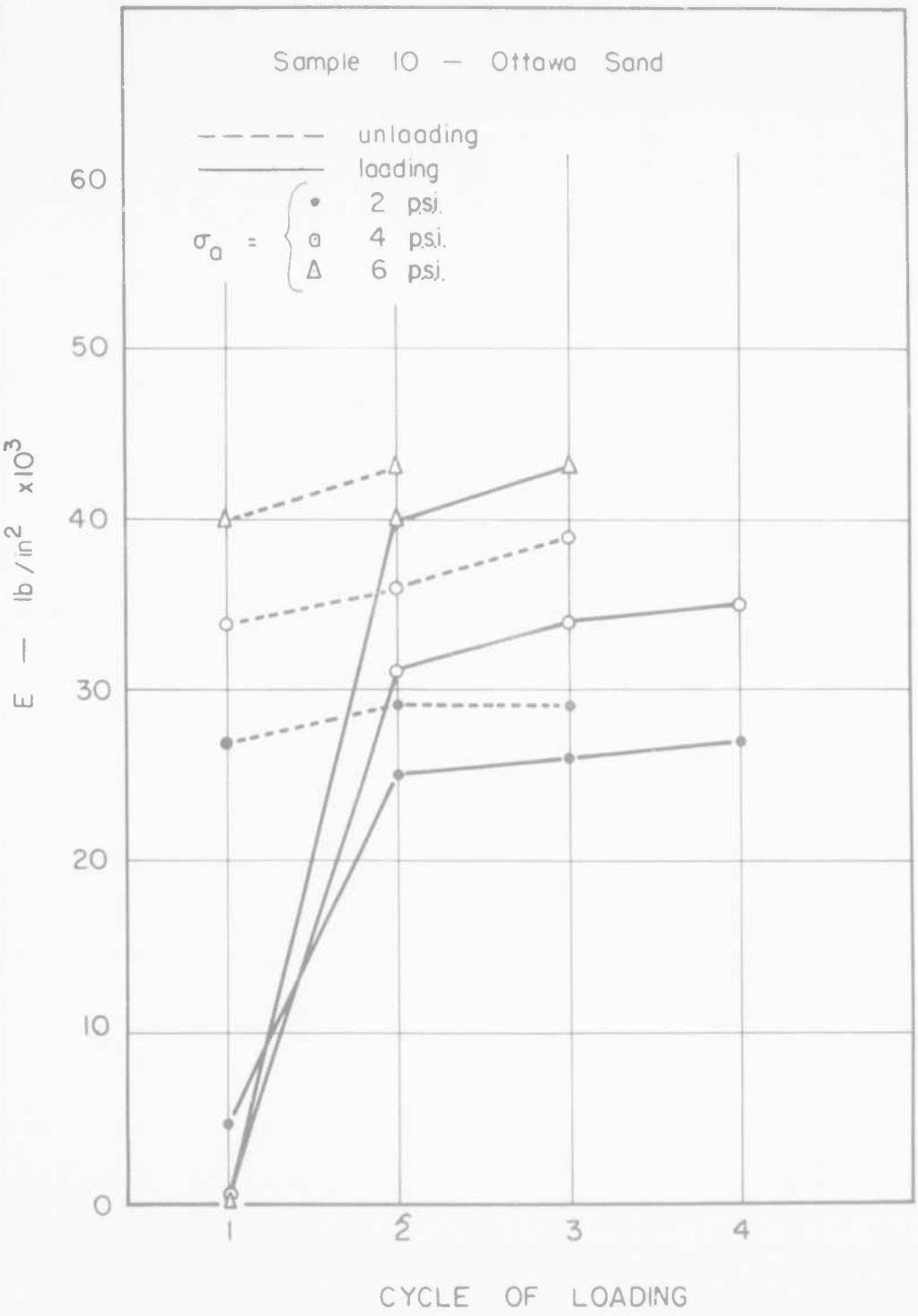

FIGURE 6 VARIATION IN MODULUS WITH CYCLES OF LOADING

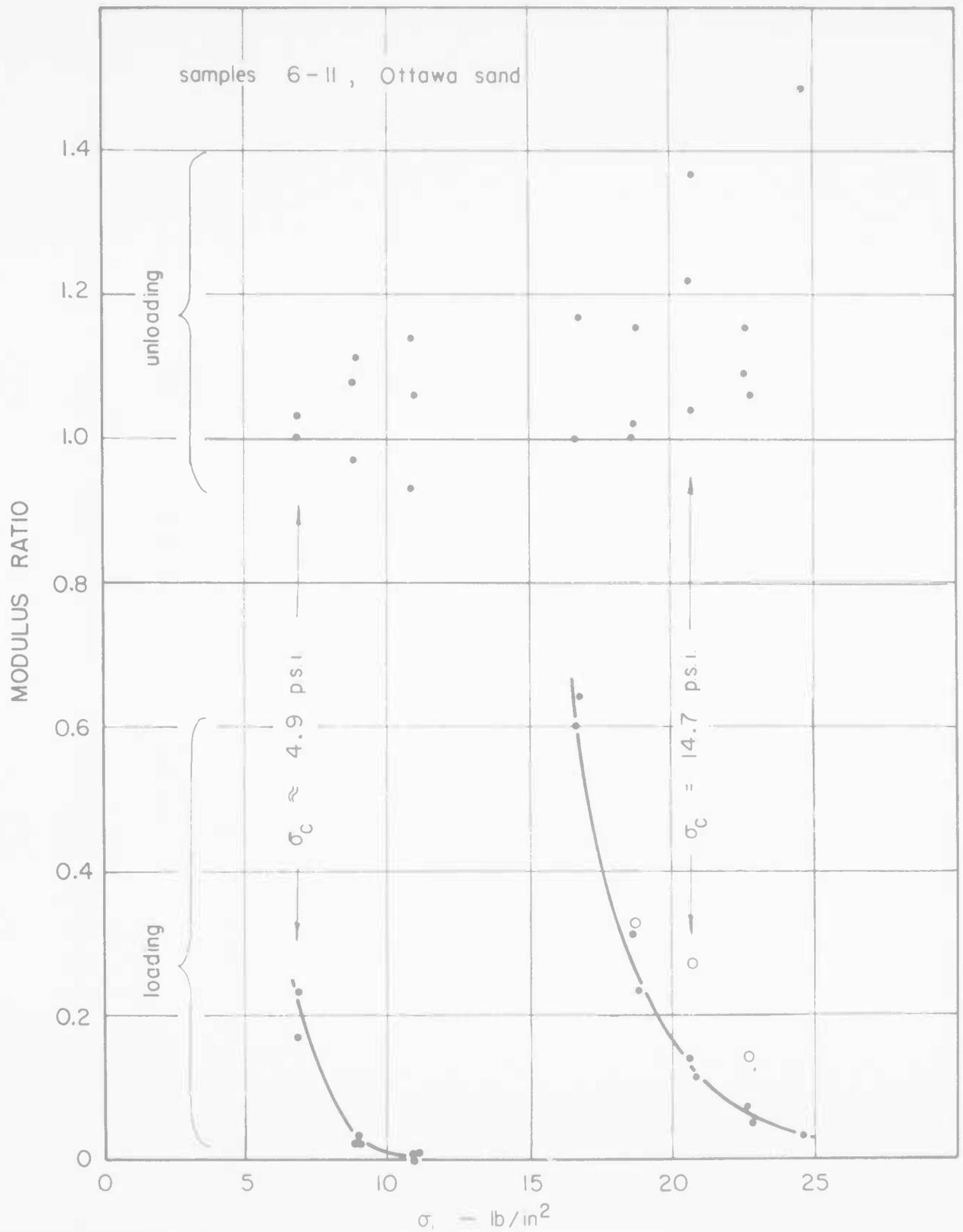

FIGURE 7 VARIATIONS OF FIRST CYCLES MODULUS RATIO WITH MAJOR PRINCIPAL STRESS

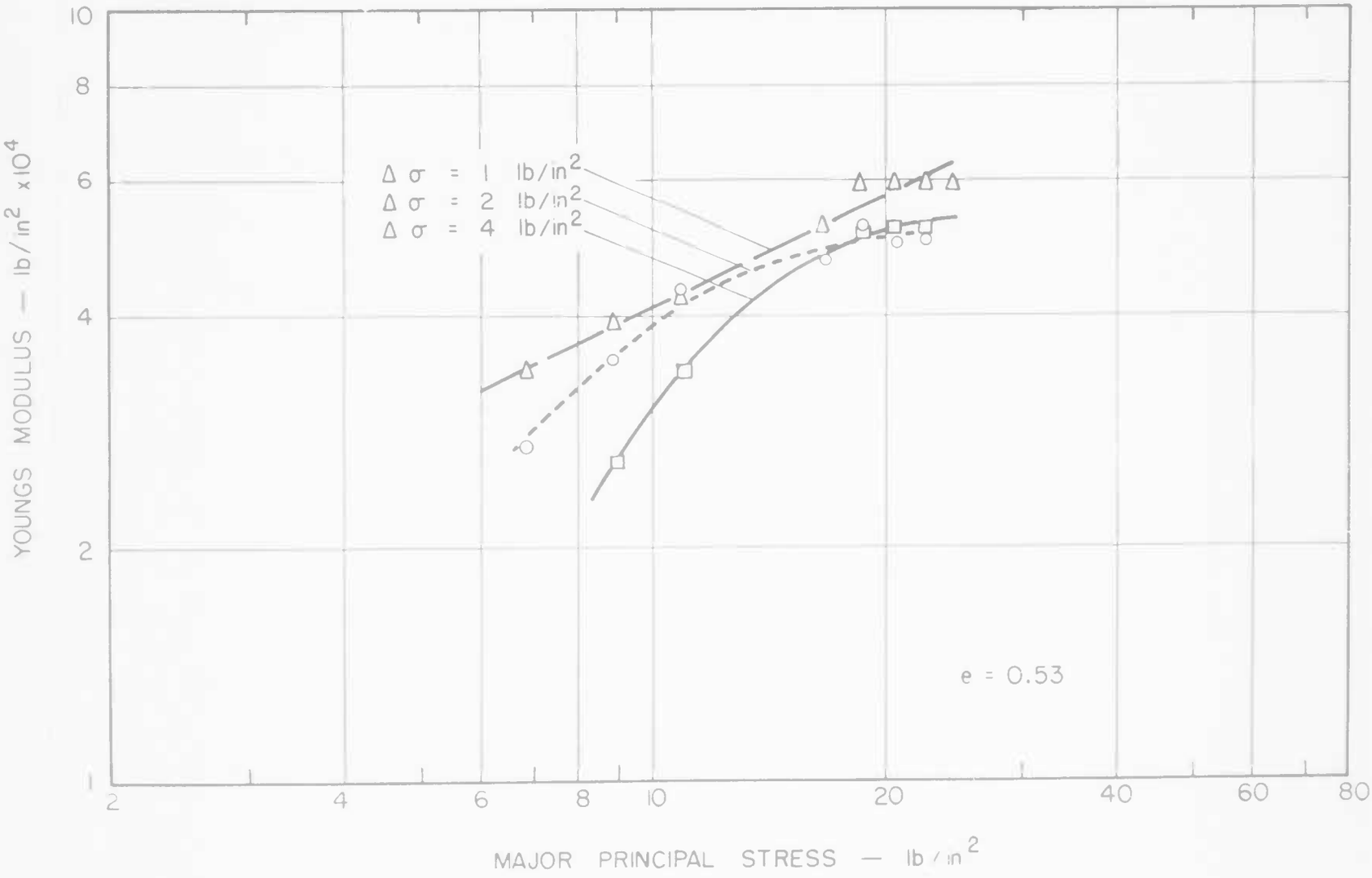

FIGURE 8 MODULUS DETERMINATIONS FROM TRIAXIAL TEST — OTTAWA SAND

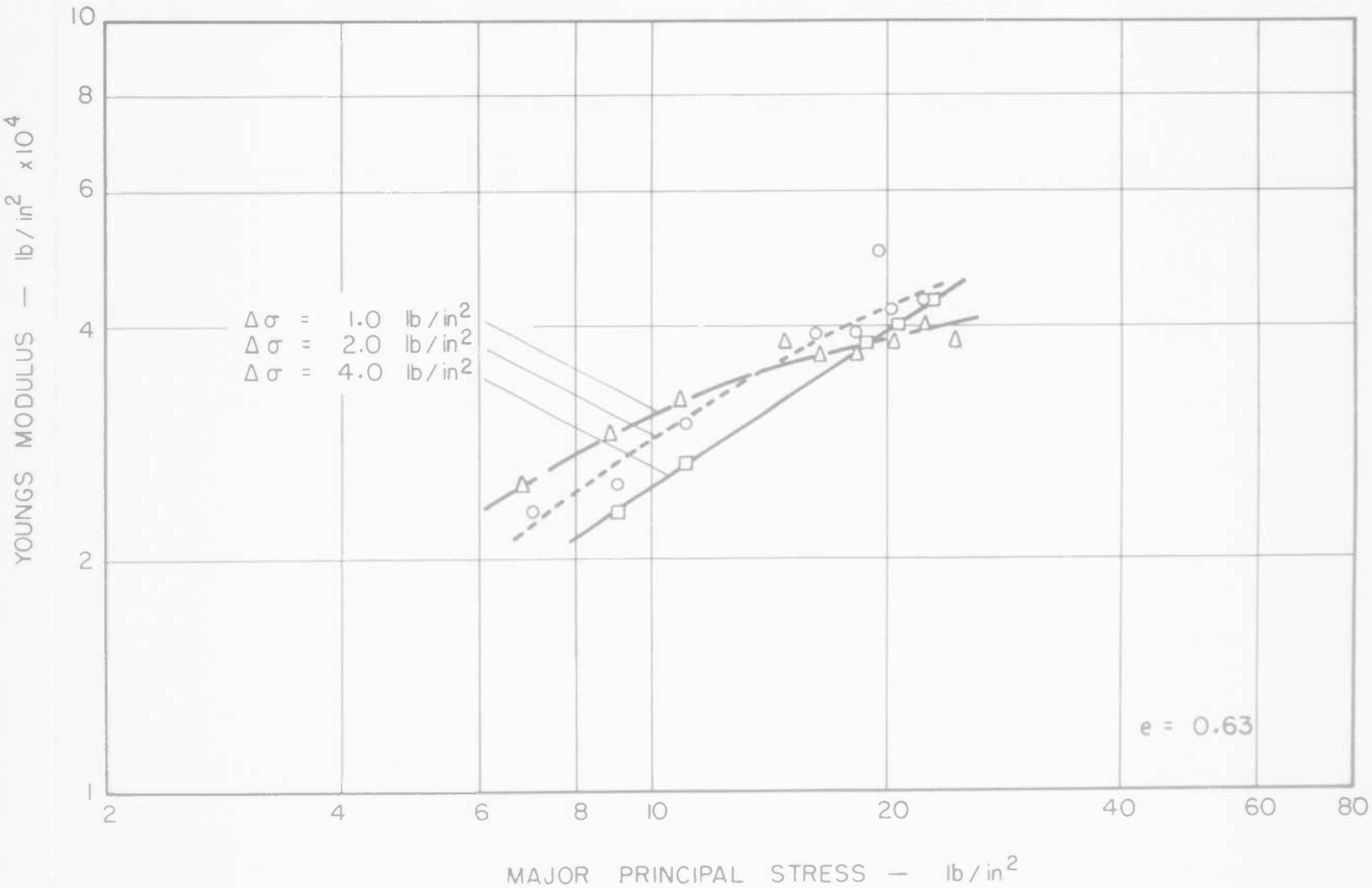

FIGURE 9 MODULUS DETERMINATIONS FROM TRIAXIAL TEST — EGLIN FIELD SAND

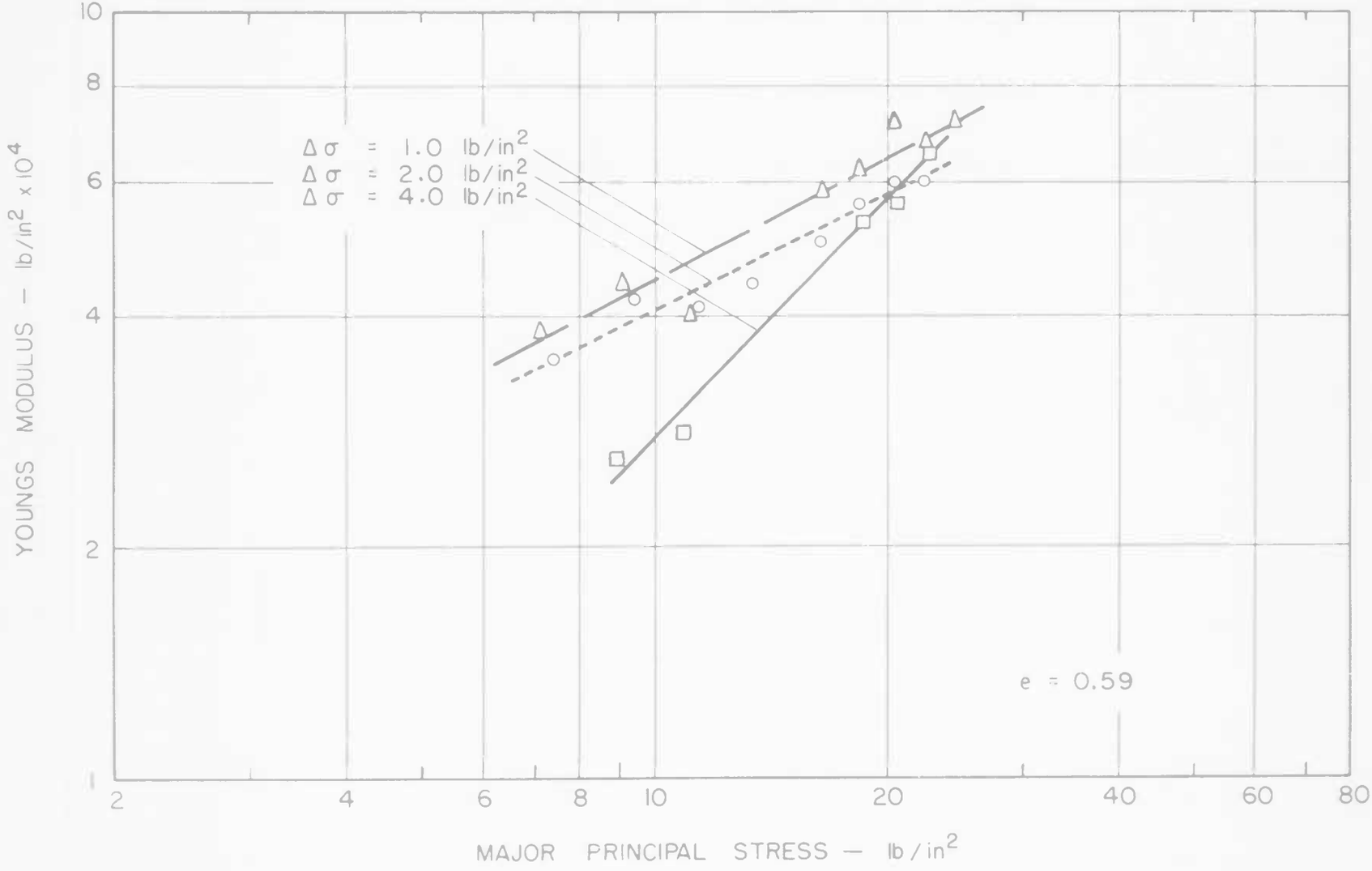

FIGURE 10 MODULUS DETERMINATIONS FROM TRIAXIAL TEST – GLASS BEADS

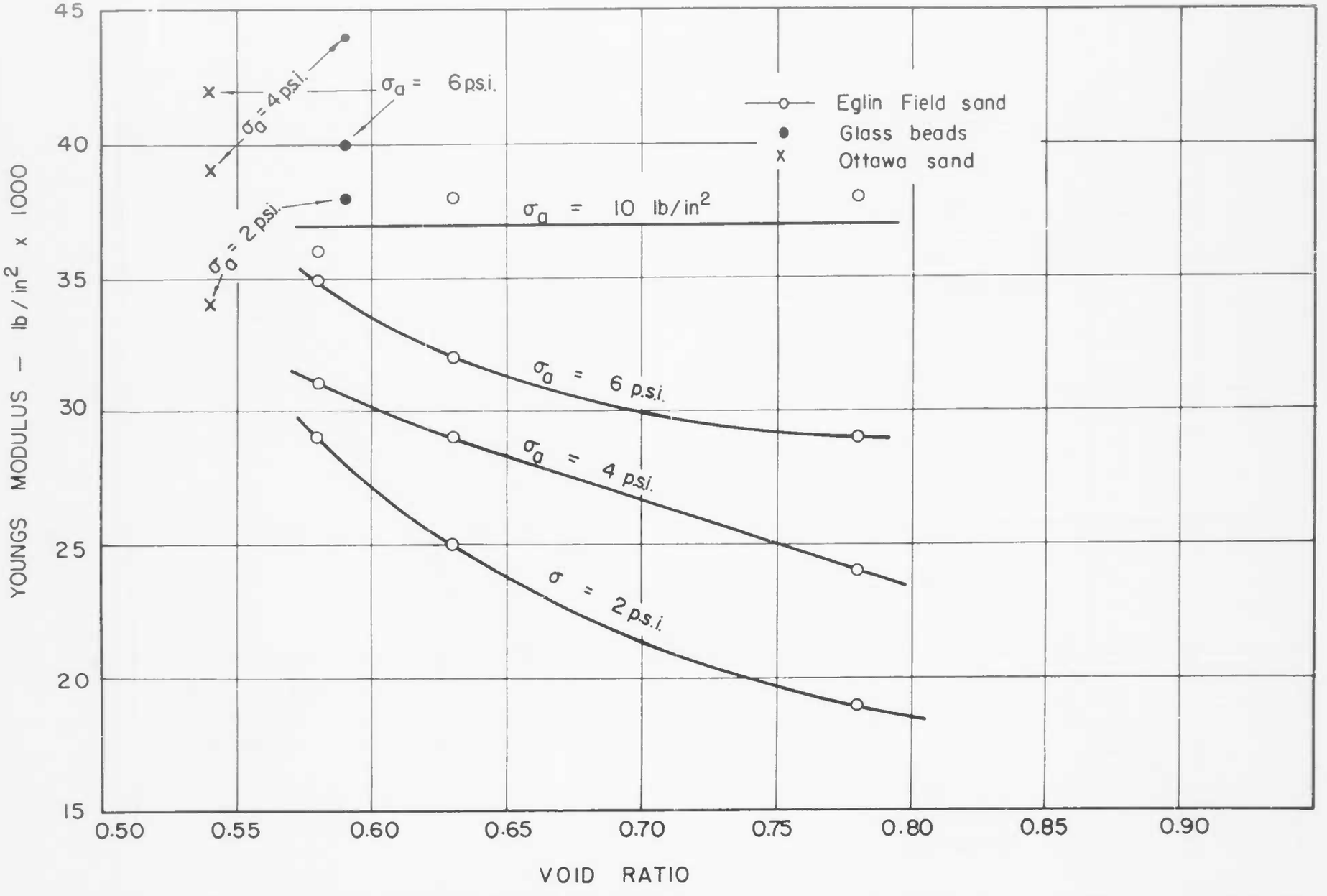

FIGURE 11 EFFECT OF VOID RATIO ON MODULUS

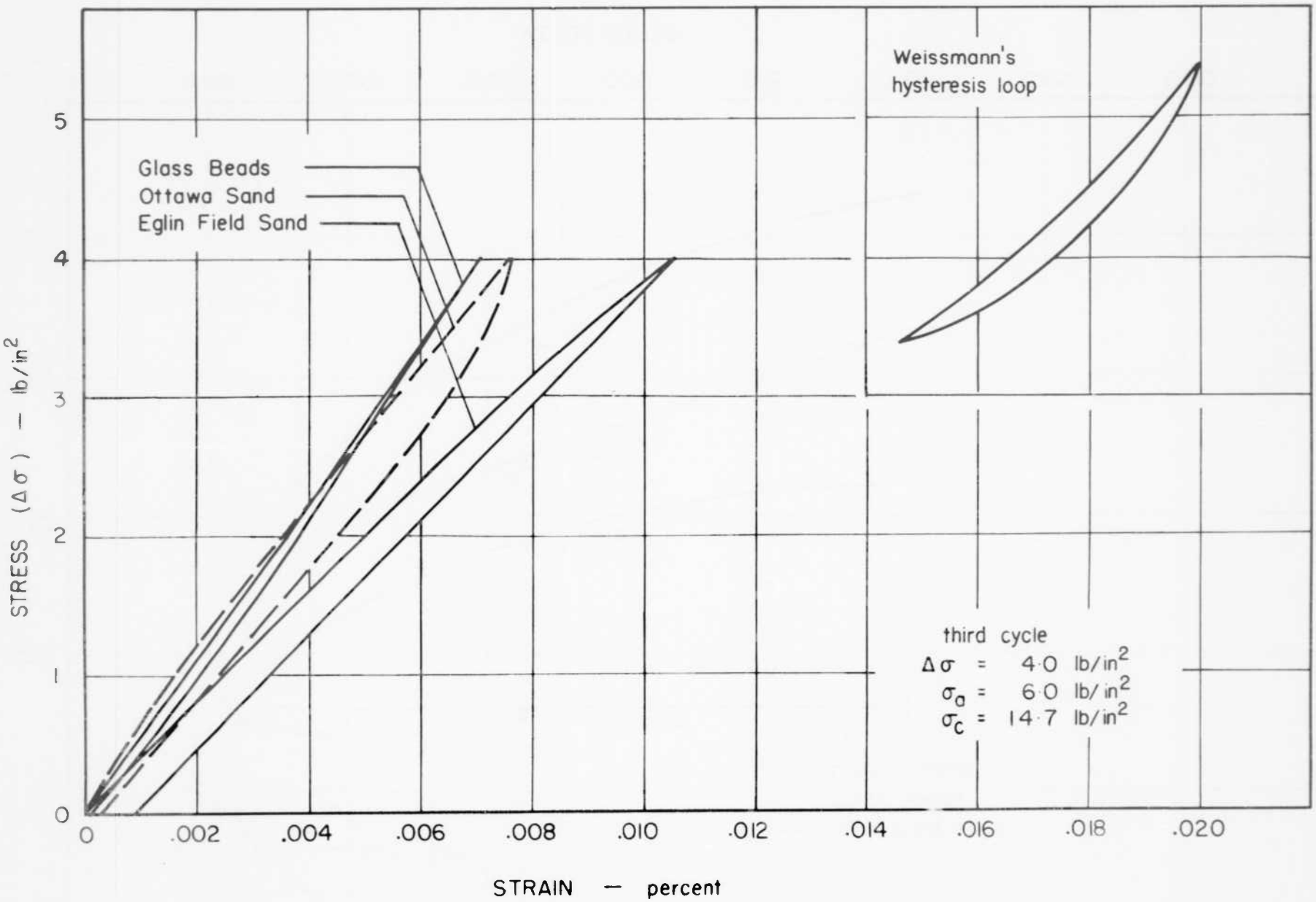

FIGURE 12 HYSTERESIS LOOPS OBTAINED ON THIRD LOADING CYCLE

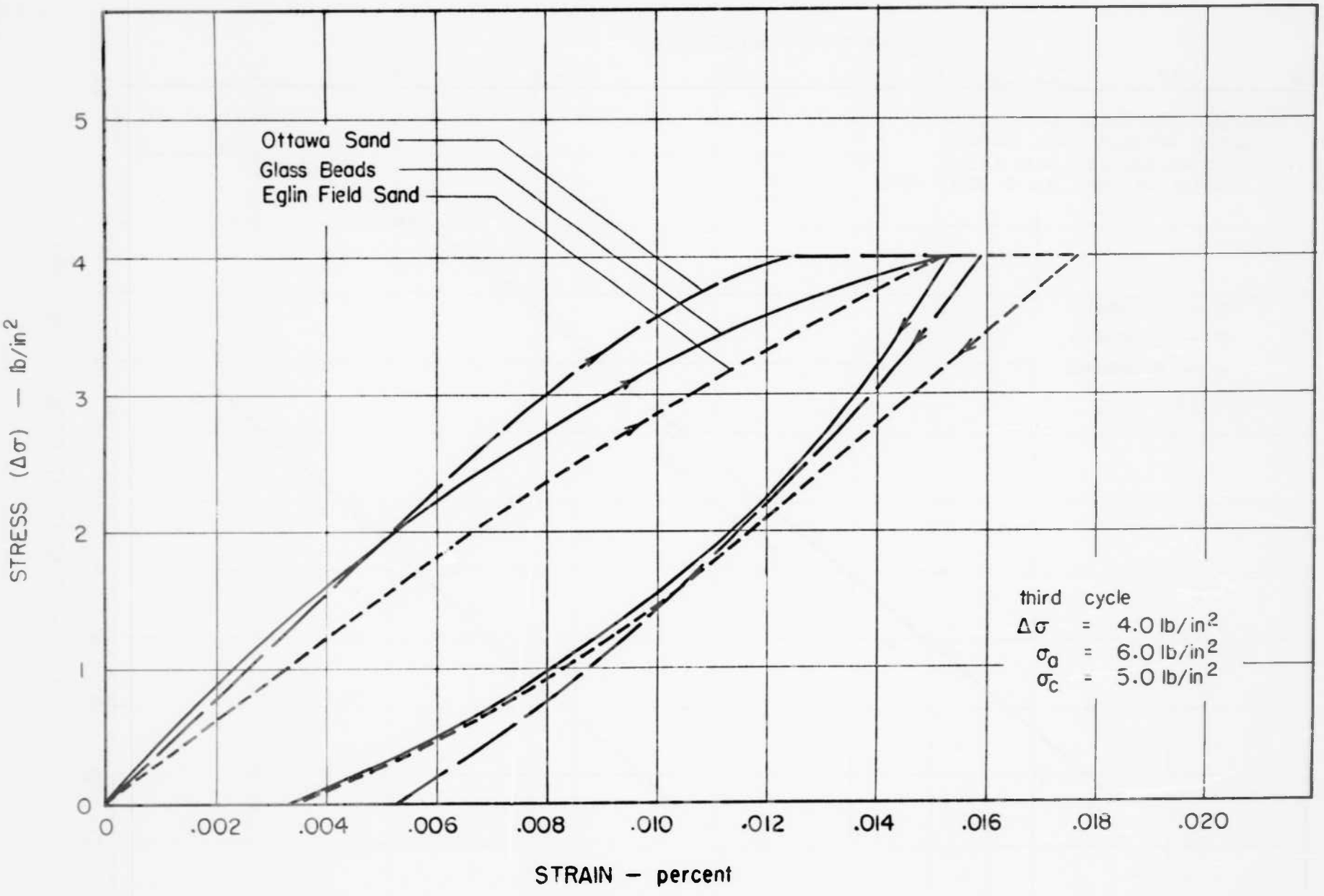

FIGURE 13 HYSTERESIS LOOPS OBTAINED ON THIRD LOADING CYCLE

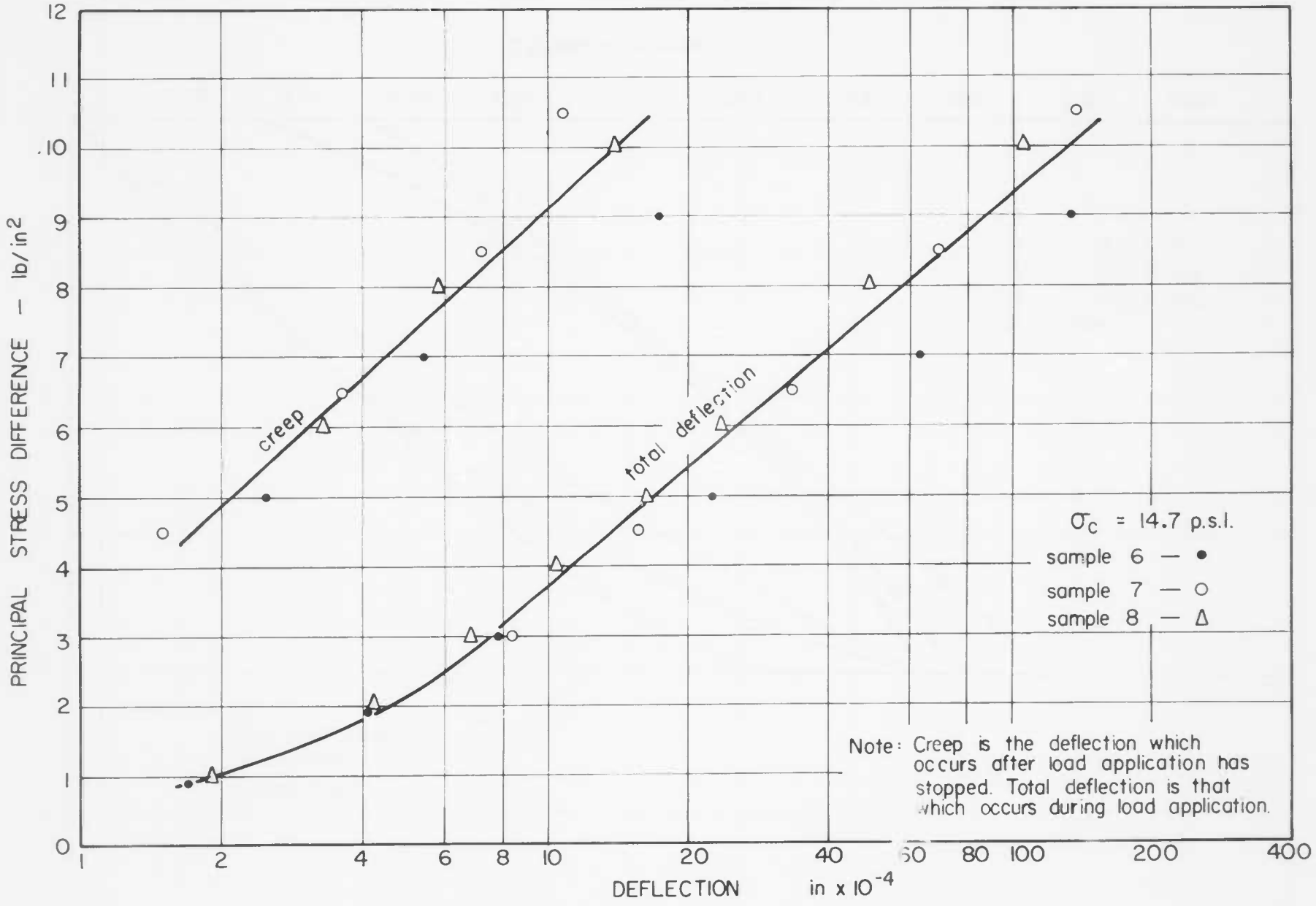

FIGURE 14 STRESS – DEFLECTION CURVES
OTTAWA SAND

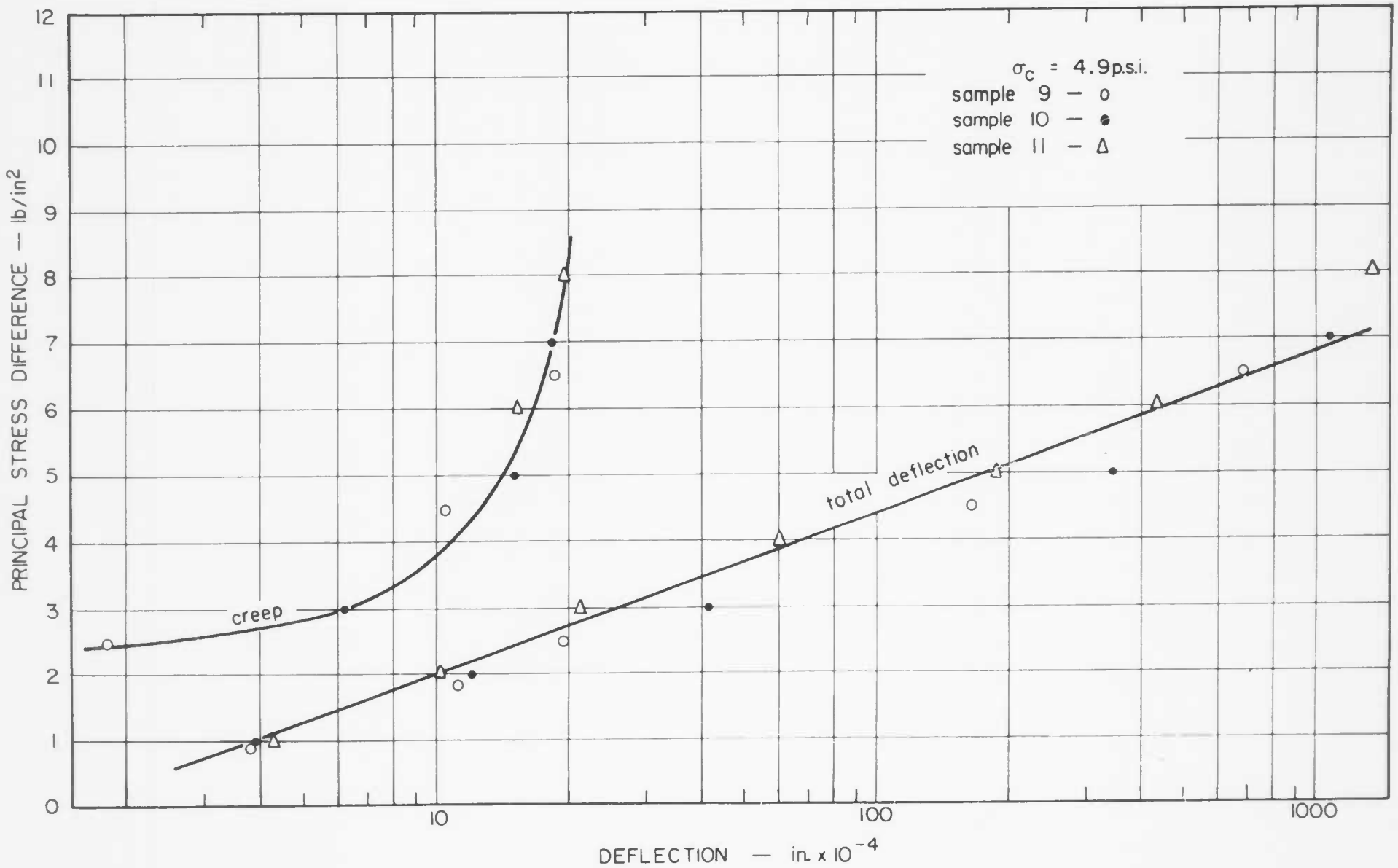

FIGURE 15 STRESS DEFLECTION CURVES — OTTAWA SAND

DISTRIBUTION LIST

Addresses	No. of Copies
Bureau of Mines, Washington, D. C., Attn: J. E. Crawford	1
Chief, Bureau of Yards and Docks, ND, Washington 25, D. C. Attn: D-440	1
Chief, Defense Atomic Support Agency, Washington 25, D. C. Attn: Document Library Attn: Major Vickery	12 1
Chief of Engineers, Department of the Army, Washington 25, D. C. Attn: ENGTE-E Attn: ENGMC-EB	1 2
Chief of Naval Operations, ND, Washington, D. C. Attn: Op-75	1
Chief of Research and Development, DA, Washington 25, D. C. Attn: Atomic Division	1
Commander, Air Force Ballistic Missile Division, Air Research and Development Command, Attn: WDFN, P. O. Box 262, Inglewood 49, California	1
Commander, Armed Services Technical Information Agency (ASTIA), Arlington Hall Station, Arlington 12, Va.	20
Commander, Air Force Special Weapons Center, Kirtland Air Force Base, Albuquerque, N. M., Attn: SWRS	4
Commander, Wright Air Development Center, Wright-Patterson Air Force Base, Ohio, Attn: WCOSI	1
Command General, U. S. Army Materiel Command, Attn: AMCRD-RS-ES, Room 2507, Building T-7, Washington 25, D. C.	3
Commanding Officer and Director, U. S. Naval Civil Engineering Laboratory, Port Hueneme, California	1
Director, Weapons Systems Evaluation Group OSD, Room 1E880, The Pentagon, Washington 25, D. C.	1
Director, U. S. Army Engineer Waterways Experiment Station, P. O. Box 631, Vicksburg, Mississippi	25

Director of Civil Engineering, Headquarters, U. S. Air Force,
Washington 25, D. C., Attn: AFOCE 1

Director of Defense Research and Engineering, Washington 25, D. C.,
Attn: Technical Library 1

Headquarters, U. S. Air Force, Washington 25, D. C.,
Attn: AFTAC, C. F. Romney 2

Space Technology Laboratory, Inglewood, California
Attn: B. Sussholz 1

U. S. Coast and Geodetic Survey, Washington, D. C.
Attn: D. S. Gardner 1

U. S. Coast and Geodetic Survey, San Francisco, California,
Attn: W. K. Cloud 1

U. S. Geological Survey, Washington, D. C.
Attn: J. R. Balsley 1

California Institute of Technology, Pasadena, California,
Attn: F. Press 1
Attn: R. Benioff 1

Columbia University, New York, N. Y., Attn: J. E. Oliver 1

Pennsylvania State College, Atomic Defense Engineering Dept.,
State College, Pennsylvania, Attn: Prof. Albright 1

Stanford Research Institute, Physical Sciences Division,
Menlo Park, California, Attn: Dr. R. B. Vaille, Jr. 2

American Machine and Foundry, 7501 North Natchez Avenue,
Niles 48, Illinois, Attn: Mr. Tom Morrison 1

Barry Wright Corporation, 700 Pleasant St., Watertown 72,
Massachusetts, Attn: Mr. Cavanaugh 1

Holmes and Narvey, Los Angeles, California, Attn: S. B. Smith 1

Dr. Harold Brode, RAND Corporation, 1700 Main Street,
Santa Monica, California 1

Dr. N. M. Newmark, Civil Engineering Hall, University of Illinois,
Urbana, Illinois 1

Dr. T. H. Schiffman, Armour Research Foundation, Illinois Institute
of Technology, Technology Center, Chicago 16, Illinois 1

Prof. F. E. Richart, Jr., Dept. of Civil Engineering, University of Michigan, Ann Arbor, Michigan 1

Prof. Robert L. Kondner, The Technological Institute, Northwestern University, Evanston, Illinois 1

Prof. Gerald A. Leonards, School of Civil Engineering, Purdue University, Lafayette, Indiana 1

Prof. H. Bolton Seed, Dept. of Civil Engineering, University of California, Berkeley, California 1

Prof. H. Neils Thompson, Civil Engineering Dept., University of Texas, Austin 12, Texas 1

Mr. Kenneth Kaplan, United Research Services, 1811 Trousdale Drive, Burlingame, California 1

Mr. W. R. Perret, 5112, Sandia Corporation, Sandia Base, Albuquerque, N. M. 1

Mr. Fred Sauer, Physics Department, Stanford Research Institute, Menlo Park, California 1

Mr. A. A. Thompson, Terminal Ballistics Laboratory, Aberdeen Proving Ground, Aberdeen, Maryland 1

Mr. C. J. Nuttall of Wilson, Nuttall, Raimond Engineers, Inc., Chestertown, Maryland 1

Dr. Grover L. Rogers, Recon, Inc., Box 3622 MSS, Tallahassee, Florida 1

Armour Research Foundation of Illinois Institute of Technology, Attn: Document Library, Chicago 16, Illinois 1